COMPUTATIONALLY GUIDED EXPLORATION IN GOLD(I)-CATALYSED REACTIONS

Eduardo García Padilla

UNIVERSITAT
ROVIRA i VIRGILI

Computationally Guided Exploration into Gold(I)-Catalysed Transformations

Eduardo García Padilla

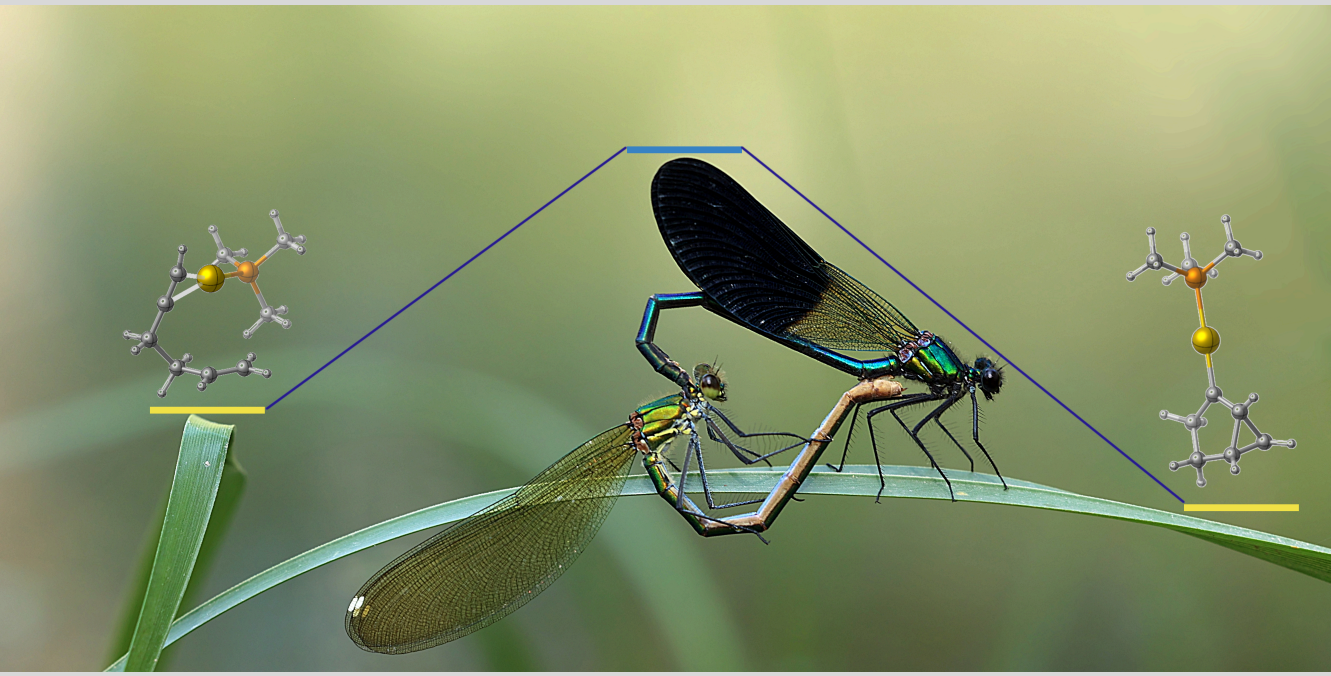

DOCTORAL THESIS
2023

UNIVERSITAT ROVIRA I VIRGILI
COMPUTATIONALLY GUIDED EXPLORATION IN GOLD(I)-CATALYSED REACTIONS
Eduardo García Padilla

UNIVERSITAT ROVIRA I VIRGILI
COMPUTATIONALLY GUIDED EXPLORATION IN GOLD(I)-CATALYSED REACTIONS
Eduardo García Padilla

Eduardo García Padilla

Computationally Guided Exploration into Gold(I)-Catalysed Transformations

DOCTORAL THESIS

Supervised by Prof. Antonio M. Echavarren and Prof. Feliu Maseras

Institut Català d'Investigació Química

UNIVERSITAT ROVIRA i VIRGILI

Tarragona 2023

UNIVERSITAT ROVIRA I VIRGILI
COMPUTATIONALLY GUIDED EXPLORATION IN GOLD(I)-CATALYSED REACTIONS
Eduardo García Padilla

ICIQ Institut Català d'Investigació Química

UNIVERSITAT ROVIRA i VIRGILI

WE STATE that the present study, entitled "Computationally Guided Exploration into Gold(I)-Catalysed Transformations", presented by Eduardo García Padilla for the award of the degree of Doctor, has been carried out under our supervision at the Institut Català d'Investigació Química.

Tarragona, 11th October 2023

Doctoral Thesis Supervisors

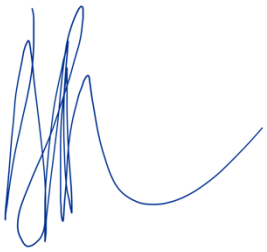

Prof. Antonio M. Echavarren

Prof. Feliu Maseras

UNIVERSITAT ROVIRA I VIRGILI
COMPUTATIONALLY GUIDED EXPLORATION IN GOLD(I)-CATALYSED REACTIONS
Eduardo García Padilla

A mis padres.

UNIVERSITAT ROVIRA I VIRGILI
COMPUTATIONALLY GUIDED EXPLORATION IN GOLD(I)-CATALYSED REACTIONS
Eduardo García Padilla

"In science we must all submit not to what seems to us attractive from one point of view or another, but to what represents an agreement between theory and experiment."

Dmitri Mendeleyev

UNIVERSITAT ROVIRA I VIRGILI
COMPUTATIONALLY GUIDED EXPLORATION IN GOLD(I)-CATALYSED REACTIONS
Eduardo García Padilla

I would like to thank Prof. Antonio Echavarren and Prof. Feliu Maseras for accepting me in their research groups as a PhD student in the Institut Català d'Investigació Química (ICIQ). Thank you for shaping my scientific judgement, for consistently showing the importance of integrity in science, for the trust and freedom granted to explore different ideas and for all the enriching scientific discussion.

Vull agrair a Sònia Gavaldà portar-nos l'efi- a la -ciència i coordinar simultàniament tots els trencaclosques administratius del grup amb una destresa legendària. Gràcies també a la Dra. Imma Escofet per ser la "superuser" per excel·lència i assegurar que tot funcione bé sempre; gràcies també per tota l'ajuda en els moments més estressants del doctorat.

I thank Prof. Dr. Robert Wolf for having me in his group for three months and allowing me to explore some great chemistry. My gratitude also extends to all the people in the research group, who made me feel at home, especially to Franzi and Karo, with whom I had the pleasure of collaborating.

I would also like to thank all members of the research support units at ICIQ, in particular HTE (gràcies, Xisco i Sílvia, per la vostra ajuda), NMR (because Baroque music improves shimming), HRMS (for ionising the unionisable), XRD (for crystallising the uncrystallisable), as well as Martín Gumbau. Likewise, thanks to the people working at the IT unit, administration, security, cleaning and also SHEQ for the help after my involuntary glass-mediated (*S*)-2-fingerpad cleavage.

During the last four years, I have had the great pleasure of spending my time alongside truly fantastic people. I extend my gratitude to all past and present members of the Echavarren and Maseras groups for the company inside and outside the lab.

Gracias a Isabel Arranz por la amistad, por haber sido la mejor (y única) alumna de armonía y análisis que he tenido e incluso haber aprendido la letra de Pequeño Cosmonauta. Neanche potrei dimenticare Andrea Cataffo per tutto quello che abbiamo fatto questi anni, le giornate in montagna, proprio distruggere i nostri cervelli contro i meccanismi, e per essere sempre lì quando ne avevo bisogno: grazie!

Gracias a las superusers "OG", Inma Martín y Ana Arroyo, por aquellas semanas frente a los equipos, los "vapores del UHPLC" y las propuestas para el Journal of Chromatography (dos métodos más y tenemos full paper).

También a Pablo Mora, Leo (del 2.2 OG, por tantas risas), Dr. Víctor García (por traer un trocito de Elche), Dr. Nicolás Fincias (por las excelentes conversaciones de química), Gala Ogalla, Laura Lerena, Dr. Anna Sadurní, Dr. Paul Beller and Dr. Anders Hammarbäck, as well as several more people for the hiking adventures, pandemic-induced boardgame evenings and for preventing me from face-planting the snow while skiing.

Thank you to all the computational labmates these years. En concreto, gracias a todos aquellos que me ayudaron con las dudas o peticiones más inusuales (Dr. Raúl Pérez, Dr. Bruna Sánchez, Lucía Morán),

благодарю Иоганна Толбатова за советы по химии и горам, i Marina Díaz per ser tan bona gent i pels seus “Ànims! Tu pots!” en els punts més crítics.

The context around the science is often a better catalyst than anything to come out of ligand design or fruitless reaction optimisations. Thank you to Dr. Matthew Stevens, Mr. Gallium if I may, for your great friendship, for teaching me how to solve XRD, and for engaging in our endless chemistry conversations for hours on end. Gracias a Dr. Mauricio Murillo, quien me inició en la química computacional y me contagió su pasión.

Especialment, i degut a la meua afició musical, gràcies a l’orquestra de la URV per tants bons moments. Gracias a Inés trompa por tu apoyo todos estos meses, també a Miquel Massana (quina meravella de director!), Alèria cello (pels consells químics, musicals i més generals), Jaume fagot, Salortet trompa, Joan violí i Àlex violí per tots els moments viscuts. También a José Luis Carrasquilla por las extraordinarias églogas acompañadas de no menos extraordinarias cenas. Thank you, Dr. John Stringer for the great conversations and for letting me play again in the Minster with my *alma mater*.

Gràcies a Tomàs y a Tomás (tú y el otro, vull dir, l’altre però també tu) per l’amistat tan extraordinària que m’heu regalat i que hem mantingut tants anys des dels primers anys en York y ahora desde no tan cerca.

También a todos mis amigos de Elche que han estado apoyándome desde la distancia: gracias a Manu, Pérez, Roca, Víctor, Germán, Carol, María, Enrique, Isma y Juanjo. Gracias por tantísimas conversaciones interesantes, surrealistas, circulares, filosóficas y a menudo útiles. En especial, por hacerme sentir cada vez que vuelvo a Elche como si siempre hubiera estado allí. Sería inconcebible olvidar en este plano ilicitano a los Achos y, en concreto, a los inigualables Enrique Girona (desde El Candil hasta Парнас) i Pablo Pastor (pels “bon dia” i perquè és un plaer estar amb tu).

Sin lugar a dudas, muchísimas gracias a mi familia: a todos mis tíos y primos de Reus (gracias, Garcías) y de Alicante, por haberme apoyado todos estos años y por haberme hecho sentir tan querido. Sois los arbotantes de esta tesis.

Especialmente, quiero agradecer a mis padres, y con la certeza de que me quedará escasa la semántica, el incondicional apoyo y amor. Gracias por haberme enseñado tanto, por confiar en mí, guiarme, escucharme y acompañarme siempre. Me siento increíblemente afortunado de teneros. Muchísimas gracias por todo.

This work was carried out with the financial support of AGAUR – FI PhD fellowship (2020FI_B 00403, predoctoral fellowship), the Ministerio de Ciencia e Innovación (PID2019-104815GB-I00), Severo Ochoa Excellence Accreditation 2020-2023 (CEX2019-000925-S), European Research Council (Advanced Grant 835080), the Agència de Gestió d'Ajuts Universitaris i de Recerca – AGAUR (project 2021 SGR 01256), and the Institute of Chemical Research of Catalonia (ICIQ) in the CERCA Program/Generalitat de Catalunya.

UNIVERSITAT ROVIRA I VIRGILI
COMPUTATIONALLY GUIDED EXPLORATION IN GOLD(I)-CATALYSED REACTIONS
Eduardo García Padilla

At the time of writing this Doctoral Thesis, part of the work detailed in this manuscript has been published in the following articles:

García-Padilla, E.; Maseras, F.; Echavarren, A. M. Gold(I)-Catalyzed 1,6-Enyne Single Cleavage Rearrangements: The Complete Picture. *ACS Org. & Inorg. Au*, **2023**, *3*, 312–320.

García-Padilla, E.; Escofet, I.; Maseras, F.; Echavarren, A. M. The Puzzling Structure of the Key Intermediates in Gold(I) Catalyzed Cyclizations of Enynes and Allenenes. **2023**. *Submitted*.

UNIVERSITAT ROVIRA I VIRGILI
COMPUTATIONALLY GUIDED EXPLORATION IN GOLD(I)-CATALYSED REACTIONS
Eduardo García Padilla

Table of Contents

UNIVERSITAT ROVIRA I VIRGILI
COMPUTATIONALLY GUIDED EXPLORATION IN GOLD(I)-CATALYSED REACTIONS
Eduardo García Padilla

UNIVERSITAT ROVIRA I VIRGILI
COMPUTATIONALLY GUIDED EXPLORATION IN GOLD(I)-CATALYSED REACTIONS
Eduardo García Padilla

Prologue

This Doctoral Thesis manuscript has been divided into four main parts: a general introduction on gold(I) catalysis and three research chapters. The latter are preceded by the abstract and the general objectives of the work presented in this Thesis. The research chapters are followed by the general conclusions. Each research chapter follows a quinquepartite structure comprising a more specific introduction, the objectives of the work, the results and discussion, the conclusions, and the experimental section. The numbering of compounds, computational geometries, schemes, tables, figures, and references is organised by chapter.

The **General Introduction** explores the development of homogeneous gold catalysis, focusing on the activation of alkynes, enyne cycloisomerisations, the evolution of the mechanistic understanding and the application of DFT methods.

Chapter I collects the computational and experimental work in the mechanistic investigation of enyne rearrangements, divided in three parts. The first section explores the nature of intermediates in 1,5-enyne and 1,5-allenene cyclisations and the description of these systems through DFT methods; initial work performed by Dr. Imma Escofet is only briefly discussed for coherence. The second section explores the stereoconvergence and changes in *exo*/*endo*-type single-cleavage gold(I)-catalysed cycloisomerisations of 1,6-enynes. The third section analyses racemisation pathways in enyne cyclisations. The experimental work corresponding to this final section was carried out by Andrea Cataffo and will be referenced in the discussion of the computational results.

Chapter II presents our studies on the gold(I)-catalysed 1,3,5-cyclotrimerisation of terminal alkynes, including both the experimental and computational work to provide mechanistic insight as well as synthetic results. Part of the experimental work was performed in collaboration with Dr. Anders Hammarbäck, but his results are excluded from the discussion.

Chapter III contains the work related to the synthesis, coordination chemistry and reactivity of bimetallic complexes containing a phosphine-bipyridine scaffold. The experimental work was carried out in collaboration with Dr. Víctor García and Dr. Nicolás Fincias, and some of their results are discussed for coherence and to put the work in context.

List of Abbreviations and Acronyms

In this manuscript, the abbreviations and acronyms most commonly used in organic and organometallic chemistry have been used following the recommendations of "Guidelines of Authors" of the Journal of Organic Chemistry.

Additional abbreviations and acronyms used in this manuscript are listed here:

APCI	atmospheric pressure chemical ionisation
$BAr^{F}{}_{4}^{-}$	tetrakis[3,5-bis(trifluoromethyl)phenyl]borate
DVV	damped velocity Verlet integrator
ECP	effective core potential
er	enantiomeric ratio
ESI	electrospray ionisation
HRMS	high-resolution mass spectrometry
IMes	1,3-bis(2,4,6-trimethylphenyl)imidazol-2-ylidene
IPr	1,3-bis(2,6-diisopropylphenyl)imidazol-2-ylidene
IRC	intrinsic reaction coordinate
JohnPhos	(2-biphenyl)di-*tert*-butylphosphine
L	ligand
LQA	local quadratic approximation
MS	mass spectrometry or molecular sieves
MW	microwave irradiation
NBO	natural bond orbital
NHC	N-heterocyclic carbene
NLMO	natural localised molecular orbital
NTf_2^-	bis(trifluoromethyl)imidate
OTf^-	trifluoromethanesulfonate
ORTEP	Oak Ridge thermal ellipsoid plot
*t*BuXPhos	di-*tert*-butyl-(2',4',6'-triisopropylbiphenyl)phosphine
TS	transition state

Abstract

Gold(I) catalysis, dominated by the activation of *sp*-hybridised carbons, has shown great versatility in organic synthesis due to their selectivity patterns, broad functional group tolerance and generally mild conditions. In the light of the lack of insight into more unusual observed reactivity, whether in shifting regio- and stereoselectivity, highly selective transformations or underexplored bimetallic systems, this Doctoral Thesis covers the explored mechanisms underpinning each of these reactions experimentally and computationally and presents rational approaches to reaction discovery.

We determined the nature of intermediates in 1,5-enynes and 1,5-allenenes, confirming the existence of tautomeric cyclopropylcarbene and vinylgold species, as well as non-classical carbocationic species. We described their bonding through NBO calculations. We also extend this study to a complete mechanistic understanding of single- and double-cleavage enyne rearrangements, uncovering the factors leading to stereoconvergence, exocyclic or endocyclic selectivity and single or double cleavage. Finally, a mechanistic investigation of enyne cyclisations and alkoxycyclisations provided the theoretical framework for the study of the role of the alcohol. Thereby, we explored the racemisation pathway in 1,6-enyne cyclisations with evidence supporting a reversible 1,2-hydride shift which is accessible at lower concentrations of alcohol.

The gold(I)-catalysed 1,3,5-selective cyclotrimerisation of alkynes was then explored. We developed the reaction for terminal arylalkynes reaching low to moderate yields. A thorough computational mechanistic investigation, validated through control experiments, suggested that the cyclotrimerisation proceeds through unique gold(I) η^1-cyclobutadiene and Dewar benzene intermediates. Hence, we developed intramolecular cyclotrimerisations that afforded formal 1,2,3-cyclotrimerised alkynes.

We finally designed a ligand platform to serve as a scaffold for bimetallic complexes containing gold(I). In addition to their synthesis and structural characterisation, we examined their reactivity and performed more in-depth combined computational and experimental work on the cyclometallated gold(I)-d^8 metal complexes. Computational insight helped develop rational self-activating catalysis with the [AuAu] complexes.

General Objectives

The objective of this Doctoral Thesis was to perform a full mechanistic exploration into gold(I) cycloisomerisations and harnessing the computational results to develop novel reactivity. Specifically, we pursued the following aims:

- The computational and experimental study in enyne cyclisations and the definitive characterisation of the nature of the underlying intermediates and mechanistic scenarios in skeletal rearrangements and alkoxycyclisations.
- The development of the 1,3,5-cyclotrimerisation of alkynes, the determination of the mechanism and the computationally guided discovery of unusual 1,2,3-cyclotrimerised products.
- The design of a ditopic ligand as a platform to study bimetallic complexes, the preparation thereof and the study of their reactivity.

A more detailed description of each of these objectives is provided in the corresponding section of each Chapter of this manuscript.

General Introduction

A Historical Prelude to Gold Chemistry

The Early Bronze Age was marked by the discovery of metal working, which deeply transformed the agrarian late Neolithic communities into more hierarchic, urbanised societies catalysed by the newly developed metallurgy.[1] In addition to gradually replacing stone tools, all metals were considered symbols of prestige or status due to the complexity in their processing. Nevertheless, it was the heavier coinage metals that were most valued in this respect, with gold objects first described in Europe towards 4600 BCE,[2] complex processing of silver objects in El Argar[3] and the recently reported earliest evidence of gold processing in Central Europe.[4]

Perhaps unsurprisingly, the atemporal value that has accompanied gold has always been defined, in addition to its scarcity, by its chemistry. In fact, the evidence for this is attested in the two known Proto-Indo-European roots for gold metal: **h₂eusom* (derivative of **h₂ewes*, "to shine"), whence Latin *aurum*; and **ǵʰelh₃* ("yellow"), whence English *gold*.[5] The occurrence of native –metallic– gold reflects its lower tendency to oxidise in air and as such would be one of the only "shiny" metals to be found in nature. Its yellow colour, unusual for most metals, is due to relativistic effects since the absorbed wavelengths shift to violet-blue.[6] In spite of these initial observations, it would take several thousand years for the thorough investigation into the chemistry of this element to begin.

Gold(I) chloride itself was only discovered in 1913 through the thermal decomposition of rigorously dried gold(III) chloride, yet even then it showed some instability in the absence of additional chloride ions.[7] Only several decades later, the first examples of gold-alkene complex were prepared[8] and then found to form under milder conditions without photoirradiation.[9] The simplest dicoordinated gold-alkene complex, with a coordinated ethylene, was much more elusive and required a large stabilising ligand. It was first isolated more than 70 years later by Campos and coworkers.[10]

The earliest gold-mediated reactions were generally stoichiometric because of the concomitant reduction to gold metal. The earliest reports by Kharasch and Isbell found that gold(III) chloride would

1 McLellan III, J. E.; Dorn, H. *Science and Technology in World History: An Introduction*. JHU Press, 41–44
2 Leusch, V.; Pernicka, E.; Armbruster, B. Chalcolithic gold from Varna – Provenance, circulation, processing, and function. *Metalle der Macht Frühes Gold und Silber*, Tagungen des Landesmuseums für Vorgeschichte Halle (Halle (Saale)), **2014**, *11*, 165–183.
3 Delgado-Raack, S.; Lull, V.; Martin, K.; Micó, R.; Rihuete Herrada, C.; Risch, R. The Silversmith's Workshop of Tira Del Lienzo (Totana, Murcia) In The Context of Iberian Bronze Age Metallurgy. *Archaeometry* **2016**, *58*, 779–795.
4 Müller, J.; Delgado-Raack, S.; Escanilla, N.; Kienle, L.; Kneisel, J.; Czebreszuk, J.; Jaeger, M.; Szmyt, M.; Schürmann, U. First Evidence for the Forging of Gold in an Early Bronze Age Site of Central Europe (2200–1800 BCE). *J. Archaeol. Sci. Rep.* **2023**, *47*, 103748.
5 Mallory, J. P.; Adams, D. Q. *The Oxford Introduction to Proto-Indo-European and the Proto-Indo-European World.* Oxford University Press, **2006**, 241–242.
6 Pyykkö, P. Relativistic Effects in Chemistry: More Common Than You Thought. *Annu. Rev. Phys. Chem.* **2012**, *63*, 45–64.
7 Diemer, M. E. Aurous Chloride. *J. Am. Chem. Soc.* **1913**, *35*, 552–559.
8 Chalk, A. J. 1,5-Cyclooctadiene Complexes of Gold(I) and Gold(III). *J. Am. Chem. Soc.* **1964**, *86*, 4733–4734.
9 Hüttel, R.; Reinheimer, H.; Dietl, H. Olefin-Gold-Komplexe, II. Gold(I)-chlorid-Komplexe cyclischer Mono-, Di- und Triolefine. *Chem. Ber.* **1966**, *99*, 462–468.
10 Navarro, M.; Miranda-Pizarro, J.; Moreno, J. J.; Navarro-Gilabert, C.; Fernández, I.; Campos, J. A Dicoordinate Gold(i)–Ethylene Complex. *Chem. Commun.* **2021**, *57* (73), 9280–9283.

chlorinate benzene to form chlorobenzenes, isolating phenylgold(III) dichloride as an intermediate and confirming that gold(III) chloride could operate catalytically in the presence of chlorine gas.[11] Later examples include the chlorination of alkenes with gold(III) chloride, shedding light on the stepwise reduction processes as well as the fate of unligated gold(III) species in the presence of alkenes (Scheme 1).[12] As was seen in these early studies, the facile decomposition to gold metal, the chemical inertness and perceived lack of general reactivity consequently led to its neglect by the chemical community for several decades.[13]

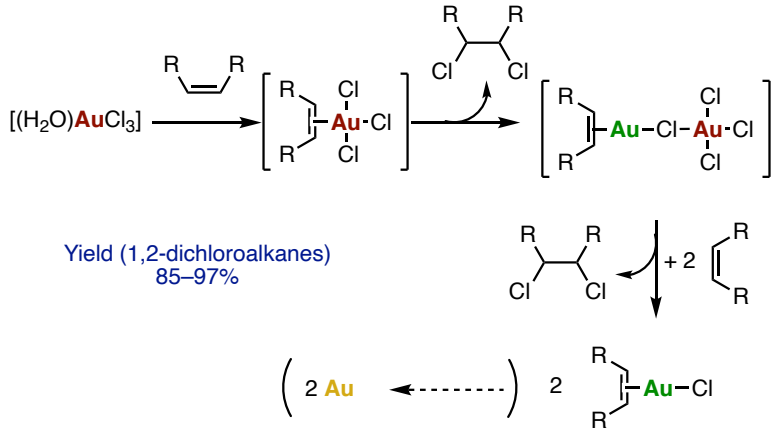

Scheme 1. Gold-mediated formation of 1,2-dichloroalkanes and overall reduction to gold(I), with [(alkene)Au_2Cl_4] proposed to be a chloride-bridged mixed-valence species. Further reduction to gold metal occurs with concomitant formation of dichloroalkane and alkene. Gold(III), gold(I) and gold(0) marked in red, green and yellow.

The first catalytic reaction reported with a preformed gold complex was asymmetric: the aldol reaction between aldehydes and an isocyanoacetate leading to chiral products in 72–97% enantiomeric excess.[14] The origin of the chiral induction was not fully understood but was confirmed to require gold.[15]

In 1991, Fukuda and Utimoto reported that sodium tetrachloroaurate as a gold(III) source was able to catalyse the hydration and alkoxylation of alkynes under mild conditions, thus constituting the first example of substoichiometric homogeneous gold catalysis in which the reaction mechanism involved the activation of an alkyne by gold.[16] Because of the previously explored decomposition pathways for

11 Kharasch, M. S.; Isbell, H. S. The Chemistry of Organic Gold Compounds. III. Direct Introduction of Gold into the Aromatic Nucleus (Preliminary Communication). *J. Am. Chem. Soc.* **1931**, *53*, 3053–3059.
12 Hüttel, R.; Reinheimer, H.; Nowak, K. Olefin-Gold-Komplexe, VI. Gold(I)-Gold(III)-Mischkomplexe von Olefinen. *Chem. Ber.* **1968**, *101*, 3761–3776.
13 Schmidbaur, H. *Naturwiss. Rundsch.* **1995**, *48*, 443-451.
14 Ito, Y.; Sawamura, M.; Hayashi, T. Catalytic Asymmetric Aldol Reaction: Reaction of Aldehydes with Isocyanoacetate Catalyzed by a Chiral Ferrocenylphosphine-Gold(I) Complex *J. Am. Chem. Soc.* **1986**, *108*, 6405–6406.
15 The coordination of the isocyanide to gold(I) centre was expected, but the proposed six-membered ring transition state with a tetrahedrally tetracoordinated gold(I) centre is now considered unlikely.
16 Fukuda, Y.; Utimoto, K. Effective Transformation of Unactivated Alkynes into Ketones or Acetals with a Gold(III) Catalyst. *J. Org. Chem.* **1991**, *56*, 3729–3731.

gold(III) salts in the presence of alkenes,[12] it would remain unclear whether gold(III) was acting as the active catalyst or an active gold(I) complex was generated from the precatalyst.

The analogous methyl acetal and methyl enol ether formation reported by Teles (Scheme 2) was, however, the first case with a well-defined catalyst with an active gold(I) centre.[17] Beyond the substitution of mercury(II) catalysts for a much less toxic alternative, this work laid the foundation of subsequent explorations into alkyne activation with gold(I) catalysis.

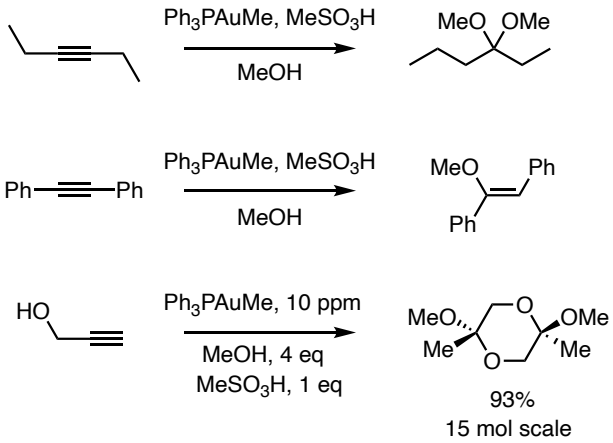

Scheme 2. Gold(I)-catalysed mono- and dialkoxylation of alkynes.

In these early works, the activity of gold was already assigned to a coordinatively unsaturated cationic gold(I) species, which would coordinate the alkyne substrate in a linear dicoordinated fashion typical for gold(I). However, accessing these species from the early precatalysts required the use of a strong acid (as seen in Scheme 2). The discovery of the activation of gold(I) chloride complexes with halide scavengers, such as silver or sodium salts of weakly-coordinating anions, allowed gold(I) catalysis to flourish by forming the active catalysts at much lower temperatures.[18] Interestingly, different weakly coordinating anions have sometimes shown different activity.

The growth of gold(I) catalysis since the discovery of the efficient activation of alkynes was facilitated by two main factors: the wide range of nucleophiles that could react with such gold-activated alkynes and the development of the mechanistic understanding behind the concept of π-acidity.[19] Although the mechanisms were broadly known, aiding in rational planning, the accessible molecular diversity with gold(I) catalysis proved to be double-edged in the overarching substrate dependence exhibited in many reactions.[20]

17 Teles, J. H.; Brode, S.; Chabanas, M. Cationic Gold(I) Complexes: Highly Efficient Catalysts for the Addition of Alcohols to Alkynes. *Angew. Chem. Int. Ed.* **1998**, *37*, 1415–1518.
18 Jia, M.; Bandini, M. Counterion Effects in Homogeneous Gold Catalysis. *ACS Catal.* **2015**, *5*, 1638–1652.
19 Fürstner, A. Gold and Platinum Catalysis—a Convenient Tool for Generating Molecular Complexity. *Chem. Soc. Rev.* **2009**, *38*, 3208.
20 Fensterbank, L.; Malacria, M. Molecular Complexity from Polyunsaturated Substrates: The Gold Catalysis Approach. *Acc. Chem. Res*. **2014**, *47*, 953–965.

Relativistic Effects

All 5d transition metals show atomic radii surprisingly close to their 4d counterparts, an observation explained by the lanthanide contraction.[21] However, in the case of 5d late transition metals and gold in particular, there is an additional contribution due to the heavy nucleus: relativistic effects. These reach a maximum for gold due to cooperative shell contraction and relativistic stabilisation of valence orbitals at the end of the d-block.[22] As lanthanide contraction effects gradually decrease in importance along the d-block, the relativistic contraction at gold is much more significant.

The relativistic effects result in the contraction of the orbitals closest to the nucleus, mainly *s* but also *p* orbitals, and the secondary enlargement of the other orbitals in the atom. The origin of this contraction can be explained by the increase in mass and time dilation for high-velocity electrons near the nucleus, resulting in an overall greater electron density closer to the nucleus. The electron density of the orbitals that penetrate closest to the nucleus is therefore shifted inwards and the orbitals contract in effective size. The outer *d* and *f* orbitals consequently experience an indirect effect, becoming more shielded and therefore increasing in size.[23]

The consequences of such effects permeate gold chemistry. Aurophilicity can be of the same order of magnitude as hydrogen bonds and the ionisation energy is surprisingly high for a group 11 metal, linked to the high electronegativity. The electronegativity and Lewis acidity are coupled to the rarity of non-dicoordinate gold(I) species, and the rarity of oxidative addition processes is also caused by the same effects.[24] Overall, this results in a very high degree of covalency in bonding. For this reason, ligands are able to modify the electronic properties of the gold atom to a very large extent. Modifications of the ligands on gold catalysts have shown divergence in a broad range of transformations, being mainly attributed to electronic rather than steric effects.[25]

The larger *d* orbitals, in particular, which are much more diffuse because of the increased shielding from the other contracted orbitals, become much softer than would be expected if relativistic effects were not taken into account. This is in line with the observed low oxophilicity and the catalytically important strong bonding interactions with soft ligands such as alkenes and alkynes.

Computationally, and more specifically with DFT methods, the omission of relativistic effects often fails to model the systems almost completely, as can be inferred from the importance that these have. The main approaches have therefore relied on the use of relativistic basis sets for gold or circumventing

21 Douglas, B. E. The Lanthanide Contraction. *J. Chem. Educ.* **1954**, *31*, 598.
22 Autschbach, J.; Siekierski, S.; Seth, M.; Schwerdtfeger, P.; Schwarz, W. H. E. Dependence of relativistic effects on electronic configuration in the neutral atoms of d- and f-block elements. *J. Comp. Chem.* **2002**, *23*, 804–813.
23 Pyykkö, P. Theoretical Chemistry of Gold. *Angew. Chem. Int. Ed.* **2004**, *43*, 4412–4456.
24 Gorin, D. J.; Toste, F. D. Relativistic Effects in Homogeneous Gold Catalysis. *Nature* **2007**, *446*, 395–403.
25 Chintawar, C. C.; Yadav, A. K.; Kumar, A.; Sancheti, S. P.; Patil, N. T. Divergent Gold Catalysis: Unlocking Molecular Diversity through Catalyst Control. *Chem. Rev.* **2021**, *121*, 8478–8558.

the problem by using effective core potentials (ECPs) that are appropriately corrected. These will be discussed more in detail later.

Gold(I) Carbenes

Among the intermediates, or geometries, most altered by the covalency and ligand effects is the gold(I) carbene. Gold(I) carbenes exist in a continuum between a singly-bonded carbocation and a fully formed carbene. They show a strong π contribution in spite of the overall bond order and are particularly sensitive to the ligand electronics (Figure 1).[26]

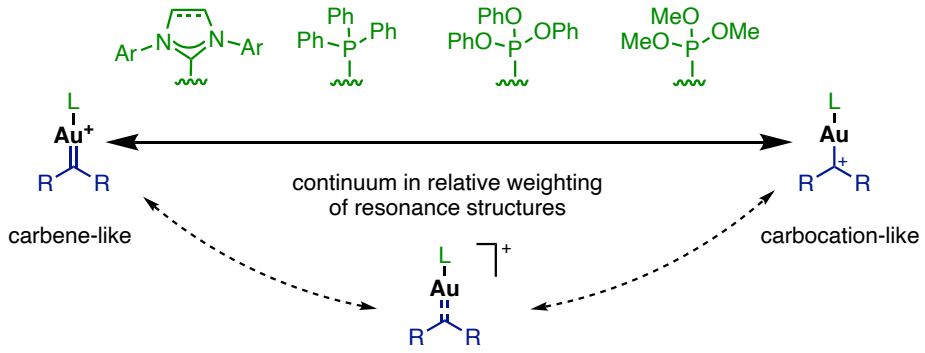

Figure 1. Ligand influence on the nature of gold(I) carbene complexes.

In order to account for this, Goddard and Toste proposed that the three-centre four-electron σ hyperbond between the two occupied ligand orbitals and the empty 6*s* orbital on gold(I) would include back-donation from the gold(I) onto any accessible empty ligand orbitals with π symmetry. When the latter was very significant, the σ bond would become more localised leading to what was described as a "double half-bond" arrangement, accounting for the bond order being smaller than 2 (Figure 2).[27]

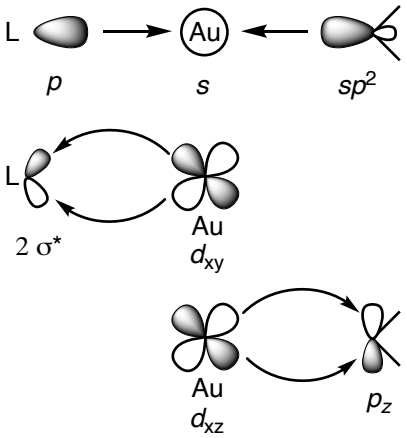

Figure 2. Metal-ligand bonding diagram for a model gold(I) carbene complex.

26 Wang, Y.; Muratore, M. E.; Echavarren, A. M. Gold Carbene or Carbenoid: Is There a Difference? *Chem. Eur. J.* **2015**, *21*, 7332–7339.

27 Benitez, D.; Shapiro, N. D.; Tkatchouk, E.; Wang, Y.; Goddard III, W. A.; Toste, F. D. A bonding model for gold(I) carbene complexes. *Nat. Chem.* **2009**, *1*, 482–486.

Far from being of purely conceptual interest, gold carbenes appear as intermediates in a wide range of catalytic processes involving gold(I). Upon initial outer-sphere nucleophilic attack to form a vinylgold, this intermediate shows nucleophilicity at the β carbon instead of the *ipso*-substitution driven by the high covalency and stability of the gold-carbon bond (Scheme 3). The formation of a gold carbene can therefore be achieved from alkynes and analogous π systems (such as cyclopropenes)[28] acting as synthons for dicarbenes.

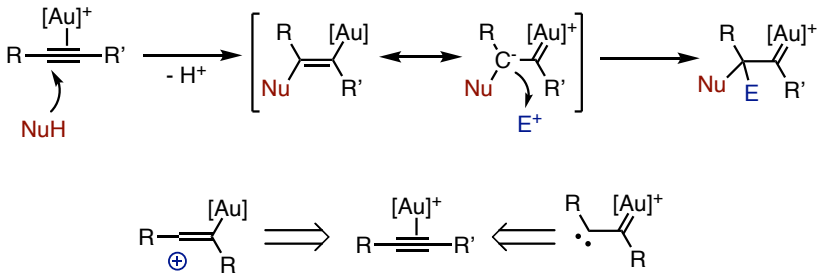

Scheme 3. Gold(I)-alkyne complexes as synthons for vinyl cations or dicarbenes.

When the nucleophile is an alkene, a carbocation is formed upon attacking the gold(I) alkyne complex. The resulting trapping of the carbocation with the nucleophilic β carbon, which generally happens in a concerted fashion, forms one of the most characteristic intermediates in gold(I) catalysis: the α-cyclopropylcarbene.[29] This intermediate is in resonance with the two derived homoallylic cations and consists of a gold-stabilised cyclopropylcarbinyl cation (Scheme 4).

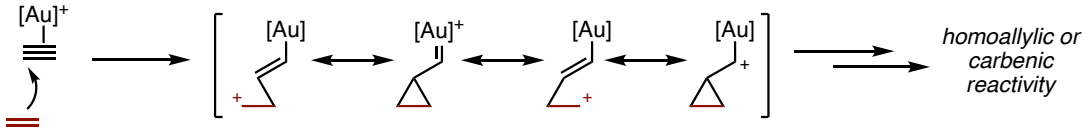

Scheme 4. Formation and resonance structures of a gold α-cyclopropylcarbene.

Gold(I)-Catalysed Enyne Cycloisomerisations

The use of alkenes for the outer-sphere nucleophilic attack on alkynes and the formation of the very versatile cyclopropylcarbene intermediates led to the development of several cycloisomerisations by carrying out the reaction intramolecularly. Tethered enynes react in the presence of cationic gold(I)

28 Bauer, J. T.; Hadfield, M. S.; Lee, A. L. Gold catalysed reactions with cyclopropenes. *Chem. Comm.* **2008**, *47*, 6405–6407.

29 Dorel, R.; Echavarren, A. M. Gold-Catalyzed Reactions via Cyclopropyl Gold Carbene-like Intermediates. *J. Org. Chem.* **2015**, *80*, 7321–7332.

complexes to form electrophilic structures that can be trapped with external or internal nucleophiles or rearrange to form a variety of new carbon skeletons.[30]

Perhaps, among all studied enynes, 1,6-enynes have been studied most in depth, not least because they can readily form two different gold(I) α-cyclopropylcarbene intermediates: 5-*exo*-dig cyclisation forms **2** and 6-*endo*-dig cyclisation forms **9** (Scheme 5). The bonding in these intermediates is usually highly dependent on the substitution patterns, with electron-donating groups on the alkene favouring the carbocationic form, often changing the reactivity.[31]

Each gold(I) α-cyclopropylcarbene can undergo a variety of processes (Scheme 5), including skeletal rearrangements, nucleophile attack and E1 or E2-like reactions (not shown). Skeletal rearrangements predominate for 5-*exo*-dig cyclisations as the main processes in the absence of a suitable nucleophile or base.[32] Single-cleavage rearrangements can lead to **3**, through exocyclic cleavage, and to **4**, through endocyclic cleavage. While the alkene is cleaved in both cases, **4** is unique in forming a six-membered ring through an initial 5-*exo*-dig cyclisation. Alternatively, **5** can be formed in a double-cleavage process which results, after 1,2-hydride shift, in **6**. The connectivity of this species shows cleavage of both the original alkyne and alkene.

Cyclobutenes can be formed in formal [2+2] reactions from both **2** and **9**. However, the former requires an isomerisation to a *syn*-cyclopropylcarbene by rotation about the carbon-carbon bond.[31] Direct 1,2-hydride shift from **9** forms vinylcyclopropane **11**.

In the presence of nucleophiles, several of these intermediates can be trapped. The most characteristic reactivity, and by far the most frequent, is the attack onto the cyclopropyl (or carbocationic) carbon atom, leading to products **7** and **12**. However, there have also been reports of direct attack onto the carbenic carbon yielding **8**.[33] With internal nucleophiles, polycyclic systems can also be formed in formal [4+2] reactions after proton shuttling.[34]

30 Nieto-Oberhuber, C.; Muñoz, M. P.; López, S.; Jiménez-Núñez, E.; Nevado, C.; Herrero-Gómez, E.; Raducan, M.; Echavarren, A. M. Gold(I)-Catalyzed Cyclizations of 1,6-Enynes: Alkoxycyclizations and Exo/Endo Skeletal Rearrangements. *Chem. - Eur. J.* **2006**, *12*, 1677– 1693,

31 Nieto-Oberhuber, C.; López, S.; Muñoz, M. P.; Cárdenas, D. J.; Buñuel, E.; Nevado, C.; Echavarren, A. M. Divergent Mechanisms for the Skeletal Rearrangement and [2+2] Cycloaddition of Enynes Catalyzed by Gold. *Angew. Chem. Int. Ed.* **2005**, *44*, 6146–6148.

32 Mattalia, J.-M.; Nava, P. Gold-Catalyzed Cycloisomerizations of 1,6-Enynes. A Computational Study. *J. Organomet. Chem.* **2014**, *749*, 335–342.

33 Amijs, C. H. M.; López-Carrillo, V.; Raducan, M.; Pérez-Galán, P.; Ferrer, C.; Echavarren, A. M. Gold(I)-Catalyzed Intermolecular Addition of Carbon Nucleophiles to 1,5- and 1,6-Enynes. *J. Org. Chem.* **2008**, *73*, 7721–7730.

34 Nieto-Oberhuber, C.; López, S.; Echavarren, A. M. Intramolecular [4 + 2] Cycloadditions of 1,3-Enynes or Arylalkynes with Alkenes with Highly Reactive Cationic Phosphine Au(I) Complexes. *J. Am. Chem. Soc.* **2005**, *127*, 6178–6179.

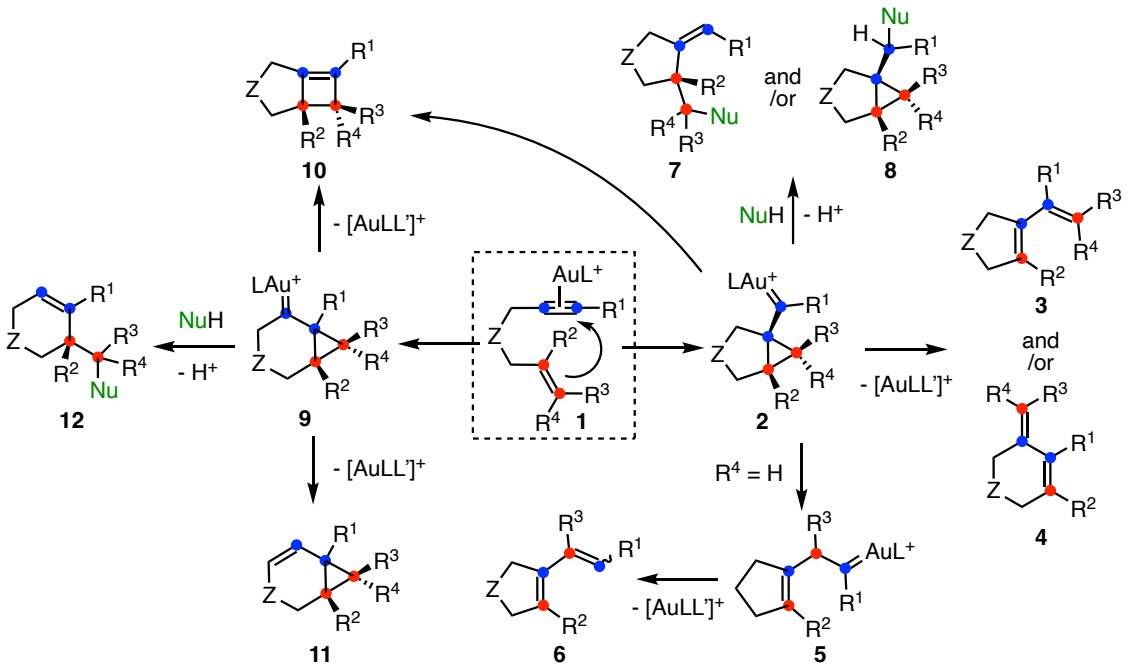

Scheme 5. Evolution of the gold cyclopropylcarbene derived from 1,6-enynes: pronucleophile trapping, single and double cleavage skeletal rearrangements. Elimination pathways are not shown.

Although the origins of selectivity skeletal rearrangements will be covered in more detail in **Chapter I**, the general picture shows that from common cyclopropylcarbene intermediates from 5-*exo*-dig (**2**) or 6-*endo*-dig (**9**) cyclisations, already three different nucleophile-trapped products (**7**, **8** and **12**) can be formed. In addition, the skeletal rearrangement processes and 1,2-hydride shifts lead to an immense array of structurally diverse products.[20] As harnessing this variation for synthetic purposes would be very valuable, this raises questions about the selectivity or specificity of these processes.

Although the formation of cyclobutenes such as **10** is generally substrate-dependent and are often outcompeted by 1,2-hydride shift or skeletal rearrangements, the intermolecular reaction between alkynes and alkenes to form cyclobutenes has been developed and there are recent reports of enantioselectivity.[35]

35 García-Morales, C.; Ranieri, B.; Escofet, I.; López-Suarez, L.; Obradors, C.; Konovalov, A. I.; Echavarren, A. M. Enantioselective Synthesis of Cyclobutenes by Intermolecular [2+2] Cycloaddition with Non-C_2 Symmetric Digold Catalysts. *J. Am. Chem. Soc.* **2017**, *139*, 13628–13631.

Through the Lens of Computational Chemistry

The advent of computation in chemistry revolutionised different fields introducing powerful tools that enabled molecular modelling to reproduced their behaviour or properties. Among the methodologies that were developed, quantum mechanical calculations were the most rigorous approaches to represent the electronic structure of complex molecules and thus became rapidly adopted in organometallic chemistry and catalysis.[36] However, more simplified models have been of paramount importance in other fields: molecular mechanics, relying on forcefields and thereby minimising computational cost,[37] and molecular dynamics, which is derived from the former and allows the calculation of motion and conformationally complex systems.[38] However, there was a problem with very large systems, unsuitable for QM calculations, with complex electronic or bonding patterns especially when including metals, preventing the full modelling of the system with molecular mechanics. The combination of quantum mechanics and molecular mechanics allowed the partition of these systems into QM and MM fragments, thereby allowing the calculation of a wide range of complex systems including very large catalysts among many other applications.[39]

Computational chemistry, through quantum mechanics, is capable of characterising the thermodynamic and kinetic stability of molecular systems and understanding the underlying electronic structure.

The electrons are modelled through basis functions that aim to reproduce the unknown molecular orbital wavefunction (or analogous unknown functions) with a set of known functions that approximate it.[40] The basis sets are therefore the groupings of such functions, which can be larger or smaller depending on how many functions they contain. Larger basis sets are more costly, computationally, whereas smaller basis sets are generally more inaccurate models. Despite the apparent incremental nature of basis sets thus described, this is an oversimplification: larger unbalanced basis sets that overrepresent some interactions can perform worse than smaller basis sets, to such an extent that they (incorrectly) predict benzene or other aromatic molecules to be non-planar.[41]

The main types of basis functions are Slater and Gaussian atomic orbitals, depending on the basic equation that models them. While both orbital models have a maximum value at a radius of zero, Slater

36 Ziegler, T.; Autschbach, J. Theoretical Methods of Potential Use for Studies of Inorganic Reaction Mechanisms. *Chem. Rev.* **2005**, *105*, 2695–2722.
37 Boeyens, J.; Comba, P. Molecular Mechanics: Theoretical Basis, Rules, Scope and Limits. *Coord. Chem. Rev.* **2001**, *212*, 3–10.
38 Wood, W. W.; Erpenbeck, J. J. Molecular Dynamics and Monte Carlo Calculations in Statistical Mechanics. *Annu. Rev. Phys. Chem.* **1976**, *27*, 319–348.
39 Maseras, F.; Morokuma, K. IMOMM: A New Integrated ab Initio + Molecular Mechanics Geometry Optimization Scheme of Equilibrium Structures and Transition States. *J. Comput. Chem.* **1995**, *16*, 1170–1179.
40 Cuevas, G.; Cortés, F. *Introducción a la Química Computacional*, 1st ed.; Sociedad Mexicana de Física: México DF, 2003, 60–72.
41 Moran, D.; Simmonett, A. C.; Leach, F. E.; Allen, W. D.; Schleyer, P. V. R.; Schaefer, H. F. Popular Theoretical Methods Predict Benzene and Arenes To Be Nonplanar. *J. Am. Chem. Soc.* **2006**, *128*, 9342–9343.

orbitals have a non-zero first derivative at that radius and show exponential decrease, whereas Gaussian orbitals have a derivative of zero.[42] Slater orbitals generally are more representative of the real systems especially at longer distances; however, Gaussian orbitals allow easier treatment of two-electron integrals, explaining their much more widespread use. Combinations thereof can approximate Slater functions while allowing easier calculations.[40]

As valence orbitals are the most important orbitals in most quantum chemical applications, increasing the basis set size by duplicating all basis functions is not generally required: those related to the core orbitals can be excluded. Such partitions are known as split-valence basis sets in which valence orbitals are represented with a greater number of basis functions.

For larger atoms, even this is impractical due to the large number of electrons involved, and a solution is to include effective core potentials (ECPs), which account for the core electrons of an atom (defined as small core or large core) without calculating these explicitly.[43] They have been of particular importance in the modelling of inorganic and organometallic systems.

As ECPs account for the most tightly bound orbitals, they can represent relativistic effects very well without adding any computational cost. As discussed earlier, this is of utmost importance for gold atoms and the modelling of catalytic cycles including gold. For very specific applications, such as NMR prediction or Mössbauer spectroscopy, the core electrons have to be explicitly modelled. A high accuracy is often required, making split-valence basis sets also less useful and potentially driving the computational cost to impractical levels. Relativistic basis sets have since been developed for these purposes, which account for the electronic changes upon relativistic treatment and can be applied with several *ab initio* methods.[44]

However, explicitly solving the required equations using these basis sets, including not only the Schrödinger equation but several related ones, is unfeasible in most cases and impossible for larger systems. Devising novel approaches to solve these approximately has been of utmost importance throughout the development of computational chemistry, especially when applied to larger systems or materials.[45]

The families of *ab initio* methods approach the solution of the wavefunction itself, therefore approximating QM equations in different ways to approach the Schrödinger equation. The original Hartree-Fock method did not result in great accuracy, whereas newer approaches including coupled-cluster (CC) methods was found as a way to tackle the many-electron correlation problem. The latter

42 Cramer, C. J. *Essentials of Computational Chemistry – Theories and Models*, 2nd ed.; John Wiley & Sons: Chichester, 2004.
43 Russo, T. V.; Martin, R. L.; Hay, P. J. Effective Core Potentials for DFT Calculations. *J. Phys. Chem.* **1995**, *99*, 17085–17087.
44 Pantazis, D. A.; Chen, X.-Y.; Landis, C. R.; Neese, F. All-Electron Scalar Relativistic Basis Sets for Third-Row Transition Metal Atoms. *J. Chem. Theory Comput.* **2008**, *4*, 908–919.
45 Marzari, N. The Frontiers and the Challenges. *Nat. Mater.* **2016**, *15*, 381–382.

have been extensively used for the accurate calculation of very small systems (due to their higher computational cost) and, in the case of non-iterative variants such as CCSD(T), also medium-sized systems;[46] however, even these show problems with potential energy surfaces due to the failure of the many-body perturbation theory.[47] Among the QM methods, and in spite of the challenges with solvation or multireference systems, *ab initio* methods have performed best, even if their computational cost limits their use to small systems.

Among the most important approaches was the development of density functional theory (DFT). The conceptual framework was constructed in 1964 by Hohenberg and Kohn, which proved that there is a universal functional dependent on the electron density of a system from which the energy of the system can be obtained, thus circumventing the problems associated to solving QM equations directly and using electron density instead.[48] In the original publication, Hohenberg and Kohn also showed that the functional could be expressed in terms of electron correlation and electronic polarisability.

As the most simplified alternative, semiempirical methods use many approximations, including parametrised integrations, which severely limit their application in very complex systems. However, their much lower computational cost and, in many instances, adequate results when the systems have been correctly parametrised have made semiempirical methods very attractive.[49] There is a strong dependence on parametrisation and, therefore, on using quality experimental data for reference. In spite of these drawbacks, current improvements in general parametrisations (and those tailored to specific applications or systems) make semiempirical methods very efficient QM methods, giving worse results than DFT but being several orders of magnitude faster.

Since their invention, DFT methods have evolved, not only with the creation of time-dependent DFT allowing for excited state calculations,[50] but with several changes to the functionals used by changing their parametrisations against a reference. As opposed to *ab initio* methods, there are no trivial ways of determining how good a particular exchange-correlation functional is, nor whether it approaches the form of the real functional, beyond comparing the results against properly validated experimental or computational benchmarks.[51] This has led to an inevitable proliferation of general exchange-correlation functionals as well as others envisioned for specific purposes.

46 Piecuch, P.; Kowalski, K.; Pimienta, I. S. O.; Mcguire, M. J. Recent Advances in Electronic Structure Theory: Method of Moments of Coupled-Cluster Equations and Renormalized Coupled-Cluster Approaches. *Int. Rev. Phys. Chem.* **2002**, *21*, 527–655.

47 The many-body perturbation theory does not converge for large internuclear separations, see Paldus, J.; Li, X.; A Critical Assessment of the Coupled Cluster Method in Quantum Chemistry, *Advances in Chemical Physics*, **1999**, *110*, 1–176.

48 Hohenberg, P.; Kohn, W. Inhomogeneous Electron Gas. *Phys. Rev.* **1964**, *136*, B864–B871.

49 Thiel, W. Semiempirical Quantum–Chemical Methods. *WIREs Comput Mol Sci* **2014**, *4*, 145–157.

50 Runge, E.; Gross, E. K. U. Density-Functional Theory for Time-Dependent Systems. *Phys. Rev. Lett.* **1984**, *52*, 997–1000.

51 Iron, M. A.; Janes, T. Evaluating Transition Metal Barrier Heights with the Latest Density Functional Theory Exchange–Correlation Functionals: The MOBH35 Benchmark Database *J. Phys. Chem.* **2019**, *123*, 3761–3781.

The attempts to judge the relative quality of functionals resulted in the often-mentioned Jacob's ladder (as applied to DFT), which ranks different functionals proportionally to their representation of the electronic systems and, therefore, also indirectly ranks their approximate computational cost.[52] The ladder shows, at the lowest level of chemical accuracy, the local density approximation (LDA) functionals, such as the Slater functional with the Vosko-Wilk-Nusair correlation functional.

Gradient-corrected methods are a step higher, with generalised gradient approximation (GGA) functionals being used in very common combinations of exchange and correlation functionals. These include examples such as BP86, from Becke's 1988 exchange functional[53] and Perdew's 1986 correlation functional, or MPWPW91, with the modified Perdew and Wang exchange functional[54] and Perdew and Wang's 1991 correlation functional.[55]

Hybrid functionals are characterised by the combined use of exchange and correlation functionals with exact Hartree-Fock exchange energy, modulated by a set of coefficients. These include some of the most frequently used functionals, such as B3LYP, which was conceived from Becke's exchange functional[53] and Lee-Yang-Parr correlation functional,[56] but includes the local spin density approximation and the Hartree-Fock exchange energy. Each of these parameters is scaled by a coefficient, which were fitted to a set of experimental data.[57]

In transition metal catalysis, the field that concerns the work in this manuscript, DFT methods, as a compromise between accuracy and computational cost, have been critical in providing mechanistic information on a variety of processes. The often elusive nature of reactive intermediates, the intricate interspecies correlations in measurable kinetics greatly hinder the study of some organometallic processes or the near-indistinguishable nature of non-rate-determining steps in the catalytic cycle (such as the specific pathway for a C-H activation). These can all be modelled by DFT methods to provide greater insight or even pave the way to their experimental identification.[58] However, DFT methods are not exempt from pitfalls or problems: the degree of accuracy required for correct mechanistic determinations, the comprehensive modelling of the conformational landscape and the exceedingly

52 Perdew, J. P. Jacob's Ladder of Density Functional Approximations for the Exchange-Correlation Energy. In *AIP Conference Proceedings*; AIP: Antwerp (Belgium), 2001; Vol. 577, pp 1–20.
53 Becke, A. D. Density-functional exchange-energy approximation with correct asymptotic behavior. *Phys. Rev. A* **1988**, *38*, 3098–3100.
54 Adamo, C.; Barone, V. Exchange functionals with improved long-range behavior and adiabatic connection methods without adjustable parameters: The *m*PW and *m*PW1PW models. *J. Chem. Phys.* **1998**, *108*, 664–675.
55 Perdew, J. P.; Wang, Y. Accurate and simple analytic representation of the electron-gas correlation energy. *Phys. Rev. B* **1992**, *45*, 13244–13249.
56 Lee, C.; Yang, W.; Parr, R. G.; Development of the Colle-Salvetti correlation-energy formula into a functional of the electron density. *Phys. Rev. B.* **1988***, 37*, 785–789.
57 Becke, A. D. Density-functional thermochemistry. III. The role of exact Exchange. *J. Chem. Phys*. **1993**, *98*, 5648–5652.
58 Sameera, W. M. C.; Maseras, F. Transition Metal Catalysis by Density Functional Theory and Density Functional Theory/Molecular Mechanics. *WIREs Comput Mol Sci* **2012**, *2*, 375–385.

small errors required to predict enantioselectivity are very important challenges.[59,60] Due to the complementarity of most of these approaches, experimental and computational insight can be used together very successfully in analysing mechanistic puzzles.

Over time, DFT has emerged as a tool not only to reproduce experimental results but to predict previously unexplored systems and rationally design new ligands, reactions or physicochemical properties.[61] The importance of the predictive power that modern computational chemistry methods have recently encountered is clear from the widespread adoption thereof in many different applications.[62,63,64,65]

A computational exploration into gold(I) catalysis, as with most calculations to gain mechanistic insight, requires a high degree of accuracy in the calculated energies. In addition, the bonding in most of the reactive intermediates is not well-defined by the Lewis structures,[66] which together with the required accuracy severely limits the application of molecular mechanics models, as QM calculations would be needed to describe the bonding. The exceptions would be mixed QM/MM methods such as ONIOM, if a large section of the calculated molecules only have steric effects, or preliminary molecular dynamics simulations to search conformational space.[67,68]

Furthermore, real systems can be relatively large and so *ab initio* calculations become impractical in the majority of cases, although simplified models can be used as benchmarks.[69]

For these reasons, DFT becomes the method of choice in the calculation of gold(I)-catalysed reactions. Nonetheless, there are several additional factors in these reactions that have to be accounted for in order to represent the systems accurately and minimise the sources of error. In addition to the previously

59 Torrent, M., Solà, M.; Frenking, G. Theoretical studies of some transition-metal-mediated reactions of industrial and synthetic importance. *Chem. Rev.* **2000**, *100*, 439–493.
60 Besora, M.; Braga, A. A. C.; Ujaque, G.; Maseras, F.; Lledós, A. The importance of conformational search: a test case on the catalytic cycle of the Suzuki–Miyaura cross-coupling. *Theor. Chem. Acc.* **2011**, *128*, 639–646.
61 Houk, K. N.; Cheong, P. H.-Y. Computational prediction of small-molecule catalysts. *Nature* **2008**, *455*, 309–313.
62 Fan, W.; Duan, Z.; Liu, W.; Mehmood, R.; Qu, J.; Cao, Y.; Guo, X.; Zhong, J.; Zhang, F. Rational Design of Heterogenized Molecular Phthalocyanine Hybrid Single-Atom Electrocatalyst towards Two-Electron Oxygen Reduction. *Nat. Commun.* **2023**, *14*, 1426.
63 Wang, J.; Xu, H.; Che, C.; Zhu, J.; Cheng, D. Rational Design of PdAg Catalysts for Acetylene Selective Hydrogenation via Structural Descriptor-Based Screening Strategy. *ACS Catal.* **2023**, *13*, 433–444.
64 Demissie, T. B.; Ruud, K.; Hansen, J. H. DFT as a Powerful Predictive Tool in Photoredox Catalysis: Redox Potentials and Mechanistic Analysis. *Organometallics* **2015**, *34*, 4218–4228.
65 Tolbatov, I.; Marrone, A.; Coletti, C.; Re, N. Computational Studies of Au(I) and Au(III) Anticancer Metallodrugs: A Survey. *Molecules* **2021**, *26*, 7600.
66 Fürstner, A.; Morency, L. On the Nature of the Reactive Intermediates in Gold-Catalyzed Cycloisomerization Reactions. *Angew. Chem. Int. Ed.* **2008**, *47*, 5030–5033.
67 Martín-Rodríguez, M.; Nájera, C.; Sansano, J. M.; de Cózar, A.; Cossío, F. P. Binap-Gold(I) versus Binap-Silver Trifluoroacetate Complexes as Catalysts in 1,3-Dipolar Cycloadditions of Azomethine Ylides. *Chem. Eur. J.* **2011**, *17*, 14224–14233.
68 Rao, W.; Koh, M. J.; Li, D.; Hirao, H.; Chan, P. W. H. Gold-Catalyzed Cycloisomerization of 1,6-Diyne Carbonates and Esters to 2,4a-Dihydro-1 *H* -Fluorenes. *J. Am. Chem. Soc.* **2013**, *135*, 7926–7932.
69 Dohm, S.; Hansen, A.; Steinmetz, M.; Grimme, S.; Checinski, M. P. Comprehensive Thermochemical Benchmark Set of Realistic Closed-Shell Metal Organic Reactions. *J. Chem. Theory Comput.* **2018**, *14*, 2596–2608.

described relativistic effects, which can be solved by the inclusion of effective core potentials, the accurate energy determinations in catalytic cycles requires some corrections to be applied.

The first observation is that most reactions catalysed by gold(I) complexes involve cationic or charge-separated intermediates and transition states. The stabilisation of such species in solution is very different to that in vacuum. As DFT calculations are generally performed in the gas phase, ion pairs under such conditions tend to experience much stronger net attraction than what would otherwise be found for the system. The outcomes of such calculations result in divergent geometries, an increase in the energy cost of charge separation and more secondary consequences. For this reason, the inclusion of implicit solvation in these systems is recommended, as it minimises the consequences of dipolar or multipolar stabilisation of charges.[70] Explicit solvation modelling, in which a number of solvent molecules are calculated together with the system of interest, is much more costly and only recommended when the solvent plays a key role in the stabilisation of a structure through a specific interaction.

The polarisable continuum model (PCM) is one of the most common implicit solvation models, in which a cage at a set distance around the molecule is treated as a continuous surface that can be polarised -developing apparent surface charges- depending on the solvent's dielectric constant and the electronics of the modelled molecule. While it greatly simplifies to solvation to the dielectric constant, it performs well except for systems in which strong directional solute-solvent interactions are expected.[71] There are a number of variants of this model including CPCM (the conductor-like polarisable continuum model).

Another early model was the conductor-like screening model (COSMO), which like CPCM considers the environment to be conductor-like to adopt approximations in the treatment of polarisation. However, this model requires correct parametrisation for treatment of the solvent-accessible surface.[72]

The solvent model based on density (SMD) was devised in 2009 by Truhlar and coworkers and includes several more parameters than PCM: two based on hydrogen bond donor and acceptor capabilities, one based on atomic surface tension, and two on aromatic and halogen components.[73] This model, also very frequently used, is proposed to be more adequate for solvents with more directional or localised interactions.

These solvation models generally perform adequately for most systems, with the greatest differences being more whether any implicit solvation models were used at all rather than the specific model chosen.

---

70 Bursch, M.; Mewes, J.; Hansen, A.; Grimme, S. Best-Practice DFT Protocols for Basic Molecular Computational Chemistry**. *Angew Chem Int Ed* **2022**, *61*, e202205735.

71 Klein, R. A.; Mennucci, B.; Tomasi, J. Ab Initio Calculations of ^{17} O NMR-Chemical Shifts for Water. The Limits of PCM Theory and the Role of Hydrogen-Bond Geometry and Cooperativity. *J. Phys. Chem. A* **2004**, *108*, 5851–5863.

72 Klamt, A.; Schüürmann, G. COSMO: A New Approach to Dielectric Screening in Solvents with Explicit Expressions for the Screening Energy and Its Gradient. *J. Chem. Soc., Perkin Trans. 2* **1993**, *5*, 799–805.

73 Marenich, A. V.; Cramer, C. J.; Truhlar, D. G. Universal Solvation Model Based on Solute Electron Density and on a Continuum Model of the Solvent Defined by the Bulk Dielectric Constant and Atomic Surface Tensions. *J. Phys. Chem. B* **2009**, *113*, 6378–6396.

However, time-dependent DFT calculations for photoexcitation are more sensitive to the implicit or explicit model, due to the relative importance of non-equilibrium solvation shells especially with compounds with large Stokes shifts.[74] The problems in such systems are overcome by the use of combined explicit and implicit solvation models, where necessary, as well as using corrected Linear Response or State-Specific models for emission instead of the more common Linear Response model, which performs well for absorption due to the full applicability of the Franck-Condon principle.

Dispersion interactions are poorly modelled with DFT methods, with weak supramolecular interactions particularly affected. This deficiency can lead to inaccurate predictions of molecular structures or energies in systems where dispersion forces play a crucial role. There have been several approaches to palliate this in DFT, with meta-GGA functionals, dispersion corrections, or the inclusion of long-range correlation in the DFT methods.[75] Among these, dispersion correction has been one of the most extensively used, due to their good performance in organic systems. Dispersion-corrected DFT has been successfully applied even to complex cases such as the van der Waals binding of dimers with errors associated more with implicit solvation than with the dispersion modelling.[76]

Grimme and coworkers derived a series of empirical dispersion corrections for all elements with stable isotopes, parametrised based on several calculable magnitudes using the Casimir-Polder formula, but requiring readjustment for different functionals.[77] However, as a rule, many organometallic systems are not perfectly parametrised with dispersion corrections due to the existence of very different oxidation states or electronic structures (with the dispersion corrections usually modelled on a neutral atom).[75] The inclusion of dispersion in such systems is generally preferred, as any problems with parametrisation are minor compared to the exclusion of dispersion.

The outlook of computational chemistry is that of a more predictive nature, as well as aiming to solve problems such as automated conformer searches, protein folding, inorganic retrosynthesis or multi-reference states in metal complexes. The advent of artificial intelligence in computational chemistry, though still in a rather early stage, is bound to allow novel approaches to these challenges if only due to large-scale data analysis and automated data fitting.[78]

74 Chibani, S.; Jacquemin, D.; Laurent, A. D. Modelling Solvent Effects on the Absorption and Emission Spectra of Constrained Cyanines with Both Implicit and Explicit QM/EFP Models. *Comp. Theor. Chem.* **2014**, *1040–1041*, 321–327.

75 Johnson, E. R.; Mackie, I. D.; DiLabio, G. A. Dispersion Interactions in Density-Functional Theory. *J. Phys. Org. Chem.* **2009**, *22*, 1127–1135.

76 Antony, J.; Sure, R.; Grimme, S. Using dispersion-corrected density functional theory to understand supramolecular binding thermodynamics. *Chem. Comm.* **2015**, *51*, 1764–1774.

77 Grimme, S.; Antony, J.; Ehrlich, S.; Krieg, H. A consistent and accurate ab initio parametrization of density functional dispersion correction (DFT-D) for the 94 elements H-Pu. *J. Chem. Phys.* **2010**, *132*, 154104.

78 Huang, B.; Von Rudorff, G. F.; Von Lilienfeld, O. A. The Central Role of Density Functional Theory in the AI Age. *Science* **2023**, *381*, 170–175.

Chapter I

Towards a Complete Mechanistic Understanding of Enyne Rearrangements

Introduction

Skeletal Rearrangements in Enyne Cycloisomerisations

As explained in the **General Introduction**, gold(I) catalysis experienced a great development in reactions involving the activation of alkynes.[1] In particular, cycloisomerisation reactions have been prolific, allowing the construction of new ring systems from linear unsaturated substrates. These transformations include those in which an external nucleophile traps the cationic intermediates, leading to the development of formal [4+2] reactions, alkoxycyclisations and aminocyclisations.[2,3] As a subset of these processes, enyne skeletal rearrangements are particularly interesting processes, in which cleavage of the substrate alkene or the alkyne can lead to new ring structures with different connectivity.[4]

One of the main appeals of such processes is that, as the exocyclic or endocyclic bond can be cleaved (single cleavage), or both the exocyclic and the bond α to the gold centre (double cleavage), a large variety of products with different structures can be accessed (Scheme 1a).[5] In this way, a model enyne **1.1** can cyclise to form gold(I) α-cyclopropylcarbene **1.2**, which is the common intermediate in any of three ulterior rearrangements leading to 1,3 dienes **1.3** (exocyclic), **1.4** (endocyclic) or **1.6** (exocyclic double cleavage). The latter is reached from vinylcarbene **1.5**, itself a product of formal insertion into the carbon-carbon bond.[6,7,8]

1 Hashmi, A. S. K. Homogeneous gold catalysts and alkynes: A successful liaison. *Gold Bull*. **2003**, 36, 3–9.
2 Obradors, C.; Echavarren, A. M. Gold-Catalyzed Rearrangements and Beyond. *Acc. Chem. Res.* **2014**, *47*, 902–912.
3 For a review on these processes and the scope of these transformations, see Dorel, R.; Echavarren, A. M. Gold(I)-Catalyzed Activation of Alkynes for the Construction of Molecular Complexity. *Chem. Rev.* **2015**, *115*, 9028–9072.
4 Jiménez-Núñez, E.; Echavarren, A. M. Gold-Catalyzed Cycloisomerizations of Enynes: A Mechanistic Perspective. *Chem. Rev.* **2008**, *108*, 3326–3350.
5 Nieto-Oberhuber, C.; Muñoz, M. P.; López, S.; Jiménez-Núñez, E.; Nevado, C.; Herrero-Gómez, E.; Raducan, M.; Echavarren, A. M. Gold(I)-Catalyzed Cyclizations of 1,6-Enynes: Alkoxycyclizations and Exo/Endo Skeletal Rearrangements. *Chem. Eur. J.* **2006**, *12*, 1677–1693.
6 Ferrer, C.; Raducan, M.; Nevado, C.; Claverie, C. K.; Echavarren, A. M. Missing Cyclization Pathways and New Rearrangements Unveiled in the Gold(I) and Platinum(II)-Catalyzed Cyclization of 1,6-Enynes. *Tetrahedron* **2007**, *63*, 6306–6316.
7 Cabello, N.; Jiménez-Núñez, E.; Buñuel, E.; Cárdenas, D. J.; Echavarren, A. M. On the Mechanism of the Puzzling "Endocyclic" Skeletal Rearrangement of 1,6-Enynes. *Eur. J. Org. Chem.* **2007**, 4217–4223.
8 Soriano, E.; Marco-Contelles, J. Mechanistic Insights on the Cycloisomerization of Polyunsaturated Precursors Catalyzed by Platinum and Gold Complexes. *Acc. Chem. Res.* **2009**, *42*, 1026–1036.

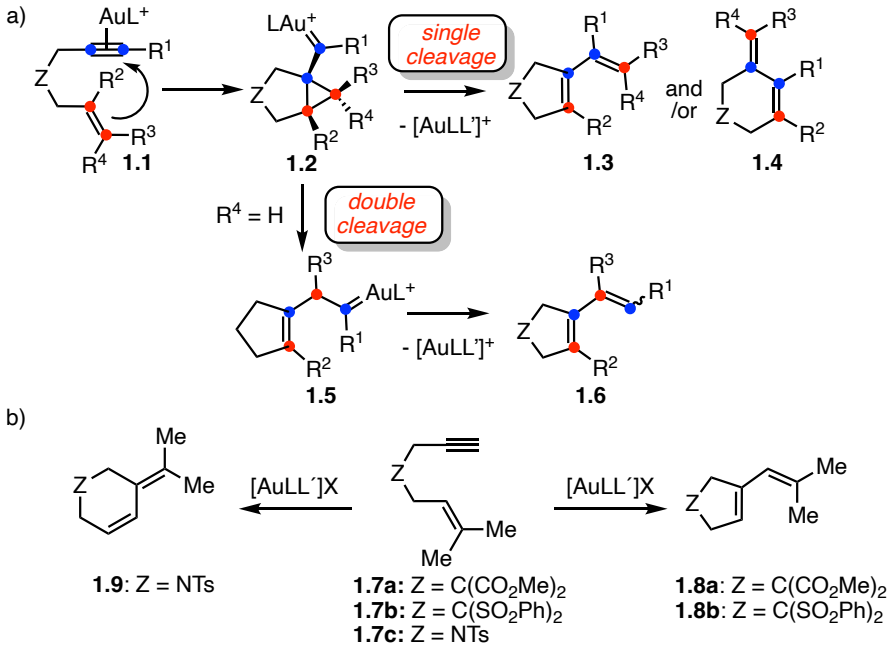

Scheme 1. a) Skeletal rearrangement of 1,6-enynes: single and double cleavage b) Exocyclic and endocyclic cleavages depend on the enyne tether.

In spite of the seemingly complex array of pathways from intermediate **1.2**, certain substitution patterns on the substrates lead to strong preferences for specific mechanisms. This greatly simplifies the reaction outcomes and what would otherwise be anticipated to afford complex low-yielding mixtures often form a single product selectively.[9] The primary factor affecting the exocyclic or endocyclic cleavage is the tether on the enyne, with toluenesulfonamides favouring the endocyclic cleavage product **1.9** and both malonate or sulfone tethers favouring the exocyclic cleavage products **1.8a** and **1.8b**. Conversely, an internal alkyne, when the alkene has a terminal methylene group, generally undergo double cleavage forming diene **1.6** as the only product. In these examples, the products are all isolated in excellent yields and no mixtures are observed (Scheme 1b).[5,7]

Many other metals have been explored in similar transformations, with most of them known to form enyne metathesis or skeletal rearrangement products before the first reports of this reactivity with gold(I) catalysis. In 1994, Chatani et al reported a ruthenium-catalysed rearrangement that showed *E*-stereoconvergence, with product dienes containing *E*-alkenes regardless of the stereochemistry on the starting material (Scheme 2).[10]

9 Nieto-Oberhuber, C.; Muñoz, M. P.; Buñuel, E.; Nevado, C.; Cárdenas, D. J.; Echavarren, A. M. Cationic Gold(I) Complexes: Highly Alkynophylic Catalysts for the Exo- and Endo-Cyclization of Enynes. *Angew. Chem. Int. Ed.* **2004**, *43*, 2402–2406.

10 Chatani, N.; Morimoto, T.; Muto, T.; Murai, S. Highly Selective Skeletal Reorganization of 1,6- and 1,7-Enynes to 1-Vinylcycloalkenes Catalyzed by $RuCH_2(CO)_3$ *J. Am. Chem. Soc.* **1994**, *116*, 6049–6050.

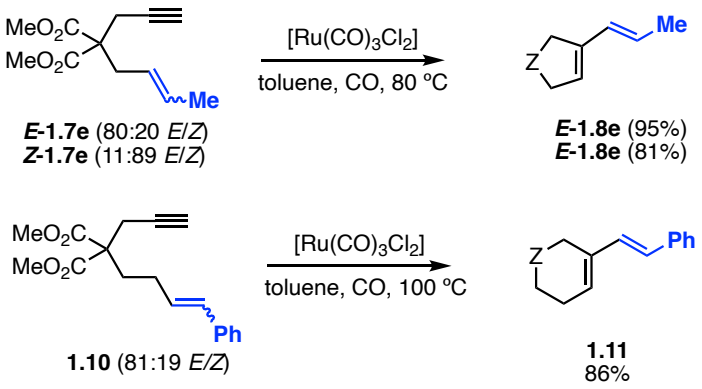

Scheme 2. Ruthenium(II) catalysis affords *E*-selective skeletal rearrangements of 1,6- and 1,7-enynes.

Later reports with platinum catalysis showed the first examples of what would later be known as double-cleavage rearrangements,[11] found strong dependence on small changes on the substrate,[12] and brought mechanistic understanding into these processes.[13] Analogous reactivities were then found for rhodium(II)[14] and iridium(I) complexes.[15] Both showed stereoconvergence to the *E*-isomers like in the ruthenium-catalysed reactions.

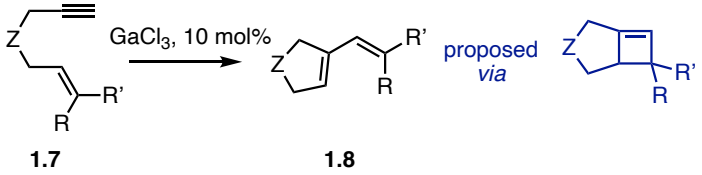

Scheme 3. Gallium(III) chloride-catalysed skeletal rearrangement of 1,*n*-enynes.

In addition, group 13 metals have been also reported to catalyse the same transformations. The skeletal rearrangement mediated by gallium trichloride was proposed to occur via cyclobutene intermediates, albeit without any specific experimental evidence (Scheme 3).[16] Indium(III) catalysts, which have since grown in importance in the activation of π systems,[17] were also found to efficiently catalyse the transformation.[18] Uniquely, the double cleavage reactions with this catalyst led exclusively to the skipped dienes. Extensive calculations later found the reason for the 1,4-diene selectivity, stemming

11 Chatani, N.; Furukawa, N.; Sakurai, H.; Murai, S. $PtCl_2$-Catalyzed Conversion of 1,6- and 1,7-Enynes to 1-Vinylcycloalkenes. Anomalous Bond Connection in Skeletal Reorganization of Enynes. *Organometallics* **1996**, *15*, 901–903.

12 Fürstner, A.; Szillat, H.; Stelzer, F. Novel Rearrangements of Enynes Catalyzed by $PtCl_2$. *J. Am. Chem. Soc.* **2000**, *122*, 6785–6786.

13 Oi, S.; Tsukamoto, I.; Miyano, S.; Inoue, Y. Cationic Platinum-Complex-Catalyzed Skeletal Reorganization of Enynes. *Organometallics* **2001**, *20*, 3704–3709.

14 Ota, K.; Lee, S. I.; Tang, J.-M.; Takachi, M.; Nakai, H.; Morimoto, T.; Sakurai, H.; Kataoka, K.; Chatani, N. Rh(II)-Catalyzed Skeletal Reorganization of 1,6- and 1,7-Enynes through Electrophilic Activation of Alkynes. *J. Am. Chem. Soc.* **2001**, *131*, 15203–15211.

15 Inoue, H.; Morimoto, T.; Muto, T.; Murai, S.; Chatani, N. Iridium(I)-Catalyzed Cycloisomerization of Enynes. *J. Org. Chem.* **2001**, *66*, 4433–4436.

16 Chatani, N.; Inoue, H.; Kotsuma, T., Murai, S. Skeletal Reorganization of Enynes to 1-Vinylcycloalkanes. *J. Am. Chem. Soc.* **2002**, *124*, 10294–10295.

17 Pérez Sestelo, J.; Sarandeses, L. A.; Martínez, M. M.; Alonso-Marañón, L. Indium(III) as π-Acid Catalyst for the Electrophilic Activation of Carbon–Carbon Unsaturated Systems. *Org. Biomol. Chem.* **2018**, *16*, 5733–5747.

18 Miyanohana, Y.; Chatani, N. Skeletal Reorganization of Enynes Catalyzed by $InCl_3$. *Org. Lett.* **2006**, *8*, 2155–2158.

from the coordination of active $[InCl_2]^+$ fragment to the alkene, disfavouring the formation of an allyl cation intermediate and facilitating the migration.[19] Finally, Yu and coworkers' work brought forward a coherent framework to understand exocyclic and endocyclic single cleavage, as well as double cleavage, rearrangements catalysed by indium(III) salts.[20]

However, and as stated earlier, one of the most interesting yet poorly understood phenomena is how the outcome of these skeletal rearrangements was found to shift completely across all metals with superficially unimportant changes in the starting materials, with different solvents or modifications on the catalyst.[21,22,23] In particular, the reasons for the changes have remained unclear. These can be summarised in why a particular set of modifications only allows a different pathway, or perhaps more importantly, how a substrate can be modified to ensure it undergoes only one specific skeletal rearrangement.

Within the exocyclic cleavage rearrangements, the majority of reactions are known to be stereospecific, with the diene stereochemistry dictated by the original alkene isomer (Scheme 4a).[8] However, and as mentioned previously, the systems can lead to the thermodynamic product in the ruthenium-, rhodium- or iridium-catalysed reactions. All of these afford *E*-dienes and were generally rationalised on the thermodynamic stability of the products.

19 Zhuo, L.-G.; Zhang, J.-J.; Yu, Z.-X. DFT and Experimental Exploration of the Mechanism of $InCl_3$ -Catalyzed Type II Cycloisomerization of 1,6-Enynes: Identifying $InCl_2^+$ as the Catalytic Species and Answering Why Nonconjugated Dienes Are Generated. *J. Org. Chem.* **2012**, *77*, 8527–8540.

20 Zhuo, L.-G.; Zhang, J.-J.; Yu, Z.-X. Mechanisms of the $InCl_3$-Catalyzed Type-I, II, and III Cycloisomerizations of 1,6-Enynes. *J. Org. Chem.* **2014**, *79*, 3809–3820.

21 Kim, N.; Brooner, R. E. M.; Widenhoefer, R. A. Unexpected Skeletal Rearrangement in the Gold(I)/Silver(I)-Catalyzed Conversion of 7-Aryl-1,6-Enynes to Bicyclo[3.2.0]Hept-6-Enes via Hidden Brønsted Acid Catalysis. *Organometallics* **2017**, *36*, 673–678.

22 Gagosz, F. Unusual Gold(I)-Catalyzed Isomerization of 3-Hydroxylated 1,5-Enynes: Highly Substrate-Dependent Reaction Manifolds. *Org. Lett.* **2005**, *7*, 4129–4132.

23 Chen, G.-Q.; Fang, W.; Wei, Y.; Tang, X.-Y.; Shi, M. Divergent Reaction Pathways in Gold-Catalyzed Cycloisomerization of 1,5-Enynes Containing a Cyclopropane Ring: Dramatic Ortho Substituent and Temperature Effects. *Chem. Sci.* **2016**, *7*, 4318–4328.

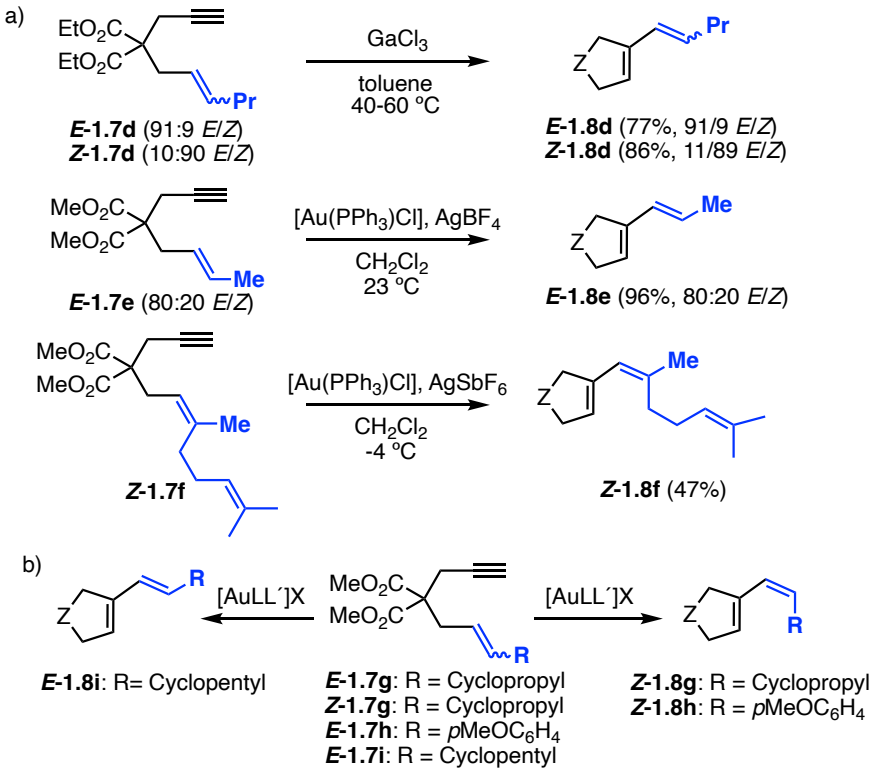

Scheme 4. a) Stereospecific single cleavage skeletal rearrangements. b) Gold(I)-catalysed *Z*-selective exocyclic single cleavage skeletal rearrangement and stereospecific counterpart.

Nevertheless, the discovery of *Z*-selective skeletal rearrangements, unexpectedly leading to a thermodynamically less favourable product, showed that stereoconvergence could favour this isomer too in spite of containing a *Z*-alkene (Scheme 4b).[24] Even though most 1,6-enynes form stereospecific products when subjected to gold(I) catalysis, sufficiently electron-rich examples like *p*-methoxyphenyl or cyclopropyl would lead to close to full stereoconvergence to the *Z*-products in good to excellent yields. The stereoconvergence was confirmed not to be a case of stereoinversion through the cycloisomerisation of substrate ***Z*-1.7g**, which led to the same product as its *E* counterpart. While some sort of interconversion pathway was proposed as the most plausible explanation for this behaviour, no explicit mechanism was found for this. The preliminary substrate scope showed that the same phenomenon extended to all very electron-rich substituents on a malonate-tethered 1,6-enyne.

24 Jiménez-Núñez, E.; Claverie, C. K.; Bour, C.; Cárdenas, D. J.; Echavarren, A. M. Cis-Selective Single-Cleavage Skeletal Rearrangement of 1,6-Enynes Reveals the Multifaceted Character of the Intermediates in Metal-Catalyzed Cycloisomerizations. *Angew. Chem. Int. Ed.* **2008**, *47*, 7892–7895.

Allenene Cycloisomerisations

Allenes, containing a single *sp*-hybridised carbon, are also amenable to activation by gold(I) complexes. However, compared to the chemistry of enynes, they have been comparatively less explored and understood, both experimentally and computationally. The main pattern observed in the activation of allenes corresponds to the reactivity on the external sp^2 carbons, which develop a partial positive charge upon coordination to the metal.[25] However, the understanding of the coordination to gold(I) is not trivial and has been analysed, with three coordination isomers known to be present for different substitution patterns (Figure 1).[26]

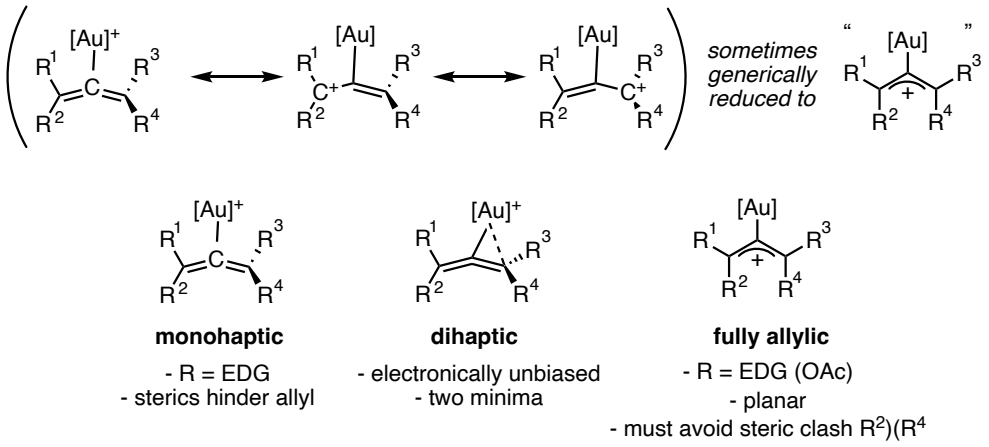

Figure 1. Resonance structures of a gold(I)-allene complex. The pure allyl cation geometry is a common oversimplification for most systems; it represents a tautomer that is only favoured when electron-donating groups are present.

An example of unusual activation of allenes, in which the nucleophile attacks the central *sp*-hybridised carbon, was reported in 2011 in the gold(I)-catalysed cyclisation of allene amides (Scheme 5). The reaction proceeded through the intermediate formation of an alkylgold(I) complex and conjugate protodemetallation.[27]

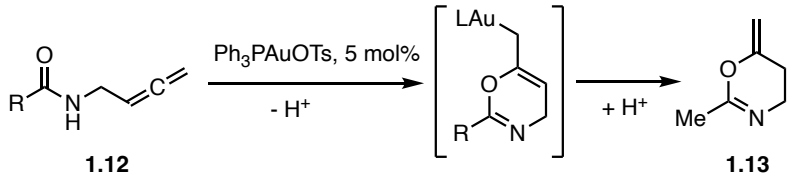

Scheme 5. Gold(I)-catalysed 6-*exo*-dig cyclisations of allene amides forming dihydrooxazines are proposed to proceed *via* the rarer alkylgold intermediates.

25 Belmont, P.; Parker, E. Silver and Gold Catalysis for Cycloisomerization Reactions. *Eur. J. Org. Chem.* **2009**, 6075–6089.

26 Gandon, V.; Lemière, G.; Hours, A.; Fensterbank, L.; Malacria, M. The Role of Bent Acyclic Allene Gold Complexes in Axis-to-Center Chirality Transfers. *Angew. Chem. Int. Ed.* **2008**, *47*, 7534–7538.

27 Hashmi, A. S. K.; Schuster, A. M.; Litters, S.; Rominger, F.; Pernpointner, M. Gold Catalysis: 1,3-Oxazines by Cyclisation of Allene Amides. *Chem. Eur. J.* **2011**, *17*, 5661–5667.

While gold complexes can activate allenes to engage in several cycloisomerisations as electrophiles, allenynes coordinate gold on the alkyne, leading to nucleophilic reactivity and downstream transformations that are varied and distinctively unrelated to typical enyne chemistry.[28] However, the appeal with allenenes, in which an additional alkene is tethered to an allene substrate, is that while the activation is similar to that of enynes, with the allene acting as an electrophile, the reactions do not follow the same pathways and lead to novel carbon skeletons and complementary families of products.

In the case of the shortest allenenes, or rather, vinylallenes, the mechanistic patterns are defined by the formation of gold(I) cyclopentenylidene complexes, as found in the theoretical and experimental studies by Gandon, Fensterbank and Malacria.[29] The peculiarity, therefore, with respect to enynes, is the absence of a single dominant gold(I) carbene motif, as the formed carbocation is not always homoallylic. Thus, vinylallene **1.14** formed a gold(I) vinylcarbene which underwent intramolecular cyclopropanation to form tetracyclic **1.15** as a single diastereoisomer (Scheme 6). The same reactivity was proven in the same work to be reached through gold-catalysed isomerisation of propargyl esters to the allenyl esters. The isomerisation and cyclisation of **1.16** afforded product **1.17** with excellent chirality transfer.

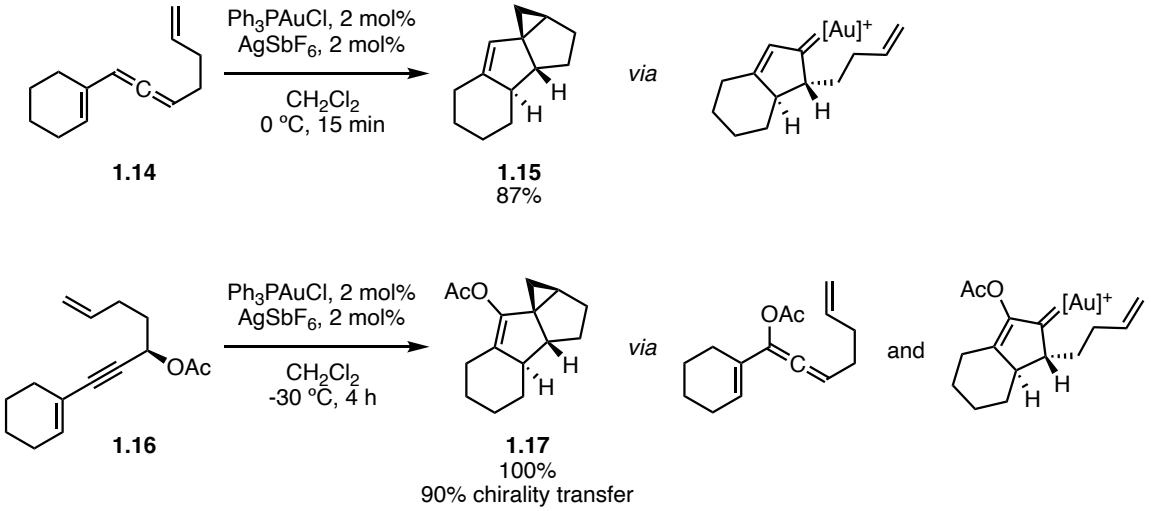

Scheme 6. Vinylallenene cyclisation trapping the carbene by intramolecular cyclopropanation.

As a general rule, allenynes react through the activation of the alkyne followed by nucleophilic attack of the allene. Therefore, they are usually not considered to constitute examples of gold(I) activation of

28 Lemière, G.; Gandon, V.; Agenet, N.; Goddard, J.-P.; De Kozak, A.; Aubert, C.; Fensterbank, L.; Malacria, M. Gold(I)- and Gold(III)-Catalyzed Cycloisomerization of Allenynes: A Remarkable Halide Effect. *Angew. Chem. Int. Ed.* **2006**, *45*, 7596–7599.

29 Lemière, G.; Gandon, V.; Cariou, K.; Hours, A.; Fukuyama, T.; Dhimane, A.-L.; Fensterbank, L.; Malacria, M. Generation and Trapping of Cyclopentenylidene Gold Species: Four Pathways to Polycyclic Compounds. *J. Am. Chem. Soc.* **2009**, *131*, 2993–3006.

allenes, but some examples have shown that allene activation, with the alkyne acting as a nucleophile, is not only feasible but perhaps the dominant pathway in similar allenyne systems.[30]

Computational Methods Applied to Gold(I) Catalysis

The activation of alkynes or allenenes in gold(I) catalysis generally result, upon cyclisation, in a plethora of diverse cationic intermediates that have led to widespread applications in synthesis precisely because of the multifaceted reactivity.[31] The computational treatment of gold(I) catalysis was significantly improved by relativistic treatment, allowing more accurate determinations of the real electronic structure.[32] In spite of the generally sound approaches to non-classical carbocations after the conclusion of the controversies surrounding their bonding paradigms,[33,34] and being revisited computationally,[35] gold(I) intermediates remained poorly defined for several years as a result of the poorly modelled extent of back-donation from the gold atom. Nevertheless, and as described in the **General Introduction**, the description by Toste and Goddard of gold carbenes as a continuum between fully fledged singlet carbenes and singly-bonded carbocations clarified the bonding and, especially, the degree of cationic character of the carbene.[36]

The intermediates in gold(I) catalysis posed an additional problem, however, as the homoallylic carbocations formed in enyne cyclisations could be viewed as comprising a homoallylic stabilisation to a cyclopropylcarbinyl cation. These are now widely known as independent entities.[37,38] The gold atom, by weakly[39] back-donating onto the carbocation, would significantly stabilise such a structure. However, the question remained as to whether they represented resonance forms or tautomers (Figure 2).

30 Yang, C.-Y.; Lin, G.-Y.; Liao, H.-Y.; Datta, S.; Liu, R.-S. Gold-Catalyzed Hydrative Carbocyclization of 1,5- and 1,7-Allenynes Mediated by π-Allene Complex: Mechanistic Evidence Supported by the Chirality Transfer of Allenyne Substrates. *J. Org. Chem.* **2008**, *73*, 4907–4914.

31 Jiménez-Núñez, E.; Echavarren, A. M. Molecular Diversity through Gold Catalysis with Alkynes. *Chem. Commun.* **2007**, *4*, 333–346.

32 Pernpointner, M.; Hashmi, A. S. K. Fully Relativistic, Comparative Investigation of Gold and Platinum Alkyne Complexes of Relevance for the Catalysis of Nucleophilic Additions to Alkynes. *J. Chem. Theory Comput.* **2009**, *5*, 2717–2725.

33 Olah, G. A.; Prakash, G. K. S.; Saunders, M. Conclusion of the Classical-Nonclassical Ion Controversy Based on the Structural Study of the 2-Norbornyl Cationt. *Acc. Chem. Res.* **1983**, *16*, 440–448.

34 Staral, J. S.; Yavari, I.; Roberts, J. D.; Surya Prakash, G. K.; Donovan, D. J.; Olah, G. A. Low-temperature carbon-13 nuclear magnetic resonance spectroscopic investigation of C_4H_7+. Evidence for an equilibrium involving the nonclassical bicyclobutonium ion and the bisected cyclopropylcarbinyl cation. *J. Am. Chem. Soc.* **1978**, *100*, 8016–8018.

35 Lobb, K. A. Isomerization of the 2-Norbornyl Carbocation: Isomerization of the 2-Norbornyl Carbocation. *Eur. J. Org. Chem.* **2015**, 5370–5380.

36 Benitez, D.; Shapiro, N. D.; Tkatchouk, E.; Wang, Y.; Goddard, W. A.; Toste, F. D. A Bonding Model for Gold(I) Carbene Complexes. *Nat. Chem*. **2009**, *1*, 482–486.

37 Creary, X.; O'Donnel, B. D.; Vervaeke, M. Homoallyl−Cyclopropylcarbinyl Cation Manifold. Trimethylsilyl versus Aryl Stabilization. *J. Org. Chem.* **2007**, *72*, 3360–3368.

38 Xie, J.; Dong, G. Cyclopropylcarbinyl Cation Chemistry in Synthetic Method Development and Natural Product Synthesis: Cyclopropane Formation and Skeletal Rearrangement. *Org. Chem. Front.* **2023**, *10*, 2346–2358.

39 Wang, Y.; Muratore, M. E.; Echavarren, A. M. Gold Carbene or Carbenoid: Is There a Difference? *Chem. Eur. J.* **2015**, *21*, 7332–7339.

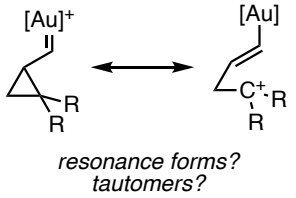

Figure 2. Homoallylic carbocation resonance structures: a vinylgold(I) and a gold(I) carbene.

This prompted a discussion on the nature of such systems with the aim of establishing which model represented the observed reactivity best. The assignment of bicyclo[3.2.0]heptenes to a gold(I) *syn*-cyclopropylcarbene complex and the separation of the cyclobutene pathways from the skeletal rearrangements suggested that the cyclopropyl forms were important.[40] Related tautomers (sometimes represented as resonance forms) also included the now disregarded cyclobut-2-ylium-1-yl complexes.[41] Similarly, the study of the endocyclic skeletal rearrangements required a fully formed exocyclic bond as the endocyclic bond was cleaved, which supported the description as a gold(I) α-cyclopropylcarbene for the key intermediates.[7] The understanding of [4+2] reactions to still be best defined as cyclopropylcarbenes, even in stabilised cases, endorsed this formalism further.[42,43] In these cases, when the gold(I) cyclopropylcarbene (hereafter, also closed form) and vinylgold(I) homoallylic cation (hereafter, also open form) coexisted as separate tautomers, their barriers towards further reactivity were distinct. This, in turn, implied that the very equilibrium between these structures –or even the mere existence thereof– could explain divergence in gold-catalysed processes or treat the unreactive form as a resting state.

For this reason, the general mechanistic understanding increased in complexity, as α-cyclopropylcarbene intermediates could exist as unique species or, fairly often, in equilibrium with their open-form tautomers. Nucleophile trapping and skeletal rearrangement would generally only proceed from a specific tautomer.[42,44]

Given the existing understanding in the substrate-dependent tautomerism and relative importance of resonance forms, a computational study to describe the effects of substitution on these equilibria was undertaken in 2020, determining that three independent tautomers were accessible.[44] Each would also contribute as resonance forms to the other ones, but the predominant resonance form would be seen in

40 Nieto-Oberhuber, C.; López, S.; Muñoz, M. P.; Cárdenas, D. J.; Buñuel, E.; Nevado, C.; Echavarren, A. M. Divergent Mechanisms for the Skeletal Rearrangement and [2+2] Cycloaddition of Enynes Catalyzed by Gold. *Angew. Chem. Int. Ed.* **2005**, *44*, 6146–6148.

41 Several examples in platinum and gold catalysis are provided in Fürstner, A.; Davies, P. W. Catalytic Carbophilic Activation: Catalysis by Platinum and Gold π Acids. *Angew. Chem. Int. Ed.* **2007**, *46*, 3410–3449.

42 Pérez-Galán, P.; Martin, N. J. A.; Campaña, A. G.; Cárdenas, D. J.; Echavarren, A. M. Carbocations or Cyclopropyl Gold Carbenes in Cyclizations of Enynes. *Chem. Asian J.* **2011**, *6*, 482–486.

43 Nieto-Oberhuber, C.; Pérez-Galán, P.; Herrero-Gómez, E.; Lauterbach, T.; Rodríguez, C.; López, S.; Bour, C.; Rosellón, A.; Cárdenas, D. J.; Echavarren, A. M. Gold(I)-Catalyzed Intramolecular [4+2] Cycloadditions of Arylalkynes or 1,3-Enynes with Alkenes: Scope and Mechanism. *J. Am. Chem. Soc.* **2008**, *130*, 269–279.

44 Escofet, I.; Armengol-Relats, H.; Bruss, H.; Besora, M.; Echavarren, A. M. On the Structure of Intermediates in Enyne Gold(I)-Catalyzed Cyclizations: Formation of *Trans* -Fused Bicyclo[5.1.0]Octanes as a Case Study. *Chem. Eur. J.* **2020**, *26*, 15738–15745.

the tautomer as it adopted geometrically very distinct structures. Moreover, it was found that even when a closed form and an open form existed as tautomers, the gold(I) cyclopropylcarbene was most stable (Scheme 7).

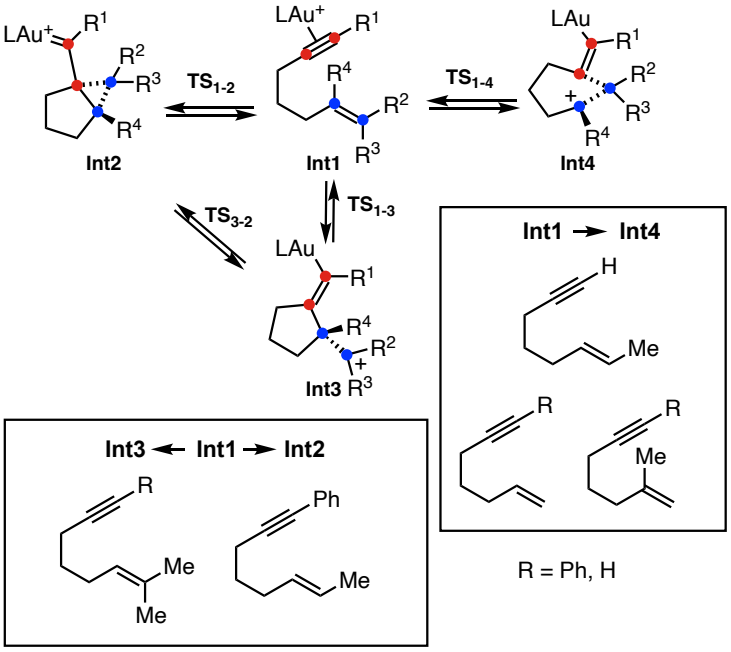

Scheme 7. Previously described intermediates in the gold(I)-catalysed cyclisation of a family of 1,6-enynes.

In gold(I) catalysis, other structures with classical bonding patterns have been identified or postulated as intermediates. Among these, cyclobutene-fused structures were proposed to be intermediates in skeletal rearrangements and further evidence came in 2009 with the isolation of said cyclobutene intermediates such as **1.19**, which reacted further under gold(I) catalysis to ring-open to skeletal rearrangement product **1.20** (Scheme 8a) and with other substituents formed naphthalene**s** or underwent an ene reaction.[45] In a later stoichiometric study, the initial [1,2]-fused cyclobutene **1.22** formed at low temperature rapidly isomerised to the [2,3]-fused cyclobutene **1.23**, affording the corresponding gold(I) complex in 96% yield (Scheme 8b).[46]

45 Odabachian, Y.; Gagosz, F. Cyclobutenes as Isolable Intermediates in the Gold(I)-Catalysed Cycloisomerisation of 1,8-Enynes. *Adv. Synth. Catal.* **2009**, *351*, 379– 386.

46 Brooner, R. E. M.; Brown, T. J.; Widenhoefer, R. A. Direct Observation of a Cationic Gold(I)-Bicyclo[3.2.0]hept-1(7)-Ene Complex Generated in the Cycloisomerization of a 7-Phenyl-1,6-Enyne. *Angew. Chem. Int. Ed.* **2013**, *52*, 6259−6261.

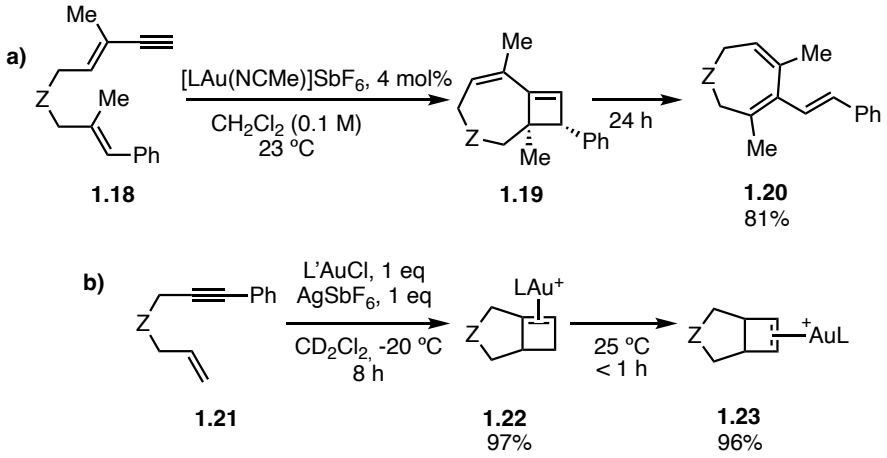

Scheme 8. a) Intermediacy of cyclobutenes in a skeletal rearrangement process. b) Isomerisation of gold(I) cyclobutene complexes at room temperature.

Objectives

Intermediates in gold(I)-catalysed 1,5-enyne and 1,5-allenene cyclisations have been presented to exist in several forms ranging from closed gold(I) cyclopropylcarbene complexes to open-form homoallylic vinylgold(I) carbocations.[25,29] The precedents in the studies of intermediates linked to 1,6-enynes[44] might not be fully applicable to 1,5-enynes due to the increased ring strain and 5-*endo*-dig reactivity. In addition, 1,5-allenenes lack the additional π bond that can back-bond to form gold(I) cyclopropylcarbenes. While the reactivity of such systems has been explored experimentally, the existence of specific structures as tautomers or resonance structures had not been determined unequivocally. The trends in reactivity can be understood by analysing the accessible intermediates with these systems. This prompted us to study the nature of intermediates in gold(I) catalysis with DFT and revisit known intermediates to contrast the bonding paradigms. We also sought to understand to what extent different functionals can be used for geometry optimisations, orbital analysis or for energy profiles. Thus, we also aim to construct a consistent framework to evaluate DFT methods in gold(I) catalysis and provide criteria for valid protocols in future computational studies.

The gold(I)-catalysed single-cleavage skeletal rearrangement of 1,6-enynes, while known for a wide range of substrates,[5] has long evaded understanding for the seemingly capricious shifts in exocyclic and endocyclic cleavage selectivity,[7] as well as the stereoconvergence of reactions when very electron-rich alkenes were present in the substrate.[24] We decided to explore both of these matters through a combined experimental and computational approach, with the aim of understanding all of the factors that lead to the changes in selectivity and, ultimately, be able to predict the outcome for a particular system with the aim of generalising the model for as many different modifications as possible. In addition, we sought to explain the reasons for double-cleavage rearrangements and why single- and double-cleavage products never form as mixtures in the same reaction.

As the final objective, we endeavoured to calculate the full mechanisms of cyclisation (elimination) and alkoxycyclisation of 1,6-enynes using three phenyl-tethered enynes as models. There have been no previous attempts to approach the full catalytic cycles comprehensively nor to explain product ratios. Furthermore, and with the mechanistic insight provided by the full picture, we set out to explain the apparent alcohol-dependence in enantioselectivity that had been observed experimentally in chiral alkoxycyclisation reactions.

Results and Discussion

Nature of Intermediates in Gold(I) Catalysis

As outlined in the introduction, our understanding of the specific nature of intermediates in gold(I) catalysis has evolved over time. The reasons for this have been that for most proposed mechanisms, any tautomeric or non-tautomeric forms could be drawn, in principle, with no major difference in reaction outcome. Only with computational chemistry were the equilibria between tautomers ascertained, as well as the extent of delocalisation in such intermediates. However, most of these intermediates were described *ad hoc* for each particular reaction and there have been far fewer comprehensive efforts to understand the substrate-dependent variations in tautomeric equilibria.[2,4,5,7]

Previous work carried out in our group on the intermediates in 1,6-enyne cyclisations highlighted the importance of closed gold(I) cyclopropylcarbene complexes. In particular, when different structures were present as independent tautomers, some of these were found to react further with the others having higher barriers or behaving as resting states for the system. Further work on the nature of this intermediates suggested that a gold(I) α-cyclopropylcarbene, an open-form exocyclic vinylgold carbocation and an endocyclic vinylgold carbocation were all possible tautomers for the cyclised 1,6-enyne system.[44] However, the latter endocyclic carbocation was never found alongside the α-cyclopropylcarbene intermediate.

We then sought to study the intermediates found in both the 5-*endo*-dig, 5-*exo*-dig and 4-*exo*-dig cyclisations of 1,5-enynes. The latter tend to be strongly disfavoured due to strain and orbital overlap, as outlined by Baldwin's rules. The inclusion of these intermediates and transition states in our study was for three main reasons: the analogy to the known 1,6-enynes should be more direct, while greatly increasing the ring strain; the calculations should reproduce the known experimental preference for the alternative pathway; and understanding how strain can shift thermodynamic preference for specific bonding arrangements, or disallow some geometries entirely.

In order to approach this problem, we decided to carry out DFT calculations on a set of gold(I) complexes of 1,5-enynes. By modelling the intermediates resulting from the cyclisation of a set of substituted substrates would be comparable to the known bonding situations with 1,6-enyne substrates, and thus direct comparisons could be made. The geometries were optimised with BP86-D3, a functional consisting of Becke's exchange functional and Perdew's 1986 correlation functional. For the reasons explained in the **General Introduction**, implicit solvation was included in all calculations, using PCM, while the weakly-coordinating anion was excluded.

A family of model 1,5-enynes were chosen to include varied alkyl substitution on the alkene fragment, with a terminal or phenyl-capped alkyne. The methyl groups on the alkene could, in principle, alter the electronics of the system to favour some tautomeric structures of cyclised intermediates, as had been

observed with 1,6-enynes. The phenyl-capped alkynes were included as internal alkynes with aryl substituents have been extensively studied experimentally; in addition, 5-*endo*-dig reactivity could show greater differences for these systems. Substrate **I** was included as a more strongly electron-donating example to see if a 4-*exo*-dig cyclisation still had an accessible reaction coordinate, or whether it would collapse unto the same reaction coordinate as the 5-*exo*-dig cyclisation.

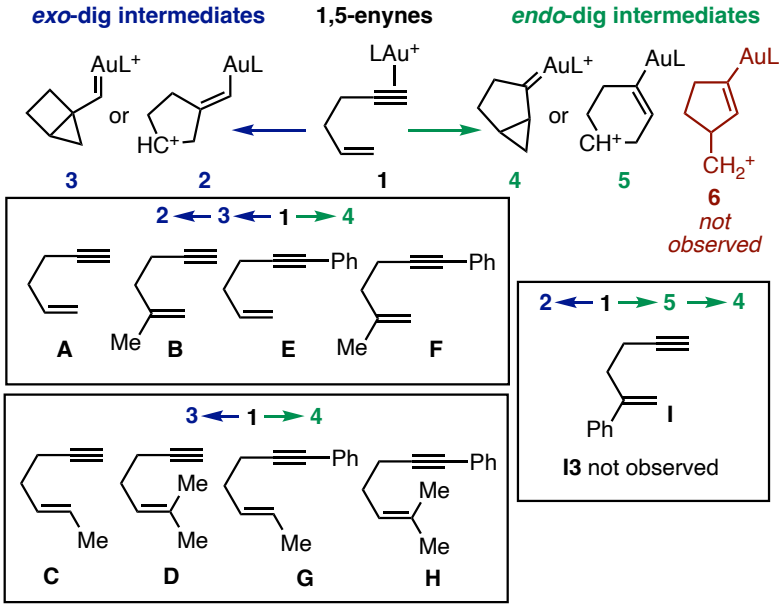

Scheme 9. Intermediates (**1**–**6**) derived from 1,5-enynes (**A**–**I**) as found to exist for differently substituted carbon skeletons.

1,5-enynes **A**–**H** with the same substitution patterns as the previously studied 1,6-enynes, as well as enyne **I**, were calculated as the gold(I) complex (**A1**–**I1**) and as the *exo* (**A2**–**I2** and **A3**–**I3**) and *endo* (**A4**–**I4, A5**—**I5** and **A6**–**I6**) intermediates (Scheme 9).

For the methyl-substituted substrates, geometries **5** and **6** were always inaccessible, converting in a barrierless manner to **4**. In addition, the **C2**, **D2**, **G2** and **H2** geometries did not constitute minima on the potential energy surface, undergoing rearrangement, and were not considered for the analysis as they did not represent the intermediates of interest in gold catalysis.

Aryl substituents next to the formed carbocation stabilise it enough for the open form to exist as an independent intermediate as seen in **I5**. This enyne was only explored in order to probe the geometry of the open form carbocation, so the bicyclopentane geometries were not studied in this case. Despite this significant benzylic stabilisation, it is remarkable how intermediate **I5** is still somewhat higher in energy than **I4**. The formation of a bicyclic structure with relatively low strain combined with a stabilised gold carbene contributes to the overall stability of the intermediate.

Table 1. Calculated bond distances and angles of optimised intermediates and transition states of enynes. Free energies in kcal mol^{-1} at BP86-D3/6-31G(d) + SDD, PCM (dichloromethane) referenced to geometry **1**. L=PMe_3. Distances expressed in Å and angles in degrees.

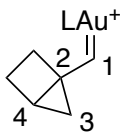

for structures **2** and **3**

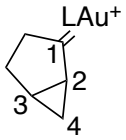

for structures **4** and **5**

Enyne	Species	*C1-C2*	*C2-C3*	*C2-C4*	*C2-C3-C4*	$\Delta G^{\ddagger}$	ΔG^{o}
A	**A2**	1.346	1.537	2.386	106.4	12.1[a]	10.9
A	**A3**	1.381	1.579	1.755	70.7	15.3	7.3
A	**A4**	1.417	1.600	1.605	63.0	8.9	-11.6
B	**B2**	1.345	1.558	2.322	102.2	3.2[a]	1.3
B	**B3**	1.368	1.573	1.914	78.4	12.2	2.9
B	**B4**	1.406	1.668	1.586	60.6	7.9	-11.0
C	**C3**	1.375	1.620	1.753	69.6	13.3	8.0
C	**C4**	1.411	1.585	1.645	65.2	8.1	-11.0
D	**D3**	1.369	1.689	1.735	66.8	10.5	9.0
D	**D4**	1.406	1.590	1.685	66.8	7.2	-9.6
E	**E2**	1.356	1.532	2.394	107.2	-16.9[a]	15.5
E	**E3**	1.412	1.551	1.705	68.7	19.1	9.6
E	**E4**	1.425	1.639	1.591	61.5	8.2	-6.0
F	**F2**	1.354	1.537	2.390	105.6	8.7[a]	7.6
F	**F3**	1.397	1.555	1.809	73.5	16.7	6.7
F	**F4**	1.409	1.759	1.575	57.8	6.8	-5.7
G	**G3**	1.396	1.628	1.691	66.3	17.4	10.8
G	**G4**	1.419	1.587	1.679	66.7	8.2	-5.8
H	**H3**	1.400	1.676	1.644	62.7	3.7	12.2
H	**H4**	1.414	1.591	1.725	68.6	15.0	-5.1
I	**I4**	1.397	1.769	1.561	56.9	-5.6[b]	-6.7
I	**I5**	1.354	2.315	1.575	42.2	11.5	-5.3

[a] TS corresponds to TS2-3. [b] TS corresponds to TS4-5, electronic energy on the PES is higher than **I5**.

After having the relative energies of all intermediates accessible for every 1,5-enyne and discarding several of the structures as inaccessible tautomers or resonance structures, we then decided to investigate the possible bonding arrangements for these intermediates. With this in mind, an NBO

analysis of selected intermediates was carried out. **H3**, **H4**, **B2**, **B3** and **I5** were chosen, representing the endocyclic gold α-cyclopropylcarbene, a strained exocyclic gold α-cyclopropylcarbene, an endocyclic carbocationic vinylgold complex, its strained cyclopropylcarbene analogue and an endocyclic carbocationic cyclohexenylgold complex.

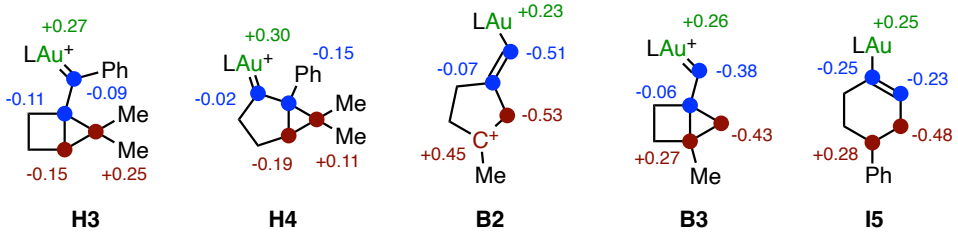

Figure 3. NPA charges of selected intermediates of 1,5-enyne cyclisations.

The NPA charges (from NBO) show a similar charge distribution for **H3** and **H4** independent from the ring size. The differences between **H3** and **B3** are much more significant, exemplifying how the charge localisation on the original alkene carbons depends on their substitution more than on their specific bonding arrangement. **B2** and **I5** are similarly comparable.

Compared to **B3**, **B2** is more polarised. However, by looking at the Second Order Perturbation Theory analysis, even open-form **B2** exhibits very significant donation from C-C π to C(cation) (89.3 kcal mol^{-1}), as well as strong C-C σ to C(cation) donation (71.8 kcal mol^{-1}), which is much stronger than either the C-H or alternative C-C σ to C(cation) donations (15 and 9 kcal mol^{-1} respectively). This strong donation from both the double bond and the adjacent single bond suggests that even the open form has significant cyclopropyl character. This is conceptualised as resonance and is likely enhanced by the constrained geometry of a small cycle allowing for better orbital overlap.

In contrast, **I5** does not show a strong vinylgold to carbocation donation (at only 8.1 kcal mol^{-1}), with more significant hyperconjugative C-C σ to carbocation donation (21.3 kcal mol^{-1}), as well as the expected benzylic stabilisation (74.6 kcal mol^{-1}).

Comparing intermediates **H3** and **H4** by NBO analysis shows how in the bicyclohexane ring, it is the outer cyclopropyl bond which is most distorted (with natural hybrid orbital -NHO- bending above 20º in both cases) whereas in the bicyclopentane, it is the inner cyclopropyl bond that experiences greater distortion. In both cases, however, it is the outer cyclopropyl bond which has the lowest occupancy, at 1.698 and 1.666 for **H3** and **H4**, respectively. This is likely a result of the potential stabilisation offered by the methyl groups. The main difference is in the occupancy of the inner cyclopropyl bond, at 1.825 for **H4** but at 1.754 for **H3**. The donation from either of the outer cyclopropyl bonds to the gold carbene is surprisingly similar (20.6 kcal mol^{-1} and 22.1 kcal mol^{-1}) despite the gold carbene being endocyclic or exocyclic. Backdonation from the carbene is nonetheless significant in the case of **H3**.

Performing the same calculations on known 1,6-enyne intermediates, with special emphasis on the second-order perturbation theory, allows the direct quantitative comparison to the explored intermediates of 1,5-enyne cyclisations.

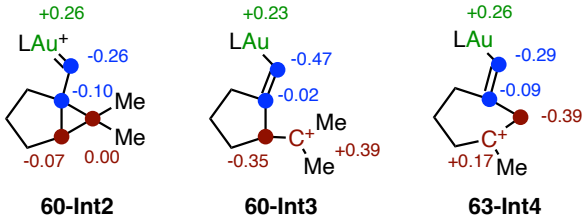

Figure 4. NPA charges of selected intermediates of 1,6-enyne cyclisations.

60-Int2 shows a lower occupancy of the endocyclic cyclopropyl bond compared to the exocyclic (1.639 and 1.750 respectively, Figure 4). This correlates with the results from Second Order Perturbation Theory, as the donation from C-C_{endo} to the gold carbene is, at 23.6 kcal mol^{-1}, higher than that from C-C_{exo} (8.0 kcal mol^{-1}). The NLMOs follow a similar delocalisation tend, with up to 17.3% contribution from the carbenic carbon to the endocyclic cyclopropyl NLMO. As substituents on both sides of the cyclopropyl are alkyls, and by analogy to **H3**, **H4** and **B3**, we can say that as a general rule it is the *endo*-bond that delocalises best for electronically unbiased gold cyclopropylcarbenes.

Open form **60-Int3** shows residual donation from the vinylgold to the carbocation (11.7 kcal mol^{-1}), compared to the stronger hyperconjugation from the C-C σ bond (24.0 kcal mol^{-1}).

The Lewis structure adopted by genNBO for **63-Int4** also presents an endocyclic cyclopropyl bond, albeit significantly less populated than the exocyclic one (1.556 and 1.824 occupancy, respectively). As evidenced by the NHO bending, there is more distortion in the endocyclic bond as the hybrid orbitals for both carbons have angular deviations above 20º. This is compounded by more delocalisation from the endocyclic bond to the carbene (35.3 kcal mol^{-1}) and almost no donation from the exocyclic bond (4.3 kcal mol^{-1}). However, and while it is clearly more polarised than other examples of cyclopropylcarbenes, this intermediate is probably best described as a more divergent version of **Int2** rather than as a separate geometric category.

We next focused our attention on 1,5-allenenes. These substrates, containing two geminal π bonds, have the peculiarity that gold α-cyclopropylcarbenes cannot form in a synchronous manner: such a geometry requires two π bonds on the same atoms. However, due to the length of the tether and, as explained before, these substrates are able to form cyclopropylcarbene intermediates too. Nevertheless, the cyclopropanation happens from the rear, meaning that even though 1,5-allenenes can lead to the same intermediates as 1,5-enynes, the bond to form in the cyclisation is not part of the cyclopropane. Lacking the constraints of enyne activations, the structures accessible from allenenes should in principle allow the formation of gold(I) α-cyclobutylcarbene intermediates instead when joined by a longer tether.

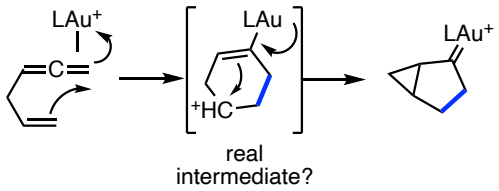

Scheme 10. Cyclisation of 1,5-allenenes results in a bicyclo[3.1.0]hexane system after rear cyclisation, but its concerted nature remained unclear.

As the transition states leading to the products could be concerted asynchronous or stepwise processes, the intermediacy of generally disfavoured endocyclic carbocations could be expected as non-stationary points in the reaction coordinate (Scheme 10). These have been described as hidden intermediates.[47] Characterised by close-to-flat potential energy surfaces (evolving in a barrierless manner), these intermediate-like structures do not have any more information than the transition state does about the eventual product formation. However, in some cases such as a vinylcyclopropane rearrangement, they proved to be instrumental in explaining the observed reaction selectivity.[48] In order to make direct comparisons to the enyne cyclisations, we studied a family of 1,5-allenenes with the same substitution patterns on the alkene (Scheme 11).

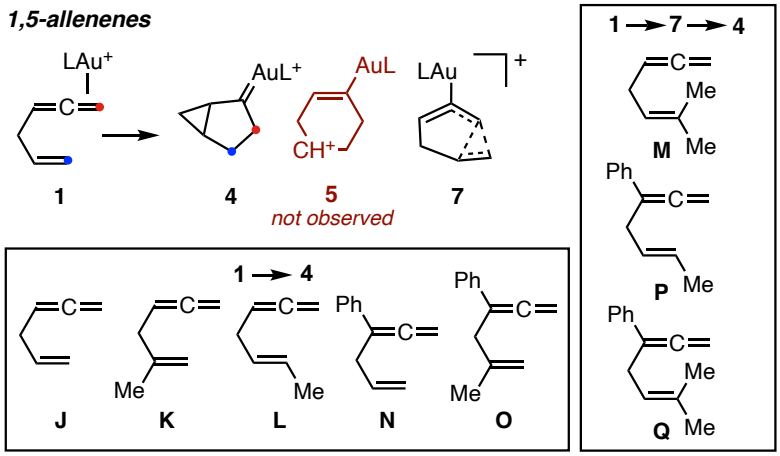

Scheme 11. Intermediates (**1**, **4**, **5**, **7**) derived from 1,5-allenenes (**J**–**Q**) as found to exist for differently substituted carbon skeletons.

As for analogous 1,5-enynes, endocyclic homoallylic cations were found to be non-stationary geometries in the PES. As such, for the studied substrates, the only real intermediate after cyclisation is the gold(I) cyclopropylcarbene complex.

47 Roca-López, D.; Polo, V.; Tejero, T.; Merino, P. Understanding Bond Formation in Polar One-Step Reactions. Topological Analyses of the Reaction between Nitrones and Lithium Ynolates. *J. Org. Chem.* **2015**, *80*, 4076–4083.

48 Garay, G.; Hurtado, J.; Pedrón, M.; García, L.; Reyes, E.; Sánchez-Díez, E.; Tejero, T.; Carrillo, L.; Merino, P.; Vicario, J. L. Organocatalytic Enantioselective Vinylcyclopropane-Cyclopentene (VCP-CP) Rearrangement. *Angew Chem Int Ed* **2023**, *62*, e202302416.

Table 2. Calculated bond distances and angles of optimised intermediates and transition states of allenenes. Free energies in kcal mol^{-1} at BP86-D3/6-31G(d) + SDD, PCM (dichloromethane) referenced to geometry **1**. L=PMe_3. Distances expressed in Å and angles in degrees.

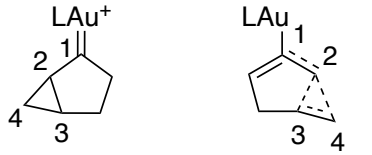

for structure **4** for structure **7**

Allenene	Species	*C1-C2*	*C2-C3*	*C2-C4*	*C2-C3-C4*	$\Delta G^{\ddagger}$	ΔG^{o}
J	**J4**	1.417	1.600	1.605	63.0	8.4	-8.9
K	**K4**	1.406	1.668	1.586	60.6	4.8	-9.7
L	**L4**	1.417	1.601	1.604	63.1	6.6	-6.5
M	**M4**	1.417	1.601	1.602	63.0	4.6[a]	-4.6
M	**M7**	1.507	1.689	2.253	91.9	8.6	0.3
N	**N4**	1.425	1.639	1.591	61.5	8.1	-6.8
O	**O4**	1.409	1.759	1.575	57.8	4.6	-8.0
P	**P4**	1.425	1.634	1.592	61.7	7.7	-4.2
P	**P7**	1.427	2.304	2.297	72.3	7.4	5.8
Q	**Q4**	1.425	1.640	1.589	61.4	9.1	-2.9
Q	**Q7**	1.500	1.674	2.273	93.4	9.1[a]	0.2

[a] Corresponds to TS4-7.

One peculiarity of allenenes is that, upon cyclisation, partial cyclopropane rings can form as a non-classical carbocation. The reason is that the lack of a second π bond to form the standard cyclopropylcarbene, when combined with an electronically unbiased alkene, can only form one weak three-centre two-electron bond. This can be observed in intermediate **P7**. Intermediates **M7** and **Q7** are similar, but more open form carbocationic in nature. The dimethyl-substituted alkenes favour the localisation of charge on the tertiary carbocation. The inaccessibility of the π system to this exocyclic carbocation allows the stabilisation of the open form, which was never observed with these substrates for the 1,5-enynes.

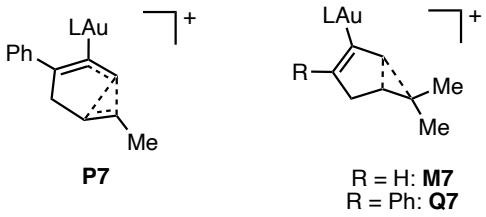

Figure 5. Intermediates **P7**, **M7** and **Q7** show non-integer bond orders and non-classical delocalisation of the carbocation. L = Me_3P.

To assess the bonding situation in these cases, NBO analysis was performed on **P7** and **Q7**. Firstly, the natural charges show a much greater localisation in **Q7**, as expected from the open geometry.

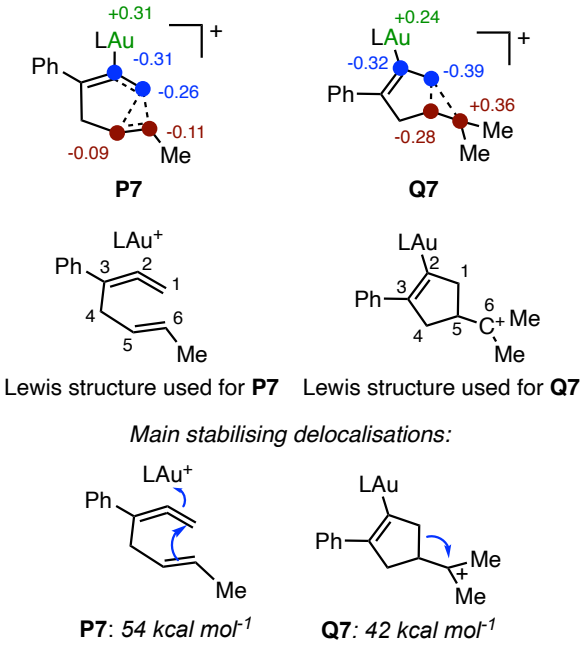

Figure 6. NPA charges of selected intermediates of 1,5-allenene cyclisations and Lewis structures used in the NBO analysis. L = Me_3P.

The non-classical carbocation in **P7** was fully supported by the NBO analysis. Using this Lewis structure, alkenes C1-C2 and C5-C6 were found to have π occupancies of 1.663 and 1.593 respectively. The corresponding antibonds had occupancies of 0.140 and 0.099, respectively. With the Second Order Perturbation Theory analysis, donation of C5-C6 π to C1-C2 π* accounted for a stabilisation of 54 kcal mol^{-1}. Finally, the NLMO corresponding to the C5-C6 π bond was found to consist only of 78.6% of its parent NBO, with a 15.3% contribution from C1 orbitals. Based on all of this, the donation is very significant and accounts for occupancies more akin to those found for aromatic π bonds than to alkenes. The non-classical carbocationic structure of this intermediate is therefore correct.

The charge localisation in **Q7** is more apparent. The C1-C5 bond has an occupancy of 1.785 and the carbocation on C6 an occupancy of 0.608. The delocalisation of the C1-C5 bond onto C6 accounts for a very significant stabilisation of 42 kcal mol^{-1}. Finally, the NLMO corresponding to C1-C5 consists of

86.6% of the parent NBO with a further 12.2% contribution from C6. This suggests a noticeable partial cyclopropylic character (as with all open-form intermediates); however, it remains much more localised than in endocyclic carbocationic cases, such as **B2**, and in full cyclopropylcarbene intermediates.

We then turned our attention to whether different functionals describe these systems appropriately and to which functionals would be most suitable for the obtention of single-point energies at a higher level of theory. A number of functionals were used to calculate single-point energy of all intermediates, using Grimme's D3 empirical dispersion in all cases. With the intention of evaluating the performance of these functionals, we also performed DLPNO-CCSD(T) calculations on the same systems with ORCA 4.0.

An analogous benchmark to that carried out for 1,6-enynes was first performed with substrate **I** to ensure that carbocationic species are described in a similar way. In addition, **TSI4-5** is really close in energy to **I5**, potentially making the system more challenging.

Table 3. Single-point energy calculated for the intermediates and transition states in the cyclisation of **I**. Functional-D3/6-311+G(d,p) + SDD. Electronic energies in kcal mol^{-1}.

	I1	**I4**	**I5**	**TSI1-5**	**TSI4-5**
BP86	0.0	-5.3	-3.8	12.5	-3.8
B3LYP	0.0	-0.8	0.5	14.0	0.6
B3PW91	0.0	-5.9	-1.6	14.6	-1.7
B97D	0.0	-1.6	-1.9	11.8	-1.7
BMK	0.0	-3.5	3.2	18.6	3.3
TPSS	0.0	-6.5	-3.9	11.3	-3.9
M062X	0.0	0.1	6.9	16.7	7.1
M06HF	0.0	2.1	10.1	17.4	10.2
M06	0.0	-2.6	2.5	15.3	2.6
M06L	0.0	-3.8	0.3	14.1	0.5
PBE0	0.0	-9.5	-4.1	13.5	-4.2
PBE	0.0	-9.3	-6.9	10.7	-6.9
DLPNO-CCSD(T)*	0.0	-1.3	3.0	14.4	3.6

* def2-TZVPP with default ECP used as present in ORCA4.0.

Out of these results B3PW91, B97 and PBE0 are the only to show an incorrect description of the shallow transition state, as its electronic energy was found to be lower than the minimum it would supposedly connect to. As these values originate from single-point calculations, it is plausible that the geometric differences depending on the functional can be large enough to misrepresent shallow transition states.

The benchmark was also carried out with the intermediates from the cyclisation of **H**, which followed a similar pattern in the energy distribution depending on the used functionals.

Table 4. Single-point energy calculated for the intermediates and transition states in the cyclisation of **H**. Functional-D3/6-311+G(d,p) + SDD. Electronic energies in kcal mol^{-1}.

	H1	**H3**	**H4**	**TSH1-3**	**TSH1-4**
BP86	0.0	14.0	-2.8	17.4	6.7
B3LYP	0.0	21.2	3.3	22.5	12.2
B3PW91	0.0	14.5	-4.0	20.0	9.5
B97D	0.0	18.5	2.7	19.2	9.2
BMK	0.0	12.8	-4.7	21.2	12.4
TPSS	0.0	13.9	-1.8	18.5	8.2
M062X	0.0	19.0	0.3	24.1	14.4
M06HF	0.0	20.6	-1.2	23.0	12.1
M06	0.0	15.8	-1.8	22.1	12.4
M06L	0.0	15.0	-0.4	22.9	13.4
PBE0	0.0	12.4	-6.3	19.8	9.2
PBE	0.0	12.6	-4.1	17.3	6.8
DLPNO-CCSD(T)*	0.0	21.8	-0.6	22.9	12.3

* def2-TZVPP with default ECP used as present in ORCA4.0.

We then revisited the observed problems with some functionals finding a lower energy for the TS geometry than for the intermediate. This could arise from functional-specific error in the orbital description. Previously, structure optimisation with different functionals had been confirmed to converge to geometrically similar species.[44] Further validation of these optimisations would be important. This prompted us to explore whether all geometries of a simpler model, such as **H4**, are described in a similar way by all functionals.

Our approach was to run NBO calculations of **H4** with all the functionals and, using NPA charges as probes for the system description, confirm whether they remain constant. NPA charges are generally relatively invariable for small changes in geometry and only diverge significantly when the electronic description is different. This serves a twofold purpose, as if the charges are found to be comparable in all cases, the system is described similarly across all functionals even if the electronic energy is different.

Table 5. NPA charges (from NBO) of selected atoms in **H4**.

	Au	**C1**	**C2**	**C3**	**C4**
BP86	+0.30	-0.02	-0.15	-0.19	+0.11
B3LYP	+0.32	0.00	-0.17	-0.18	+0.11

B3PW91	+0.32	-0.01	-0.17	-0.19	+0.11
B97D	+0.29	-0.01	-0.15	-0.18	+0.11
BMK	+0.35	-0.01	-0.19	-0.19	+0.12
TPSS	+0.31	-0.03	-0.16	-0.18	+0.10
M062X	+0.36	0.00	-0.19	-0.19	+0.12
M06HF	+0.32	0.00	-0.21	-0.20	+0.10
M06	+0.35	+0.01	-0.19	-0.18	+0.12
M06L	+0.34	-0.01	-0.16	-0.18	+0.12
PBE0	+0.33	-0.01	-0.18	-0.19	+0.12
PBE	+0.30	-0.03	-0.15	-0.19	+0.10

The results collected in Table 5 show negligible variations in NPA charges. Our results therefore support the usage of any of these functionals to carry out geometry optimisations of gold(I)-catalysed processes. However, and as evidenced by the oft significant differences in energy when using different functionals for the single-point energy corrections, a higher level of theory single-point calculation with B3LYP-D3 or M06-D3 would be preferred to obtain the final energy profiles.

The same functional benchmark was performed on the geometries from allenene **Q**.

Table 6. Single-point energy calculated for the intermediates and transition states in the cyclisation of **Q**. Functional-D3/6-311+G(d,p) + SDD. Electronic energies in kcal mol^{-1}.

	Q1	**Q4**	**Q7**	**TSQ1-4**	**TSQ4-7**
BP86	0.0	-2.3	1.7	5.9	8.7
B3LYP	0.0	1.1	5.7	8.0	13.0
B3PW91	0.0	-4.8	2.5	8.3	10.5
B97D	0.0	1.8	4.7	5.8	10.8
BMK	0.0	-6.0	2.3	11.1	10.1
TPSS	0.0	-2.3	3.3	6.0	9.8
M062X	0.0	-1.5	8.4	12.6	15.0
M06HF	0.0	-1.4	9.4	14.6	13.7
M06	0.0	-3.6	6.2	10.5	14.0
M06L	0.0	-1.5	5.8	8.2	14.4
PBE0	0.0	-7.4	0.7	8.2	9.5
PBE	0.0	-3.9	0.7	5.7	8.4
DLPNO-CCSD(T)*	0.0	-3.3	3.4	10.0	10.7

* def2-TZVPP with default ECP used as present in ORCA4.0.

We then calculated the geometric average (root mean square) of the deviations of each geometry for which a benchmark was calculated with –enynes **H** and **I**, as well as allenene **Q**– with respect to the

DLPNO-CCSD(T) reference. The results showed large disparities depending on the functional, as shown in Table 7.

Table 7. RMSD of the differences between the predicted energies with functional-D3/6-311+G(d,p) [C,H,P] + SDD [Au] and DLPNO-CCSD(T), with implicit solvation. Functionals marked in red gave a lower energy for **TSI4-5** than for intermediate **I5**.

	RMSD
BP86	4.8
B3LYP	2.3
B3PW91	3.6
B97D	3.5
BMK	3.3
TPSS	4.6
M062X	2.9
M06HF	3.9
M06	2.3
M06L	2.8
PBE0	5.4
PBE	6.3

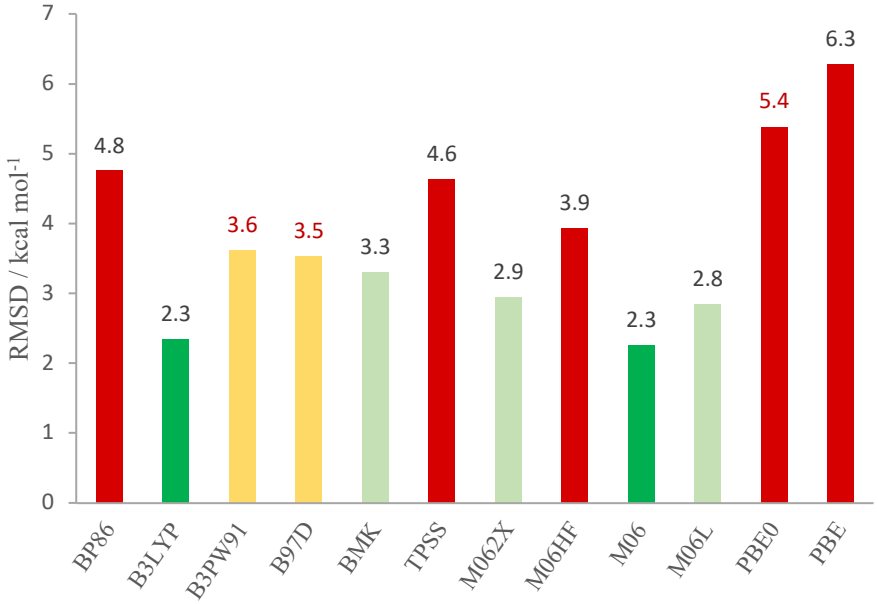

Figure 7. RMSD of the differences between the predicted energies with functional-D3/6-311+G(d,p) [C,H,P] + SDD [Au] and DLPNO-CCSD(T), with implicit solvation. Functionals for values marked in red gave a lower energy for **TSI4-5** than for intermediate **I5**.

In accordance with previous studies on the effect of the functional, B3LYP-D3 and M06-D3 proved to be the most accurate functionals for the single-point energy calculation at a higher level of theory.

Gold-Catalysed Skeletal Rearrangements: Stereoconvergence and Selectivity

The examples of cycloisomerisations mentioned in the introduction show that the influence of tethers is non-trivial and often results in changes in selectivity. We then set to explore a set of substrates that comprehended borderline cases and unexplored parts of the stereoelectronic substrate space, with the intention of drawing information from every example to explain all factors determining the selectivity. The catalyst used was commercially available [JohnPhosAu(NCMe)]SbF_6.

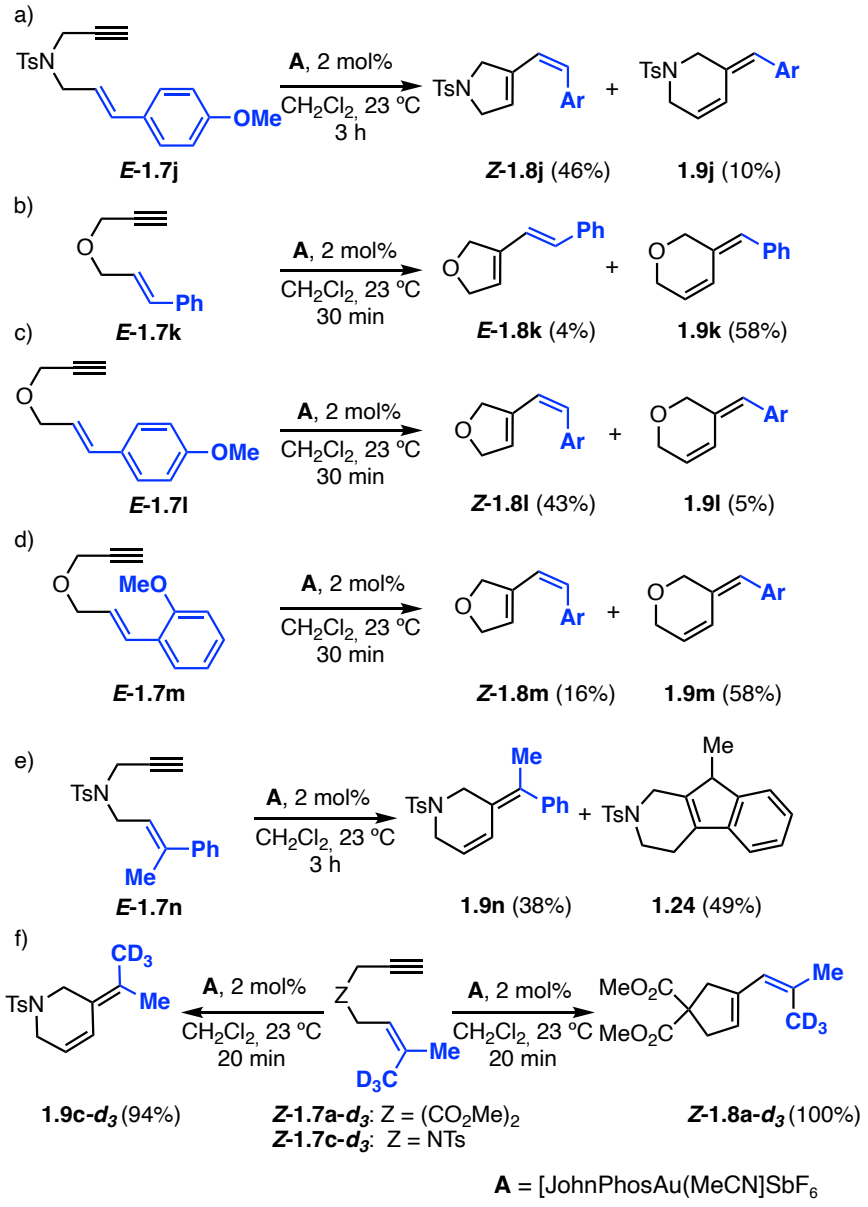

Scheme 12. Gold(I)-catalysed single cleavage skeletal rearrangements of 1,6-enynes

Initially, the prenyl propargyl substrates ***Z*-1.7a-*d*$_3$** and ***Z*-1.7c-*d*$_3$**, with a malonate and a tosylamide tether respectively, were prepared. The unlabelled substrates constituted examples of less electron-rich alkenes. The inclusion of an isotopically labelled methyl group would allow the direct determination of isomeric scrambling. In fact, while electron-rich substituents had been found to lead to *Z*-selective stereoconvergent transformations, the other substrates were assumed to be stereospecific. However, the same observation could result from a switch to an *E*-selective mechanism. Such a process would result in perfect scrambling for **1.8a-*d*$_3$** and **1.9c-*d*$_3$**, as both methyl groups would be essentially identical. These deuterated substrates, however, showed full stereospecificity in the formation of ***Z*-1.8a-*d*$_3$** and (*Z*-) **1.9c-*d*$_3$**. These results confirm that a stereoconvergent process appears only for very electron-donating alkenes and is otherwise not present.

We chose enyne ***E*-1.7j** as a first model, as all known sulfonamide-tethered substrates had resulted in *endo*-type cleavage to the best of our knowledge. This electron-rich substrate reacted to form the *exo*-type cleavage product ***Z*-1.8j**, along with a smaller quantity of the usual six-membered ring **1.9j**.

Methylcinnamyl substrate ***E*-1.7n**, however, showed full selectivity for the *endo*-cleavage. A tricyclic product **1.24** derived from **1.9n** was observed, arising from either an intramolecular acid-catalysed Friedel-Crafts alkylation or a Nazarov-type cyclisation.

Cinnamyl propargyl ethers, which had not been explored in the past, were explored as the least sterically encumbered tether. Enyne ***E*-1.7k** formed *endo*-type product **1.9k** selectively, with only a small amount of the stereospecific dihydrofuran ***E*-1.8k**. However, when an electron-rich substituent was placed in the *para* position, the selectivity switched to stereoconvergent *exo*-type ***Z*-1.8l**, as observed with the tosylamide analogues. On the other hand, o*rtho*-substitution in ***E*-1.7m** resulted in a greater selectivity for dihydropyran **1.9m**, even though the *exo*-type product ***Z*-1.8m** also showed *Z* selectivity as in all electron-rich substrates. This suggested some degree of steric influence on the different pathways, although the *Z* selectivity in the minor product suggests that the same stereoconvergent pathway is still active.

These observations, while hinting at the mechanism, showed an intricate competition between *exo* and *endo*-type cleavage together with the presence of stereoconvergent or stereospecific processes. We approached this problem with DFT calculations, with the objective of presenting a mechanistic framework capable of explaining each of these observations while remaining consistent. The calculations were performed with B3LYP-D3, and implicit solvation in dichloromethane modelled by using PCM.[49]

We used a simplified model that excluded the weakly-coordinating anion from the calculations and used trimethylphosphine as the ligand. Both of these simplifications are justified, as the former is not

49 See Experimental Section for details on the computational methods.

expected to play a significant role in determining the selectivity and the latter is a good compromise: many families of ligands work similarly in the single-cleavage rearrangements. The substrates with tosylamide tethers were simplified to a methanesulfonamide, as the tether can always reorient the nitrogen lone pair and so steric clash can be generally avoided. This is not the case for the dimethyl malonate tethers and, in order to model the selectivity correctly, this tether was not simplified.

As the malonate tethers gave *exo*-type bond cleavage selectivity in all cases, the system would show the stereoconvergence question in isolation. Therefore, it was the first system we approached with the intention of explaining the origin of stereoconvergence (Scheme 13). For this reason, we chose enyne **smS1** as the model substrate, in both the *E* and the *Z* configurations. The gold(I) complexes ***E*-S1** and ***Z*-S1** could undergo facile 5-*exo*-dig cyclisation yielding intermediates ***E*-S2** and ***Z*-S2**, respectively. These intermediates, best described as vinylgold(I) complexes with a homoallylic carbocation, showed a bond angle <100 º for both isomers, which is consistent with the structures explored previously and summarised in the previous subsection of this Chapter.

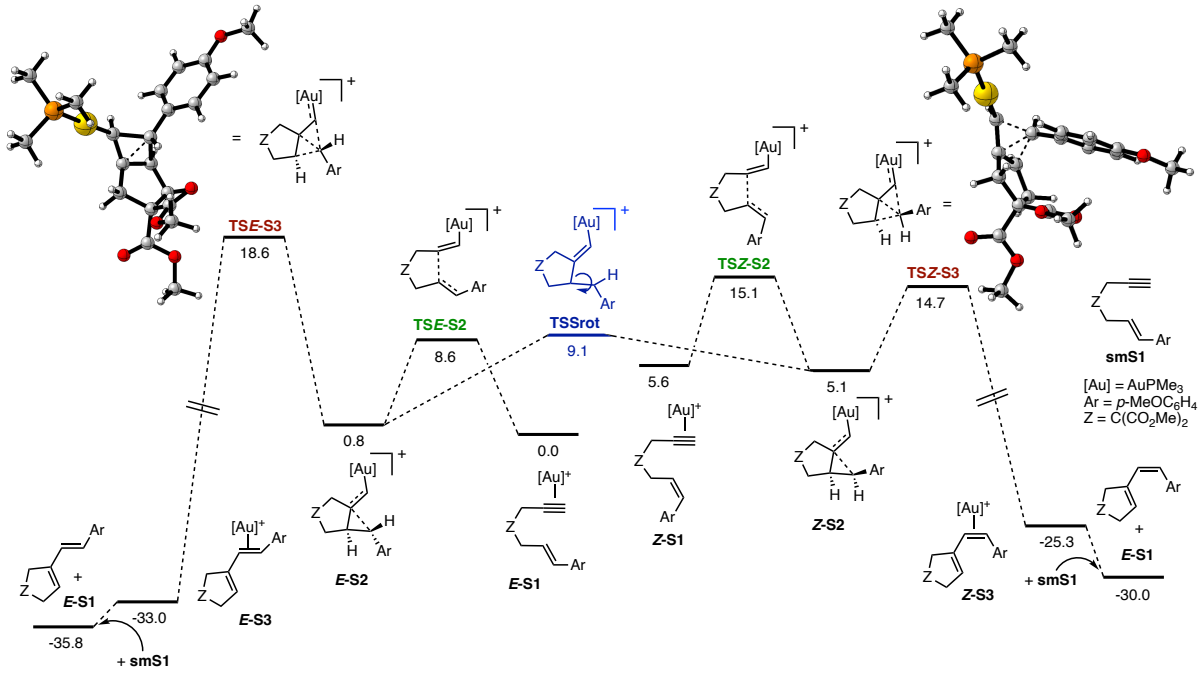

Scheme 13. Gold(I)-catalysed stereoconvergent single cleavage skeletal rearrangement of 1,6-enyne **smS1** featuring rotational interconversion. Free energy (B3LYP-D3/6-311G+(d,p) + SDD, PCM) in kcal mol^{-1}.

The subsequent rearrangements to yield dienes proceed through transition states **TS*E*-S3** and **TS*Z*-S3**. There is a very clear difference in energy, however, between the *E* and *Z* transition states. **TS*E*-S3** shows a much higher barrier, at 18.6 kcal mol^{-1}, compared to **TS*Z*-S3**, at only 14.7 kcal mol^{-1}. This difference is so significant that if ***Z*-S1** was used as the starting material (and in the absence of any interconversion mechanisms), the rate-determining step would actually be the 5-*exo*-dig cyclisation and not the migration. This is in sharp contrast to all previous intermediates and transition states, which are

significantly more stabilised in the *E* isomeric forms. The final *Z*-product ***Z*-S3** (or its dissociated form **prodS-*Z***) is, as expected, less thermodynamically favourable than its isomer ***E*-S3**, by 5.8 kcal mol^{-1}.

In order for a stereoconvergent process to occur and given that the observed stereoconvergence leads to the kinetic product, there should be an accessible isomerisation process from intermediates **S1** or **S2**. The former would require rotation about a fully-fledged π system of an intact alkene. Rotation about the single bond in intermediates **S2** was considered more likely, as it would only require cleavage of a partial cyclopropylic interaction and minor steric hindrance. A comparatively shallow transition state, **TSSrot**, was located, linking these intermediates and resulting in both sides to be in equilibrium. This rotation results in access to the favoured *Z* migration for both isomers of the starting material, fully reproducing the experimental observations.

Transition states **TS*E*-S3** and **TS*Z*-S3** are concerted processes. The process common to both isomers is a 1,3-migration of the *p*-methoxybenzylidene fragment across a delocalised π system. If we consider the stabilisation by gold(I) backdonation, the system is best described as a migration of a neutral carbene fragment across an allyl cation. The geometry of the TS shows very similar distances from the carbene to every carbon on the allyl system (1.70-1.71 Å). These distances are rather short, indicative of strong back-bonding. As the proposed model for the migration involves an η^3-allyl carbon(II) complex, it is reasonable to expect this.

Similar geometries with three partly formed bonds are known as bicyclobutonium cations, non-classical structures generally present as intermediates.[34]

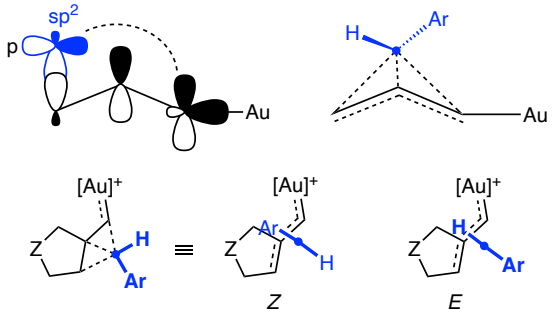

Figure 8. Configurations of the carbene migration transition state shown as a cyclobutonium cation. The orbital description is akin to a neutral carbene migrating over an allylic cation and the matching phases account for the bonding interaction across all involved carbon atoms.

While a concerted migration, as explored in Scheme 13, leads to the product, there are several examples in the literature of alternative pathways in the formation of dienes.[45,50] Among these, some strained cyclobutenes have been known to undergo ring-opening reactions. As gold(I)-catalysed [2+2] reactions

50 Escribano-Cuesta, A.; Pérez-Galán, P.; Herrero-Gómez, E.; Sekine, M.; Braga, A. A. C.; Maseras, F.; Echavarren, A. M. The Role of Cyclobutenes in Gold(I)-Catalysed Skeletal Rearrangement of 1,6-Enynes. *Org. Biomol. Chem.* **2012**, *10*, 6105−6111.

of alkynes and alkenes are also known, it was important to confirm whether these mechanisms could be present in the studied 1,6-enyne systems.

Several transition states of the ring-opening of bicyclo[3.2.0]heptenes were located (Scheme 14). As the precursor intermediates are chiral, coordination of the gold atom to each side of the alkene gave a pair of diastereomers (from the combination of central and planar chirality – **S4** and **S4b**), which would be expected to interconvert rapidly either intermolecularly or intermolecularly. Each of these four intermediates led to an accessible ring-opening transition state yielding ***E*-S3** and ***Z*-S3**. However, and while these ring-opening pathways would be competitive, no transition states were located connecting **S2** and **S4**, with any scans leading to an unreasonably high activation energy and interpolative methods failing.

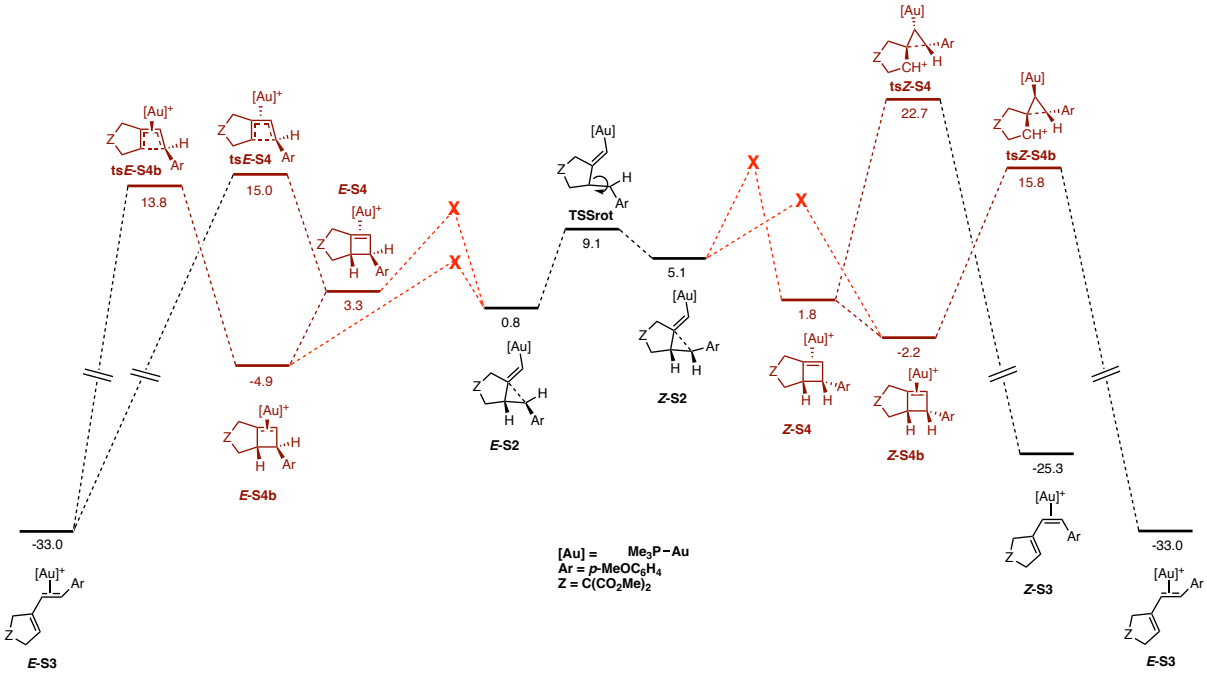

Scheme 14. Gold(I)-catalysed stereoconvergent single cleavage of ***Z*-** and ***E*-S2** is not feasible through initial formation of cyclobutenes. Free energy (B3LYP-D3/6-311G+(d,p) + SDD, PCM) in kcal mol^{-1}.

We propose an explanation for this, stemming from the result of a retro-scan of the bicyclo[3.2.0]heptene formation: its ring closure would come from a *Z*-vinylgold complex. Due to the partial double-bond character, rotation about C1-C2 is severely hindered and, hence, all subsequent intermediates are inaccessible. It is to be noted, however, that in other gold(I)-catalysed [2+2] cycloadditions, the formation of the cyclobutene does not require isomerisation of this bond. The absence of such a pathway in this case stems from the similarity between the described single-cleavage migration and the cyclobutene-forming reaction coordinates: they involve the formation of the same bond. In an analogous manner, single-cleavage rearrangements are inaccessible for some of the [2+2]

substrates. There is, therefore, a strong substrate dependence. Through this analysis, we then decided to discard these bicyclo[3.2.0]heptene intermediates from consideration in the other analysed mechanisms.

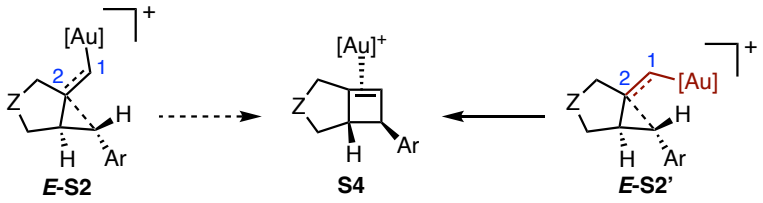

Scheme 15. Only *Z*-vinylgold(I) precursors can cyclise *ipso* to form cyclobutenes; no direct pathway exists from the *E*-vinylgold(I) species ***E*-S2**.

In order for this mechanism to explain the shift between *E*- and *Z*-configured products depending on the substitution of the alkene and, given that our experimental results with the cyclisation of ***E*-7a-*d*$_3$** suggest that the reaction becomes stereospecific, less electron-rich substrates should not allow as facile rotation. The cinnamyl and *p*-chlorocinnamyl analogues were calculated, as well as the simpler but-2-enyl substituted analogue.

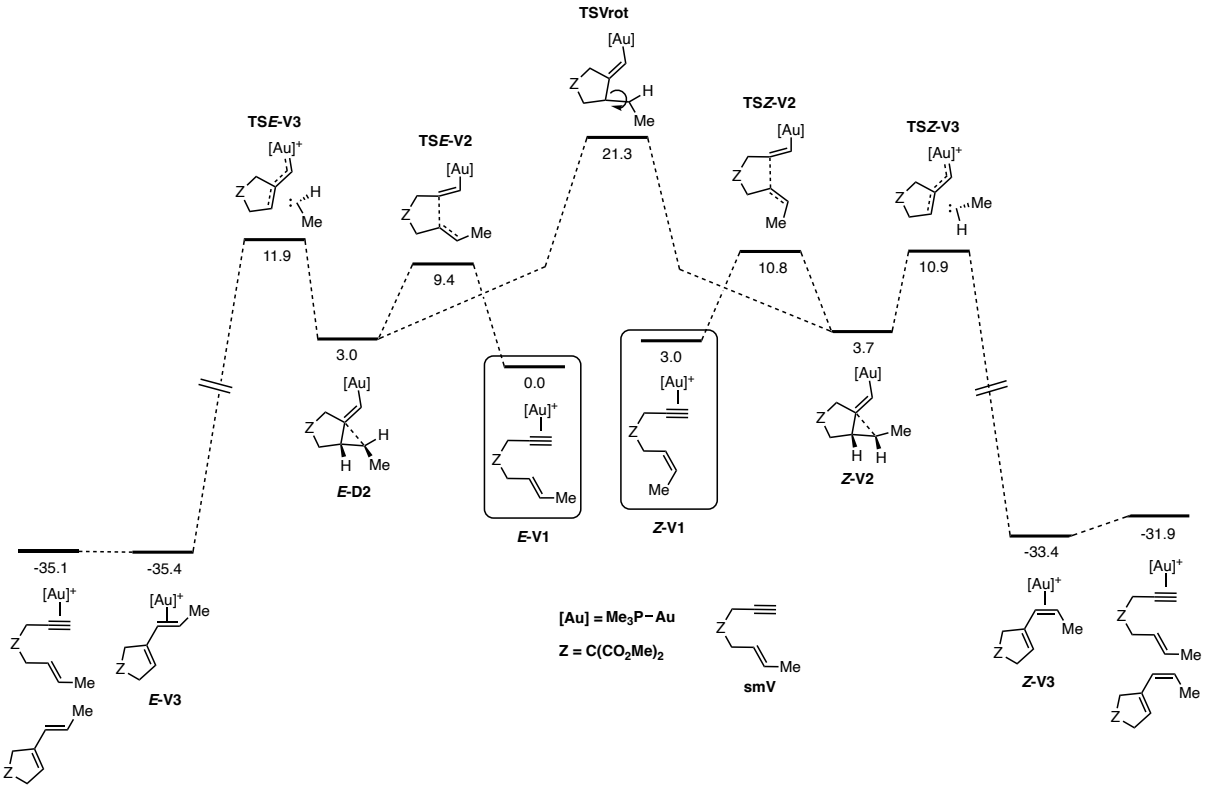

Scheme 16. Gold(I)-catalysed stereospecific single cleavage skeletal rearrangement of 1,6-enyne **smV**. Free energy (B3LYP-D3/6-311G+(d,p) + SDD, PCM) in kcal mol^{-1}.

The but-2-enyl fragment results in a much higher cyclopropylic character for intermediates ***Z*-U2** and ***E*-U2**, being a classical example of a gold(I) cyclopropylcarbene complex. Bond rotation, which in this case requires cleavage of a cyclopropyl bond, is not competitive when compared to the single-cleavage 1,3-migrations. This coincides with the stereospecific outcomes observed.

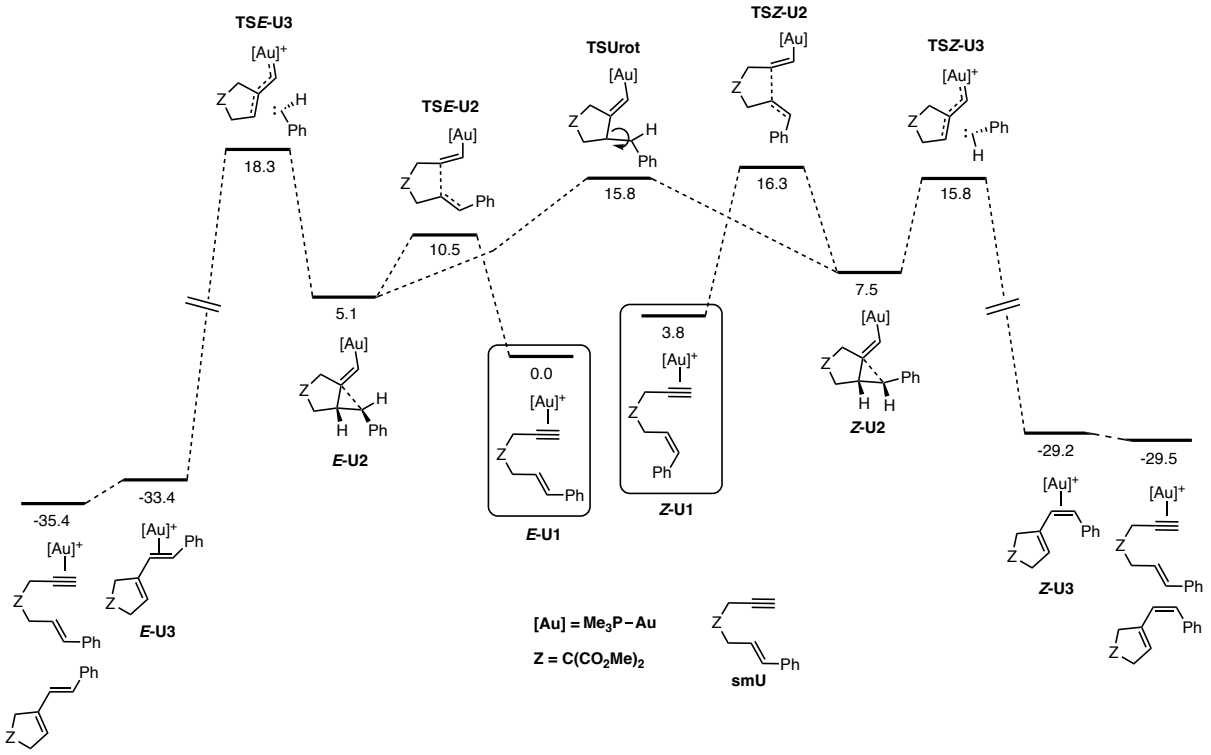

Scheme 17. Gold(I)-catalysed single cleavage skeletal rearrangement of 1,6-enyne **smU**. Free energy (B3LYP-D3/6-311G+(d,p) + SDD, PCM) in kcal mol^{-1}.

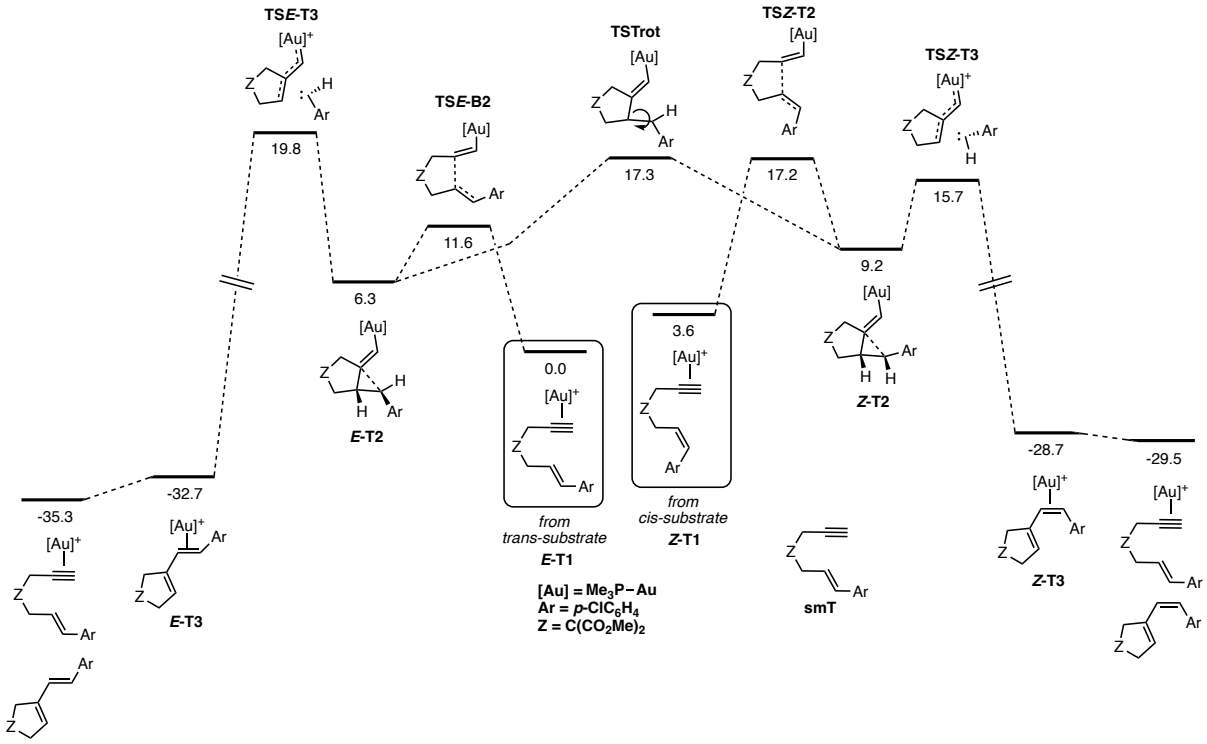

Scheme 18. Gold(I)-catalysed single cleavage skeletal rearrangement of 1,6-enyne **smT**. Free energy (B3LYP-D3/6-311G+(d,p) + SDD, PCM) in kcal mol^{-1}.

In all cases, the barrier leading to *Z*-migration is lower than that leading to *E*-migration, (cinnamyl, *p*-chlorocinnamyl and *p*-methoxycinnamyl showing a $\Delta\Delta G^{\ddagger}$ of 2.5, 4.1 and 3.9 kcal mol^{-1} respectively).

However, the overall situation is not so clear with the aryl substituents. While there is a higher barrier to rotation in both cases, the modelled system would not result in stereoconvergence in the two cases. We considered the stereoelectronic environment provided by the ligand to be a possible cause for this mismatch. We then used JohnPhos instead of trimethylphosphine for a series of calculations to probe the competition between *E*-migration and rotation for all studied substrates, while freezing the structure of all the atoms in the substrate as an approximation of the real TS geometry. This more complete model accurately reproduced the shift from stereospecific reactions (with *p*-methoxycinnamyl) to stereospecific reactions in all other cases.

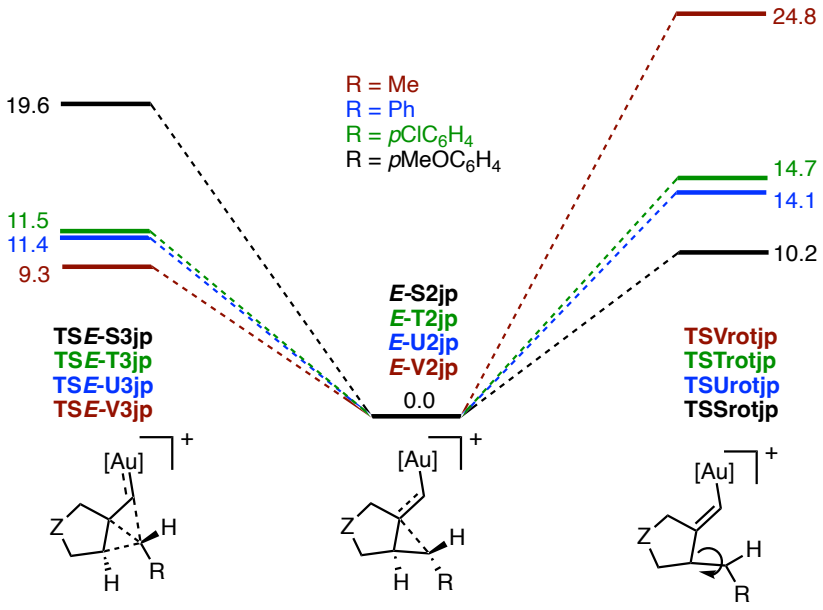

Scheme 19. Competition between rotational interconversion and *E*-migration in the JohnPhosgold(I)-catalysed single cleavage skeletal rearrangement of 1,6-enynes. Transition states modelled as frozen approximations. Electronic energy (B3LYP-D3/6-311G+(d,p) + SDD, PCM) in kcal mol^{-1}.

These calculations now matched the experimental observations related to stereoconvergence. A higher cyclopropylic character hinders rotation, which explained the appearance of stereoconvergence when sufficiently electron-donating groups stabilise the open-form vinylgold(I) carbocation.

The origin of the selectivity, nevertheless, was to be found in the 1,3-migration: even in stereospecific cases, the *Z*-migration was always favourable. This proved to be challenging, as the geometric differences in either isomeric transition state are not great. In addition, the electronic effect of having an aryl *syn*- or *anti*- to the gold remained very unclear, as similar orbital overlap was expected. Reconsidering the model with the η^3-allyl cation and a migrating carbene, the concept of "lowering the energy of the transition state" is an analogous premise to favouring such a geometric arrangement. Therefore, the question is "why does the *Z*-configuration favour η^3 coordination of the allyl fragment?" The alternative η^1 coordination would refer to the initial carbocation or the final diene product.

In order to address this question, we first substituted the tether in a set of simplified models of migration transition states. If steric effects played a role, there should be very significant differences in energy for the *Z*- and *E*-isomers depending on the tether. The opposite was observed, as shown in Table 8. Substitution on the carbene did not affect the outcome either, and increasing the steric hindrance on the allyl system only made a relatively minor impact favouring the *Z*-configuration even more. This last effect, however, would not be responsible for the other experimental observations, as no substrates with this substitution were explored.

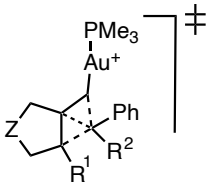

Table 8. Difference in free energy between *Z* and *E* migration transition states.

Code	Z	R^1	R^2	$\Delta\Delta G^{\ddagger}$ / kcal mol^{-1}
TSU2	$C(CO_2Me)_2$	H	H	2.5
TSX2	CH_2	H	H	2.9
TSY2	CMe_2	H	H	2.9
TSZ2	CH_2	H	Me	2.7
TSAA2	CH_2	Me	H	4.6

Now that supramolecular interactions and steric clashes were discarded as reasonable causes for the selectivity, we focused our attention on the electronic description of the system. NBO analysis was carried out on the preoptimised geometries of **TS*E*-X2** and **TS*Z*-X2**. The Lewis structure selected during the NBO analysis was the same in both isomers. Second order perturbation theory analysis showed very significant differences between both configurations: the delocalisation of the NBOs corresponding to the formal σ bonds between C1-C7 and C6-C7 onto the C2 carbocation accounted for an additional stabilisation of 64 kcal mol^{-1} for **TS*Z*-X2** when compared to **TS*E*-X2**. Additional interactions, each with around 5 kcal mol^{-1} of delocalisation energy are present in the *Z*-isomer, of which the C7-C_{Ph} to carbocation donation is the most prominent at 7 kcal mol^{-1}. While there is no analogous C7-H to carbocation donation in **TS*E*-X2**, this stabilisation is weak and, at best, a secondary contribution.

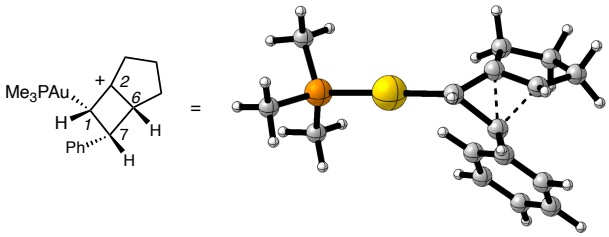

Table 9. Selected NBO interactions in the second order perturbation analysis of the single-cleavage migration transition state.

Occupied NBO	Lewis representation	Vacant NBO	Lewis representation	E (cis)[a]	E (trans)[a]
2	C1-C7 σ	72	C2(p)	164	111
11	C6-C7 σ	72	C2(p)	183	170

13	C7-C_{Ph} σ	72	C2(p)	7	0

[a] Delocalization energy in kcal mol^{-1}.

In terms of the charge localisation and potential differences therein, the NBO charges for the Me_3PAu fragment were identical in both configurational isomers (at +1.13). Any changes in charge separation were also discarded for the migrating benzylidene (*E* = +0.17 and *Z* = +0.18).

Table 10. NBO charges of atoms and fragments of the single-cleavage migration transition state.

Atom or fragment	Charge (cis)	Charge (trans)
C1	-0.51	-0.56
C2	+0.15	+0.24
C6	-0.11	-0.13
C7	-0.16	-0.14
P + Au	+1.13	+1.13
Ph + C7 + H14	+0.18	+0.17

Thus, we isolate the responsible electronic phenomenon for the stabilisation of the favoured transition state to the delocalisation described with the second order perturbation theory analysis. As the resonance onto the allyl is described in a very different way, and only with regards to the ease of donating onto an η^3 system, it is consistent with the derived interpretation that we suggested earlier. The improved overlap in aromatic $\pi \rightarrow \sigma^*$ donation allows the weakening of the bicyclobutonium σ bonds, allowing more extensive delocalisation and therefore lowering the energy of the geometry of the transition state. Stable bicyclobutonium cations present as intermediates had been studied according to their stability in the past and, while not directly analogous, comparable substituent effects were observed.[51]

To validate this analysis, **TS*E*-X2** should not show the same degree of delocalisation in other measurable properties. The NBO (NPA) charges of the carbocation are somewhat higher for the *E*-isomer, at +0.24, when compared to the *Z*-isomer, at +0.15. While the difference seems small, it must be noted that both cases benefit from σ delocalisation and no huge changes were expected.

The *endo*-type cleavage results in the formation of six-membered ring products, but the initial step is also a 5-*exo*-dig cyclisation. Of the known substrates, 1,6-enynes with sulfonamide or ether tethers have been found to favour the *endo*-type skeletal rearrangement instead of the more common *exo*-type single-cleavage.[9] This is the case as long as the alkene does not contain very electron-rich substitution, such as in substrate ***E*-1.7j**, for which *Z*-selective *exo*-type cleavage was the major product. However, as this

[51] Creary, X. 3-*t*-Butyl-1-methylcyclobutyl Cation. Experimental vs Computational Insights into Tertiary Bicyclobutonium Cations. *J. Org. Chem.* **2020**, *85*, 7086-7096.

substrate also showed the formation of tetrahydropyridine **1.9j**, we explored this system with the intention of reproducing the stereoconvergence as well as the competition of the *endo*-pathways. As mentioned previously, the tosylamide tether was simplified to a methanesulfonamide.

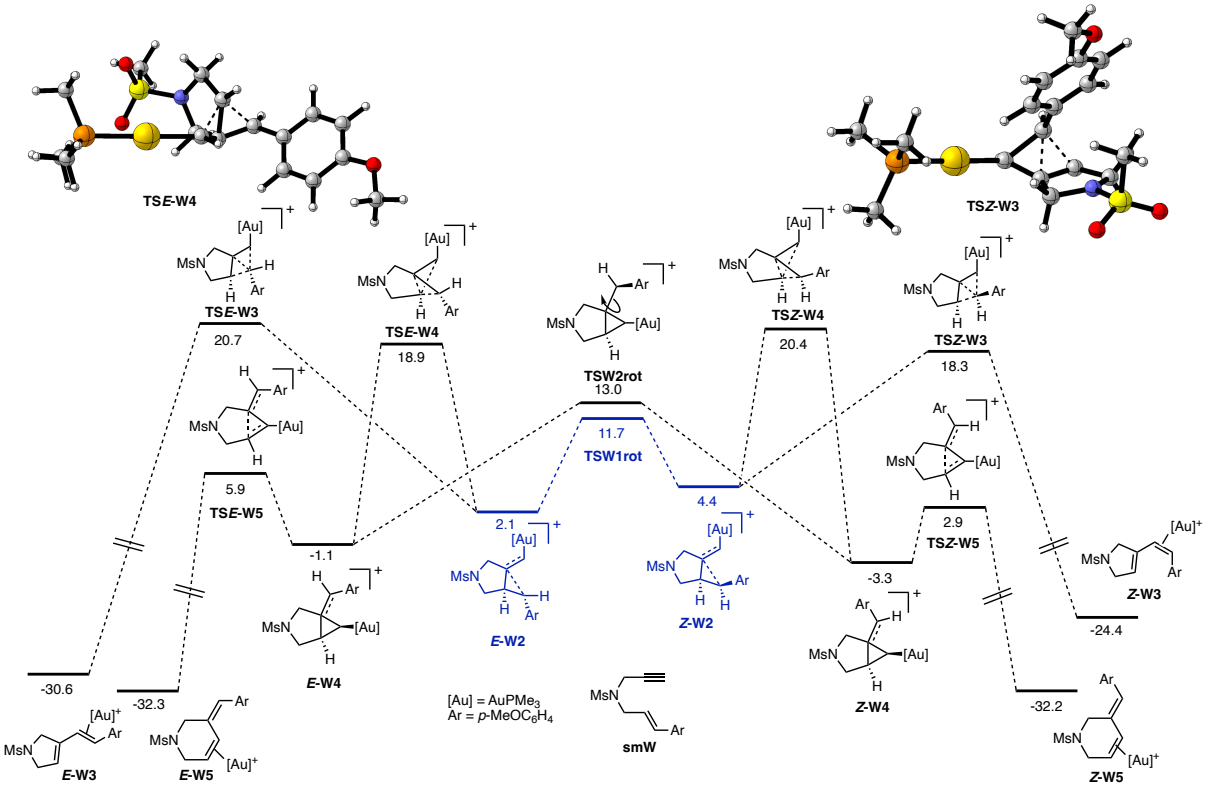

Scheme 20. Gold(I)-catalysed exocyclic and endocyclic single cleavage skeletal rearrangement of 1,6-enyne **smW**. Free energy (B3LYP-D3/6-311G+(d,p) + SDD, PCM) in kcal mol^{-1}.

Referencing the system to ***E*-W1**, not shown in Scheme 20 for clarity, the system reaches analogous intermediates to those in Scheme 13 by 5-*exo*-dig cyclisation. These can interconvert through transition state **TSW1rot**, which is energetically accessible and much lower in energy than any migration process. This results in scrambling ***E*-** and ***Z*-W2** through bond rotation as with malonate tethers. The system then displays a complex fourfold competition, which was found experimentally to favour ***E*-W5** and ***Z*-W3**. The computational model fully reproduces this selectivity, showing a 2.4 kcal mol^{-1} preference for ***Z*-W3** of the two *exo* pathways. In addition, the most favoured *endo*-type TS, ***E*-W5**, lies less than 1 kcal mol^{-1} above the major product, which is fully consistent with the experimental observation of **1.9j** as a minor product.

While *exo*-cleavage proceeds in a concerted manner, *endo*-cleavage is a stepwise process with cyclopropylgold(I) carbocation intermediates ***Z*-** and ***E*-W4**, followed by a concerted asynchronous process in which initial ring-opening is followed by change in hapticity.

Intermediates ***Z***- and ***E*-W4** are in principle capable of bond rotation, which could allow further scrambling of stereochemical information (and stereoconvergence would depend on the difference in energy between ring-opening barriers **TS*E*-W5** and **TS*Z*-W5**). Bond rotation barrier **TSW2rot** was found to be much higher than either of the ring opening transition states, and thus was not relevant in the reaction mechanism. Stereoconvergence in the case of the *endo*-cleavage products is also determined by **TSW1rot**; hence, the computational results suggest that the *endo*-cleavage process is stereoconvergent and selective for ***E*-W5**.

The energy profile reproduces the experimental evidence for the ratio of *exo* and *endo* products, taking into account that these have been performed with a simplified model. Nevertheless, the explanation for the substrate dependence of this selectivity, both for the tether and the alkene substituents, remained to be explained.

Carbene migration transition states **TS*E*-W4** and **TS*Z*-W4**, as the rate-determining steps in the endocyclic cleavage, are comparable to the *exo*-cleavage alternatives in that they consist of a carbene fragment migrating across an allylic system (even if distorted and heavily sp^3). Critically, in both cases, there is a fully formed bond to the benzylic carbon. As electron-donating substituents drive the bonding situation away from gold(I) cyclopropylcarbene structures and towards open-form carbocations, as we have widely discussed, the TS geometry for endocyclic cleavage would be less accessible than the exocyclic cleavage, in which the TS geometry requires a partial cleavage of all bonds to the benzylic carbon. Less electron-donating substituents, apart from not showing the Curtin-Hammett behaviour leading to stereoconvergence, also allow the *endo*-type cleavage to proceed.

Moreover, there is an important steric effect: intermediates ***E*-W4** and ***Z*-W4** both show the {LAu} fragment as being oriented *endo* with respect to the bicyclic system. This is not problematic for the studied sulfonamide tether, which can reorient the nitrogen lone pair towards that region of space. However, a dimethyl malonate or a diphenyl sulfone tether is always too sterically encumbered to facilitate the pivoting of the gold fragment towards this position. This derivation would address the question of why bulkier tethers invariably favour exocyclic cleavage processes.

We then focused our attention on the double-cleavage skeletal rearrangement of 1,6-enynes. This process, which is preferred for internal alkynes especially when the alkene moiety is monosubstituted, had not been comprehensively explored computationally. Even though some trends had been observed with regards to the substitution patterns,[40] there had been no unified explanation for all the observed substrate-dependent switches in single- to double-cleavage selectivity. We explored a simplified model substrate with the aim of explaining the origin of this reactive pathway.

1-Octen-6-yne was chosen as the model substrate, as our previous results suggested that the impact of the tether only affected *exo*- and *endo*-type cleavage selectivity, which is not present in double cleavage

reactions. The gold(I) complex **R1** undergoes a 5-*exo*-dig cyclisation leading to gold(I) α-cyclopropylcarbene **R2**. This species can then undergo the same carbene migration as found in the exocyclic single cleavage processes through transition state **TSR3**, which is the rate-limiting step. Relaxation of this transition state proceeds through a non-stationary geometry, or hidden intermediate, shown in blue, which is reminiscent of cyclopropylgold carbocations ***E*-W4** and ***Z*-W4** in the endocyclic single-cleavage mechanism. However, these geometries relax in a barrierless manner to **R3**. Intermediate **R3** presents a C_{alkene}-C-CAu bond angle of 90.1°, which is consistent with a strong donation from the alkene to a gold carbene species. Similar bond angles are found for various intermediates presented in section 1.3.1 of this manuscript. Rearrangement to open form **R4** through a shallow transition state affords, after facile hydrogen migration, product **R5**. The final transition state, **TSR5**, is actually a concerted asynchronous process in which 1,2-hydride shift facilitated by the alkene is only afterwards followed by hapticity change.

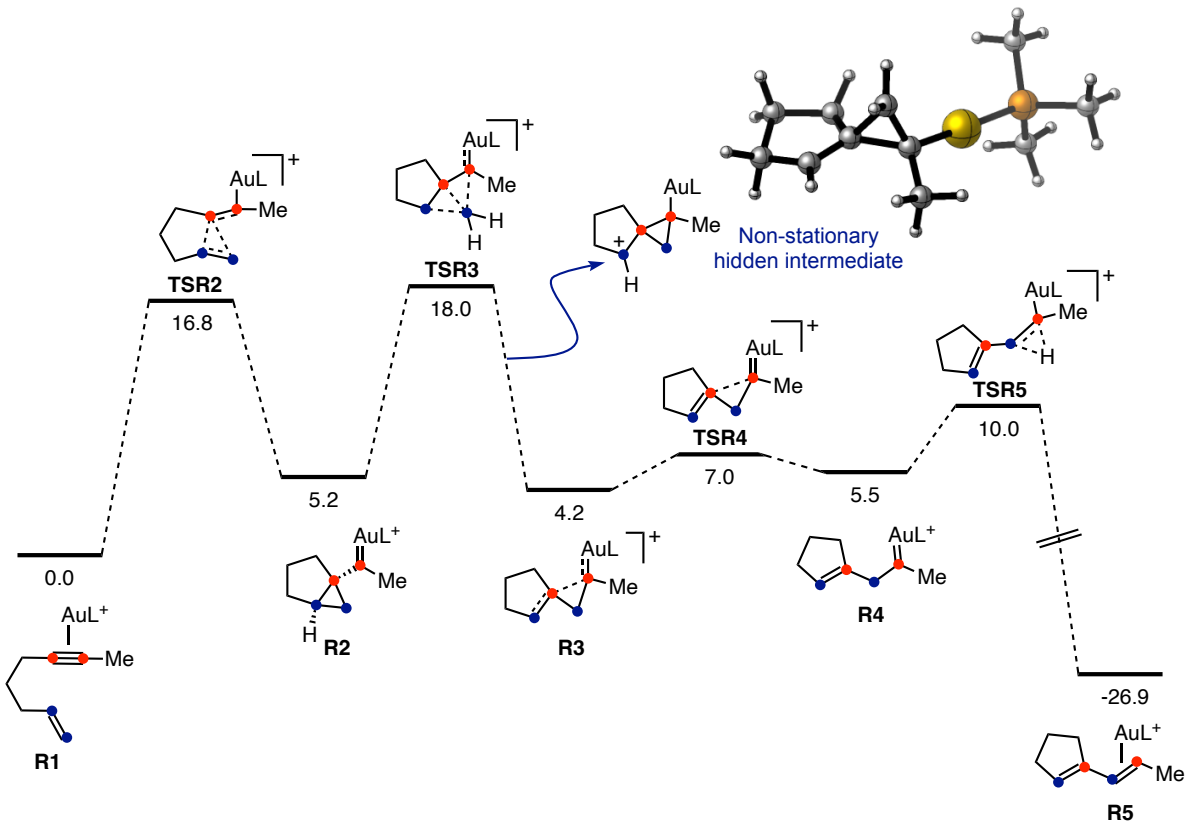

Scheme 21. Gold(I)-catalysed double cleavage skeletal rearrangement of a methyl-capped 1,6-enyne. Free energy (B3LYP-D3/6-311G+(d,p) + SDD, PCM) in kcal mol^{-1}.

What determines whether a substrate leads to single cleavage or double cleavage depends primarily on the barrierless relaxation of the cyclopropylgold-carbocation hidden intermediate or, in the event that there is a real minimum for this geometry, on the relative cleavage barriers of either cyclopropylic bond

(Scheme 22). Therefore, the electronic properties of this geometry are critical in understanding the outcome of enyne skeletal rearrangements.

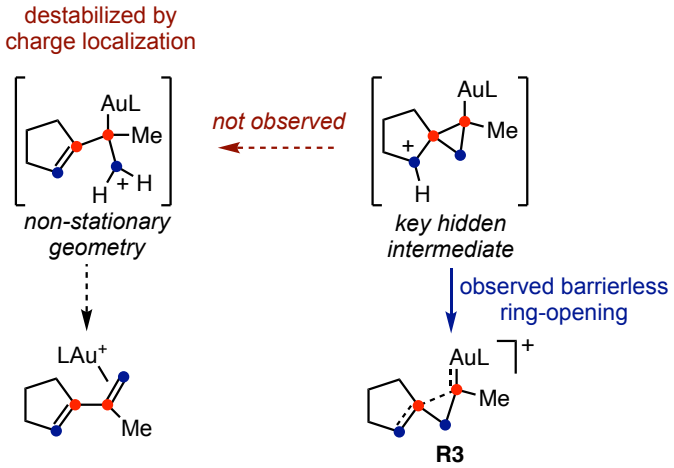

Scheme 22. After reaching the common hidden intermediate after the rate-determining step, the subsequent barrierless evolution thereof is what determines whether a single-cleavage or double-cleavage process occurs.

The preference for enynes consisting of internal alkynes with terminal alkenes to undergo this mechanism is fully explained by this analysis: the relative stabilisation of each carbocation (Scheme 22) leads to the immediate cleavage of what was the remaining alkyne bond. The close geometric proximity of all processes in these intrinsic reaction coordinates, both in single-cleavage and double-cleavage mechanisms, results in direct product formation for only one of the two pathways. A stepwise process would result in several stages of competition between pathways, which would be more likely to lead to mixtures of single- and double-cleavage products. The coalescence of the carbene migration and cyclopropyl ring-opening into one single TS is fully consistent with the experimental observation that all known substrates undergo one of these two gold(I)-catalysed cycloisomerisations selectively and never both.

It can be observed that analogous processes should, in principle, exist for the endocyclic migration pathways too (Scheme 23). The most likely reason for no such endocyclic double cleavage products being reported in the literature is that, for any known substitution patterns, the single-cleavage ring-opening is likely to be favoured. Nonetheless, it would not be far-fetched to assume that appropriate substrate design based on this mechanistic reasoning could lead to the first experimental examples of endocyclic double-cleavage products, especially as the *endo*-type cleavage of ***Z*-W2** and ***E*-W2** were found to have a cyclopropylgold(I) species not as a non-stationary hidden intermediate but as a minimum.

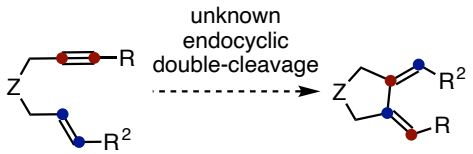

Scheme 23. Bond connectivity that would arise from a hypothetical endocyclic double-cleavage process.

An alternative mechanism for the formation of product **R5** from **R4** would involve deprotonation alpha to the intermediate carbene followed by protodemetallation of the vinylgold species that would form. However, the hydrogen migration is remarkably accessible, at a $\Delta G^{\ddagger} = 4.5$ kcal mol^{-1}, and the reactions proceed in the absence of external proton shuttles. A mechanism involving deprotonation should also lead to a skipped diene product, by deprotonation of the less sterically hindered methyl group, but these compounds are never observed experimentally. Our proposed pathway, which involves 1,2-hydride shift at the peak of the TS, would explain the full 1,3-diene selectivity because the alkene greatly stabilises the build-up of positive charge on the allylic carbon (whereas 1,2-hydride shift from the methyl group would be disfavoured).

Enyne alkoxycyclisations and racemisation pathways[52]

As explained in the introduction, gold(I) complexes in catalysis, in addition to skeletal rearrangements, can undergo reactions with external nucleophiles or bases. When an alcohol is used as the intermolecular partner, it can have the role of either a nucleophile or a base, leading to alkoxycyclisation of enynes or, when acting as a base (through elimination), cycloisomerisation of enynes. In the enantioselective versions of such processes, an enantiodetermining cyclisation forms gold(I) cyclopropylcarbene or vinylgold(I) intermediates, whereafter trapping with an external nucleophile fixes the configuration of the stereogenic centre that had already formed (Scheme 24)

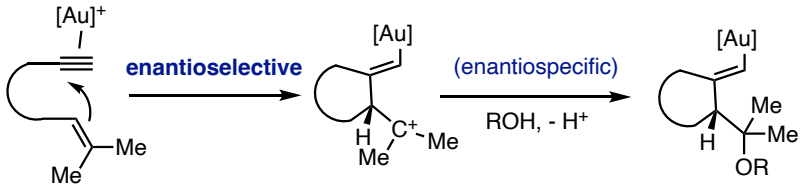

Scheme 24. Straightforward model of enantiodetermination in an enyne alkoxycyclisation.

A unique phenomenon sporadically noticed, although rarely reported, in enantioselective gold(I)-catalysed alkoxycyclisation of enynes is the observed dependence of the enantiomeric ratio on the

52 All experimental work described in this subsection was performed by Andrea Cataffo and Anna Arnanz. Such work is mentioned for context, coherence and discussion of the computational work.

quantity or type of nucleophile.[53,54,55] This is counterintuitive, as the enantiodetermining step should be the gold(I)-catalysed enyne cyclisation. According to the simplified picture (Scheme 24), one would expect the enantiomeric ratio to be fully independent of the equivalents of nucleophile used. The only effect that would be expected would be down to changes in the solvent composition at higher concentrations of alcohol.

However, in the case of some enynes, we found that the outcome of the reaction catalysed with a chiral gold(I) complex would vary greatly both in terms of chemoselectivity (between alkoxycyclisation and elimination) and in terms of enantiomeric excess, varying as a function of the equivalents of alcohol nucleophile down to 1 equivalent with respect to the substrate (Scheme 25 and Table 11).[52] With the intention of exploring these effects and understanding what processes can lead to such racemisation, loss of enantioselectivity or other forms of enantiomeric scrambling, we carried out DFT calculations which, in combination with (and guiding) control experiments, could explain the observed abnormal alcohol dependence.

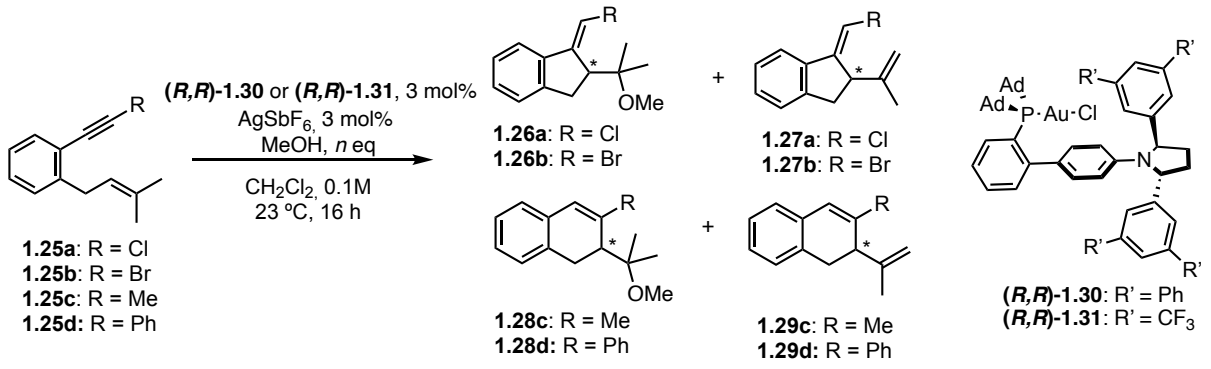

Scheme 25. General reactivity pattern of 1,6-enynes in enantioselective gold(I)-catalysed cyclisation and alkoxycyclisation reactions.

Table 11. Results of the enantioselective (alkoxy)cyclisation reactions from Scheme 25, reported as yield%, *er*. Reactions performed under inert atmosphere using dry solvents. Yields reported are NMR unless otherwise stated.

MeOH	1.26a	1.27a[a]	1.26b[b]	1.27b[b]	1.28c[c]	1.29c[a]	1.28d[d]	1.29d[d]
0 eq	/	25%, 58:42	/	7%, 50:50	/	/ [e]	/	/ [e]
1 eq	26%, 63:37	50%, 57:43	47%, 66:34	18%, 63:37	6% n/d	37%,	3%, 89:11	42%, 89:11

53 Martínez, A.; García-García, P.; Fernández-Rodríguez, M. A.; Rodríguez, F.; Sanz, R. Gold(I)-Catalyzed Enantioselective Synthesis of Functionalized Indenes. *Angew. Chem. Int. Ed.* **2010**, *49*, 4633–4637.

54 Zuccarello, G.; Mayans, J. G.; Escofet, I.; Scharnagel, D.; Kirillova, M. S.; Pérez-Jimeno, A. H.; Calleja, P.; Boothe, J. R.; Echavarren, A. M. Enantioselective Folding of Enynes by Gold(I) Catalysts with a Remote C_2-Chiral Element. *J. Am. Chem. Soc.* **2019**, *141*, 11858–11863.

55 Franchino, A.; Martí, À.; Echavarren, A. M. H-Bonded Counterion-Directed Enantioselective Au(I) Catalysis. *J. Am. Chem. Soc.* **2022**, *144*, 3497–3509.

					~ 67:33			
2.5 eq	40%, 71:29	2% n/d	80%, 74:26	16%, 64:36	9% n/d	59% n/d	10%, 89:11	67%, 90:10
5 eq	82%, 72:28	7% n/d	77%, 78:22	11%, ~ 60:40	20%, 85:15	17% n/d	39%, 89:11	20%, 89:11
10 eq	89%, 71:29	/	77%, 80:20	10%, ~ 60:40	65%, 87:13	6% n/d	67%, 93:7	18% n/d
50 eq	94%, 72:28	/	88%, 76:24	/	71%, 95:15	/	75%, 85:15	/

[a] Due to stability, *er* determined from crudes.[b] Isolated yields.[c] Some 5-*exo*-dig products also observed. [d] **(*R,R*)-1.31** used instead of **(*R,R*)-1.30**. [e] Elimination products formed as traces, substituted naphthalenes were the major products.

In order to study this behaviour, we focused on chloroenynes, methyl-capped and phenyl-capped enynes. Initial control experiments with bromoenynes showed that the preformed products did not undergo racemisation under the reaction conditions. Any observed changes in overall enantiomeric ratio of the products would therefore have to occur during the reaction itself.

Modelling Alkoxycyclisations and Eliminations

Our first hypothesis was that the racemisation occurred to the reaction intermediates, which was supported by experimental evidence that the products were stable (and did not lose enantiopurity) under the reaction conditions (Scheme 26).

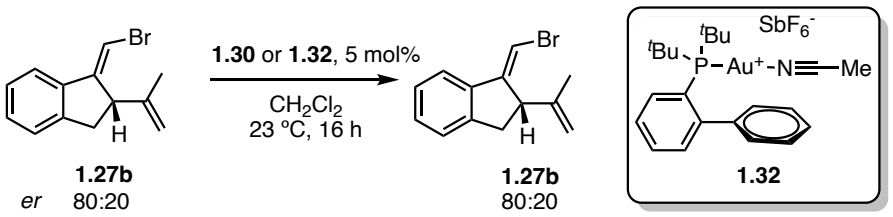

Scheme 26. Control experiments show no racemisation of the final products.

To address this issue, and as the system must present a case of racemisation and not of enantioselectivity if the two products have different enantiomeric ratios, we searched the possible pathways that could interconvert the two chiral products. In that way, and as the enantioselectivity with the chiral ligand was not to be modelled, the ligand on gold was simplified to trimethylphosphine (which proved robust for most applications in our previous work detailed in **Chapter I**, except when sterics played a significant role).

As in previous studies of cycloisomerisation mechanisms, the calculations were performed with B3LYP-D3, modelling the solvent (dichloromethane) with implicit solvation using the polarisable continuum model. Similarly, the counteranion was excluded – even though previous work had described non-trivial involvement of hexafluoroantimonate,[56] there were some important methodological flaws[57] and, when we addressed these, we confirmed that the anion did not have any significant directional interaction. Thus, the weakly coordinating anions were excluded.

The cyclisation of haloenynes, with a halogen substituent on the alkyne, has been found to be selective for *exo*-dig cyclisations presumably to prevent build-up of positive charge α to the electronegative halogen atom. In the reactions carried out with chloroenynes with our system, this was also observed experimentally, with no 6-*endo*-dig products found. We decided to model the different cyclisation transition states and intermediates with the aim of reproducing this experimental observation, also serving as validation for the model (Scheme 27).

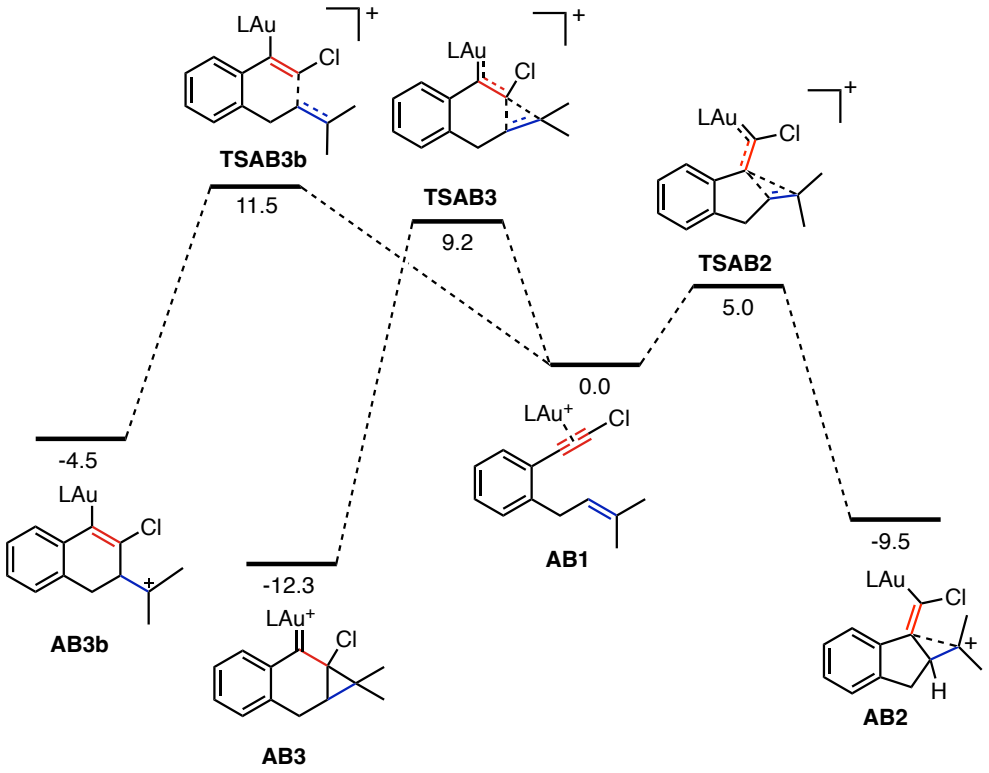

Scheme 27. Competition between 5-*exo*-dig and 6-*endo*-dig barriers with gold(I) chloroenyne complex **AB1**, consistent with the experimental observations. Free energy in kcal mol^{-1} at B3LYP-D3/6-311+G(d,p) + SDD, PCM.

56 Zhou, L.; Zhang, Y.; Fang, R.; Yang, L. Computational Exploration of Counterion Effects in Gold(I)-Catalyzed Cycloisomerization of *Ortho*-(Alkynyl)Styrenes. *ACS Omega* **2018**, *3*, 9339–9347.

57 Optimisation without implicit solvation of the ion pairs resulted in very short cation–anion distances; when we included PCM in the optimisation of the same structures, these short contacts disappeared and no other reported stabilisations were reproduced.

With intermediate **AB1** as the starting point, transition states **TSAB3** and **TSAB3b** led to 6-*endo*-dig-type products and transition state **TSAB2** led to the 5-*exo*-dig product **AB2**. The difference in energy was larger than 4 kcal mol^{-1}, consistent with the full selectivity towards **AB2** as found experimentally.

Our objective was to model all productive pathways from intermediate **AB2**, that is, the alkoxycyclisation and the elimination pathways. Both of these processes require the alcohol, whether to act as a nucleophile or as a base. However, to understand the nucleophile dependence, it would be necessary to model the full mechanisms including the deprotonation and the nucleophilic attack of the alcohol (with eventual product formation). That last section of the mechanisms was something which had not been calculated in previous computational studies, which stopped at the carbocationic precursors.[58,59] This was reasonable, seeing as the ulterior chemistry was expected to be unimportant (and thermodynamically downhill) and the inclusion of alcohols presented significant computational challenges that would not improve the mechanistic explanations in those studies.

One of the unsolved questions was the correct model to use: is methanol present as a monomer in dichloromethane? The implications of the speciation are not trivial, with the most important difference being the pKa of oligomeric species due to the better solvation of the proton. Previous work on the methanol cluster speciation in methanol had suggested tetramers, hexamer, octamers and tridecamers were the major structures.[60,61]

To approach this question, we calculated several neutral and protonated clusters of methanol, optimising the structures with B3LYP-D3/6-31G(d) and running single-point calculations with 6-311+G(d,p), with dichloromethane implicit solvation (PCM). The results showed that the main neutral species would be monomeric methanol, whereas the protonated species would generally favour clusters of higher order (Figure 9). However, the hexamers that had been found to be the major species in pure methanol could not compete entropically with the smaller clusters.

58 Virumbrales, C.; Suárez-Pantiga, S.; Marín-Luna, M.; Silva López, C.; Sanz, R. Unlocking the 5-*exo* Pathway with the Au^{I} -Catalyzed Alkoxycyclization of 1,3-Dien-5-ynes. *Chem. Eur. J.* **2020**, *26*, 8443–8451.

59 Martín-Torres, I.; Ogalla, G.; Yang, J.; Rinaldi, A.; Echavarren, A. M. Enantioselective Alkoxycyclization of 1,6-Enynes with Gold(I)-Cavitands: Total Synthesis of Mafaicheenamine C. *Angew. Chem. Int. Ed.* **2021**, *60*, 9339–9344.

60 Boyd, S. L.; Boyd, R. J. A Density Functional Study of Methanol Clusters. *J. Chem. Theory Comput.* **2007**, *3*, 54–61.

61 Teh, S.; Hsu, P.-J.; Kuo, J.-L. Size of the Hydrogen Bond Network in Liquid Methanol: A Quantum Cluster Equilibrium Model with Extensive Structure Search. *Phys. Chem. Chem. Phys.* **2021**, *23* , 9166–9175.

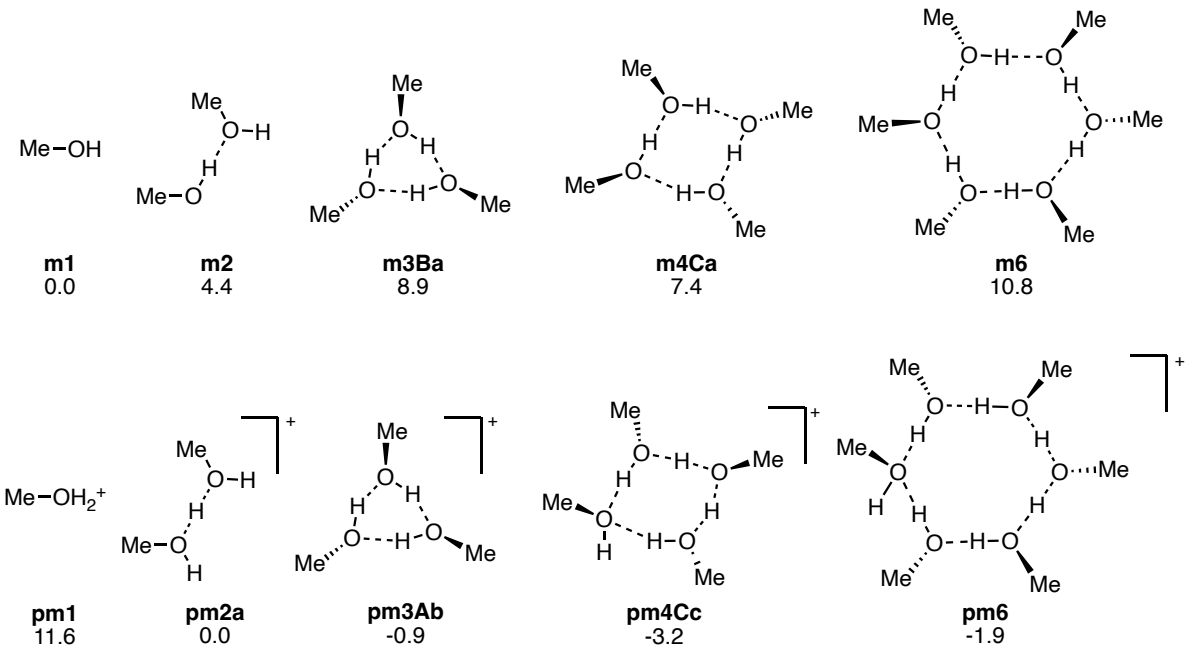

Figure 9. Calculated neutral and protonated methanol clusters in dichloromethane (modelled with PCM). Free energy in kcal mol^{-1} at B3LYP-D3/6-311+G(d,p), PCM (dichloromethane).

From these results, we decided to use monomeric methanol where possible as the main neutral alcohol reference, but due to the high destabilisation of protonated methanol (**pm1**, $CH_3OH_2^+$) with respect to the protonated dimer or higher oligomers, we used $[H(MeOH)_2]^+$ **pm2a** as the simplest model that approximates the real behaviour in solution. Implicitly, the deprotonated intermediates can all be stabilised by a further 3.2 kcal mol^{-1} by coordination of two additional methanol molecules to the protonated dimer (forming **pm4Cc**).

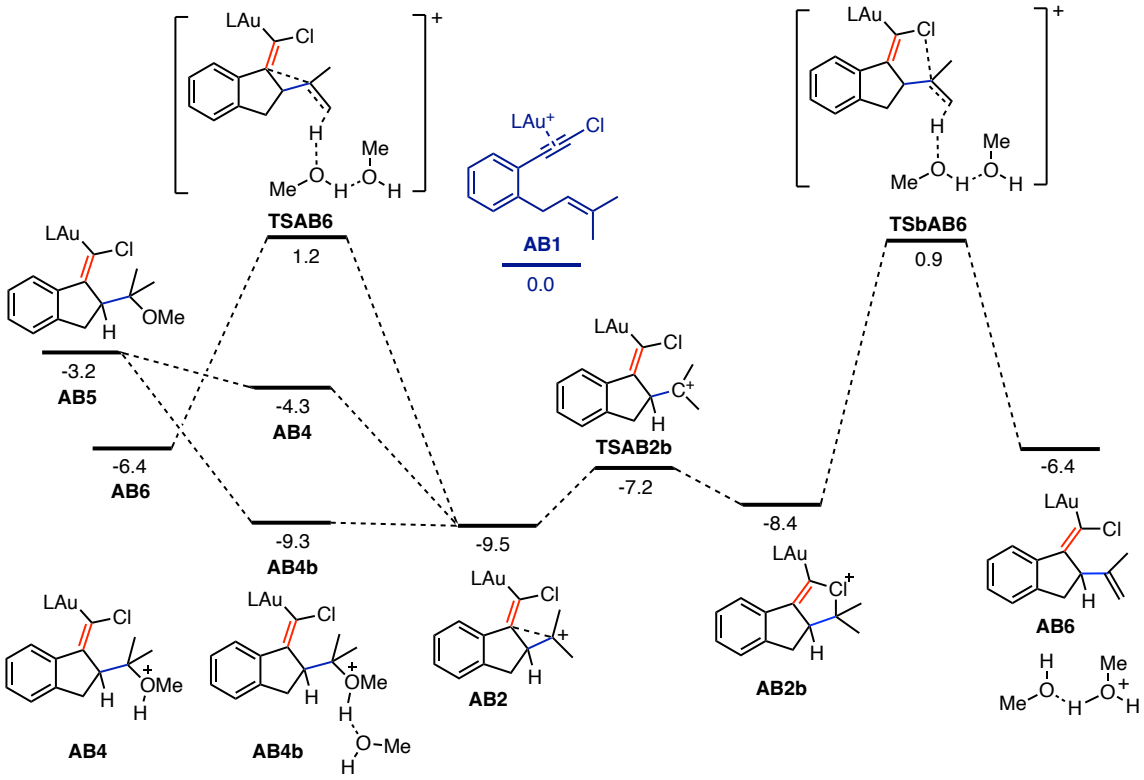

Scheme 28. Evolution of intermediate **AB2** in elimination or alkoxycyclisation processes. Free energy in kcal mol^{-1} at B3LYP-D3/6-311+G(d,p) + SDD.

The first observation that can be made is the existence of an equilibrium between a cyclopropylcarbene intermediate **AB2**, which is formed directly in the cyclisation, and a cyclic chloronium species, **AB2b**, only marginally destabilised with respect to the former. Intermediate **AB2** can undergo elimination, through transition state **TSAB6**, or methanol addition to form **AB4** (and **AB4b**). On the other hand, chloronium **AB2b** can only undergo E2 elimination (**TSbAB6**) due to sterics.

It is remarkable that **AB4** is higher in energy than **AB2** while being a barrierless process: this would imply the immediate dissociation of methanol from the cation. This suggests that the alkoxycyclisation needs a larger cluster than the monomer to be attacked directly in a productive process to prevent charge build-up on the oxygen atom. For this reason, we modelled the intermediate with the dimer (**AB4b**), trimer (**AB4c**) and tetramer (**AB4d**) to understand which would be the most accurate (Scheme 29). The dimer was found to be the most favourable structure.

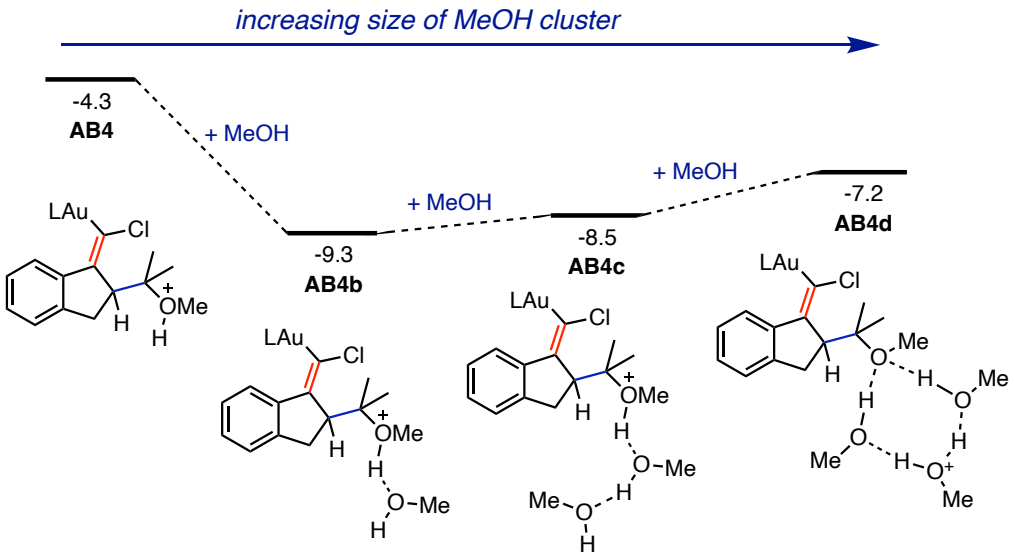

Scheme 29. In the methanol addition to the carbocation, the preferred cluster (from the most stable intermediate) was found to be the dimer. Free energy in kcal mol^{-1} at B3LYP/6-311+G(d,p) + SDD.

Unsurprisingly, attempts to find the transition state to deprotonate alkoxycyclisation intermediate **AB4** failed both directly and through interpolative methods, hinting at a close-to-barrierless process. Since a wide range of methanol-containing species are accessible, several almost isoenergetic pathways presumably coexist. This is due both to the poor characterisation of the methanol clusters when attached to the gold(I) complexes and the sheer combinatorial branching out of accessible mechanisms. Indeed, **AB4b** could evolve to deprotonated **AB5** in a number of ways: (1) by deprotonation with methanol dimer **m2**, followed by loss of methanol; (2) by formation of trimeric adduct **AB4c**, followed by loss of a protonated dimer; (3) by formation of higher-order adducts followed by loss of protonated clusters and/or free methanol. Moreover, the proton transfer barriers or dissociation of methanol clusters are always expected to be relatively low, especially when larger clusters are involved. Because of this, we focused on the thermodynamics of these steps. We considered **AB4b** (the most stable species) and deprotonated **AB5** as models for the alkoxycyclisation.

From first principles, and by comparison to Figure 9 with the relative stabilities of protonated clusters, it seems unlikely than a simple dimer could effect this transformation in the reaction, as that would require decoordination of **pm1** which was found to be greatly disfavoured. Our previous results indicate that the speciation of protonated methanol in dichloromethane is probably that of a tetramer (which lowers the concentration of free –neutral– methanol in solution). We propose that higher-order clusters are therefore needed to undergo the full alkoxycyclisation pathway than the elimination. At the very least, with three molecules of methanol, two can stabilise the residual proton and one forms the methyl ether in the alkoxycyclisation, whereas the elimination needs a minimum of two to stabilise the proton from the deprotonation.

The product, **AB5**, was calculated independently as a reference, with the residual proton modelled separately as $[H(MeOH)_2]^+$, **pm2a**. We modelled this solvated proton as a dimer for simplicity. As the elimination product **AB6** is also modelled with a dimer, any differences in the stabilisation of the proton itself cancel out. Therefore, they are independent of whether a dimer, trimer or tetramer are used as the minimum expression for $[H(MeOH)_n]^+$. This model is therefore satisfactory to explain alkoxycyclisation and elimination processes.

On the origin of racemisation

The model presented in Scheme 28, without any further calculations, would represent the general accepted stereospecific cyclisations. The quenching mechanisms therein, whether by deprotonation or overall alkoxycyclisation, do not alter the chirality at the adjacent stereogenic carbon centre.

The difference in enantiomeric ratios has to be the result of a process that racemises intermediates **AB2** or **AB2b**, as the products would not lose optical purity under the reaction conditions. For these reasons, we decided to explore the reactions that could lead to racemisation. The common denominator would be that the stereogenic carbon atom should become sp^2 hybridised. As no reversible interchange (S_N2-type) pathway could be possibly envisioned, the reversible formation of an sp^2 centre was far more likely. In this line, we considered two main possibilities: a 1,2-hydride shift from the stereogenic carbon to the carbocation or deprotonation of the hydrogen on the stereogenic carbon.

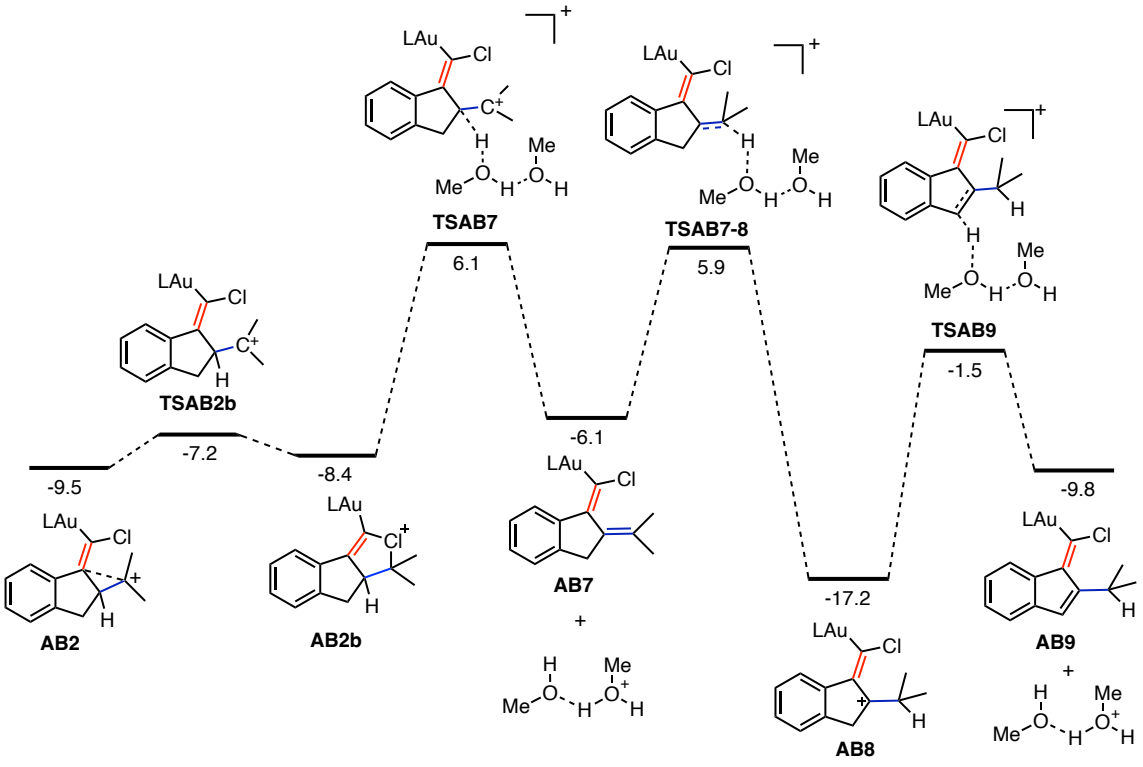

Scheme 30. Racemisation pathway with chloroenyne *via* reversible deprotonation.

The deprotonation pathway initially seemed a very reasonable suggestion: the formation of a conjugated diene **AB7**, in spite of the associated torsional strain, could lead to enantiomeric scrambling by re-protonation **TSAB7** on the other face of the alkene (Scheme 30, same transition state for both enantiomeric[62] protonations).

However, upon closer inspection, there are several reasons why this mechanism is unlikely. The barrier **TSAB7** is 5.2 kcal mol^{-1} higher than the direct elimination (**TSbAB6**), requiring in both cases two molecules of methanol and so having identical molecularity (so no entropic contributions can result in changes in rate with concentration). In addition, vinylgold(I) **AB7** constitutes an example of a neutral gold(I) complex subject to protodemetallation. Hence, an explanation would be necessary for why **AB7** would be apparently unable to undergo protodeauration, when the reverse reaction also requires protonated methanol.

In addition, the protonation on the isopropylic carbon through **TSAB7-8** is of practically the same energy as the reverse reaction. Although within error, **AB8** could be formed under these conditions. Deprotonation **TSAB9** at the benzylic position would be significantly more favourable than the reverse reaction (by 7.4 kcal mol^{-1}). As both processes require a methanol dimer, **AB8** effectively never leads to the major products – assuming a 1:1 ratio between **TSAB7** and **TSAB9**, the enantiomeric scrambling would show a significant quantity of benzofulvene derived from **AB8** if this mechanism were correct.

Continuing the search of racemisation pathways, the 1,2-hydride shift was found to be lower in energy than the deprotonation **TSAB7** (Scheme 31). Along with the fact that the 1,2-hydride shift pathway does not require methanol to operate, it is entropically more likely than intermolecular **TSAB7** and it is more favoured with respect to intermolecular processes at low concentrations of alcohol. In fact, that key observation also matches better with the dependence on the equivalents of alcohol used, because the racemisation would be independent of the alcohol concentration whereas every quenching pathway requires methanol. In spite of the fact that 1,2-hydride shifts are generally associated with thermodynamically downhill (and thus irreversible) processes, there are some examples of reversibility in these processes[63] including the racemisation of a stereogenic sp^3 carbon atom.[64]

62 Diastereomeric in the real system with a chiral catalyst, but due to the larger conformational landscape of non-directed protonations, it is less likely to discriminate *Re* or *Si* faces than the cyclisation step.

63 Hudson, H. R.; Koplick, A. J.; Poulton, D. J. Competitive 1,2- and 1,3-Hydride Shifts in the Thermal Decomposition of n-Alkyl Chloroformates. *Tetrahedron Lett.* **1975**, *17*, 1449–1452.

64 Shapirot, S. S.; Dennis, D. Lactic Acid Racemization in Clostridium Butylicum. Evidence for a Direct Internal Hydride Shift. *Biochemistry*, **1965**, *4*, 2283–2288.

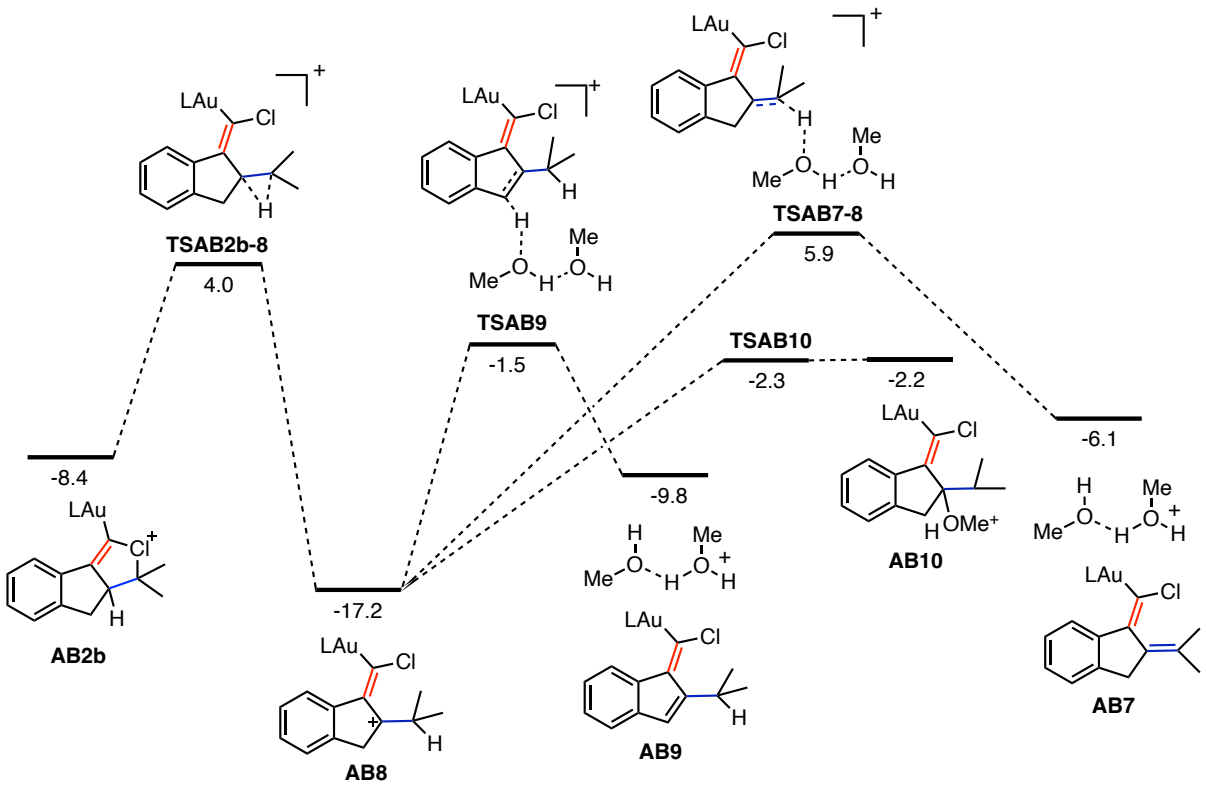

Scheme 31. Racemisation pathway with chloroenyne *via* 1,2-hydride shift. Note that **AB2** has a free energy of -9.5 kcal mol^{-1} and links to **AB2b**.

TSAB2b-8 lies about 3 kcal mol^{-1} higher in energy than the elimination transition states **TSAB6** and **TSbAB6**. This is energetically accessible at lower methanol concentrations. If this process were responsible for racemisation, it should be more important for the examples with lower concentration of methanol, in line with the experimental results.

Intermediate **AB8** can be deprotonated through transition states **TSAB9** or **TSAB7-8**, as well as undergoing a rather unfavourabvle addition to **AB10**. While the benzylic deprotonation can seem very competitive on first impression, at low enough concentrations of methanol in which **TSAB2b-8** is accessed, the reversibility of the intramolecular hydride shift is reasonable.

Our proposal for the disparity in enantiomeric ratios of products **1.26** and **1.27** (modelled with **AB5** and **AB6**) is that initially, when a large quantity of methanol is present, alkoxycyclisation dominates. This reaction happens at a much faster rate than 1,2-hydride shift or than elimination because, in the presence of enough methanol, the residual proton from **AB5** (Scheme 28) can be better stabilised also by higher-order clusters. The effect of methanol concentration on the rate of elimination is smaller because the transition state does not depend as strongly on the presence of higher-order methanol oligomers. At a specific threshold of relative concentrations, elimination becomes favoured because it requires fewer molecules of methanol to complete the catalytic cycle. Simultaneously, the 1,2-hydride shift becomes competitive (not requiring alcohol), which leads to racemisation of the intermediates. Additionally, **AB5** can undergo methanol dissociation in close-to-barrierless process in the presence of any protons,

whereas this reversibility is less facile for **AB6**. This racemisation affects the elimination products more strongly as at lower concentrations of methanol, the alkoxycyclisation products are unlikely to re-form even if the methanol dissociates.

An additional experiment in which 10 equivalents of hexafluoroisopropanol (HFIP) were added to an otherwise dry reaction mixture was carried out. The hypothesis was that due to the very poor nucleophilicity of this alcohol, no alkoxycyclisation product should form, whereas the proton-shuttle involving deprotonation (of a very acidic hydrogen) and subsequent facile protodemetallation should still operate as usual; thus, we expected to isolate the elimination product **1.27b** without any loss in enantiomeric ratio. In accordance with this prediction and consequently with the calculated mechanism, **1.27b** was isolated in an 80:20 *er*, fully comparable of that of alkoxycyclisation and much higher than any enantiopurities of the elimination product hitherto observed (Scheme 32).

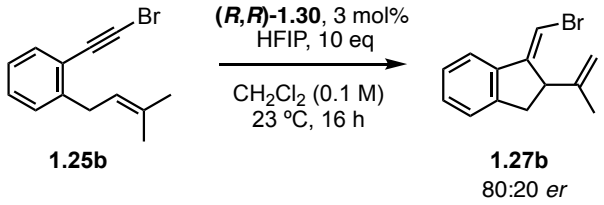

Scheme 32. Enantioselective cycloisomerisation of bromoenyne **1.25b** with high enantiomeric ratios in the presence of a non-nucleophilic alcohol.

We performed a more comprehensive search of mechanisms that could have led to these observed drops in enantioselectivity, but we found them to be less likely. Silver catalysis or Brønsted acid catalysis, with varying kinetics, could in principle form racemic products along the enantioenriched ones from the gold(I)-catalysed pathway. The former was disproven by experiments using a cationic version of the chiral catalyst, which showed high racemisation of the elimination product regardless. Brønsted acid involvement has been found in isomerisation of gold(I)-catalysed products, and such acidic protons are well-understood to originate from cationic intermediates such as **AB2** or **AB2b**.[21] It remained unclear whether these protons could catalyse these same cycloisomerisations as gold(I), potentially explaining the partially racemic product formation.

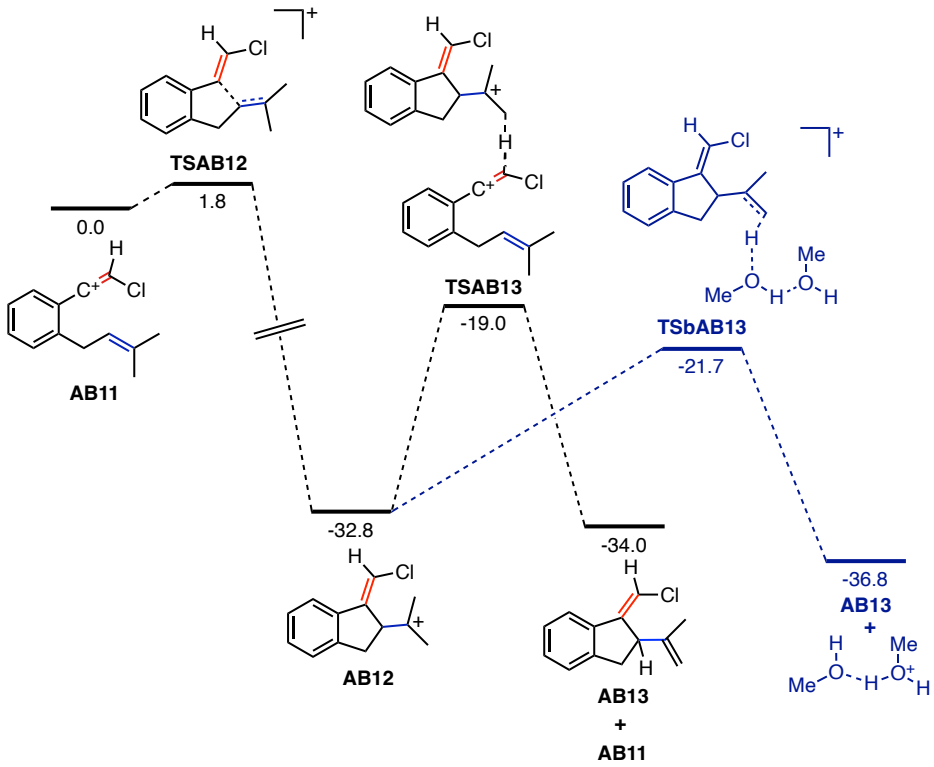

Scheme 33. Mechanism of the proton-catalysed cyclisation. In blue, methanol model for side-deprotonations.

The Brønsted acid-catalysed cyclisation was calculated, displaying low barriers for cyclisation (**TSAB12**) and moderately high barriers for proton transfer to the next enyne (**TSAB13**). Nevertheless, the feasibility of this catalytic cycle does not depend exclusively on having accessible transition states: the reaction medium can intercept most of these intermediates. This is because even if all barriers are acceptable for room temperature processes, all intermediates in this system are extremely acidic. As a consequence, the presence of traces of alcohol, water or any suitable proton shuttles that would be protonated preferentially stop the chain reaction (Scheme 33, pathway shown in blue) – from the relative energies, even 10 mol% of methanol (or water) would completely deprotonate these structures.

Similarly, either intermediate **AB12**, other protonated organic fragments,[65] or the protonated traces of methanol or water can protodemetallate the catalyst: the process is completely barrierless (Scheme 34). Hence, we conclude that the Brønsted acid-catalysed pathway is not competitive under the reaction conditions and cannot be responsible for the racemisation.

65 See Additional Computational Results, in the Experimental Section of **Chapter I**.

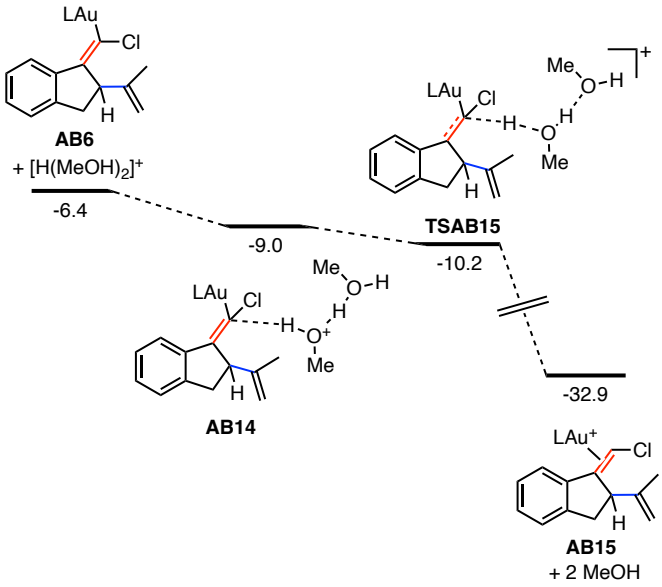

Scheme 34. Mechanism of the protodemetallation of **AB6** with the protonated methanol dimer **pm2a**. **AB14** has a lower electronic energy than **TSAB15**.

Subsequent control experiments confirmed that strong acids could not carry out the enyne cyclisation even in the absence of gold, presumably because of traces of water (Scheme 35).

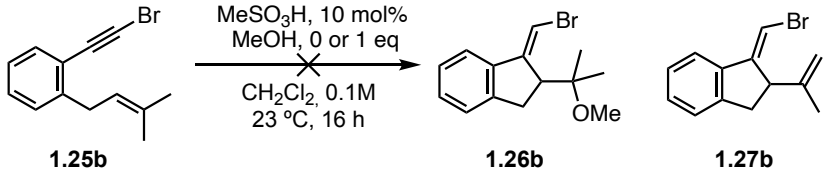

Scheme 35. Control experiment excluding the racemisation via proton-catalysed pathways.

Even if we ignore entropic contributions and consider the protonated methanol tetramer to be the real speciation of the free proton (Figure 9), as the difference in energy between the two methanol clusters is of only 3.2 kcal mol^{-1}, the greatest overall barrier for the protodemetallation would be of about 0.8 kcal mol^{-1} after adding the predissociation cost for **pm4Cc**. This is an upper bound, however, as it is very likely that the dissociation of two neutral methanol molecules can be aided by precoordination to **AB6**. The model presented in Scheme 34 is therefore our best proposal for protodemetallation in spite of simplifying the methanol speciation in such a pKa-sensitive process.

Extension to 6-*endo*-dig mechanisms

In spite of the 6-*endo*-dig pathways becoming energetically feasible for the other studied enynes, the methyl-capped and the phenyl-capped alkynes (hereafter, methylenyne **1.25c** and phenylenyne **1.25d**), both of these substrates should present an analogous 1,2-hydrogen shift pathway. However, the elimination products were found experimentally not to depend on the quantity of nucleophile. In the

same line, alkoxycyclisation and elimination products for the phenylenyne were formed in the same enantiomeric ratios (Table 11), with further formation of 2,3-disubstituted naphthalene products. This presents a conceptual problem, as there would have to be a reason why either the 1,2-hydrogen shift does not occur or why it does not lead to racemisation.

For these reasons and as the results could not be extrapolated in a simple manner, we endeavoured to explain these experimental observations by modelling the methylenyne and phenylenyne systems and contrasting them with the chloroenyne mechanisms.

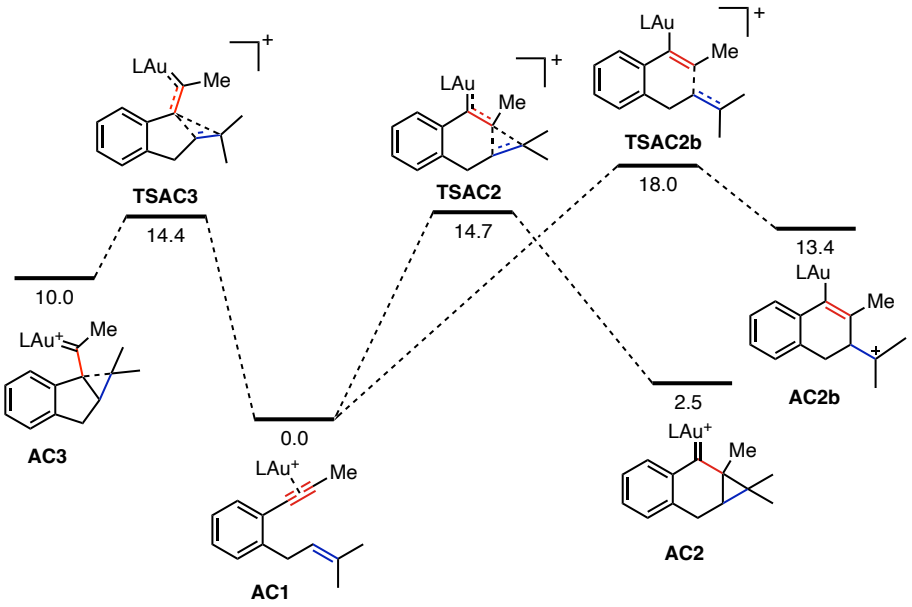

Scheme 36. Competition between 5-*exo*-dig and 6-*endo*-dig barriers for methylenyne **1.25c** consistent with the experimental observations. Free energy in kcal mol^{-1} at B3LYP-D3/6-311+G(d,p) + SDD, PCM.

The methyl-capped substrate complex **AC1** displays almost isoenergetic barriers for the 5-*exo*-dig (**TSAC3**) and the 6-*endo*-dig (**TSAC2**) processes (Scheme 36). This coincides with the product distribution using JohnPhos as the ligand, although the (bulkier) chiral ligand used in the enantioselective reactions proved to be significantly more selective towards 6-*endo*-dig cyclisation.

It is presumed that there could be a transition state for interconversion between **AC2** and **AC2b**, but it was not searched.

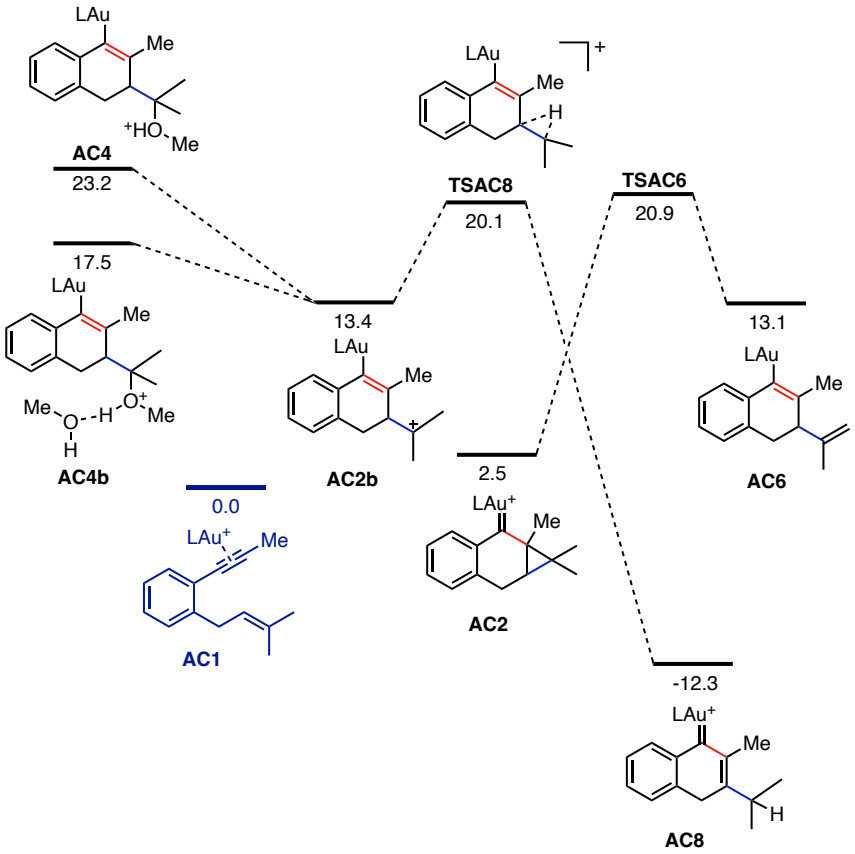

Scheme 37. Evolution of intermediates **AC2** and **AC2b** in elimination or alkoxycyclisation processes, together with irreversible 1,2-hydride shift. Free energy in kcal mol^{-1} at B3LYP-D3/6-311+G(d,p) + SDD, PCM.

As opposed to the case with the chloroenyne substrate, the 1,2-hydride shift through **TSAC8** is completely irreversible, beyond any kinetic consideration, as to return from **AC8** would require more than 32 kcal mol^{-1}. This is consistent with the methylenyne substrate not showing the same racemisation pattern experimentally.

The barrier of 1,2-hydride shift **TSAC8** is, at 20.1 kcal mol^{-1} from the initial complex **AC1**, comparable to elimination and (presumably) alkoxycyclisation. Experimentally, and in particular under dry conditions, 2-methyl-3-isopropylnaphthalene **1.33c** can be the major product (Figure 10, maximum in a 7:2 ratio). In the presence of HFIP as a proton shuttle-mediator, the elimination product and the naphthalene product are formed in an equimolar ratio. **AC8** is reasonably anticipated to form 2-methyl-3-isopropylnaphthalene after deprotonation and protodemetallation, analogously to chloroenyne **TSAB9**. This brings forth more evidence for the mediation of 1,2-hydride shifts in gold(I)-catalysed cyclisations.

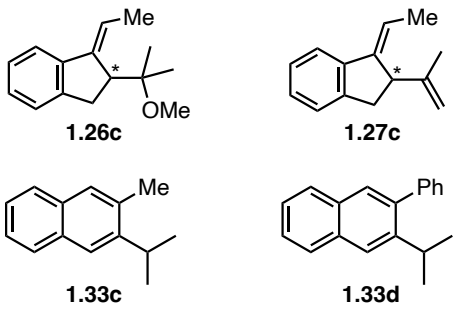

Figure 10. Additional products formed in the alkoxycyclisation/cycloisomerisation reactions of **1.25c** and **1.25d**.

Phenylenyne **1.26d** behaves very similarly to the methyl-capped substrate, showing a slight preference for the 6-*endo*-dig pathway – experimentally, this preference is much clearer, justifying the exclusion of 5-*exo*-dig intermediates in the subsequent computational studies. Similarly, and yet more clearly than for **1.26c**, there is no observed racemisation.

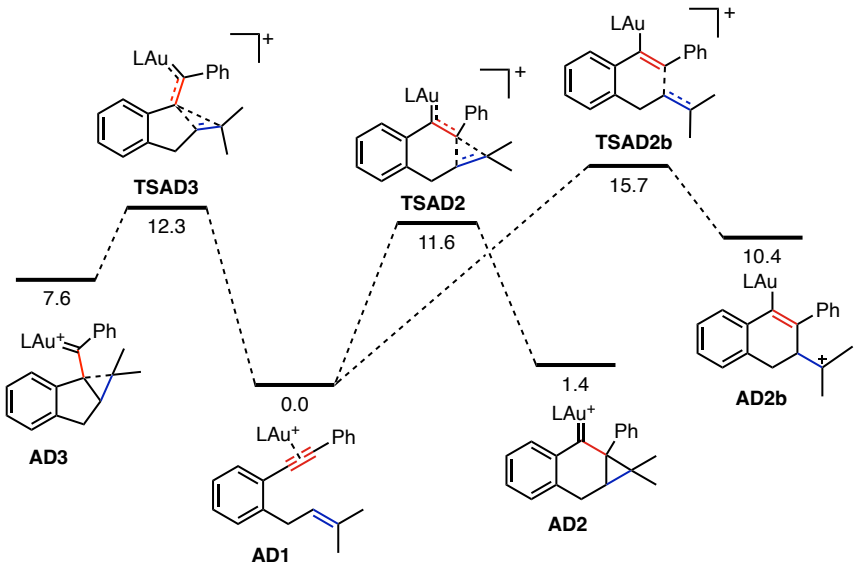

Scheme 38. Competition between 5-*exo*-dig and 6-*endo*-dig barriers for phenylenyne **1.26d** consistent with the experimental observations. Free energy in kcal mol^{-1} at B3LYP-D3/6-311+G(d,p) + SDD, PCM.

In line with the experimental findings, which also find no racemisation on neither the elimination nor alkoxycyclisation products, the 1,2-hydride shift **TSAD8** in this case is also irreversible (Scheme 38). Similarly to the previously described case, 2-phenyl-3-isopropylnaphthalene **1.33d** was also detected experimentally and was the major product under dry conditions.

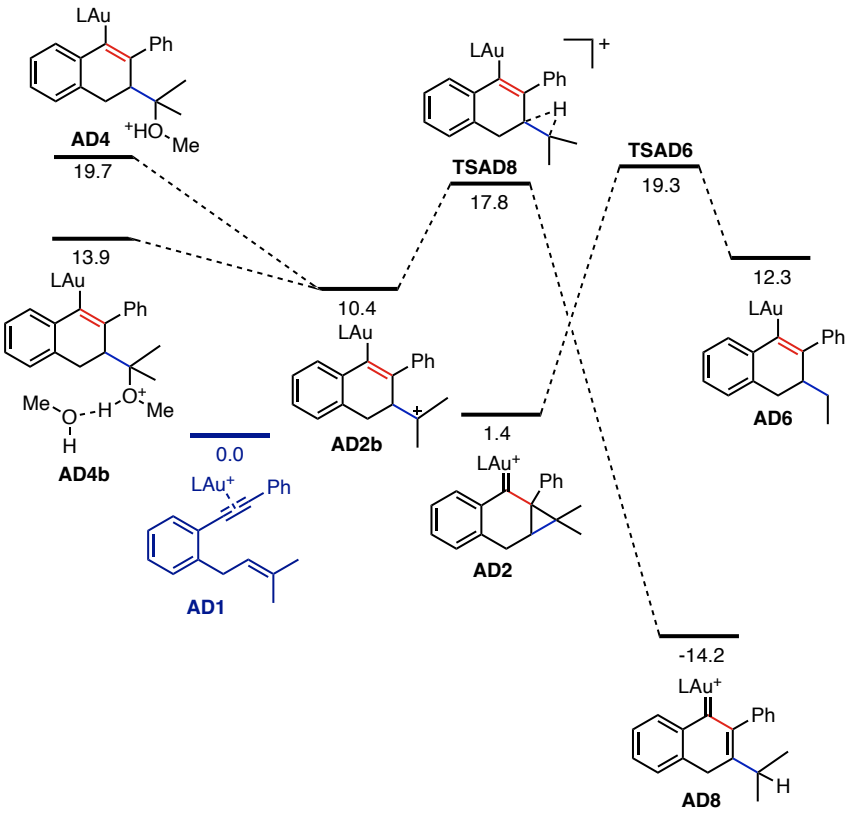

Scheme 39. Evolution of intermediates **AD2** and **AD2b** in elimination or alkoxycyclisation processes, together with irreversible 1,2-hydride shift. Free energy in kcal mol^{-1} at B3LYP-D3/6-311+G(d,p) + SDD, PCM.

The same pathways for racemisation involving deprotonation (**TSAB7** of chloroenyne) were also calculated for the methylenyne and phenylenyne substrates, as well as deprotonations from open-form **AC2b** and **AD2b**. However, all of these pathways were found to be non-competitive. As they were all discussed in more detail with the chloroenyne, they have been excluded from these schemes but their energies are included in the Experimental Section for reference.

Conclusions

The intermediates present in gold(I)-catalysed cyclisations of 1,5-enynes consist of gold(I) α-cyclopropylcarbenes and vinylgold complexes with an endocyclic carbocation. These bonding arrangements occur in both *endo*-dig and *exo*-dig cyclisations. Even though more electron-donating substituents are likely to stabilise exocyclic carbocations, as evidenced in the study of stereoconvergent reactions, it is notable that dimethyl-substituted alkenes do not suffice, whereas this open-form is known for 1,6-enynes with the same substitution. Ring strain is proposed to contribute to this effect.

Endocyclic carbocations are invariably less stable than the cyclopropylcarbene structure, even in the most stabilised cases, and independently from substitution. However, according to the NBO analysis, the *endo*-cyclopropylic bonds are less populated than the *exo* bonds except for some dimethyl-substituted cases, even for 1,6-enyne examples where an open-form *exo*-carbocationic structure is known but no *endo*-carbocationic intermediate exists. **Int4** geometries are just particularly polarised **Int2** structures, and do not show huge differences in the NBO analysis as seen for fully open vinyl-carbocations. They are best understood as a divergent cyclopropylcarbene system.

1,5-Allenenes generally behave analogously to enynes but can form non-classical carbocationic intermediates. However, all can rearrange to form a bicyclo[3.1.0]hexane structure, transannulating from the rear. This is unique to 1,5-allenene systems, as lengthening the tether does not allow the formation of a cyclopropane ring.

With respect to the computational methods, we validate the usage of most functionals for geometry optimisations by indirectly probing their electronic representation of the system. We propose B3LYP-D3 and M06-D3 to be the preferred choices for higher level of theory single-point calculations for energy profiles in gold(I)-catalysed cyclisations.

Gold(I)-catalysed single-cleavage skeletal rearrangements of 1,6-enynes owe their stereoselectivity to the access to a Curtin-Hammett scenario: sufficiently electron-rich alkenes in the substrate will allow a bond rotation that interconverts the *Z* and *E* pathways. The factors determining the *Z*-selective migration are present also in substrates that cannot access the rotational equilibrium. These factors are exclusively electronic and independent of the ligand, stemming from the stabilisation of the bicyclobutonium geometry.

The pathways leading to *endo*-type single-cleavage products are only accessible when the tether does not present a steric impediment. For small tethers, most substrates would be expected to favour this mechanism. Nonetheless, alkenes with strongly electron-donating substituents revert this trend, due to the weakening of one of the key bonds required in the *endo*-migration.

The *endo*-cleavage is expected to be stereoconvergent with electron-rich substituents. Specifically, a preference for the products that would form stereospecifically from *E*-substrates is predicted. While electron-rich substitution also leads to a preference for exocyclic migrations, *Z-ortho*-methoxycinnamyl propargyl ether would be a good candidate to prove this, as the *exo*-type product showed stereoconvergence while the *endo*-type product was still the major product.

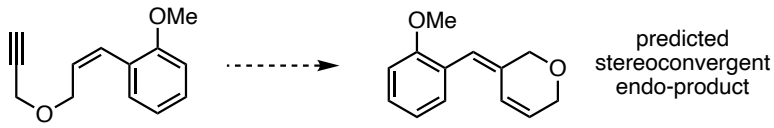

Scheme 40. Stereoconvergence is also expected in the endocyclic single-cleavage skeletal rearrangement.

We also conclude that the single- and double-cleavage selectivity of skeletal rearrangements is explained by the relative cleavage preferences of the cyclopropylgold carbocation non-stationary geometry present in both cycloisomerisations. This dependence on the outcome of a barrierless isomerisation of a common intermediate explains why, experimentally, mixtures of single- and double-cleavage products have never been observed. Our findings explain the origin of the substrate dependence in these processes and hints at the plausible existence of hitherto unreported endocyclic double-cleavage products. We also reassign the final stage of the double-cleavage skeletal rearrangement to the direct formation of the product alkene *via* an initial 1,2-hydride shift, which matches the known experimental regioselectivity.

We have performed the first full calculations of eliminative cyclisation and alkoxycyclisation of 1,6-enynes, confirming that methanol dimers are the minimal alcohol oligomer that can drive the reaction, whereas protonate tetramers are the most stable solvated proton species. While alkoxycyclisation adduct formation is effectively barrierless, the overall deprotonation (or dissociation of protonated methanol clusters) is similar or higher in energy than elimination pathways when methanol dimers serve as proton shuttles. This explained why alkoxycyclisation reactions generally need more alcohol. Protodemetallation of the studied chloroenyne was found to be barrierless, whereas most Brønsted acid-catalysed pathways have moderately high barriers. Thus, acid-catalysed cyclisations are unlikely to mediate these cyclisations, especially in the presence of alcohol or traces of water. We ascribe the racemisation process in phenyl-tethered 1,6-haloenyne cyclisations to be mediated by a reversible 1,2-hydride shift. Methyl- or phenyl-capped enynes show an irreversible 1,2-hydride shift and, consequently, no racemisation is observed. This is consistent with experimental evidence and with the detected naphthalenes that are formed under anhydrous conditions.

Experimental Section

Computational Methods

All calculations were carried out on Gaussian09.[66] The geometry optimisations of the intermediates and transition states in section 1.3.1 were performed with BP86[67]. The geometry optimisations of the complexes in the mechanisms were performed with B3LYP[68]. For both functionals, these calculations were carried out using Grimme's D3 dispersion correction[69] with the 6-31G(d) basis set[70] for non-metal atoms and the SDD[71] basis set and ECP for gold. Single-point energy calculations were performed with the 6-311+G(d,p) basis set for non-metal atoms and SDD basis set and ECP for gold. The implicit polarisable continuum model (PCM)[72] for dichloromethane was used in all calculations and the cationic complexes were modelled with the exclusion of the counter-anions. All stationary points were verified by the absence of imaginary vibrations and transition states confirmed by IRC[73] calculations with the LQA or DVV algorithms. The transition states for the hindered rotations were confirmed with IRC relaxation with Hratchian and Schlegel's damped velocity Verlet algorithm (DVV).[74] The reported free energies were calculated at 298 K and 1 atm. NBO analysis was performed with the NBO3.0 program[75] with B3LYP-D3, the 6-311+G(d,p) basis set for non-metal atoms and SDD basis set and ECP for gold.

Additional Computational Results

In addition to the methanol clusters described in the Results and Discussion, several other cyclic and acyclic trimers and tetramers were calculated and found to be less stable than their counterparts. These are presented here (Figures 11 and 12).

---

66 Gaussian 09, Revision B.1, Frisch, M. J., Trucks, G. W., Schlegel, H. B., Scuseria, G. E., Robb, M. A., Cheeseman, J. R., Scalmani, G., Barone, V., Mennucci, B., Petersson, G. A., Nakatsuji, H., Caricato, M., Li, X., Hratchian, H. P., Izmaylov, A. F., Bloino, J., Zheng, G., Sonnenberg, J. L., Hada, M., Ehara, M., Toyota, K., Fukuda, R., Hasegawa, J., Ishida, M., Nakajima, T., Honda, Y., Kitao, O., Nakai, H., Vreven, T., Montgomery, J. A., Peralta, Jr. J. E., Ogliaro, F., Bearpark, M., Heyd, J. J., Brothers, E., Kudin, K. N., Staroverov, V. N., Kobayashi, R., Normand, J., Raghavachari, K., Rendell, A., Burant, J. C., Iyengar, S. S., Tomasi, J., Cossi, M., Rega, N., Millam, J. M., Klene, M., Knox, J. E., Cross, J. B., Bakken, V., Adamo, C., Jaramillo, J., Gomperts, R., Stratmann, R. E., Yazyev, O., Austin, A. J., Cammi, R., Pomelli, C., Ochterski, J. W., Martin, R. L., Morokuma, K., Zakrzewski, V. G., Voth, G. A., Salvador, P., Dannenberg, J. J., Dapprich, S., Daniels, A. D., Farkas, Ö., Foresman, J. B., Ortiz, J. V., Cioslowski, J., Fox, D. J. Gaussian, Inc., Wallingford CT 2009.

67 (a) Becke, A. D. *Phys. Rev. A.* **1988**, *38*, 3098-3100. (b) Perdew, J. P. *Phys. Rev. B.* **1986**, *33*, 8822-8824.

68 (a) Becke, A. D. *J. Chem. Phys.* **1993**, *98*, 5648; (b) Becke, A. D. *J. Chem. Phys.* **1993**, *98*, 1372; c) Lee, C.; Yang, W.; Parr, R. G. *Phys. Rev. B* **1988**, *37*, 785.

69 Grimme, S. Density Functional Theory with London Dispersion Corrections. *WIREs Comput Mol Sci* **2011**, *1*, 211–228.

70 Hehre, W. J.; Ditchfield, R.; Pople, J. A. Self–Consistent Molecular Orbital Methods. XII. Further Extensions of Gaussian–Type Basis Sets for Use in Molecular Orbital Studies of Organic Molecules. *J. Chem. Phys.* **1972**, *56*, 2257–2261.

71 Andrae, D.; Häußermann, U.; Dolg, M.; Stoll, H.; Preuß, H. Energy-adjusted ab initio pseudopotentials for the second and third row transition elements. *Theor. Chim. Acta* **1990**, *77*, 123–141.

72 Cancès, E.; Mennucci, B.; Tomasi, J. A new integral equation formalism for the polarizable continuum model: Theoretical background and applications to isotropic and anisotropic dielectrics. *J. Chem. Phys.* **1997**, *107*, 3032−3041.

73 Gonzalez, C.; Schlegel, H. B. Reaction path following in mass-weighted internal coordinates. *J. Phys. Chem.* **1990**, *94*, 5523−5527.

74 Hratchian, H. P.; Schlegel, H. B. Following Reaction Pathways Using a Damped Classical Trajectory Algorithm. *J. Phys. Chem. A* **2002**, *106*, 165–169.

75 Glendening, E. D.; Badenhoop, J. K.; Reed, A. E.; Carpenter, J. E.; Bohmann, J. A.; Morales, C. M.; Weinhold, F. NBO, 5.0 Theoretical Institute, University of Wisconsin: Madison, WI, 2011.

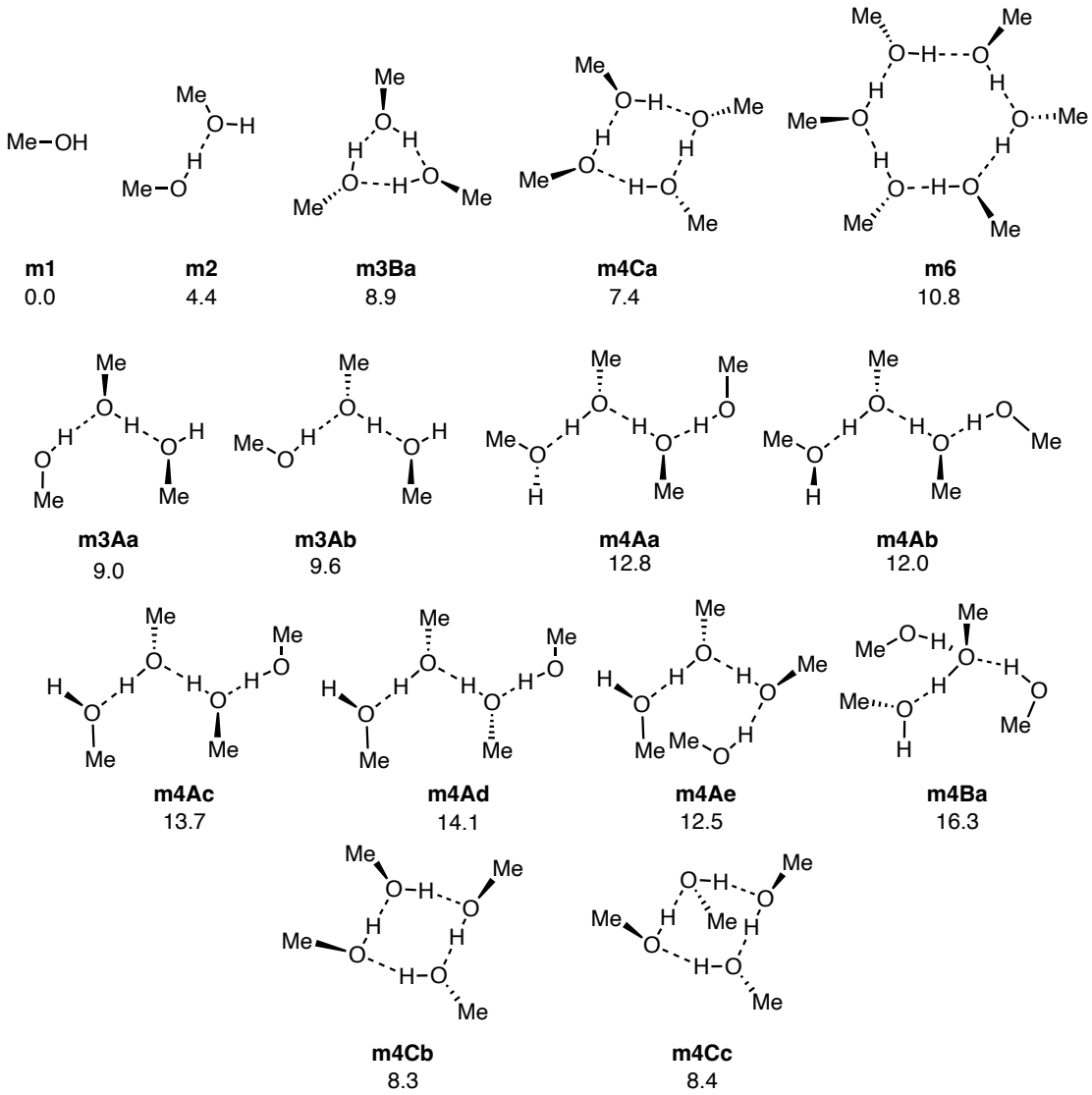

Figure 11. Structures and free energies (kcal mol^{-1}) of all studied neutral methanol clusters. Energies calculated at B3LYP-D3/6-311+G(d,p), PCM (dichloromethane).

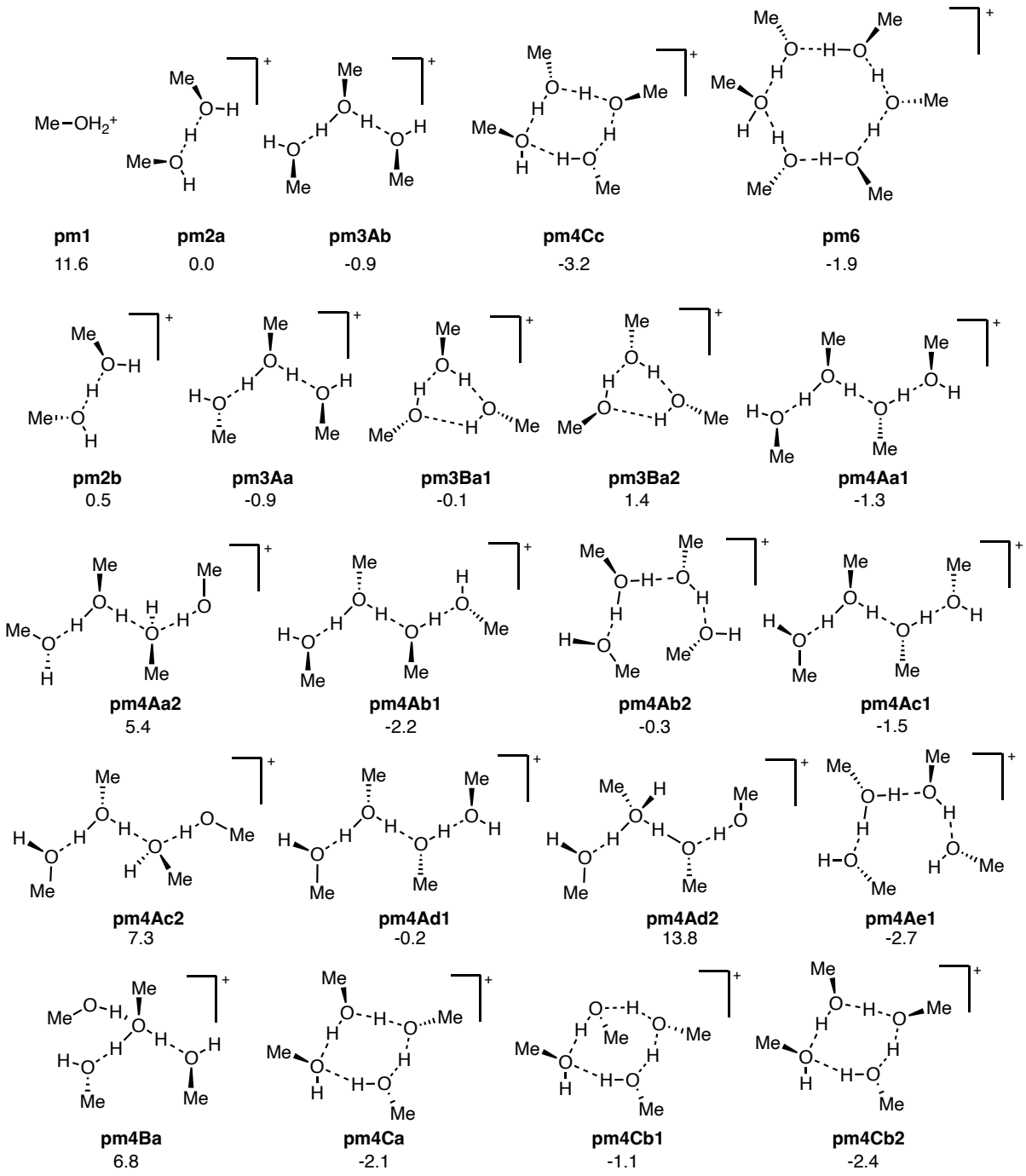

Figure 12. Structures and free energies (kcal mol^{-1}) of all studied protonated methanol clusters. Energies calculated at B3LYP-D3/6-311+G(d,p), PCM (dichloromethane).

In the calculation of the Brønsted acid-catalysed pathways, and in order to find the most basic positions of the chloroenyne or its cyclised product (**AB13**), the respective protonated species were also calculated. While protonated alkene **AB12**, in the catalytic cycle, was among the most favourable, other resting states were calculated and shown here. Some are lower in energy by 3.3 kcal mol^{-1}, constituting a resting state but ultimately not affecting the conclusions.

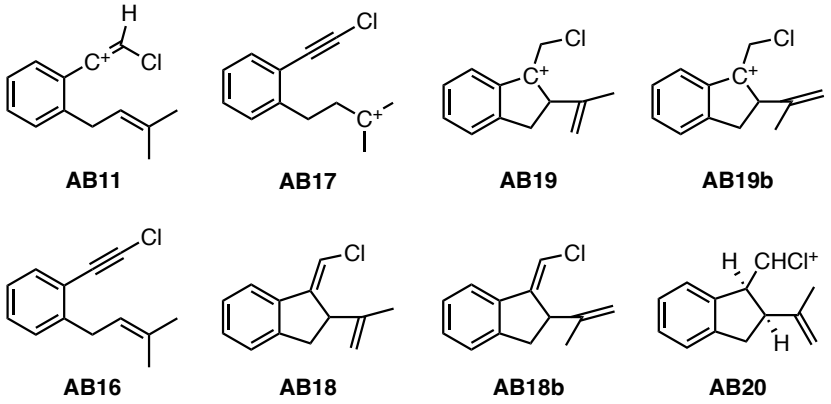

Figure 13. Structures of neutral and protonated chloroenynes and cyclised products. Energies listed in Computed Structures and Energies.

General Experimental Methods

Anhydrous reactions were performed under nitrogen or argon in solvents dried by passing through an activated alumina column on a PureSolv^{TM} solvent purification system (Innovative Technologies, Inc., MA). Otherwise, HPLC-grade solvents were used. Reactions were followed by GC-MS, UHPLC-MS, TLC (thin layer chromatography) or ^{1}H NMR analysis on aliquots. Analytical thin layer chromatography was carried out using TLC aluminium sheets with 0.2 mm of silica gel (Merck 60 F_{254}) using UV light as the visualizing agent, and an acidic solution of vanillin in ethanol or a basic aqueous solution of $KMnO_4$ as stains. UHPLC-MS analyses were carried out on an Agilent Technologies 1290 Infinity II instrument with single-quad detector using APCI for the ionisation. Purifications by chromatography were carried out using flash grade silica gel (SDS Chromatogel 60 ACC, 40-63 mm) or preparative thin-layer chromatography plates (Analtech, 1000 μm or 2000 μm). The reported yields refer to isolated pure compounds or, in the case of isolation as pure mixtures as ratios, weighed and the ratio determined by NMR and subsequently validating with an internal standard. NMR spectra were recorded at 298 K on a Bruker Avance 300, Bruker Avance 400 Ultrashield or a Bruker Avance 500 Ultrashield apparatus. The signals are given as δ / ppm (multiplicity, coupling constant (Hertz), number of protons) downfield from tetramethylsilane, with calibration on the residual solvent used (δ_H = 7.26 ppm and δ_C = 77.16 ppm for $CDCl_3$). Mass spectra were recorded on a Waters UPLC-QqTOF (Maxis Impact, Bruker Daltonics) with ESI and APCI, or a Waters Alliance HPLC-TOF (MicroTOF Focus, Bruker Daltonics) with ESI and APCI. Melting points were determined using a Büchi melting point apparatus or MP70 Melting Point System (Mettler Toledo).

All reagents were used as purchased with no further purification. N-Propargyltoluenesulfonamide,[76] *p*-methoxycinnamyl alcohol,[77] 3-phenylbut-2-en-1-ol,[78] prenyl-d_3 bromide,[79] 3-propargyloxy-1-propen-1-yl-4-methoxybenzene (***E*-1.7l**),[80] 3-propargyloxy-1-propen-1-yl-2-methoxybenzene (***E*-1.7m**)[81] cinnamyl propargyl ether (***E*-1.7k**),[82] and *p*-methoxycinnamyl *tert*-butyl carbonate[83] were synthesised according to previously reported procedures. The NMR data are in agreement with the ones reported in the literature.

Synthetic Procedures and Characterisation Data

(*E*)-N-*p*-Methoxycinnamyl-N-propargyl-*p*-toluenesulfonamide (*E*-1.7j)

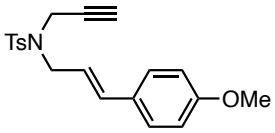

N-Propargyltoluenesulfonamide (364 mg, 1.74 mmol), (E)-*p*-methoxycinnamyl alcohol (300 mg, 1.83 mmol, 1.05 eq) and triphenylphosphine (456 mg, 1.74 mmol, 1.0 eq) were dissolved in anhydrous THF (6 mL) and cooled to 0 ºC. To the stirred solution was added dropwise diisopropyl azodicarboxylate (360 mg, 1.77 mmol, 1.02 eq) and the mixture allowed to warm up to room temperature and react for 63 h. After this time, aqueous NaOH (10%, 10 mL) was added, followed by saturated aqueous sodium bicarbonate (20 mL) and the mixture extracted with ethyl acetate (2 x 50 mL). The combined organic extracts were washed with saturated brine (10 mL), dried with sodium sulfate and concentrated. The crude product was purified by column chromatography on silica (5:1 cyclohexane:EtOAc), affording the title compound as an off-white solid (221 mg, 36%).

Spectral data consistent with the values reported in the literature.[84]

(*Z*)-3-(4-Methoxystyryl)-1-tosyl-2,5-dihydro-1H-pyrrole (*Z*-1.8j)

76 Bodinier, F.; Sanogo, Y.; Ardisson, J.; Lannou, M.-I.; Sorin, G. Low-Valent Dialkoxytitanium(ii): A Useful Tool for the Synthesis of Functionalized Seven-Membered Ring Compounds. *Chem. Commun.* **2021**, *57*, 3603–3606.

77 Meiß, R.; Kumar, K.; Waldmann, H. Divergent Gold(I)-Catalyzed Skeletal Rearrangements of 1,7-Enynes. *Chem. Eur. J.* **2015**, *21*, 13526–13530.

78 Porta, E. O. J.; Vallejos, M. M.; Bracca, A. B. J.; Labadie, G. R. Experimental and Theoretical Studies of the [3,3]-Sigmatropic Rearrangement of Prenyl Azides. *RSC Adv.* **2017**, *7* (75), 47527–47538.

79 Choi, S.; Breugst, M.; Houk, K. N.; Poulter, C. D. δ-Deuterium Isotope Effects as Probes for Transition-State Structures of Isoprenoid Substrates. *J. Org. Chem.* **2014**, *79*, 3572–3580.

80 Pal, S.; Lucarini, F.; Ruggi, A.; Kilbinger, A. F. M. Functional Metathesis Catalyst Through Ring Closing Enyne Metathesis: One Pot Protocol for Living Heterotelechelic Polymers. *J. Am. Chem. Soc.* **2018**, *140*, 3181–3185.

81 Galland, J.-C.; Dias, S.; Savignac, M.; Genêt, J.-P. Cycloisomerization of 1,6-Enynes in Organoaqueous Medium: An Efficient and Eco-Friendly Access to Furan Derivatives. Synthesis of a Key Intermediate of Podophyllotoxin. *Tetrahedron* **2001**, *57*, 5137–5148.

82 Barreiro, E. M.; Boltukhina, E. V.; White, A. J. P.; Hii, K. K. M. Atropisomeric [(Diphosphine)Au_2Cl_2] Complexes and Their Catalytic Activity Towards Asymmetric Cycloisomerisation of 1,6-Enynes. *Chem. Eur. J.* **2015**, *21*, 2686–2690.

83 Zheng, J.; Nopper, C.; Bibi, R.; Nikbakht, A.; Bauer, F.; Breit, B. Regio- and Diastereoselective Decarboxylative Allylation of *N*- Aryl α-Amino Acids by Dual Photoredox/Nickel Catalysis. *ACS Catal.* **2022**, *12*, 5949–5960.

84 Yang, J.; Zhang, R.; Wang, W.; Zhang, Z.; Shi, M. Axially Chiral N-Heterocyclic Carbene Gold(I) Complex Catalyzed Asymmetric Friedel–Crafts/Cyclization Reaction of Nitrogen-Tethered 1,6-Enynes with Indole Derivatives. *Tetrahedron: Asymmetry* **2011**, *22*, 2029–2038.

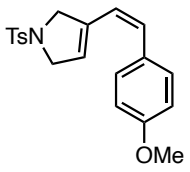

To a stirred solution of ***E*-1.7j** (87.7 mg, 247 μmol) in dichloromethane (1.5 mL) at 23 ºC was added [JohnPhosAu(NCMe)]SbF_6 (3.6 mg, 4.7 μmol, 2 mol %). After stirring for 2 hours, the reaction was quenched with a drop of triethylamine and the solution concentrated *in vacuo*. Purification by column chromatography on neutral alumina (1:1 cyclohexane:EtOAc) afforded the product as a colourless oil (46%) mixed with *endo*-cleavage product (10%). **^{1}H NMR** (500 MHz, $CDCl_3$) δ 7.62 (d, *J* = 8.3 Hz, 2H), 7.32 (dd, *J* = 8.6, 0.8 Hz, 2H), 7.05 – 7.01 (m, 2H), 6.81 (d, *J* = 8.7 Hz, 2H), 6.49 (d, *J* = 11.9 Hz, 1H), 6.04 – 5.99 (m, 1H), 5.60 (br s, 1H), 4.08 (ddq, *J* = 5.7, 3.4, 1.2 Hz, 2H), 3.84 (s, 3H), 3.82 (tq, *J* = 3.4, 1.0 Hz, 2H), 2.44 (s, 3H) ppm. **^{13}C{^{1}H} NMR** (126 MHz, $CDCl_3$) δ 159.2, 143.6, 136.4, 134.0, 132.1, 129.9, 129.8, 129.6, 127.6, 124.9, 122.4, 113.6, 55.4, 55.2, 54.5, 21.7 ppm. **HRMS** (ESI) *m/z*: $[M+Na]^+$ calculated for $C_{20}H_{21}NNaO_3S$ 378.1134; found 378.1142.

(*E*)-3-styryl-2,5-dihydrofuran (*Z*-1.8k) and (*E*)-3-benzylidene-3,6-dihydro-2*H*-pyran (1.9k)

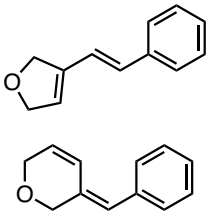

To a stirred solution of cinnamyl propargyl ether (***E*-1.7k**, 128.0 mg, 743 μmol) in dichloromethane (7.5 mL) at 23 ºC was added [JohnPhosAu(NCMe)]SbF_6 (11.5 mg, 14.9 μmol, 2 mol %). After stirring for 30 minutes, the reaction was quenched with a drop of triethylamine and the solution concentrated *in vacuo*. The crude product was purified further by column chromatography on neutral alumina (toluene). Mixture of both products isolated in a 1:14 ratio (major: **1.9k**) as a colourless oil (79.7 mg, 62%).

Major product, **1.9k**: **^{1}H NMR** (500 MHz, $CDCl_3$) δ 7.36 – 7.32 (m, 2H), 7.31 – 7.28 (m, 2H), 7.26 – 7.22 (m, 1H), 6.75 (dtd, *J* = 10.3, 2.2, 1.1 Hz, 1H), 6.25 (s, 1H), 5.97 (dtd, *J* = 10.3, 3.0, 1.6 Hz, 1H), 4.35 (d, *J* = 1.3 Hz, 2H), 4.33 (ddd, *J* = 3.1, 2.2, 1.0 Hz, 2H) ppm. **^{13}C{^{1}H} NMR** (126 MHz, $CDCl_3$) δ 136.5, 131.7, 130.0, 129.2, 128.4, 127.0, 124.2, 123.0, 70.5, 66.5 ppm.

Minor product, ***Z*-1.8k**: **^{1}H NMR** (500 MHz, $CDCl_3$) δ 6.97 – 6.93 (ddt, *J* = 16.6, 0.8, 0.8 Hz, 1H), 6.30 (d, *J* = 16.6 Hz, 1H), 5.95 (s, 1H), 4.89 – 4.86 (m, 2H), 4.79 – 4.75 (m, 2H) ppm. Aromatic signals were obscured by the major product. **^{13}C{^{1}H} NMR** (126 MHz, $CDCl_3$) δ 137.0, 130.9, 128.8, 128.0, 127.5, 126.5, 125.4, 121.2, 76.2, 74.4 ppm. **HRMS** (APCI) *m/z*: $[M+H]^+$ Calculated for $C_{12}H_{13}O$ = 173.0961; found 173.0964. **FTIR** (neat): 3026 (w), 2824 (w), 1723 (w), 1492 (m), 1448 (m), 1155 (m), 1090 (s), 963 (m), 697 (s), 572 (w) cm^{-1}.

(*Z*)-3-(4-Methoxystyryl)-2,5-dihydrofuran (*Z*-1.8l) and (*E*)-3-(4-methoxybenzylidene)-3,6-dihydro-2*H*-pyran (1.9l)

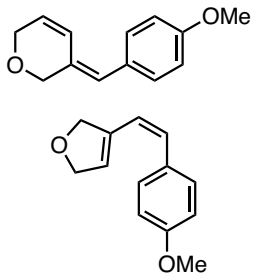

To a stirred solution of 3-propargyloxy-1-propen-1-yl-4-methoxybenzene (***E*-1.7l**, 86.0 mg, 425 μmol) in dichloromethane (4.3 mL) at 23 ºC was added [JohnPhosAu(NCMe)]SbF_6 (6.5 mg, 8.5 μmol, 2 mol %). After stirring for 30 minutes, the reaction was quenched with a drop of triethylamine and the solution concentrated *in vacuo*. The crude product was purified further by column chromatography on neutral alumina (toluene). Mixture of products isolated in a 78:9:19 ratio as a pale-yellow oil (51.7 mg, 60%).

Major product, ***Z*-1.8l**: **^{1}H NMR** (500 MHz, $CDCl_3$) δ 7.16 – 7.13 (m, 2H), 6.85 – 6.82 (m, 3H), 6.54 (d, *J* = 11.9 Hz, 1H), 6.23 (dq, *J* = 11.8, 1.0 Hz, 1H), 5.88 (pd, *J* = 2.1, 1.0 Hz, 1H), 4.61 (dddt, *J* = 5.1, 4.2, 2.1, 1.1 Hz, 2H), 4.30 (dddd, *J* = 4.6, 3.1, 2.2, 1.1 Hz, 2H), 3.81 (s, 3H) ppm. **^{13}C{^{1}H} NMR** (126 MHz, $CDCl_3$) δ 159.1, 151.5, 137.7, 131.3, 130.0, 126.9, 122.5, 113.5, 75.4, 75.0, 55.4 ppm.

Dihydro-2*H*-pyran **1.9l** characteristic signals: **^{1}H NMR** (500 MHz, $CDCl_3$) δ 6.74 (dtd, *J* = 10.3, 2.3, 1.1 Hz, 1H), 6.18 (s, 1H), 5.94 (dtd, *J* = 10.2, 3.0, 1.7 Hz, 1H), 4.32 (d, *J* = 1.2 Hz, 2H), 3.82 (s, 3H) ppm. Other signals obscured by overlap. Assigned by analogy to **9m** and **9k**.

Unassigned impurity: **^{1}H NMR** (500 MHz, $CDCl_3$) δ 7.10 (dd, *J* = 8.6, 0.6 Hz, 2H), 4.96 (q, *J* = 2.1 Hz, 1H), 4.90 (q, *J* = 2.3 Hz, 1H), 3.86 (dd, *J* = 8.7, 6.8 Hz, 1H), 3.79 (s, 3H), 3.59 (dd, *J* = 8.6, 5.9 Hz, 1H), 2.95 – 2.84 (m, 2H), 2.58 (dd, *J* = 13.2, 9.0 Hz, 1H) ppm. **^{13}C{^{1}H} NMR** (126 MHz, $CDCl_3$) δ 158.2, 130.3, 129.9, 114.0, 104.2, 73.7, 71.8, 45.6, 38.1 ppm.

HRMS (APCI) *m/z*: $[M+H]^+$ calculated for $C_{13}H_{15}O_2$ 203.1067; found 203.1062. **FTIR** (neat): 2933 (m), 2837 (m), 1725 (m), 1605 (m), 1510 (s), 1246 (s), 1174 (m), 1029 (m), 821 (w) cm^{-1}.

(*Z*)-3-(2-Methoxystyryl)-2,5-dihydrofuran (*Z*-1.8m) and (*E*)-3-(2-methoxybenzylidene)-3,6-dihydro-2*H*-pyran (1.9m)

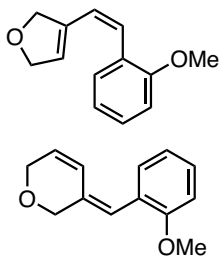

To a stirred solution of 3-propargyloxy-1-propen-1-yl-2-methoxybenzene (***E*-1.7m**, 113.0 mg, 559 μmol) in dichloromethane (5.6 mL) at 23 ºC was added [JohnPhosAu(NCMe)]SbF_6 (8.6 mg, 11 μmol, 2 mol %). After stirring for 30 minutes, the reaction was quenched with a drop of triethylamine and the solution concentrated *in vacuo*. The crude product was purified further by column chromatography on neutral alumina (toluene). Mixture of products isolated in a 7:25 ratio as a colourless oil (84.3 mg, 75%).

Major product, **1.9m**: **^{1}H NMR** (500 MHz, $CDCl_3$) δ 7.29 (ddd, *J* = 7.7, 1.9, 0.7 Hz, 1H), 7.26 – 7.23 (m, 1H), 6.94 (tdd, *J* = 7.5, 1.1, 0.5 Hz, 1H), 6.88 (dd, *J* = 8.2, 1.1 Hz, 1H), 6.66 (dtd, *J* = 10.3, 2.2, 1.1 Hz, 1H), 6.37 (s, 1H), 5.93 (dtd, *J* = 10.3, 3.0, 1.7 Hz, 1H), 4.39 (d, *J* = 1.3 Hz, 2H), 4.32 (ddd, *J* = 3.1, 2.2, 1.0 Hz, 2H), 3.83 (s, 3H) ppm. **^{13}C{^{1}H} NMR** (126 MHz, CDCl3) δ 157.4, 131.4, 131.0, 129.4, 128.6, 125.3, 123.3, 120.2, 119.9, 110.5, 70.5, 66.4, 55.5 ppm.

Minor product, ***Z*-1.8m**: **^{1}H NMR** (500 MHz, $CDCl_3$) δ 7.19 – 7.17 (m, 1H), 7.12 (ddd, *J* = 7.4, 1.8, 0.9 Hz, 1H), 6.92 – 6.89 (m, 1H), 6.85 (dd, *J* = 8.3, 1.0 Hz, 1H), 6.55 (d, *J* = 11.9 Hz, 1H), 6.39 (ddt, *J* = 11.8, 0.9, 0.9 Hz, 1H), 5.89 (tt, *J* = 2.1, 0.8 Hz, 1H), 4.59 (ddq, *J* = 5.0, 3.1, 1.0 Hz, 2H), 4.26 – 4.23 (m, 2H), 3.82 (s, 3H) ppm. **^{13}C{^{1}H} NMR** (126 MHz, $CDCl_3$) δ 157.2, 130.6, 129.2, 128.4, 127.6, 127.5, 126.8, 125.4, 123.6, 120.1, 110.2, 75.2, 74.8 ppm.

HRMS (APCI) *m/z*: $[M+H]^+$, calculated for $C_{13}H_{15}O_2$ = 203.1067; found 203.1065. **FTIR** (neat): 2935 (m), 2834 (m), 1595 (m), 1486 (m), 1461 (m), 1436 (m), 1377 (w), 1289 (w), 1243 (s), 1100 (m), 1089 (m), 1025 (m),752 (w) cm^{-1}.

(*E*)-N-3-Phenylbut-2-en-1-yl-N-propargyl-*p*-toluenesulfonamide (*E*-1.7n)

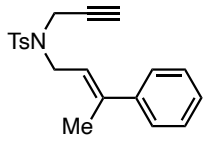

N-Propargyltoluenesulfonamide (144.1 mg, 687 μmol), (*E*)-3-phenylbut-2-en-1-ol (107.2 mg, 723 μmol, 1.05 eq) and triphenylphosphine (180.6 mg, 687 μmol, 1.0 eq) were dissolved in anhydrous THF (2.3 mL) and cooled to 0 ºC. To the stirred solution was added dropwise diisopropyl azodicarboxylate (142.0 mg, 702 μmol, 1.02 eq) and the mixture allowed to warm up to room temperature and react for 23 h. After this time, aqueous NaOH (10%, 5 mL) was added, followed by saturated aqueous sodium bicarbonate (10 mL) and the mixture extracted with ethyl acetate (2 x 15 mL). The combined organic extracts were washed with saturated brine (10 mL), dried with sodium sulfate and concentrated. The crude product was purified by column chromatography on silica (8:1 cyclohexane:EtOAc), affording the title compound as a white resin (161.2 mg, 69%) as an 8:1 E:Z mixture. **^{1}H NMR** (400 MHz, $CDCl_3$) δ 7.80 – 7.74 (m, 2H), 7.66 – 7.62 (*cis*, m, 2H), 7.34 – 7.26 (m, 7H), 7.20 – 7.17 (*cis*, m, 2H), 7.15 – 7.10 (*cis*, m, 1H), 5.68 (ddt, *J* = 7.3, 5.9, 1.4 Hz, 1H), 5.48 – 5.41 (*cis*, m, 1H), 4.13 (d, *J* = 2.5 Hz, 2H), 4.05 (d, *J* = 6.9 Hz, 2H), 2.44 (s, 3H), 2.41 (*cis*, s, 3H), 2.09 (dt, *J* = 1.5, 0.7 Hz, 3H), 2.04 (t, *J* = 2.4 Hz, 1H), 1.97 (*cis*, t, J = 2.5 Hz, 1H) ppm. Some resonances of the minor isomer not observed due to overlap. **^{13}C{^{1}H} NMR** (101 MHz, $CDCl_3$) δ 143.7, 142.7, 141.0, 136.2, 129.7, 128.4, 128.0, 127.6, 125.9, 121.1, 77.4, 73.8, 44.7, 36.1, 21.7, 16.1 ppm. **HRMS** (ESI) *m/z*: $[M+Na]^+$ calculated for $C_{20}H_{21}NNaO_2S$ 362.1185; found 362.1183.

(*E*)-3-(1-Phenylethylidene)-1-tosyl-1,2,3,6-tetrahydropyridine (1.9n) and 9-methyl-2-tosyl-2,3,4,9-tetrahydro-1H-indeno[2,1-c]pyridine (1.10)

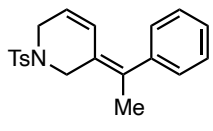

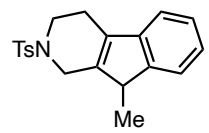

To a stirred solution of ***E*-1.7n** (66.7 mg, 196 μmol) in dichloromethane (2 mL) at 23 ºC was added [JohnPhosAu(NCMe)]SbF_6 (3.0 mg, 3.9 μmol, 2 mol %). After stirring for 2 hours, the reaction was quenched with a drop of triethylamine and the solution concentrated *in vacuo*. Purification by column chromatography (100% toluene) afforded the mixture of products as a colourless oil (both products: 58.1 mg, 87%) in a roughly 4:3 ratio. The tricyclic product forms due to further reaction of the cyclization product with silica gel.

Major product, **1.10**: **^{1}H NMR** (500 MHz, $CDCl_3$) δ 7.67 – 7.62 (m, 2H, tosyl MM'), 7.34 – 7.20 (m, 4H, Ph overlapping), 7.20 – 7.17 (m, 2H, tosyl AA'), 4.12 (ddd, *J* = 18.4, 2.5, 0.6 Hz, 3H, $NC\boldsymbol{H_A}H_A{\cdot}C_{alkene}$), 4.05 (ddd, *J* = 18.4, 2.5, 0.6 Hz, 1H, $NCH_A\boldsymbol{H_A}{\cdot}C_{alkene}$), 3.11 (qdd, *J* = 13.7, 8.8, 6.2 Hz, 2H, $NC\boldsymbol{H_2}C_{sec}$), 2.76 (h, *J* = 7.0 Hz, 1H, Ar***C*H**), 2.40 (s, 3H, tosyl $C\boldsymbol{H_3}$), 1.93 – 1.80 (m, 2H, $NCH_2C\boldsymbol{H_2}$), 1.27 (d, *J* = 6.9 Hz, 3H, ArCH-$C\boldsymbol{H_3}$) ppm. Assigned ^{13}C peaks: **^{13}C{^{1}H} NMR** (126 MHz, $CDCl_3$) δ 45.1 ($N\boldsymbol{C}H_2C_{sec}$), 37.4 (Ar***C*H**), 36.6 ($N\boldsymbol{C}H_2C_{alkene}$), 35.8 ($NCH_2\boldsymbol{C}H_2$), 22.4 (ArCH-$\boldsymbol{C}H_3$), 21.7 (tosyl $\boldsymbol{C}H_3$) ppm.

Minor product, **1.9n**: **^{1}H NMR** (500 MHz, $CDCl_3$) δ 7.72 – 7.69 (m, 2H), 7.34 – 7.17 (m, 5H, overlapping), 6.93 – 6.88 (m, 2H), 5.97 (dt, *J* = 10.3, 2.2 Hz, 1H), 5.46 (dtd, *J* = 10.2, 3.5, 0.7 Hz, 1H), 4.11 (d, *J* = 0.9 Hz, 2H), 3.88 (ddt, *J* = 3.4, 2.2, 1.0 Hz, 2H), 2.43 (s, 3H), 2.08 (br s, 3H) ppm. Assigned ^{13}C peaks: **^{13}C{^{1}H} NMR** (126 MHz, $CDCl_3$) δ 126.3 ($NCH_2CH=\boldsymbol{C}H$), 122.0 ($NCH_2\boldsymbol{C}H=CH$), 45.3 ($N\boldsymbol{C}H_2{}^A$), 45.2 ($N\boldsymbol{C}H_2{}^B$), 21.6 (tosyl $\boldsymbol{C}H_3$), 20.3 (allylic $\boldsymbol{C}H_3$) ppm.

^{13}C{^{1}H} NMR (126 MHz, $CDCl_3$) δ 146.5, 143.6, 143.5, 142.1, 135.9, 135.0, 134.4, 129.7, 129.6, 128.7, 128.6, 128.1, 127.8, 127.8, 127.7, 127.1, 127.1, 126.4, 126.3, 124.6, 122.0, 45.3, 45.2, 45.1, 37.4, 36.6, 35.8, 22.4, 21.7, 21.6, 20.3 ppm. Some peaks missing due to overlap.

HRMS (ESI) *m/z*: $[M+Na]^+$ calculated for $C_{20}H_{21}NNaO_2S$ = 362.1185; found 362.1182.

(*Z*)-Dimethyl (prenyl-4,4,4-*d*$_3$)propargylmalonate (1.7a-*d*$_3$)

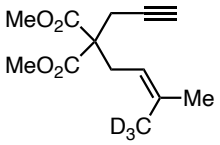

(*Z*)-Prenyl-4,4,4-*d*$_3$ bromide (351 mg, 2.31 mmol) and dimethyl propargylmalonate (393 mg, 2.31 mmol, 1 eq) were dissolved in ethyl acetate (23 mL) and cesium carbonate (903 mg, 2.77 mmol, 1.2 eq) was added to the stirring mixture. The reaction was stirred at 60 ºC in an oil bath for 16 h. Filtration through silica gel (washing with EtOAc) afforded the crude product, which was purified by column chromatography (7:1 cyclohexane:EtOAc) to yield the title compound as a colourless oil (422 mg, 76%). **^{1}H NMR** (400 MHz, $CDCl_3$) δ 4.90 (td, *J* = 7.8, 1.6 Hz, 1H), 3.73 (s, 6H), 2.79 – 2.76 (m, 4H), 2.00 (t, *J* = 2.7 Hz, 1H), 1.69 (q, 3H, *J* = 1.4 Hz) ppm. **^{13}C{^{1}H} NMR** (101 MHz, $CDCl_3$) δ 170.6, 137.0, 117.1, 79.4, 71.3, 57.3, 52.8, 30.9, 26.1, 22.7 ppm. The CD_3 carbon signal is missing. **HRMS** (ESI) *m/z*: $[M+Na]^+$ calculated for $C_{13}H_{15}D_3NaO_4$ 264.1286; found 264.1296. **FTIR** (neat): 3285 (m), 2955 (m), 2111 (w), 1734 (s), 1436 (m), 1291 (m), 1201 (m), 1054 (m), 976 (w), 854 (w), 645 (w) cm^{-1}.

(*Z*)-N-(Prenyl-4,4,4-*d*$_3$)-N-propargyl-*p*-toluenesulfonamide (1.7c-*d*$_3$)

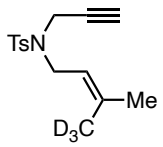

N-Propargyltoluenesulfonamide (150 mg, 717 µmol), (Z)-4,4,4-*d*$_3$-prenol (67 mg, 753 µmol, 1.05 eq) and triphenylphosphine (188 mg, 717 µmol, 1.0 eq) were dissolved in anhydrous THF (2.4 mL) and cooled to 0 ºC. To the stirred solution was added dropwise diisopropyl azodicarboxylate (148 mg, 731 µmol, 1.02 eq) and the mixture allowed to warm up to room temperature and react for 47 h. After this time, aqueous NaOH (10%, 5 mL) was added, followed by

saturated aqueous sodium bicarbonate (10 mL) and the mixture extracted with ethyl acetate (2 x 15 mL). The combined organic extracts were washed with saturated brine (10 mL), dried with sodium sulfate and concentrated. The crude product was purified by column chromatography on silica (4:1 cyclohexane:EtOAc), affording the title compound as a white solid (194 mg, 97%). **Melting point** (EtOAc): 61.0-61.5 °C. **^{1}H NMR** (400 MHz, $CDCl_3$) δ 7.77 – 7.70 (m, 2H), 7.31 – 7.27 (m, 2H), 5.10 (tq, *J* = 7.3, 1.4 Hz, 1H), 4.06 (d, *J* = 2.5 Hz, 2H), 3.80 (dd, *J* = 7.4, 1.1 Hz, 2H), 2.42 (s, 3H), 1.98 (t, *J* = 2.5 Hz, 1H), 1.72 (q, *J* = 1.1 Hz, 3H) ppm. **^{13}C{^{1}H} NMR** (101 MHz, $CDCl_3$) δ 143.5, 139.1, 136.3, 129.5, 128.0, 118.1, 77.2, 73.5, 44.1, 35.5, 25.9, 21.7 ppm. **HRMS** (ESI) *m/z*: $[M+Na]^+$ calculated for $C_{15}H_{16}D_3NNaO_2S$ 303.1217; found 303.1217. **FTIR** (neat): 3259 (s), 2974 (m), 2919 (m), 2115 (w), 1675 (w), 1597 (w), 1428 (m), 1374 (w), 1343 (s), 1330 (s), 1267 (w), 1202 (w), 1157 (s), 1009 (m), 895 (m), 816 (m), 657 (w), 545 (w) cm^{-1}.

Dimethyl (Z)-3-(2-methylprop-1-en-1-yl-3,3,3-*d*$_3$)cyclopent-3-ene-1,1-dicarboxylate (*Z*-1.8a-*d*$_3$)

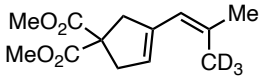

To a stirred solution of **1.7a-*d*$_3$** (116.5 mg, 483 μmol) in dichloromethane (4.8 mL) at 23 ºC was added [JohnPhosAu(NCMe)]SbF_6 (7.4 mg, 9.6 μmol, 2 mol %). After stirring for 30 minutes, the reaction was quenched with a drop of triethylamine and the solution concentrated *in vacuo*. The crude product, while already relatively free of impurities, can be purified further by column chromatography (6:1 cyclohexane:EtOAc). Product isolated as a colourless oil (116.3 mg, quant.). **^{1}H NMR** (500 MHz, $CDCl_3$) δ 5.74 (pseudo p, *J* = 1.3 Hz, 1H), 5.39 – 5.37 (m, 1H), 3.74 (s, 6H), 3.19 (dt, *J* = 2.4, 1.2 Hz, 2H), 3.04 (ddt, *J* = 3.0, 2.1, 1.0 Hz, 2H), 1.79 – 1.76 (m, 3H) ppm. **^{13}C{^{1}H} NMR** (101 MHz, $CDCl_3$) δ 172.8, 138.9, 135.7, 124.6, 120.8, 59.5, 53.0, 43.4, 40.4, 27.4 ppm. **HRMS** (ESI) *m/z*: $[M+Na]^+$ calculated for $C_{13}H_{15}D_3NaO_4$ 264.1286; found 264.1293. **FTIR** (neat): 2954 (m), 1732 (s), 1434 (m), 1249 (m), 1197 (m), 1159 (m), 1072 (w), 870 (w) cm^{-1}.

(Z)-3-(Isopropylidene-1,1,1-*d*$_3$)-1-tosyl-1,2,3,6-tetrahydropyridine (1.9c-*d*$_3$)

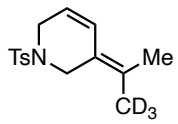

To a stirred solution of **1.7c-*d*$_3$** (28.6 mg, 102 μmol) in dichloromethane (1.0 mL) at 23 ºC was added [JohnPhosAu(NCMe)]SbF_6 (1.6 mg, 2.0 μmol, 2 mol %). After stirring for 20 minutes, the reaction was quenched with a drop of triethylamine and the solution concentrated *in vacuo*. Purification by column chromatography (4:1 cyclohexane:EtOAc) afforded the product as a colourless resin (26.8 mg, 94%). **^{1}H NMR** (500 MHz, $CDCl_3$) δ 7.66 – 7.63 (m, 2H), 7.26 (dt, *J* = 8.0, 0.8 Hz, 2H), 6.33 (dt, *J* = 10.3, 2.2 Hz, 1H), 5.52 (dt, *J* = 10.3, 3.7 Hz, 1H), 3.89 (q, *J* = 1.3 Hz, 2H), 3.76 (ddd, *J* = 3.8, 2.2, 0.8 Hz, 2H), 2.40 (s, 3H), 1.66 (s, 3H) ppm. **^{13}C{^{1}H} NMR** (126 MHz, $CDCl_3$) δ 143.5, 134.3, 130.0, 129.5, 127.8, 124.6, 122.4, 121.0, 45.2, 45.1, 21.6, 19.7, 19.6 (CD_3, J_{CD} = 19.4 Hz). **HRMS** (ESI) *m/z* $[M+Na]^+$ calculated for $C_{15}H_{16}D_3NNaO_2S$ 303.1217; found 303.1218.

Computed Structures and Energies

Table 12. Enynes, their cyclised intermediates and associated transition states. BP86-D3/6-31G(d) + SDD(Au); PCM (dichloromethane)

Code	E / Hartree	G / Hartree
A1	-830.276397	-830.09262
A2	-830.257503	-830.07532
A4	-830.297826	-830.11116
A3	-830.268681	-830.08099
B1	-869.38779	-869.59679
B2	-869.59377	-869.38568
B4	-869.61883	-869.40526
B3	-869.59543	-869.40529
C1	-869.59625	-869.38725
C4	-869.61801	-869.40475
C3	-869.58693	-869.37447
D1	-908.9150	-908.67901
D4	-908.93358	-908.6943
D3	-908.9031	-908.66464
E1	-1061.3458	-1061.0900
E2	-1061.3204	-1061.0653
E4	-1061.3587	-1061.0995
E3	-1061.3347	-1061.0747
F1	-1100.6701	-1100.3872
F2	-1100.6557	-1100.3751
F4	-1100.6822	-1100.3963
F3	-1100.6619	-1100.3765
G1	-1100.6663	-1100.3846
G4	-1100.6796	-1100.3939
G3	-1100.6525	-1100.3674
H1	-1139.9846	-1139.6765
H4	-1139.9944	-1139.6847
H3	-1139.9682	-1139.6570
I1	-1061.3450	-1061.0874
I5	-1061.3568	-1061.0959
I4	-1061.3590	-1061.0982
TSA1-2	-830.251141	-830.06820

TSA1-4	-830.261856	-830.07838
TSA2-3	-830.257357	-830.07327
TSB1-3	-869.57619	-869.36829
TSB1-4	-869.58394	-869.37521
TSB2-3	-869.59372	-869.38273
TSC1-4	-869.58278	-869.37429
TSC1-3	-869.57462	-869.36598
TSD1-4	-908.90117	-908.66749
TSD1-3	-908.89566	-908.66233
TSE1-3	-1061.3164	-1061.0596
TSE1-4	-1061.3340	-1061.0770
TSE2-3	-1061.3191	-1061.0631
TSF1-3	-1100.6416	-1100.3605
TSF1-4	-1100.6581	-1100.3763
TSF2-3	-1100.6556	-1100.3733
TSG1-4	-1100.6546	-1100.3715
TSG1-3	-1100.6397	-1100.3569
TSH1-4	-1139.9772	-1139.6707
TSH1-3	-1139.9596	-1139.6526
TSI4-5	-1061.3248	-1061.0691
TSI1-4	-1061.3567	-1061.0964

Table 13. Allenenes, their cyclised intermediates and associated transition states. BP86-D3/6-31G(d) + SDD(Au); PCM (dichloromethane).

Code	E / Hartree	G / Hartree
J1	-830.27780	-830.09703
K1	-869.59772	-869.38986
L1	-869.59712	-869.3903
L4	-869.61425	-869.40069
M1	-908.91547	-908.68323
M4	-908.93058	-908.69061
M7	-908.91864	-908.68278
N1	-1061.34464	-1061.08877
O1	-1100.66488	-1100.38354
P1	-1100.66406	-1100.38323
P4	-1100.67569	-1100.38996

P7	-1100.65364	-1100.37406
Q1	-1139.98284	-1139.67618
Q4	-1139.99245	-1139.68078
Q7	-1139.98423	-1139.67585
TSJ1-4	-830.26838	-830.08368
TSK1-4	-869.59141	-869.38225
TSL1-4	-869.58950	-869.37984
TSM1-4	-908.91010	-908.67583
TSM4-7	-908.90919	-908.66956
TSN1-4	-1061.33208	-1061.07583
TSO1-4	-1100.65565	-1100.37616
TSP1-4	-1100.65426	-1100.37101
TSP1-7	-1100.65356	-1100.37137
TSQ1-4	-1139.97499	-1139.66863
TSQ2-7	-1139.97363	-1139.66171

Table 14. Benchmark of H geometries. Functional-D3/6-311+G(d,p) + SDD(Au); PCM (dichloromethane).

	H1	**H4**	**H3**	**TSH1-4**	**TSH1-3**
BP86	-1140.19696	-1140.20140	-1140.17465	-1140.18623	-1140.16923
B3LYP	-1140.10269	-1140.09740	-1140.06890	-1140.08324	-1140.06684
B3PW91	-1139.84665	-1139.85301	-1139.82360	-1139.83157	-1139.81472
B97D	-1139.81953	-1139.81526	-1139.78998	-1139.80495	-1139.78897
BMK	-1138.82541	-1138.83287	-1138.80493	-1138.80562	-1138.79165
TPSS	-1140.13822	-1140.14109	-1140.11603	-1140.12519	-1140.10866
M062X	-1139.53340	-1139.53299	-1139.50316	-1139.51043	-1139.49498
M06HF	-1139.54949	-1139.55142	-1139.51663	-1139.53024	-1139.51277
M06	-1139.45219	-1139.45513	-1139.42703	-1139.43250	-1139.41691
M06L	-1139.97367	-1139.97434	-1139.94978	-1139.95238	-1139.93725
PBE0	-1139.05669	-1139.06682	-1139.03693	-1139.04204	-1139.02511
PBE	-1138.98661	-1138.99309	-1138.96658	-1138.97578	-1138.95898
DLPNO-CCSD(T)	-1137.80012	-1137.80115	-1137.76542	-1137.78058	-1137.76358

Table 15. Benchmark of I geometries. Functional-D3/6-311+G(d,p) + SDD(Au); PCM (dichloromethane).

	I1	I5	I4	TSI1-5	TSI4-5
BP86	-1061.53556	-1061.54165	-1061.54397	-1061.51564	-1061.54163
B3LYP	-1061.43698	-1061.43619	-1061.43831	-1061.41472	-1061.43599
B3PW91	-1061.20963	-1061.21223	-1061.21896	-1061.18637	-1061.21233
B97D	-1061.21651	-1061.21950	-1061.21900	-1061.19775	-1061.21920
BMK	-1060.22750	-1060.22238	-1060.23304	-1060.19790	-1060.22217
TPSS	-1061.46064	-1061.46692	-1061.47096	-1061.44259	-1061.46691
M062X	-1060.91901	-1060.90796	-1060.91878	-1060.89246	-1060.90763
M06HF	-1060.92788	-1060.91185	-1060.92449	-1060.90010	-1060.91161
M06	-1060.86024	-1060.85631	-1060.86436	-1060.83590	-1060.85606
M06L	-1061.32577	-1061.32527	-1061.33176	-1061.30325	-1061.32501
PBE0	-1060.49267	-1060.49919	-1060.50784	-1060.47121	-1060.49939
PBE	-1060.43640	-1060.44734	-1060.45115	-1060.41932	-1060.44747
DLPNO-CCSD(T)	-1059.31168	-1059.30695	-1059.31376	-1059.28867	-1059.30595

Table 16. Benchmark of Q geometries. Functional-D3/6-311+G(d,p) + SDD(Au); PCM (dichloromethane).

	Q1	Q4	Q7	TSQ1-4	TSQ4-7
BP86	-1140.19566	-1140.19934	-1140.19293	-1140.18629	-1140.18180
B3LYP	-1140.09873	-1140.09694	-1140.08960	-1140.08594	-1140.07805
B3PW91	-1139.84442	-1139.85208	-1139.84048	-1139.83118	-1139.82764
B97D	-1139.81735	-1139.81446	-1139.80993	-1139.80818	-1139.80020
BMK	-1138.82194	-1138.83147	-1138.81833	-1138.80424	-1138.80584
TPSS	-1140.13602	-1140.13968	-1140.13072	-1140.12652	-1140.12043
M062X	-1139.53117	-1139.53354	-1139.51773	-1139.51113	-1139.50727
M06HF	-1139.55117	-1139.55332	-1139.53620	-1139.52797	-1139.52931
M06	-1139.44990	-1139.45569	-1139.44002	-1139.43317	-1139.42760
M06L	-1139.96977	-1139.97223	-1139.96048	-1139.95675	-1139.94681
PBE0	-1139.05459	-1139.06642	-1139.05342	-1139.04154	-1139.03940
PBE	-1138.98527	-1138.99149	-1138.98410	-1138.97620	-1138.97187
DLPNO-CCSD(T)	-1137.79693	-1137.80213	-1137.79156	-1137.78093	-1137.77993

Table 17. *p*MeOcinnamyl substrate and cyclization. B3LYP-D3/6-31G(d) + SDD(Au); PCM (dichloromethane); HLT: B3LYP-D3/6-311+G(d,p) + SDD(Au).

Code	E / Hartree	G / Hartree	E_{HLT} / Hartree
smS-Z	-1074.0218	-1073.7298	-1074.3482
smS-E	-1074.0257	-1073.7353	-1074.3524
prodS-Z	-1074.0874	-1073.7901	-1074.4070
prodS-E	-1074.0936	-1073.7983	-1074.4142
Z-S1	-1670.8476	-1670.4491	-1671.2286
E-S1	-1670.8577	-1670.4603	-1671.2363
Z-S2	-1670.8591	-1670.4577	-1671.2321
E-S2	-1670.8630	-1670.4632	-1671.2375
Z-S3	-1670.9059	-1670.5035	-1671.2817
E-S3	-1670.9176	-1670.5162	-1671.2928
tsSrot	-1670.8499	-1670.4498	-1671.2245
tsZ-S2	-1670.8337	-1670.4381	-1671.2105
tsE-S2	-1670.8418	-1670.4473	-1671.2197
tsZ-S3	-1670.8425	-1670.4420	-1671.2159
tsE-S3	-1670.8350	-1670.4357	-1671.2086

Table 18. *p*Clcinnamyl substrate and cyclization. B3LYP-D3/6-31G(d) + SDD(Au); PCM (dichloromethane); HLT: B3LYP-D3/6-311+G(d,p) + SDD(Au).

Code	E / Hartree	G / Hartree	E_{HLT} / Hartree
smT-Z	-1419.1117	-1418.8607	-1419.4113
smT-E	-1419.1156	-1418.8666	-1419.4152
prodT-Z	-1419.1767	-1418.9201	-1419.4698
prodT-E	-1419.1830	-1418.9287	-1419.4770
Z-T1	-2015.9140	-2015.5582	-2016.2911
E-T1	-2015.9244	-2015.5670	-2016.2984
Z-T2	-2015.9167	-2015.5579	-2016.2851
E-T2	-2015.9190	-2015.5611	-2016.2888
Z-T3	-2015.9766	-2015.6161	-2016.3473
E-T3	-2015.9822	-2015.6226	-2016.3526
tsTrot	-2015.8993	-2015.5418	-2016.2710
tsZ-T2	-2015.8977	-2015.5422	-2016.2690
tsE-T2	-2015.9050	-2015.5501	-2016.2774
tsZ-T3	-2015.9075	-2015.5469	-2016.2766
tsE-T3	-2015.9011	-2015.5409	-2016.2696

Table 19. Cinnamyl substrate and cyclization. B3LYP-D3/6-31G(d) + SDD(Au); PCM (dichloromethane); HLT: B3LYP-D3/6-311+G(d,p) + SDD(Au).

Code	E / Hartree	G / Hartree	E_{HLT} / Hartree
smU-Z	-959.51289	-959.25006	-959.78585
smU-E	-959.5167	-959.25587	-959.78979
prodU-Z	-959.57767	-959.30960	-959.84409
prodU-E	-959.58427	-959.31804	-959.85166
Z-U1	-1556.3185	-1555.9515	-1556.6645
E-U1	-1556.3299	-1555.9607	-1556.6729
Z-U2	-1556.3237	-1555.9540	-1556.6614
E-U2	-1556.3264	-1555.9565	-1556.6654
Z-U3	-1556.3829	-1556.0102	-1556.7230
E-U3	-1556.3886	-1556.0171	-1556.7285
tsUrot	-1556.3068	-1555.9380	-1556.6473
tsZ-U2	-1556.3039	-1555.9367	-1556.6447
tsE-U2	-1556.3117	-1555.9451	-1556.6536
tsZ-U3	-1556.3136	-1555.9404	-1556.6517
tsE-U3	-1556.3078	-1555.9363	-1556.6459

Table 20. Butenyl substrate and cyclization. B3LYP-D3/6-31G(d) + SDD(Au); PCM (dichloromethane); HLT: B3LYP-D3/6-311+G(d,p) + SDD(Au).

Code	E / Hartree	G / Hartree	E_{HLT} / Hartree
smV-Z	-767.76473	-767.55063	-767.99327
smV-E	-767.76618	-767.55335	-767.99474
prodV-Z	-767.82869	-767.61012	-768.05133
prodV-E	-767.83362	-767.61521	-768.05628
Z-V1	-1364.5675	-1364.2493	-1364.8668
E-V1	-1364.5776	-1364.2578	-1364.8732
Z-V2	-1364.584	-1364.2598	-1364.8718
E-V2	-1364.584	-1364.2602	-1364.8726
Z-V3	-1364.6386	-1364.3147	-1364.9306
E-V3	-1364.6422	-1364.318	-1364.9341
tsVrot	-1364.5421	-1364.2255	-1364.8361
tsZ-V2	-1364.56	-1364.2428	-1364.8536
tsE-V2	-1364.5627	-1364.2453	-1364.8558
tsZ-V3	-1364.5699	-1364.2457	-1364.8602

tsE-V3	-1364.5678	-1364.2443	-1364.858

Table 21. Methanesulfonamide *p*MeOcinnamyl Exo- and Endo-Cleavage. B3LYP-D3/6-31G(d) + SDD(Au); PCM (dichloromethane); HLT: B3LYP-D3/6-311+G(d,p) + SDD(Au).

Code	E / Hartree	G / Hartree	E_{HLT} / Hartree
Z-W1	-1819.0090	-1818.6645	-1819.3435
E-W1	-1819.0265	-1818.6824	-1819.3576
Z-W2	-1819.0248	-1818.6786	-1819.3526
E-W2	-1819.0306	-1818.6834	-1819.3573
Z-W3	-1819.0667	-1818.7208	-1819.3982
E-W3	-1819.0830	-1818.7343	-1819.4109
Z-W4	-1819.0447	-1818.6943	-1819.3691
E-W4	-1819.0390	-1818.6912	-1819.3630
Z-W5	-1819.0887	-1818.7375	-1819.416
E-W5	-1819.0891	-1818.7378	-1819.4163
tsW1rot	-1819.0164	-1818.6682	-1819.3431
tsZ-W2	-1818.9913	-1818.6516	-1819.3243
tsE-W2	-1819.0017	-1818.6590	-1819.3348
tsZ-W3	-1819.0058	-1818.6565	-1819.3337
tsE-W3	-1818.9966	-1818.6502	-1819.3269
tsW2rot	-1819.0210	-1818.6695	-1819.3443
tsZ-W4	-1819.0088	-1818.6564	-1819.3333
tsE-W4	-1819.0086	-1818.6591	-1819.3330
tsZ-W5	-1819.0298	-1818.6813	-1819.3575
tsE-W5	-1819.0253	-1818.6769	-1819.3525

Table 22. JohnPhos migration/rotation competition, frozen substrate. B3LYP-D3/6-31G(d) + SDD(Au); PCM (dichloromethane); HLT: B3LYP-D3/6-311+G(d,p) + SDD(Au).

Code	E / Hartree	E_{HLT} / Hartree
E-S2jp	-2329.5614	-2330.1069
tsE-S3jp	-2329.5367	-2330.0757
tsSrotjp	-2329.5449	-2330.0906
E-T2jp	-2215.0260	-2215.5352
tsE-T3jp	-2215.0088	-2215.5171
tsTrotjp	-2215.0009	-2215.5128
E-U2jp	-2674.6193	-2675.1598

tsE-U3jp	-2674.6026	-2675.1415
tsUrotjp	-2674.5934	-2675.1364
E-V2jp	-2023.2822	-2023.7413
tsE-V3jp	-2023.2658	-2023.7265
tsVrotjp	-2023.2365	-2023.7017

Table 23. Smaller model substrates to study tether influence. B3LYP-D3/6-31G(d)+SDD(Au); PCM (dichloromethane); HLT: B3LYP-D3/6-311+G(d,p)+SDD(Au)

Code	E / Hartree	G / Hartree	E_{HLT} / Hartree
tsZ-X2[a]	-1100.5559	-1100.2571	-1100.7508
tsE-X2[a]	-1100.5501	-1100.2526	-1100.7449
tsZ-Y2	-1179.1903	-1178.8388	-1179.4074
tsE-Y2	-1179.1848	-1178.8340	-1179.4021
tsZ-Z2	-1139.8691	-1139.5422	-1140.0745
tsE-Z2	-1139.8627	-1139.5373	-1140.0687
tsZ-AA2	-1139.8783	-1139.5527	-1140.0842
tsE-AA2	-1139.8720	-1139.5457	-1140.0775

[a] These transition states were used for NBO analysis.

Table 24. Structures from the double-cleavage rearrangement mechanism. B3LYP-D3/6-31G(d)+SDD(Au); PCM (dichloromethane); HLT: B3LYP-D3/6-311+G(d,p)+SDD(Au)

Code	E / Hartree	G / Hartree	E_{HLT} / Hartree
R1	-908.82328	-908.57996	-908.97783
R2	-908.82888	-908.57923	-908.97586
R3	-908.82632	-908.57898	-908.97511
R4	-908.82050	-908.57528	-908.97099
R5	-908.87578	-908.62703	-909.02605
TSR2	-908.80385	-908.55705	-908.95447
TSR3	-908.80879	-908.55950	-908.95514
TSR4	-908.82006	-908.57306	-908.97036
TSR5	-908.81239	-908.56738	-908.96351
TSR3-R3 hidden int.	-908.81482	N/A	-908.96250

Table 25. Chloroenyne alkoxycyclisations and eliminations. B3LYP-D3/6-31G(d)+SDD(Au); PCM (dichloromethane); HLT: B3LYP-D3/6-311+G(d,p)+SDD(Au)

Code	E / Hartree	G / Hartree	E_{HLT} / Hartree

AB1	-1560.14643	-1559.86888	-1560.37830
AB3	-1560.18199	-1559.89613	-1560.40628
AB3b	-1560.16403	-1559.88029	-1560.39169
AB2	-1560.17308	-1559.88862	-1560.40030
AB2b	-1560.17286	-1559.88678	-1560.40026
AB4	-1675.91807	-1675.57925	-1676.18875
AB4b	-1791.67123	-1791.28355	-1791.98796
AB4c	-1907.41313	-1906.97808	-1907.77634
AB4d	-2023.16365	-2022.67571	-2023.56949
AB6_cisoid	-1559.75412	-1559.48183	-1559.98850
AB6_transoid	-1559.75482	-1559.48245	-1559.98881
AB8	-1560.18681	-1559.90162	-1560.41331
AB10	-1675.91375	-1675.57617	-1676.18426
AB7	-1559.75527	-1559.48331	-1559.98782
AB9	-1559.76242	-1559.48939	-1559.99477
AB5	-1675.50909	-1675.18282	-1675.77993
AB14	-1791.65686	-1791.27443	-1791.98223
AB15	-1560.21018	-1559.92433	-1560.43908
TSAB2	-1560.14277	-1559.86317	-1560.37236
TSAB2b	-1560.16750	-1559.88431	-1560.39539
TSAB6	-1791.63640	-1791.25956	-1791.96037
TSbAB6	-1791.63343	-1791.25962	-1791.95780
TSAB2b-8	-1560.14674	-1559.86547	-1560.37569
TSAB10	-1675.91278	-1675.57558	-1676.18394
TSAB7-8	-1791.63036	-1791.25372	-1791.95271
TSAB9	-1791.64228	-1791.26483	-1791.96524
TSAB3	-1560.13509	-1559.85529	-1560.36582
TSAB3b	-1560.13246	-1559.85246	-1560.36249
TSAB15	-1791.65321	-1791.27806	-1791.97682
TSAB7	-1791.63207	-1791.25345	-1791.95430

Table 26. Protonated chloroenyne intermediates and Brønsted acid-mediated transition states. B3LYP-D3/6-31G(d) + SDD(Au); PCM (dichloromethane); HLT: B3LYP-D3/6-311+G(d,p) + SDD(Au).

Code	E / Hartree	G / Hartree	E_{HLT} / Hartree
AB16	-963.33602	-963.15979	-963.50938
AB17	-963.73963	-963.55263	-963.90782

AB11	-963.74652	-963.55842	-963.91134
AB18	-963.39829	-963.21625	-963.56847
AB19	-963.81138	-963.61815	-963.97405
AB20	-963.75392	-963.56475	-963.92030
AB18b	-963.39948	-963.21746	-963.56929
AB19b	-963.81198	-963.61738	-963.97495
AB12	-963.80394	-963.61202	-963.96737
TSAB12	-963.74527	-963.55611	-963.90954
TSAB13	-1927.14080	-1926.75340	-1927.47410
TSbAB13	-1195.27656	-1194.98874	-1195.53486

Table 27. Methylenyne alkoxycyclisations and eliminations. B3LYP-D3/6-31G(d)+SDD(Au); PCM (dichloromethane); HLT: B3LYP-D3/6-311+G(d,p)+SDD(Au).

Code	E / Hartree	G / Hartree	E_{HLT} / Hartree
AC1	-1139.89809	-1139.58126	-1140.11037
AC3	-1139.89339	-1139.57114	-1140.09979
AC2	-1139.91008	-1139.58564	-1140.11405
AC2b	-1139.88461	-1139.56456	-1140.09218
AC8	-1139.93143	-1139.60784	-1140.13669
AC4	-1255.62729	-1255.24846	-1255.87768
AC4b	-1371.38163	-1370.95431	-1371.67760
AC6_cisoid	-1139.47123	-1139.16037	-1139.68441
AC6_transoid	-1139.47432	-1139.16448	-1139.68781
AC7	-1139.47544	-1139.16614	-1139.68769
AC5	-1255.21765	-1254.85216	-1255.46802
TSAC3	-1139.88036	-1139.56214	-1140.08883
TSAC2	-1139.88003	-1139.56107	-1140.08910
TSAC2b	-1139.87572	-1139.55626	-1140.08435
TSAC2b-8	-1139.87139	-1139.55275	-1140.08015
TSAC6 cisoid	-1371.35259	-1370.93902	-1371.65597
TSAC6 transoid	-1371.35520	-1370.94143	-1371.65866
TSbAC6	-1371.35143	-1370.93871	-1371.65372
TSAC7-8	-1371.36185	-1370.94787	-1371.66429
TSAC7	-1371.35291	-1370.93952	-1371.65521

Table 28. Phenylenyne alkoxycyclisations and eliminations. B3LYP-D3/6-31G(d) + SDD(Au); PCM (dichloromethane); HLT: B3LYP-D3/6-311+G(d,p) + SDD(Au).

Code	E / Hartree	G / Hartree	E_{HLT} / Hartree
AD1	-1331.64504	-1331.27826	-1331.90458
AD3	-1331.64125	-1331.27105	-1331.89583
AD2	-1331.65775	-1331.28456	-1331.90880
AD2b	-1331.63523	-1331.26629	-1331.89011
AD8	-1331.67977	-1331.30850	-1331.93166
AD4	-1447.37601	-1446.95076	-1447.67393
AD4b	-1563.13038	-1562.65696	-1563.47366
AD6_cisoid	-1331.21994	-1330.86035	-1331.48095
AD6_transoid	-1331.22127	-1330.86192	-1331.48298
AD7	-1331.22638	-1330.86796	-1331.48606
AD5	-1446.96615	-1446.55378	-1447.26415
TSAD3	-1331.62799	-1331.26163	-1331.88449
TSAD2	-1331.63013	-1331.26334	-1331.88611
TSAD2b	-1331.62457	-1331.25726	-1331.88005
TSAD2b-8	-1331.62122	-1331.25306	-1331.87751
TSAD6 cisoid	-1563.10236	-1562.63992	-1563.45354
TSAD6 transoid	-1563.10346	-1562.64033	-1563.45480
TSbAD6	-1562.63848	-1562.63848	-1563.44953
TSAD7-8	-1562.64878	-1562.64878	-1563.46140
TSAD7	-1562.63887	-1562.63887	-1563.45150

Table 29. Methanol clusters, neutral and protonated. B3LYP-D3/6-31G(d) + SDD(Au); PCM (dichloromethane); HLT: B3LYP-D3/6-311+G(d,p) + SDD(Au).

Code	E / Hartree	G / Hartree	E_{HLT} / Hartree
m1	-115.71753	-115.68892	-115.77095
m2a	-231.44894	-231.37568	-231.55089
m3Aa	-347.18581	-347.06447	-347.33398
m3Ab	-347.18621	-347.06409	-347.33379
m3Ba	-347.19120	-347.06844	-347.33560
m4Aa	-462.91964	-462.75266	-463.11603
m4Ab	-462.91704	-462.75296	-463.11435
m4Ac	-462.92175	-462.75309	-463.11616
m4Ad	-462.92134	-462.75161	-463.11660
m4Ae	-462.91962	-462.75287	-463.11618
m4Ba	-462.92093	-462.74893	-463.11537

m4Ca	-462.93417	-462.76548	-463.12630
m4Cb	-462.93455	-462.76452	-463.12622
m4Cc	-462.93485	-462.76428	-463.12651
m6	-694.40525	-694.14719	-694.69483
pm1	-116.11177	-116.07015	-116.16045
pm2a	-231.86924	-231.78377	-231.96507
pm2b	-231.86908	-231.78287	-231.96504
pm3Aa	-347.61601	-347.48003	-347.75928
pm3Ab	-347.61657	-347.48011	-347.75989
pm3Ba1	-347.61374	-347.48034	-347.75549
pm3Ba2	-347.61320	-347.47791	-347.75495
pm4Aa1	-463.35503	-463.17494	-463.54641
pm4Aa2	-463.34621	-463.16431	-463.53760
pm4Ab1	-463.35576	-463.17747	-463.54614
pm4Ab2	-463.35748	-463.17519	-463.54711
pm4Ac1	-463.35554	-463.17566	-463.54653
pm4Ac2	-463.34644	-463.16171	-463.53742
pm4Ad1	-463.35676	-463.17462	-463.54672
pm4Ad2	-463.32905	-463.14892	-463.52242
pm4Ae1	-463.35834	-463.17867	-463.54821
pm4Ba	-463.34349	-463.16137	-463.53559
pm4Ca	-463.36402	-463.17992	-463.55165
pm4Cb1	-463.36299	-463.17870	-463.55030
pm4Cb2	-463.36399	-463.18046	-463.55162
pm4Cc	-463.36431	-463.18178	-463.55191
pm6	-694.84076	-694.56696	-695.12572

Chapter II

Gold(I)-Catalysed 1,3,5-Cyclotrimerisation of Alkynes

Introduction

Alkynes as Nucleophiles in Gold(I) Catalysis

Gold(I) catalysis, notable for catalysing a wide range of cyclisations, additions and cycloisomerisations of unsaturated systems, shows excellent or perfect atom economy for the majority of these processes.

Regarding the discovery of atom-economic reactions, those related to additions to unsaturated compounds have been some of the most successful processes, among which alkyne dimerisations and trimerisations are key examples.[1] Furthermore, selective trimerisations between unlike molecules can allow the creation of molecular complexity in a modular manner.[2]

In gold(I) chemistry, there have been very limited advances in such reactions due to the greater difficulties associated to intermolecular reactivity in carbon-carbon bond formations.[3] An exception is the dimerisation of push-pull alkynes to form triarylnaphthalene products (Scheme 1).[4] However, this was limited to very specific electronically biased alkynes and formed compounds with a limited substitution pattern.

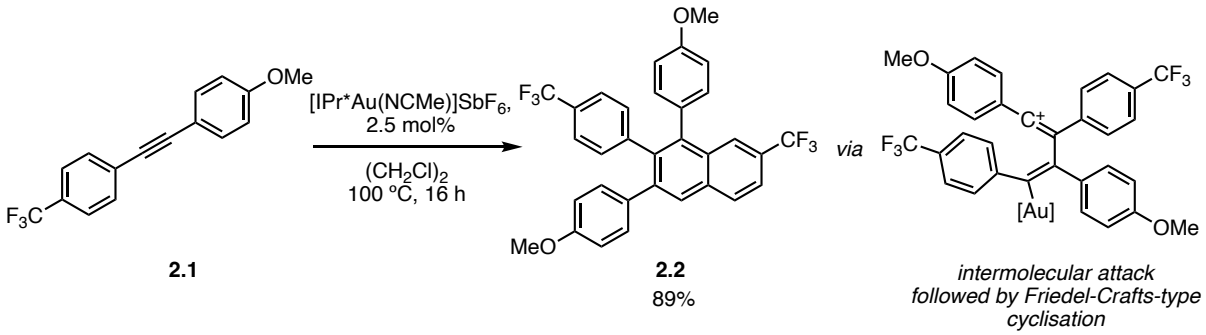

Scheme 1. Only known example of gold(I)-catalysed direct intermolecular attack of two alkynes.

However, there are several examples of gold(I)-catalysed cyclisations of diynes in which alkynes react intramolecularly.[5] The intermediates are then trapped by external pronucleophiles, isomerisation or Friedel-Crafts-type reactions. Many of the transformations that have been explored do not show a direct alkyne attack as a nucleophile. Instead, many involve the isomerisation of a propargylic ester or

1 Trost, B. M. On Inventing Reactions for Atom Economy. *Acc. Chem. Res.* **2002**, *35*, 695–705.
2 Ogata, K.; Sugasawa, J.; Fukuzawa, S. Highly Chemoselective Nickel-Catalyzed Three-Component Cross-Trimerization of Three Distinct Alkynes Leading to 1,3-Dien-5-Ynes. *Angew. Chem. Int. Ed.* **2009**, *48*, 6078–6080.
3 Dorel, R.; Echavarren, A. M. Gold(I)-Catalyzed Activation of Alkynes for the Construction of Molecular Complexity. *Chem. Rev.* **2015**, *115*, 9028–9072.
4 Weingand, V.; Wurm, T.; Vethacke, V.; Dietl, M. C.; Ehjeij, D.; Rudolph, M.; Rominger, F.; Xie, J.; Hashmi, A. S. K. Intermolecular Desymmetrizing Gold-Catalyzed Yne-Yne Reaction of Push-Pull Diarylalkynes. *Chem. Eur. J.* **2018**, *24*, 3725–3728.
5 Ohno, H. Gold-Catalyzed Cascade Reactions of Alkynes for Construction of Polycyclic Compounds. *Isr. J. Chem.* **2013**, *53*, 869–882.

carbonate to the allenyl ester, followed by further cyclisation,[6] or similar isomerisations through hydrogen migration.[7]

Several examples are known to involve the direct cyclisation of two alkynes. With the discovery of dual activation of a 1,5-diyne substrate by Zhang and coworkers, the cyclisation of 1,2-dialkynylbenzenes could be conducted leading to cyclic benzofulvenes.[8] The σ-bonded gold catalyst is proposed to become a gold(I) vinylidene which then undergoes C-H insertion onto the alkyl chain (Scheme 2a).

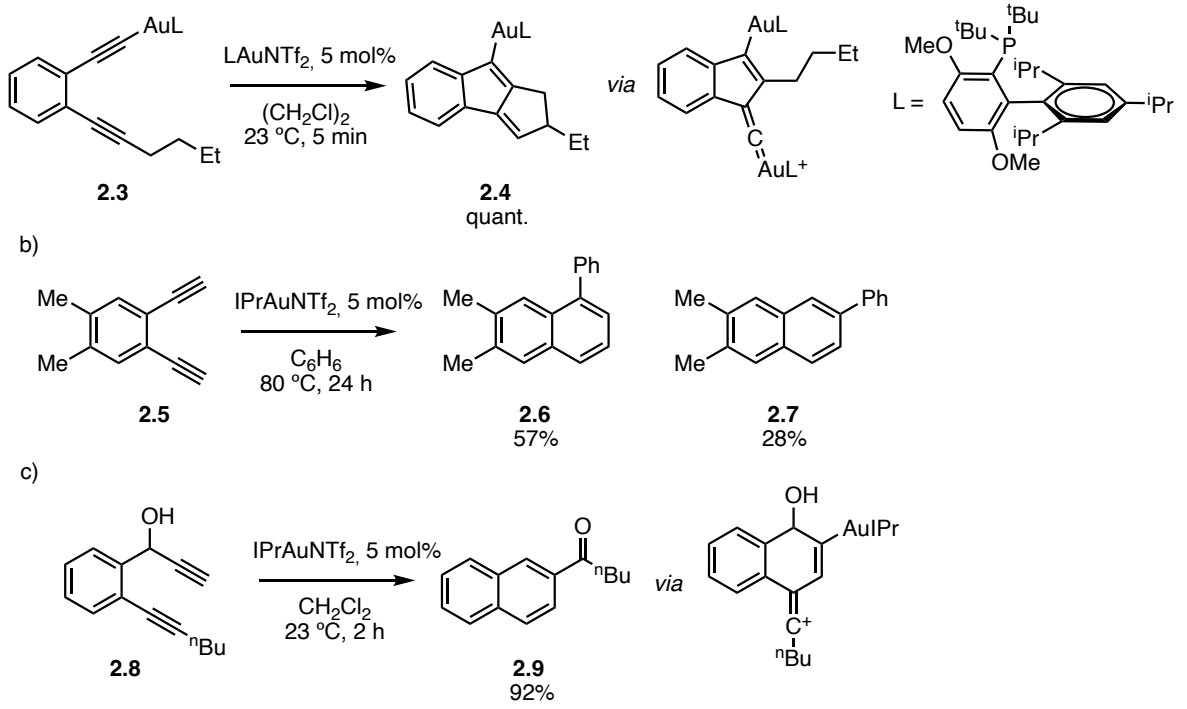

Scheme 2. a) Dual catalysis leading to benzofulvene products through vinylidene intermediates. b) Gold(I)-catalysed diyne cyclisation with intermolecular arylation. c) Formation of 2-acylnaphthalenes proposed to involve vinyl carbocations after alkyne attack.

The same year, Hashmi reported the intermolecular reaction between **2.5** and benzene to form phenylnaphthalene products **2.6** and **2.7**, showing some further evidence that dual activation of an alkyne could take place (Scheme 2b).[9] In a subsequent publication, the reasons for the selectivity of the

6 For a review on this reactivity: Day, D. P.; Chan, P. W. H. Gold-Catalyzed Cycloisomerizations of 1, *n* -Diyne Carbonates and Esters. *Adv. Synth. Catal.* **2016**, *358*, 1368–1384.

7 Pandit, Y. B.; Liu, R. Gold-Catalyzed Aminoaromatizations of 1,2-Bis(Alkynyl)Benzenes with Anthranils to Yield 1-Amino-2-napthaldehyde Products. *Adv. Synth. Catal.* **2020**, *362*, 3183–3189.

8 Ye, L.; Wang, Y.; Aue, D. H.; Zhang, L. Experimental and Computational Evidence for Gold Vinylidenes: Generation from Terminal Alkynes via a Bifurcation Pathway and Facile C–H Insertions. *J. Am. Chem. Soc.* **2012**, *134*, 31–34.

9 Hashmi, A. S. K.; Braun, I.; Rudolph, M.; Rominger, F. The Role of Gold Acetylides as a Selectivity Trigger and the Importance of *Gem* -Diaurated Species in the Gold-Catalyzed Hydroarylating-Aromatization of Arene-Diynes. *Organometallics* **2012**, *31*, 644–661.

diyne cyclisations were explored, demonstrating that the selectivity came from electronic effects and the presence of a bifurcation for very stabilised carbocationic intermediates.[10]

Likewise, the formation of 2-acylnaphthalene products *via* gold-catalysed rearrangement of diynols such as **2.8** were proposed to undergo an initial alkyne attack onto the other one, coordinated to the gold(I) atom (Scheme 2c).[11]

Cyclotrimerisation of Alkynes

The cyclotrimerisation of alkynes to form trisubstituted benzenes, driven by the energy gain upon carbon-carbon bond formation and aromatisation, has been a particularly prolific area of research, both from a synthetic[12] and a mechanistic point of view,[13] with new developments including helical chirality or selective cross-trimerisations.[14] Although there has been continued interest in this transformation, it was one of the first well-defined oligomerisations to be studied.

In 1948, Reppe and Schweckendiek discovered that metal complexes could function as catalysts in the [2+2+2] cycloaddition of alkynes.[15] In this early report, the nickel-catalysed process afforded mixtures of the two possible regioisomers, the 1,2,4- and 1,3,5-trisubstituted benzenes generally in approximately 1:1 mixtures. Styrene was also formed when acetylene was used as the substrate (in a tetramerisation), as well as dihydrobenzoic acids when alkynes were co-trimerised with acrylates.

Since this very early report, there were many examples of metal-catalysed cyclotrimerisations, including iron, molybdenum, manganese, cobalt,[16] palladium[17] as well as later discovered ones with ruthenium[18] among other metals. Most of these reactions afforded mixtures of regioisomers in varying degrees, with a limited number being selective towards the 1,2,4-cyclotrimerised product.

10 Hansmann, M. M.; Tšupova, S.; Rudolph, M.; Rominger, F.; Hashmi, A. S. K. Gold-Catalyzed Cyclization of Diynes: Controlling the Mode of 5-*Endo* versus 6-*Endo* Cyclization-An Experimental and Theoretical Study by Utilizing Diethynylthiophenes. *Chem. Eur. J.* **2014**, *20*, 2215–2223.

11 Lauterbach, T.; Arndt, S.; Rudolph, M.; Rominger, F.; Hashmi, A. S. K. Gold Catalysis: β-Ketonaphthalenes *via* Molecular Gymnastics of 1,6-Diyne-4-En-3-Ols. *Adv. Synth. Catal.* **2013**, *355*, 1755–1761.

12 Dominguez, G.; Perez-Castells, J. Recent advances in [2 + 2 + 2] cycloaddition reactions. *Chem. Soc. Rev.* **2011**, *40*, 3430−3444.

13 Roglans, A.; Pla-Quintana, A.; Solà, M. Mechanistic Studies of Transition-Metal-Catalyzed [2 + 2 + 2] Cycloaddition Reactions. *Chem. Rev.* **2021**, *121*, 1894–1979.

14 Broere, D. L. J.; Ruijter, E. Recent Advances in Transition-Metal-Catalyzed [2+2+2]-Cyclo(co)trimerization Reactions. *Synthesis* **2012**, *44*, 2639–2672.

15 Reppe, W.; Schweckendiek; W. J. Cyclisierende Polymerisation von Acetylen. III Benzol, Benzolderivate und hydroaromatische Verbindungen. *Justus Liebigs Ann. Chem.* **1948**, *560*, 104–116.

16 Hübel, W.; Hoogzand, C. Die cyclisierende Trimerisierung von Alkinen mit Hilfe von Metallcarbonyl-Verbindungen. *Chem. Ber.* **1960**, *93*, 103–115.

17 Blomquist, A. T.; Maitlis, P. M. Reactions of Palladium Compounds with Acetylenes. I. Tetraphenylcyclobutadiene-palladium(II) Chloride. J. Am. Chem. Soc. **1962**, *84*, 2329–2334.

18 Das, S. K.; Roy, R. Mild Ruthenium-Catalyzed Intermolecular Alkyne Cyclotrimerization. *Tetrahedron Letters* **1999**, *40*, 4015–4018.

However, the early understanding of the mechanism was very limited by the lack of analytical techniques suited to this purpose. The chromium-catalysed reaction in particular was proposed to form an η^4-cyclobutadiene chromium complex with subsequent insertion of the third alkyne to yield substituted benzenes. However, Whitesides and Ehmann conclusively disproved this mechanism (Scheme 3) by studying the outcome in the cyclotrimerisation of 1,1,1-d_3-2-butyne.[19] As product **2.14** was not formed, which should have formed in a 12.5% yield ignoring the negligible isotopic effects, the reaction mechanism could not be mediated by η^4-cyclobutadiene complexes. To confirm the ratio of products formed, the authors reduced the hexamethylbenzenes to the 1,4-cyclohexadienes and characterised the ozonolysis products by mass spectrometry.

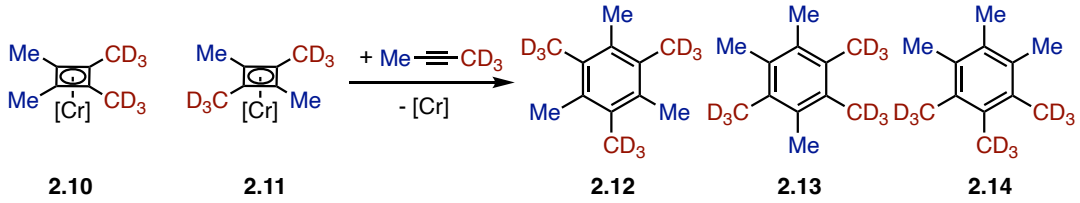

Scheme 3. Chromium-catalysed trimerisation of alkynes. Product **2.14** was not observed. If the proposed mechanism was correct, the predicted product ratio should have been 2:5:1 (**2.12**:**2.13**:**2.14**).

In a subsequent publication, the metallacyclopentadiene mechanism is proposed as a mechanism that forms **2.12** and **2.13** exclusively, which is now known to be the pathway operating in most of these transformations (Scheme 4).[20] However, by running the same cyclotrimerisation with aluminium trichloride as the catalyst, they found that **2.14** formed in 12% yield, suggesting intermediacy of a cyclobutadiene fragment **2.16** (Scheme 4). This was supported by the isolation of hexamethyl-Dewar benzene if the reaction was run under milder conditions.

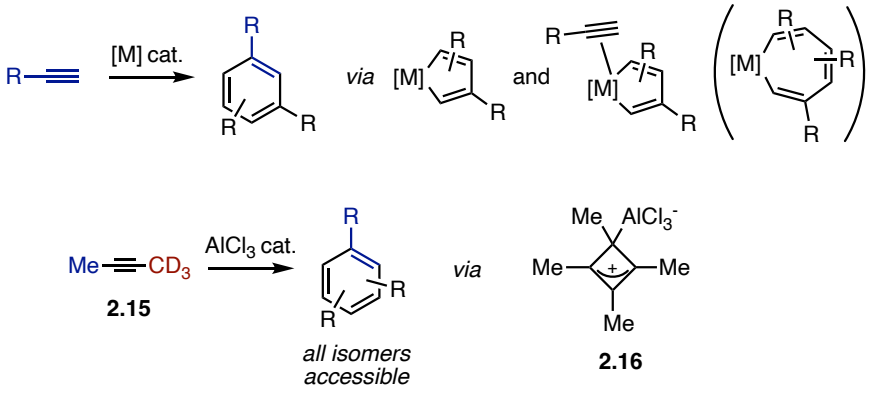

Scheme 4. a) Intermediates present in the metal-catalysed cyclotrimerisation of alkynes, M = Ni, Co, Cr, Mn, Mo, Fe, Pd, among others. b) Key intermediate in aluminium-catalysed cyclotrimerisations.

19 Whitesides, G. M.; Ehmann, W. J. Cyclotrimerization of 2-butyne-1,1,1-d3 by triphenyltris(tetrahydrofuran)-chromium(III). *J. Am. Chem. Soc*. **1968**, *90*, 804–805.

20 Whitesides, G. M.; Ehmann, W. J. The Cyclotrimerization of 2-Butyne-1,1,1-d, by Transition Metal Catalysts. *J. Am. Chem. Soc*. **1969**, *90*, 804–805.

The exact mechanism remained controversial for several years, with Nenitzescu and coworkers reporting the formation of tri-*tert*-butyl Dewar benzenes from trimerisation of *tert*-butylacetylene with a palladium catalyst (Figure 1).[21] They suggested reversible interconversion between isomers and a product ratio dependent on the final ring-opening aromatisation. However, Maitlis's group discredited the previous assignment of the Dewar benzene complexes: attempting to coordinate a palladium source to independently synthesised Dewar benzene led to decomposition faster than complex formation, conclusively determining that "Dewar benzene complexes [did] not appear to be direct intermediates in the [palladium-catalysed] trimerisation of *tert*-butylacetylene".[22]

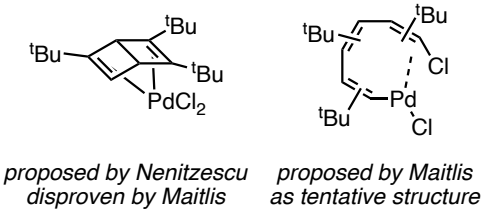

Figure 1. Proposed intermediates in the palladium-catalysed cyclotrimerisation of *tert*-butylacetylene.

While the general mechanism involving the formation of a metallacycloheptatriene was supported experimentally for several metals, later theoretical studies found the direct intramolecular [4+2] reaction between a cobaltacyclopentadiene and a coordinated alkyne to be more likely for cyclopentadienyl cobalt catalysts (Scheme 5).[23]

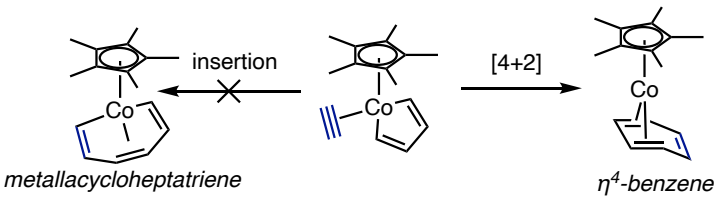

Scheme 5. The [4+2] mechanism is calculated to be preferred. The metallacycloheptatriene pathway is the more accessible one for other metals.

The reaction still involved the formation of a metallacyclopentadiene intermediate by oxidative coupling of the alkynes, preserving the initial step common to palladium catalysis. The majority of later experimental examples of cyclotrimerisation reactions with a variety of different transition metals

21 Avram, M.; Avram, E.; Mateescu, G. D.; Dinulescu, I. G.; Chiraleu, F.; Nenitzescu, C. D. Untersuchungen in der Cyclobutanreihe, XXIII. Cyclisierende Trimerisierung von tert.-Butylacetylen zu einem Dewar-Benzol-Palladiumchlorid-Komplex. *Chem. Ber.* **1969**, *102*, 3996–4007.

22 Kaiser, K. L.; Maitlis, P. M. On the Existence and Stability of a Tri-t-Butyl("Dewar Benzene")Palladium Chloride Complex. *J. Chem. Soc. D* **1970**, 942–943.

23 Hardesty, J. H.; Koerner, J. B.; Albright, T. A.; Lee, G.-Y. Theoretical Study of the Acetylene Trimerization with CpCo. *J. Am. Chem. Soc.* **1999**, *121*, 6055–6067.

would find identical pathways or refer to this mechanism to propose catalytic cycles.[24,25,26] On occasion, this would be likely an oversimplification and several experimental observations would not be fully accounted by the previously described mechanisms. Some of these examples will be discussed in more detail.

Parallelly to the development of mid or late transition metal-catalysed cyclotrimerisations, groups exploring the reactivity of main group metals (sometimes in conjunction with early transition metals) found similarly efficient reactions. The cyclotrimerisation of internal alkynes to afford the hexasubstituted benzenes was discovered in the late 1950s to be catalysed by mixtures of triisobutylaluminium and titanium tetrachloride in a range of 1:1 to 3:1 molar ratio.[27] Under optimised conditions, this bimetallic catalyst system was found to yield hexamethylbenzene quantitatively from 2-butyne.

An issue in most of the cyclotrimerisation reactions was that of regioselectivity, in particular when mixtures were obtained. This severely limited the possibility to carry out cross-trimerisations between two or more alkynes, as the resulting complex mixtures would lead to lower yields.[13]

A typical approach was to tether the alkynes, thereby cyclotrimerising a diyne with an alkyne.[28] This relied on geometric constraints to achieve one single well-defined precursor and rely on combined steric and electronic effects to obtain good regioselectivity with the cross-trimerisation partner. Alternatively, the reaction could also be performed completely intramolecularly with triyne substrates.[29] These reactions allowed the wide applicability of cyclotrimerisations in synthesis of more complex molecules by overcoming the usual limitations with regioselectivity, but consequentially required multi-step syntheses of the precursors. While the tethered substrates generally furnished approaches to 1,2,4-cyclotrimerised products, modification of the tether also provided new routes towards 1,3,5-like substitution patterns (**2.18** and **2.19**, Scheme 6).[30] Due to the scarcity of experimental protocols to reach the latter family of products, these methods of achieving high or perfect regioselectivity proved to be valuable.

24 Dachs, A.; Torrent, A.; Pla-Quintana, A.; Roglans, A.; Jutand, A. Rates and Mechanism of Rhodium-Catalyzed [2+2+2] Cycloaddition of Bisalkynes and a Monoalkyne. Organometallics **2009**, *28*, 6036-6043.

25 Dahy, A. A.; Koga, N. Trimerization of Alkynes in the Presence of a Hydrotris(pyrazolyl)borate Iridium Catalyst and the Effect of Substituent Groups on the Reaction Mechanism: A Computational Study. Organometallics **2015**, *34*, 4965-4974.

26 Smith, P. J; Tong, Z.; Ragus, J.; Solon, P.; Shimkin, K. W.; Anderson, E. A. Rhodium-Catalyzed [2+2+2] Cyclotrimerizations of Yndiamides with Alkynes. Organic Letters **2022**, *24*, 7522-7526.

27 Franzus, B.; Canterino, P. J.; Wickliffe, R. A. Titanium Tetrachloride–Trialkylaluminium Complex – A Cylcizing Catalyst for Acetylenic Compounds. *J. Am. Chem. Soc.* **1959**, *81*, 1514.

28 Vollhardt, K. P. C. Cobalt-Mediated [2 + 2 + 2]-Cycloadditions: A Maturing Synthetic Strategy. *Angew. Chem. Int. Ed. Engl.* **1984**, *23*, 539–556.

29 Yamamoto, Y. Recent Advances in Intramolecular Alkyne Cyclotrimerization and Its Applications. *Curr. Org. Chem.* **2005**, *9*, 503−519.

30 Chouraqui, G.; Petit, M.; Aubert, C.; Malacria, M. Totally Chemo- and Regioselective Cobalt(I)-Mediated Formal Intermolecular Cyclotrimerization of Alkynes. *Org. Lett.* **2004**, *6*, 1519–1521.

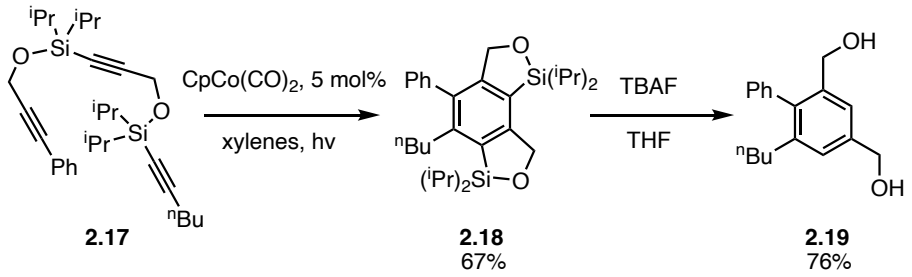

Scheme 6. Triyne substrate tethered with silyl groups as a template for 1,3,5-like cyclotrimerisations.

1,3,5-Selective Cyclotrimerisation of Alkynes

Remarkably for a field that developed over several decades, the 1,3,5-selective cyclotrimerisation remained comparatively elusive. This is surprising as there would be no shortage of applications for the products: 1,3,5-trisubstituted benzenes have found widespread applications in ligand design,[31] synthesis,[32] photophysical applications,[33] precursors for discotic liquid crystals,[34] and in polymer chemistry.[35] Additionally, current methodologies have relied heavily on condensation reactions with precursors that require multistep syntheses,[36] or cross-coupling reactions.[37]

Early transition metals have also been successful in improving the selectivity towards the less common 1,3,5-cyclotrimer. Reduced niobium chloride complexes were found to preferentially form the 1,3,5-cyclotrimerised products, becoming the only observed product for alkynes with electron-withdrawing groups.[38] The mechanistic understanding for this selectivity was limited, as the authors proposed an identical mechanism to those observed with other metals that yield mixtures or are 1,2,4-selective. However, they proposed that the dinuclear nature of the catalysts could be responsible for divergent activation.

31 Tsui, E. Y.; Day, M. W.; Agapie, T. Trinucleating Copper: Synthesis and Magnetostructural Characterization of Complexes Supported by a Hexapyridyl 1,3,5-Triarylbenzene Ligand. *Angew. Chem. Int. Ed.* **2011**, *50*, 1668–1672.

32 Kotha, S.; Lahiri, K.; Sreevani, G. Design and Synthesis of Aromatics through [2+2+2] Cyclotrimerization. *Synlett* **2018**, *29*, 2342−2361.

33 Jagadesan, P.; Whittemore, T.; Beirl, T.; Turro, C.; McGrier, P. L. Excited-State Intramolecular Proton-Transfer Properties of Three Tris(*N* -Salicylideneaniline)-Based Chromophores with Extended Conjugation. *Chem. Eur. J.* **2017**, *23*, 917–925.

34 Several examples mentioned in Sergeyev, S.; Pisula, W.; Geerts, Y. H. Discotic Liquid Crystals: A New Generation of Organic Semiconductors. *Chem. Soc. Rev.* **2007**, *36*, 1902.

35 Colson, J. W.; Dichtel, W. R. Rationally Synthesized Two-Dimensional Polymers. *Nat. Chem.* **2013**, *5*, 453–465.

36 Zhang, C.-L.; Ye, S. N-Heterocyclic Carbene-Catalyzed Construction of 1,3,5-Trisubstituted Benzenes from Bromoenals and α-Cyano-β-Methylenones. *Org. Lett.* **2016**, *18*, 6408–6411.

37 Lee, D.-H.; Jin, M.-J. An Extremely Active and General Catalyst for Suzuki Coupling Reaction of Unreactive Aryl Chlorides. *Org. Lett.* **2011**, *13*, 252–255.

38 Kakeya, M.; Fujihara, T.; Kasaya, T.; Nagasawa, A. Dinuclear Niobium(III) Complexes [{$NbCl_2(L)$}$_2$(μ-Cl)$_2$(μ-L)](L = Tetrahydrothiophene, Dimethyl Sulfide): Preparation, Molecular Structures, and the Catalytic Activity for the Regioselective Cyclotrimerization of Alkynes. *Organometallics* **2006**, *25*, 4131–4137.

Vanadium diketiminate complexes were also found to be 1,3,5-selective when a sufficiently sterically encumbered ligand was used, with the selectivity dropping significantly with smaller ligands.[39]

A quintuple-bonded dimolybdenum complex **2.22** was found to catalyse the fully selective 1,3,5-cyclotrimerisation of 1-pentyne (Scheme 7). It was found to undergo a [2+2+2] cycloaddition with two equivalents of 1-pentyne to form an aromatic C_4Mo_2 ring **2.23**, which was then confirmed to be an intermediate in the catalytic cycle.[40] This unique transformation, with perfect selectivity towards the unusual product, was studied computationally in depth, revealing the importance of the metal-metal bonded dinuclear core.[41]

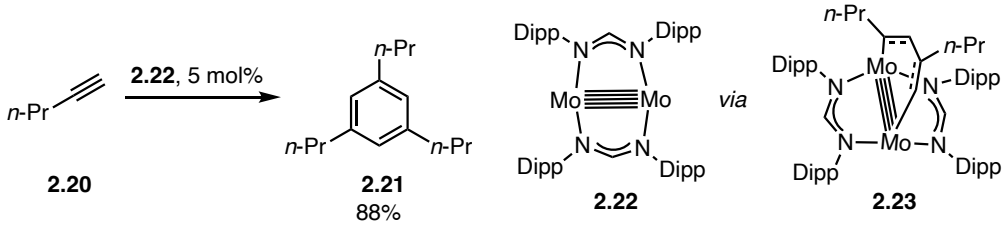

Scheme 7. Molybdenum-catalysed 1,3,5-cyclotrimerisation of a terminal alkyne.

As we see in several of these examples and, as found in most mechanistic investigations in this line,[42] the multiply-bonded nature of a bimetallic core is a key feature present in most early (or mid) transition metal catalysts that lead to high selectivity.

Mid to late first-row transition metals, in spite of their better-known selectivity towards 1,2,4-trisubstituted products[43] or the formation of regioisomeric mixtures, have also been employed successfully in 1,3,5-cyclotrimerisations.[13]

An iron diiminopyridine catalyst was found to give extremely high 1,3,5 regioselectivity for propargylic terminal alkynes, reaching excellent yields with more than 95% regioselectivity for a wide variety of substrates.[44] It showed perfect tolerance for functional groups such as alkyl tosylates, esters, or boronic esters. However, the unusual selectivity dropped to regioisomeric ratios of about 1:1 for simple arylacetylenes, which incidentally had been found to perform in other transformations with other

39 Chang, K.-C.; Lu, C.-F.; Wang, P.-Y.; Lu, D.-Y.; Chen, H.-Z.; Kuo, T.-S.; Tsai, Y.-C. Ligand-Controlled Synthesis of Vanadium(I) β-Diketiminates and Their Catalysis in Cyclotrimerization of Alkynes. *Dalton Trans.* **2011**, *40*, 2324–2331.

40 Chen, H.-Z.; Liu, S.-C.; Yen, C.-H.; Yu, J.-S. K.; Shieh, Y.-J.; Kuo, T.-S.; Tsai, Y.-C. Reactions of Metal-Metal Quintuple Bonds with Alkynes: [2+2+2] and [2+2] Cycloadditions. *Angew. Chem. Int. Ed.* **2012**, *51*, 10342–10346.

41 Chen, Y.; Sakaki, S. The Important Role of the Mo–Mo Quintuple Bond in Catalytic Synthesis of Benzene from Alkynes. A Theoretical Study. *Dalton Trans.* **2014**, *43*, 11478–11492.

42 For examples in cyclotrimerisations and related oligomerisations: Rej, S.; Tsurugi, H.; Mashima, K. Multiply-Bonded Dinuclear Complexes of Early-Transition Metals as Minimum Entities of Metal Cluster Catalysts. *Coord. Chem. Rev.* **2018**, *355*, 223–239.

43 Liu, Y.; Yan, X.; Yang, N.; Xi, C. Highly regioselective cyclotrimerization of terminal alkynes catalyzed by Fe(II) complexes bearing 2-(benzimidazolyl)-6(1-(arylamino)ethyl)pyridines. *Catal. Commun.* **2011**, *12*, 489−492.

44 Doll, J. S.; Eichelmann, R.; Hertwig, L. E.; Bender, T.; Kohler, V. J.; Bill, E.; Wadepohl, H.; Roşca, D.-A. Iron-Catalyzed Trimerization of Terminal Alkynes Enabled by Pyrimidinediimine Ligands: A Regioselective Method for the Synthesis of 1,3,5-Substituted Arenes. *ACS Catal.* **2021**, *11*, 5593–5600.

catalysts (Scheme 8). The suggested mechanism attributes the selectivity to destabilising steric clashes. An anionic metallacyclopentadiene was prepared and characterised, but beyond its likely involvement in analogous mechanisms, no further in-depth mechanistic study was carried out. The proposed model did not account for the differences observed with non-propargylic alkynes.

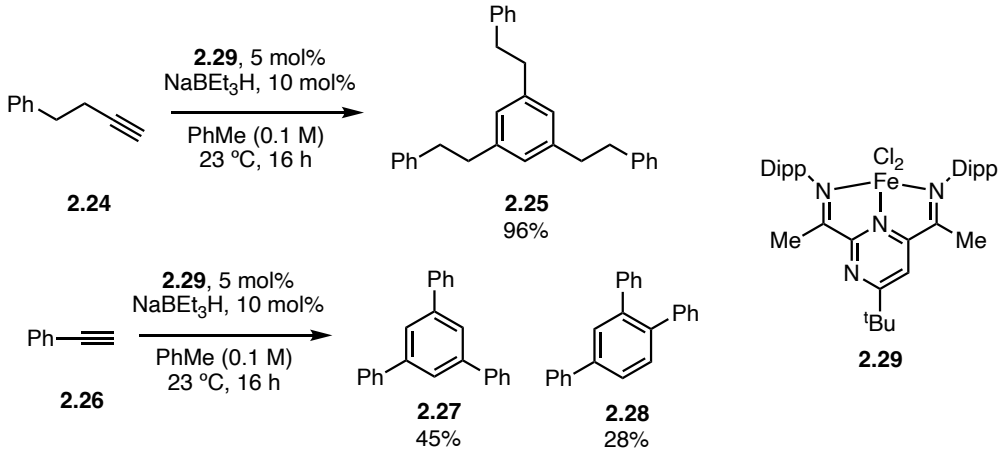

Scheme 8. Diiminopyridineiron as a catalyst for the 1,3,5-selective trimerisation of alkynes. Divergence in selectivity with propargylic alkynes and arylalkynes.

Cobalt catalysts have been known to catalyse the 1,2,4-selective cyclotrimerisation. In a particular example, however, the selectivity was found to switch dramatically depending on the solvent system when a bidentate bis(thioether) ligand was used, reaching a maximum of 2.6:1 for the 1,3,5-trimer (Scheme 9).[45] Again, no mechanism was proposed to account for the differing selectivity as well as no discussion on the possible effects of using zinc powder and zinc iodide as additives.

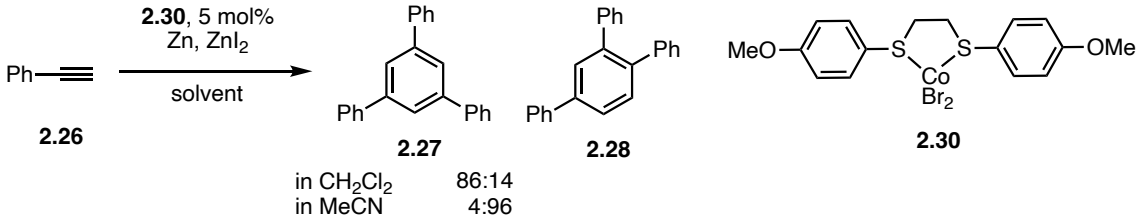

Scheme 9. Solvent-dependent regioselectivity in a cobalt-catalysed cyclotrimerisation.

In a similar line, Yang and coworkers report a nickel-catalysed cyclotrimerisation, in the presence of zinc metal as a reducing agent.[46] In this case, the addition or exclusion of zinc iodide drives the selectivity change: without this additive, the 1,2,4-cyclotrimer is produced in a 97:3 selectivity, switching to a 4:96 selectivity when the additive was added (Scheme 9). Both reactions are shown to tolerate a wide variety of substrates, including cyclopropylacetylene. The iodide was found to be crucial,

45 Hilt, G.; Hengst, C.; Hess, W. Solvent-Dependent Regiochemical Cyclotrimerisation of Phenylacetylene with Cobalt Catalysts Containing Disulfide Ligands: A Case Study. *Eur. J. Org. Chem.* **2008**, 2293–2297.

46 Fan, J.-T.; Fan, X.-H.; Gao, C.-Y.; Wei, J.; Yang, L.-M. Regioselectively Switchable Alkyne Cyclotrimerization Catalyzed by a Ni(ii)/Bidentate P-Ligand/Zn System with ZnI_2 as an Additive. *Org. Chem. Front.* **2022**, *9*, 2357–2367.

as substitution for other zinc halides led to 1:1 or 2:1 regioisomeric mixtures. However, there are several methodological inconsistencies which are not clarified. While the authors propose two mechanisms, these exclude the zinc iodide from the explanation and are effectively regioisomeric variants of the same basic mechanism.

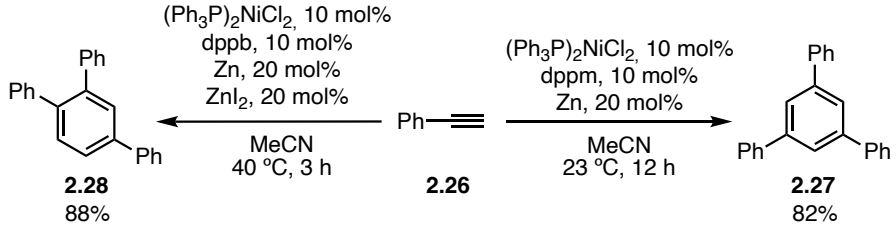

Scheme 10. Switching the regioselectivity by addition of zinc iodide in a nickel-catalysed cyclotrimerisation.

A trinickel(0) complex formed by sodium metal reduction of the halide precursor, stabilised by diimine ligands, was isolated and found to cyclotrimerise alkynes.[47] The reaction was not specific except for some alkynes, such as ethyl but-2-ynoate, which cyclotrimerised in a 91:9 1,3,5:1,2,4 ratio. However, the selectivity changes were not predictable as the propiolate or phenylpropiolate analogues were selective for the other isomer. This reaction exhibited a dramatic solvent effect, with the regioselectivity switching from a 2:1 to a 1:2 ratio from *n*-hexane to acetonitrile or diethyl ether. In addition, tetrameric products were sometimes observed in low to moderate yields.

An additional variant with nickel catalysts was found to be selective for the rarer 1,3,5-trisubstituted products: the use of tetrahydroxydiboron, or hypoboric acid, as an additive (Scheme 11).[48] A variety of alkynes could be trimerised in good to excellent yields, and practically perfect regioselectivity. Some cross-trimerisation reactions involving two different alkynes were explored, showing good yields (Scheme 11). The authors propose a complex pathway with boronickelation of an alkyne directed by hydrogen bonding to the alkynic hydrogen, as well as subsequent insertions directed by this very weak hydrogen bond. However, no evidence is given for this mechanism nor is the absence of oligomerisation discussed.

47 Shen, L.; Zhao, Y.; Luo, Q.; Li, Q.-S.; Liu, B.; Redshaw, C.; Wu, B.; Yang, X.-J. Cyclotrimerization of Alkynes Catalyzed by a Self-Supported Cyclic Tri-Nuclear Nickel(0) Complex with α-Diimine Ligands. *Dalton Trans.* **2019**, *48*, 4643–4649.

48 Yang, K.; Wang, P.; Sun, Z.-Y.; Guo, M.; Zhao, W.; Tang, X.; Wang, G. Hydrogen-Bonding Controlled Nickel-Catalyzed Regioselective Cyclotrimerization of Terminal Alkynes. *Org. Lett.* **2021**, *23*, 3933–3938.

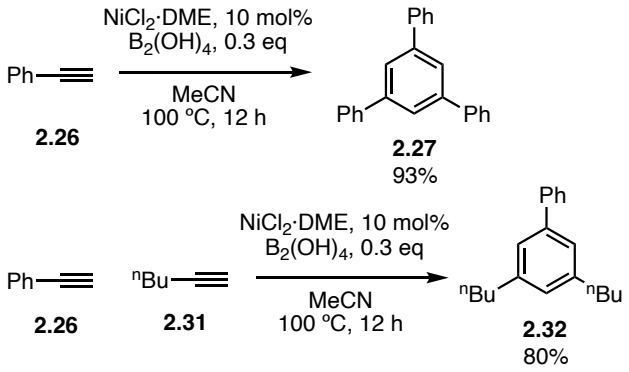

Scheme 11. Nickel and tetrahydroxydiboron-catalysed 1,3,5-selective cyclotrimerisation of terminal alkynes.

The cyclotrimerisation catalysed by indium trichloride in the presence of 2-iodophenol afforded a variety of 1,3,5-trisubstituted benzenes in good to excellent yields by refluxing in chlorobenzene.[49] The reaction works for both alkyl- and arylacetylenes. The authors report a number of unsuccessful substrates with alkyl halides or cyclopropanes. Their proposed mechanism, as well as differing substantially from the one proposed for aluminium trichloride analogues,[20] does not account for the presence of 2-iodophenol, which was found experimentally to be a critical additive (with unsubstituted phenol leading to only 10% yield). The reaction is also reported to be extended to other catalysts maintaining the same selectivity, such as iron(III) triflate or copper(II) triflate.

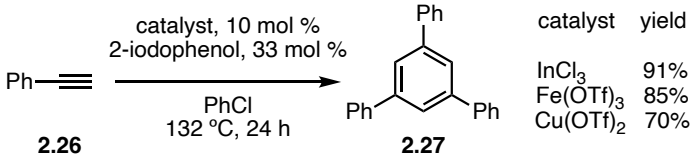

Scheme 12. 1,3,5-Selective cyclotrimerisation directed by 2-iodophenol.

49 Xu, Y.; Pan, Y.; Wu, Q.; Wang, H.; Liu, P. Regioselective Synthesis of 1,3,5-Substituted Benzenes via the $InCl_3$/2-Iodophenol-Catalyzed Cyclotrimerization of Alkynes. *J. Org. Chem.* **2011**, *76*, 8472–8476.

Objectives

Gold(I)-catalysis has been widely explored using alkynes as electrophiles upon coordination to the metal centre. However, the plausible intermolecular reaction of alkynes to afford well-defined oligomeric products had not been extensively studied.

We aimed to explore the cyclotrimerisation of alkynes and fully explain the observed selectivity towards 1,3,5-trisubstituted products through a combined computational and experimental approach. Additionally, we aspired to applying the gained mechanistic insight in guiding novel reactivity with intramolecular substrates.

Results and Discussion

Intermolecular Gold(I)-Catalysed 1,3,5-Trimerisation of Alkynes

A preliminary reaction of phenylacetylene in the presence of [JohnPhosAu(NCMe)]SbF_6 as a cationic gold(I) catalyst afforded, after heating, 1,3,5-triphenylbenzene as the only detectable and isolable triphenylbenzene isomer (Scheme 13). As the major separable molecular impurity, 1-phenylnaphthalene was also observed, which presumably originated from the tail-to-tail dimerisation of phenylacetylene followed by Friedel-Crafts-type trapping of the intermediate carbocation. However, the reaction was by far dominated by the formation of phenylacetylene oligomers, in a cationic polymerisation chain growth process by consecutive nucleophilic attacks of phenylacetylene molecules.

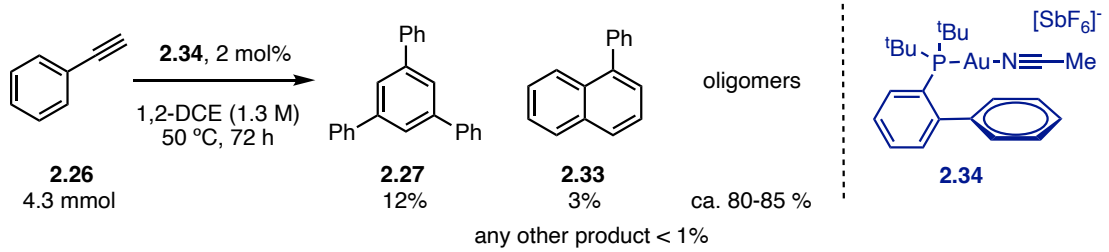

Scheme 13. Isolated products from a larger scale reaction with unoptimised conditions.

As discussed in the Introduction, the selective formation of 1,3,5-triarylbenzenes in these reactions is highly atypical. In this case, not only was a preference observed but complete absence of the 1,2,4-trisubstituted product. With the aim of minimising the formation of ill-defined oligomers and increasing the very modest yield of triphenylbenzene, we ran screenings aided by high-throughput experimentation (HTE) to determine the effect of the ligand choice and the concentration.

Table 1. HTE results of preliminary catalyst and concentration screening. UV yields determined with respect to internal standard (naphthalene, calibration curve).

L	**JohnPhos**	**tBuXPhos**	**tBuXPhos**	**PMe_3**	**Ph_3P**	**IPr**
L'	**MeCN**	**MeCN**	**PhCN**	**-**	**MeCN**	**PhCN**
X	**SbF_6**	**SbF_6**	**$BAr^F{}_4$**	**NTf_2**	**SbF_6**	**$BAr^F{}_4$**
0.8 M	14	21	17	1	3	26
1.2 M	11	20	13	1	3	17
2 M	10	17	12	1	2	18
4 M	7	12	9	1	2	15

A six-point calibration curve for 1,3,5-triphenylbenzene was performed to determine the yield from the UV traces (Table 1). The tabulated results show a strong dependence on concentration (Figure 2), with

higher concentrations leading to more oligomerisation. Only Buchwald phosphines and NHCs led to yields above 10%. The conversion was low for trimethylphosphine and triphenylphosphine complexes.

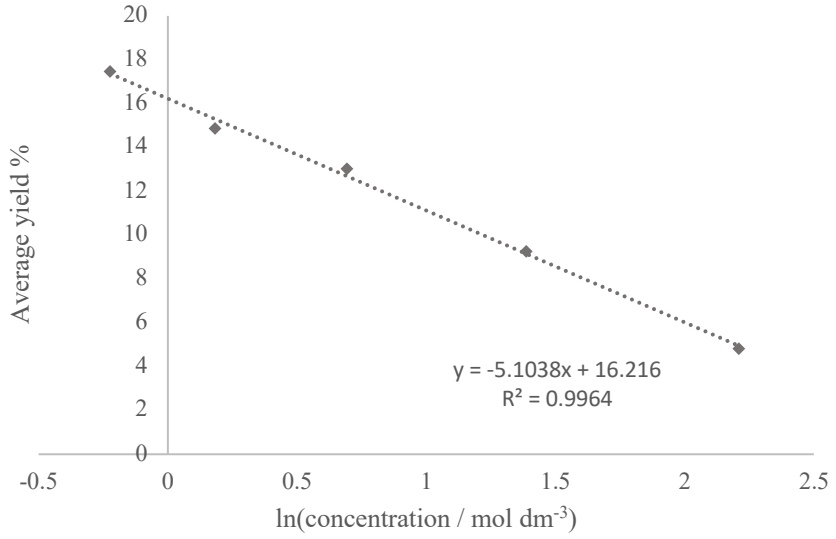

Figure 2. Average yield of 1,3,5-triphenylbenzene using [JohnPhosAu(NCMe)]SbF_6, [^{t}BuXPhosAu(NCMe)]SbF_6 and [^{t}BuXPhosAu(NCPh)]$BAr^F{}_4$ plotted against ln(concentration).

Using the JohnPhos complex for practical reasons, we explored whether lowering the concentration could improve the yields further. To determine the yields by NMR, we found trichloroethylene to be a suitable standard, with the singlet of the internal proton in **2.27** sufficiently separate from the oligomers to integrate. We used this internal standard across all other NMR yields reported in this section, weighing the trichloroethylene. Lowering the concentration down to 0.1 M improved the NMR yields somewhat, up to 18%; NMR yields at 0.8 M and 1.2 M matched the UV yields from HTE to within 1–2%.

Initially, and as IPr was found to be the best-performing ligand in this initial screening, we studied a set of NHC ligands: IPr, IMes and IAd. However, we failed to reproduce the observed yield with IPr. Even at 0.1 M, we found **2.27** (13%), **2.33** (4%) and 1,3-diphenylbutenyne (23%) by NMR. Presumably, a degree of overlap in the UV traces could be responsible for the HTE results. The other NHC complexes showed lower conversion and, due to the large amount of gold powder formed, it was attributed to catalyst deactivation. IAdAuCl with silver hexafluoroantimonate only reached 6% yield, whereas the same reaction with IMesAuCl and sodium $BAr^F{}_4$ did not form any product.

As the counteranion was found to have a moderate effect on the yield, we ran a second, more focused screening of different bulky phosphine complexes (mainly dialkylbiarylphosphines) in combination with different chloride scavenger additives.

Table 2. HTE results of ligand and chloride scavenger screening. UV yields determined with respect to internal standard (naphthalene, calibration curve).

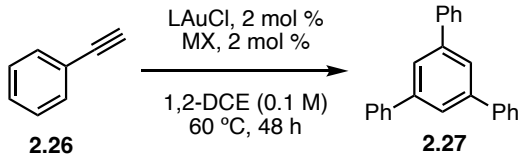

2.26 **2.27**

	tBuBrettPhos	RuPhos	SPhos	tBu_2NpP	CataCXium	TrixiePhos	QPhos	$Me_4tBuXPhos$
$AgSbF_6$	15	14	14	1	11	16	1	6
$AgNTf_2$	7	2	2	<1	1	2	<1	4
AgOTf	2	1	1	<1	<1	1	<1	2
$NaBAr^F$	9	1	1	0	0	8	0	0

Silver hexafluoroantimonate seemed to perform optimally across the studied phosphine, yet none of the studied ligand were found to lead to higher yields than *t*BuXPhos. This was confirmed later by mesoscale tests with TrixiePhos and RuPhos as ligands. The clear preference for hexafluoroantimonate for all ligands was interesting, especially when compared to weakly coordinating $BAr^F{}_4$ but ultimately did not allow an improvement in the modest yields we obtained with the standard procedure.

We then carried out a solvent screening including common chlorinated and aromatic solvents (Table 3). All studied solvents performed either comparably to 1,2-dichloroethane or somewhat worse. The solvents less frequently encountered in gold(I) catalysis, such as dioxane or ethyl benzoate, shut down the reactivity almost completely potentially through the stabilisation (or side-reactivity) of some carbocationic reactive intermediates. In addition, chlorobenzene showed lower conversion that steadily increased over time, implying significantly slower kinetics; the reaction was stopped before reaching full conversion.

Table 3. Solvent screening, 0.4 mmol scale reactions were run at 60 ºC using as catalyst [*t*BuXPhosAu(MeCN)]SbF_6 (2 mol %). NMR yields based on (weighed) trichloroethylene as internal standard.

Solvent	NMR Yield
1,2-DCE	24
$CHCl_3$	22
Tetrachloroethane	13
$PhCF_3$	19
Dioxane	1
PhCl[a]	15
BzOEt[a]	5

1,2-DCE[b]	26

[a]Slower reaction, run for three days. [b]Reaction was run at 80 ºC.

An unexpected observation was that temperature had no measurable effect on yields. We had contemplated the possibility that the temperature could change the outcome of the oligomerisation, due to entropic effects in such reactions. Because of this, we had expected to see an increase in yield with increasing temperature. Unfortunately, further tests at up to 110 ºC in sealed vials gave comparable results to the standard methods. This was reproduced in chlorobenzene, which gave marginally higher yields only because the reaction at lower temperatures was not stopped at completion.

Based on the limited precedent of $AlCl_3$-catalysed trimerisation of 2-butyne, and because of the likely 1,3,5-selectivity of the proposed mechanism,[20] a small number of catalysts were tested under the same conditions. However, of all the ones tested, only InI_3 was successful. However, it still performed worse than most gold(I) complexes (Table 4).

Table 4. Non-gold(I) catalyst screening. NMR yields based on (weighed) trichloroethylene as internal standard.

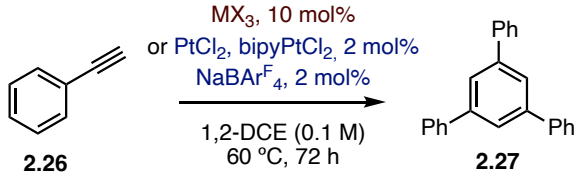

Catalyst	Yield %
InI_3	13
$In(NTf_2)_3$	<1
$BiCl_3$	0
$bipyPtCl_2$	<1
$PtCl_2$	1

At the optimal conditions, the trimerisation of phenylacetylene afforded 1,3,5-triphenybenzene in 33% isolated yield (Scheme 14).

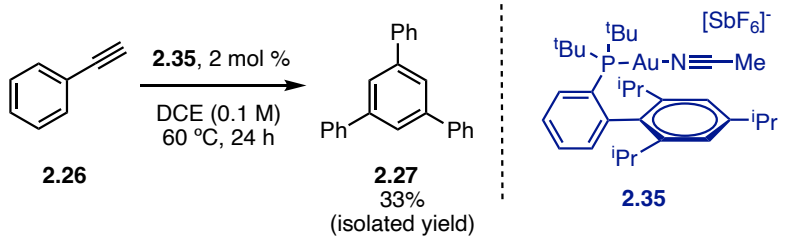

Scheme 14. 1,3,5-Selective cyclotrimerisation of phenylacetylene under the optimised conditions.

An additional bulkier ligand, tris(*o*-biphenyl)phosphine, was tested in the reaction. This ligand had been previously found to lead to orthogonal reactivity in gold(I) catalysis due to its steric environment.[50] Pleasingly, the catalyst shut down the formation of oligomers almost completely; however, 1-phenylnaphthalene was formed in a 1:1 molar ratio with respect to the product. The reasons for this selectivity were already reported by Gagosz and coworkers in different reactions,[50] with steric hindrance favouring internal coordination of the gold atom when activating terminal alkynes. While the reaction did not lead to an improvement in the overall yield, the absence of oligomers strongly indicated that sterics played a key role in preventing the formation of undesired products. Other tris(biaryl)phosphine complexes, including a more hindered *tert*-butyl-substituted one, did not lead to better yields.

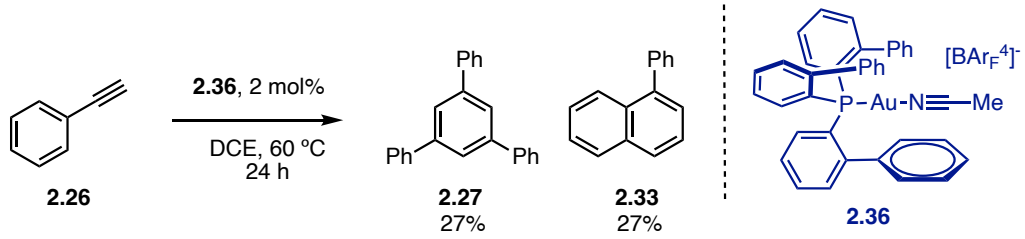

Scheme 15. Formation of an equimolar ratio of **2.27** and **2.33** with a tris(biaryl)phosphine.

A key question in the reaction was whether there was any oligomer inhibition. Poly(phenylacetylene) or related compounds would have an abundance of conjugated alkenes that, besides binding gold and creating competitive resting states, could also lead to decomposition pathways of gold(I) and deplete the catalyst. However, a control experiment in which three additional equivalents of starting material were added after full consumption of the first portion resulted in an almost identical yield, in spite of the overall catalyst loading being halved due to the setup. This confirmed that oligomers did not block the catalytic activity of gold(I) complexes.

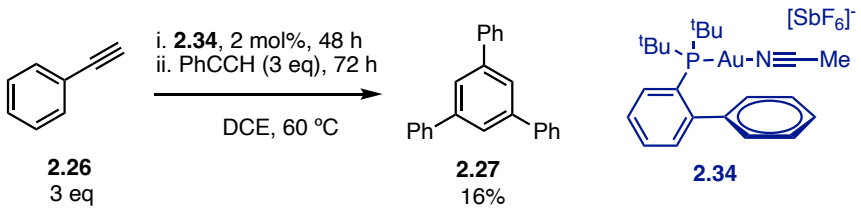

Scheme 16. Control experiment to confirm whether oligomers poison the gold(I) catalyst.

A substrate scope of several arylalkynes was then carried out. Most of the substrates that reacted successfully resulted in comparable yields to those seen with phenylacetylene, always due to the competition with oligomerisation. However, very electron-rich substrates such as *p*-methoxyphenylacetylene failed to yield any product. Electron-withdrawing substituents led to lower overall yields and either higher temperatures or prolonged reaction times were required to reach high

50 Muratov, K.; Gagosz, F. Confinement-Induced Selectivities in Gold(I) Catalysis—The Benefit of Using Bulky Tri-(*Ortho* -biaryl)Phosphine Ligands. *Angew Chem Int Ed* **2022**, *61*, e202203452.

conversion (although full conversion was not always reached). This was not entirely unexpected as cyclotrimerisation would require the same substrate to act as an electrophile (when bound to gold) and as a nucleophile.

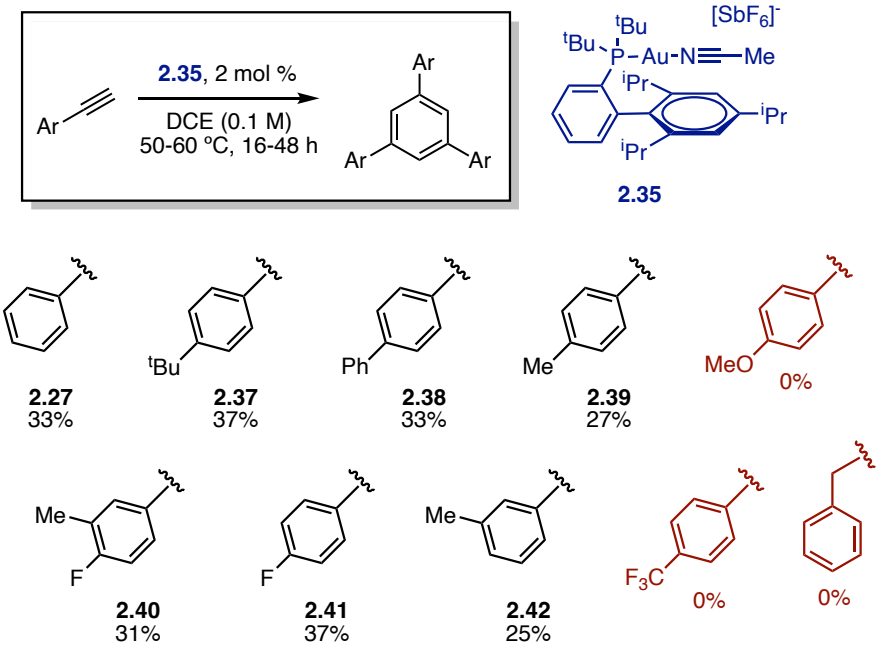

Scheme 17. Substrate scope of the gold(I)-catalysed cyclotrimerisation of terminal alkynes. Internal alkynes failed to react intremolecularly.

Cross-cyclotrimerisation tests were performed but, unfortunately, led to low selectivity. Combined with the generally low to moderate yields, the cross-trimerisation was not pursued further. In particular, the combinations of *para*-chlorophenylacetylene and electron-rich *para*-methoxyphenylacetylene did not lead to any measured cross-trimer formation, whether combined in 2:1 or 1:2 ratios.

In the light of these results and, in particular, to explain the complete 1,3,5-selectivity of this trimerisation reaction, we turned to DFT calculations to reproduce all the observed trends.

Mechanistic Study

The main intention of the mechanistic study was not only to find a plausible mechanism for the formation of the product, but, ideally, to systematically discard alternative pathways that could lead to product formation.

Analogously to the studies detailed in **Chapter I** in which we demonstrated the validity of trimethylphosphine as a prototypical ligand for gold, we decided to begin our computational study with the same catalyst model using its phenylacetylene complex, **A1**, as its starting point and referencing the free energy to this system.

Nucleophilic attack of a second molecule of phenylacetylene afforded adduct **A2**, with a benzylic sp carbocation. The head-to-tail selectivity is dictated by the stabilisation through mesomeric effects.

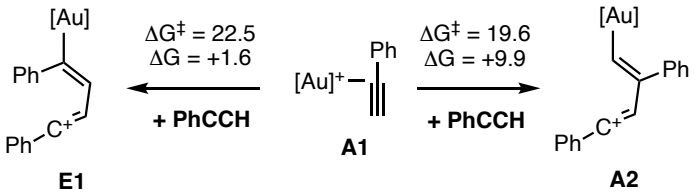

Scheme 18. Competition between head-to-tail and tail-to-tail attack. Intermediate **E1** is subsequently trapped to form 1-phenylnaphthalene, observed experimentally as traces.

This intermediate can then undergo a cyclisation to form **A3**, with only a relatively small energy barrier (Scheme 19). This intermediate, a gold(I) η^1-cyclobutadiene complex, was found to be responsible for the strict 1,3,5-selectivity. As an η^1 fragment, the charge distribution in the organic moiety is akin to a cyclobuten-2-ium-1-yl; however, and in line with standard organometallic nomenclature, we will refer to this geometry as an η^1-cyclobutadiene ligand.

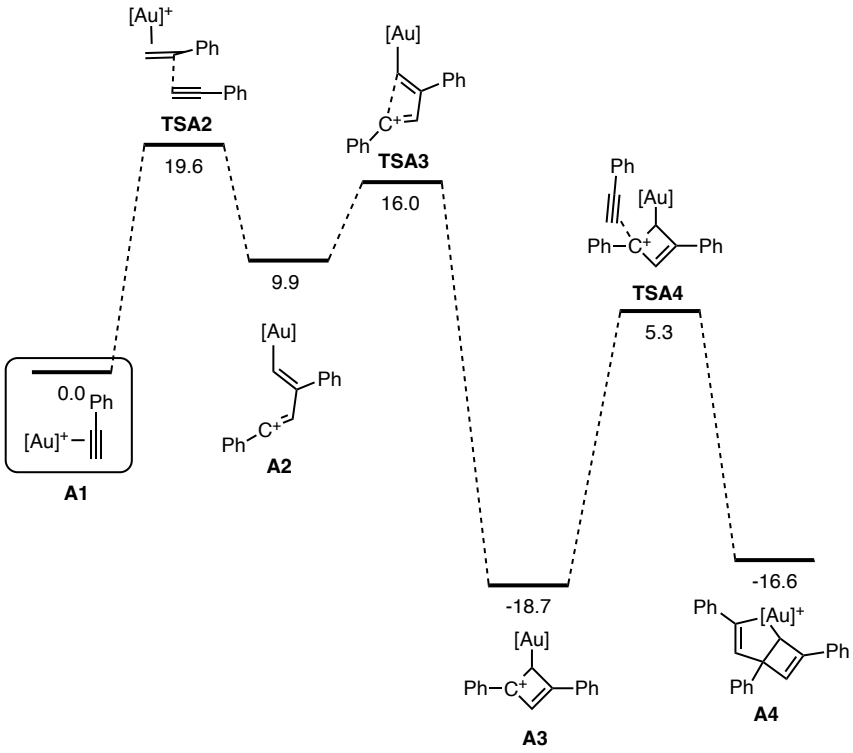

Scheme 19. Formation of key gold(I) η^1-cyclobutadiene complex and *endo*-attack to form cyclometallated **A4**.

Attack of the third alkyne can occur from two faces: the *endo*, *syn* to the gold fragment, or *exo*, *anti* to the gold fragment. Both processes have similar activation energies and lead to the same product through slightly different pathways. The former results in a concerted asynchronous cyclometallation to form a gold(III) species, **A4**. Coordination of a fourth alkyne to form **A4b** is entropically disfavoured and, due

to the geometric constraints, no further oligomerisation is possible for this intermediate (Scheme 20). Reductive elimination to form a gold(I) *endo*-Dewar benzene complex is followed by gold(I)-catalysed ring opening of the Dewar benzene to form triphenylbenzene.

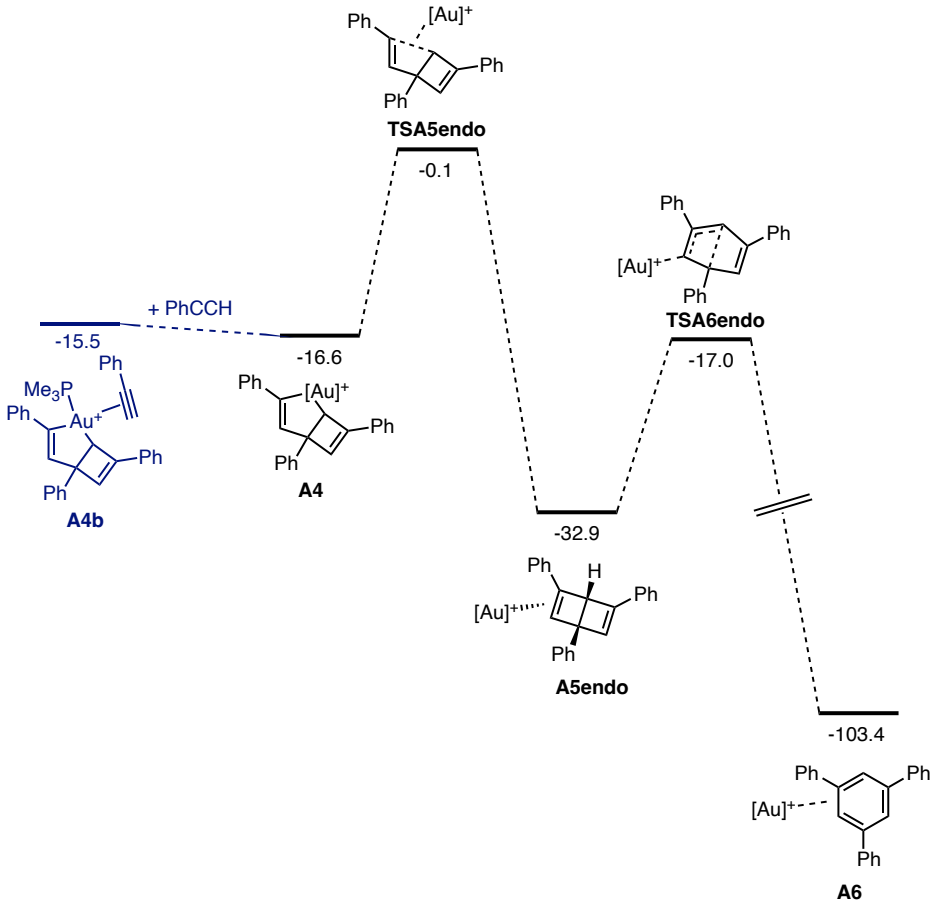

Scheme 20. Evolution of cyclometallated **A4** involves reductive elimination and ring opening. Entropically disfavoured resting state shown in blue.

The alternative *exo* attack of the third alkyne leads to concerted asynchronous formation of a gold(I) *exo*-Dewar benzene complex (Scheme 21). While this complex can undergo ring-opening, the higher energy barrier suggests that rapid migration to gold(I) *endo*-Dewar benzene followed by ring-opening is most likely (shown in green).

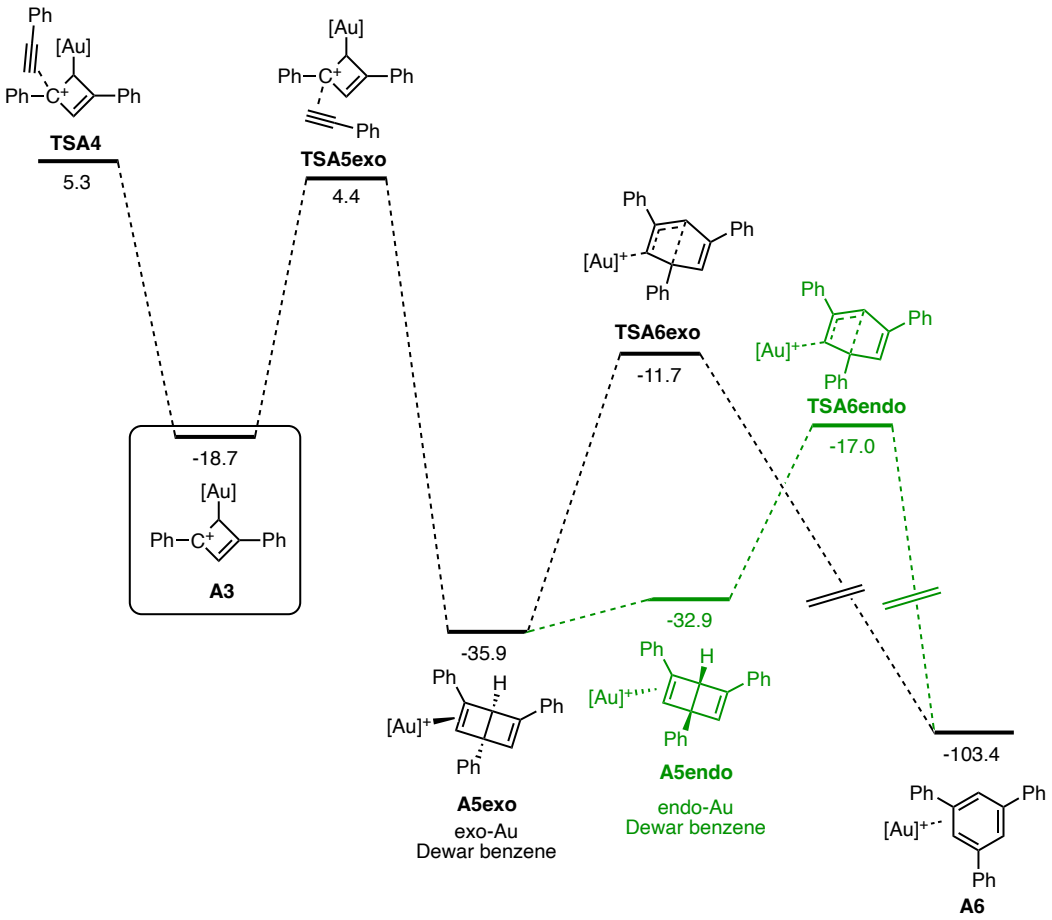

Scheme 21. Precursor **A3** can undergo *anti*-attack through **TSA5exo**. Ring-opening after isomerisation shown in green.

The main difference between these two processes, beyond the intermediacy of gold(III) intermediates, lies in the carbon atoms that form new bonds (Figure 3). Apart from either of the carbon 2 atoms (red), in the *endo* process, carbon 1 (blue) also forms a bond to the newly coordinated alkyne (yellow), *ipso* to the original gold(I) coordination. However, in the *exo* mechanism, the new bond is invariably formed to carbon 3 (green). While these lead to identical products with phenylacetylene, intramolecular variants would be able to distinguish these two mechanisms.

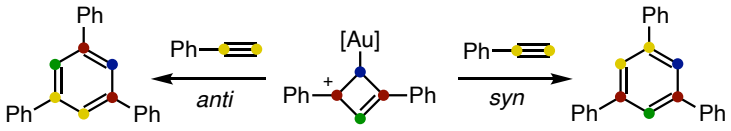

Figure 3. The connectivity of product 1,3,5-triphenylbenzene depends on whether the pathway is *anti* or *syn*.

We initially considered a direct electrocyclic cycloreversion of the cyclobutene in **A4** to be a potential productive mechanism. The reasoning behind this was that analogous metallacycloheptatrienes were often seen in cyclotrimerisation reactions with other metals and that the steps leading to this precursor had already determined the 1,3,5-selectivity irreversibly. However, due to the conrotatory ring-opening

constraint, the thermal energy barrier was inaccessible. As symmetry selection rules were deemed surmountable by a spin flip, we considered the photochemically activated pathway (Scheme 22). Preliminary TD-DFT results showed that intermediate **A4** showed relatively strong absorption in the visible region, potentially leading to further photochemical reactivity after intersystem crossing. However, disrotatory ring-opening was still comparable in energy to thermal reductive elimination through **TSA5endo** and so the photoinitiated pathways were discarded.

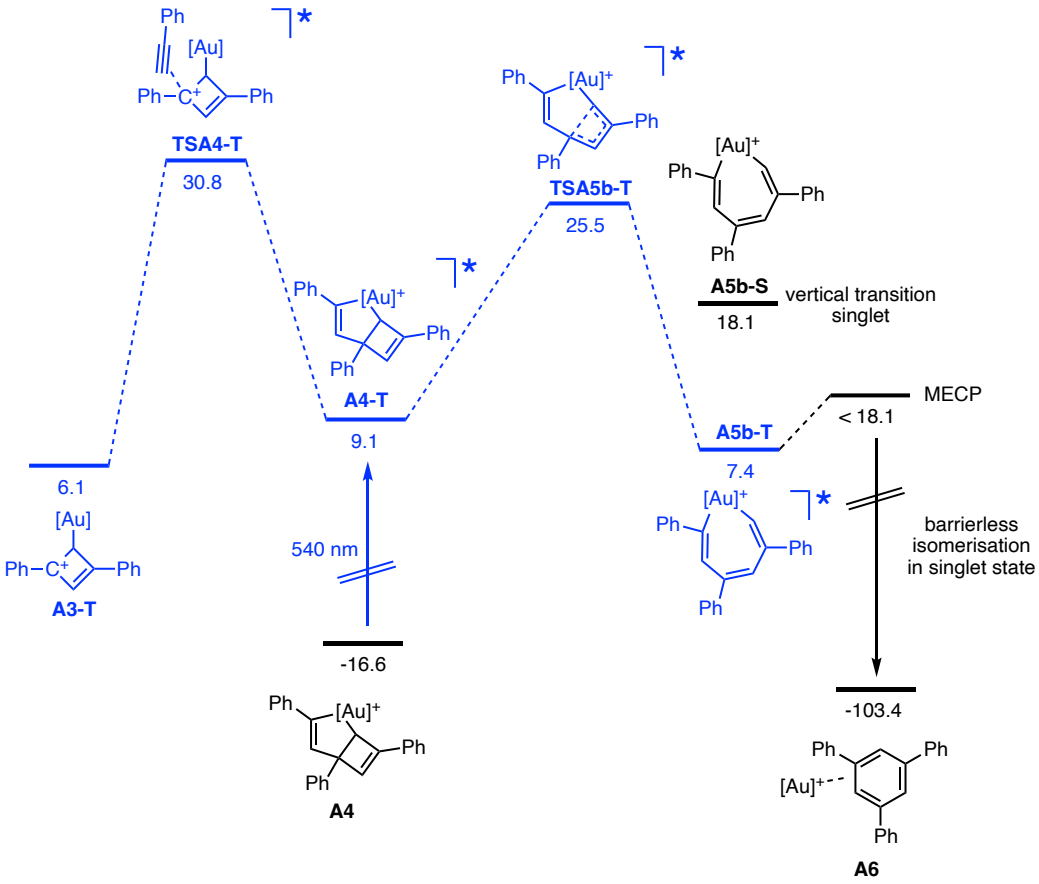

Scheme 22. Calculated photochemical pathway for the electrocyclic cyclobutene ring opening, including uncompetitive reversal to **A3-T**. Triplet-state structures in blue.

Similarly, decoordination of Dewar benzene followed by uncatalysed ring-opening was found to be much higher in energy and, at 26.2 kcal mol^{-1}, inaccessible at the temperatures at which the reactions were carried out.

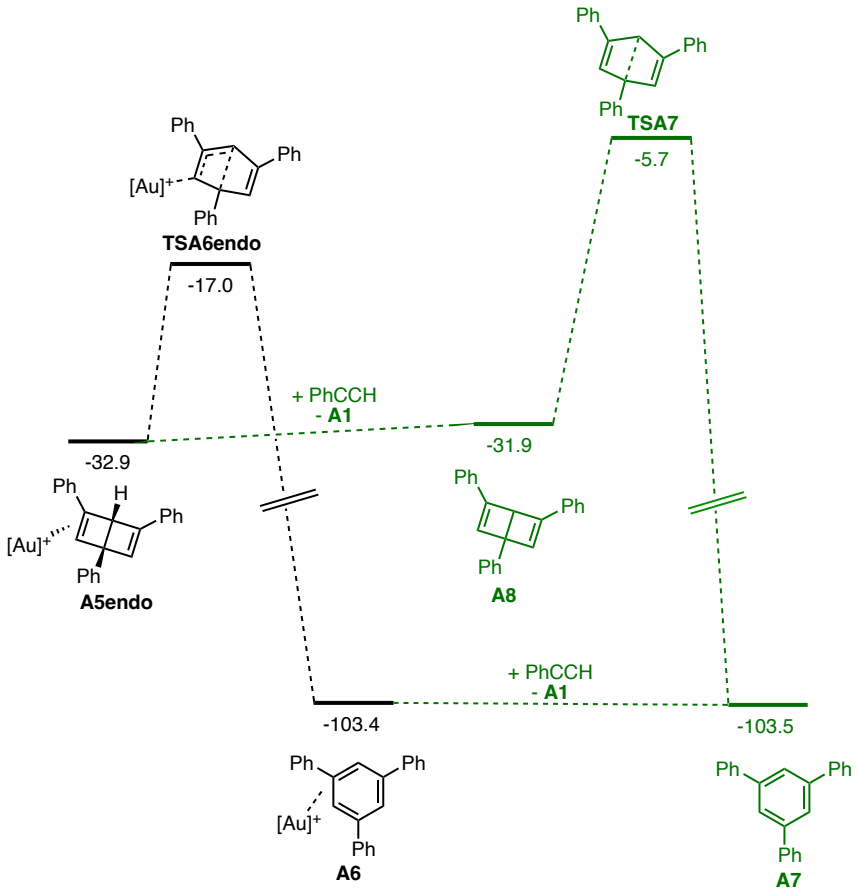

Scheme 23. Comparison of gold(I)-catalysed (in black) and uncatalysed (in green) ring opening of triphenyl-Dewar benzene.

We then returned to intermediate **A4**, which forms spontaneously in the *syn*-attack of the third alkyne, with the aim of understanding its nature. The cyclometallation to form an apparent gold(III) species, which occurred in a concerted asynchronous fashion after **TSA4**, was studied by NBO analysis. We aimed to identify the bonding and formal oxidation state of this intermediate as there were two main options: **A4** could either be a fully-fledged tricoordinate gold(III) complex or, perhaps, it could be best described as a gold complex with a *Z*-type ligand. Given that this distinction is the result of a formalism, the answer would depend primarily on the strength of the interaction.[51]

The Lewis structure adopted suggested strong gold–carbon bonds and, therefore, a gold(III) . We also found that forcing the Lewis structure to omit either of the gold–carbon bonds resulted in disproportionately large donations in the second-order perturbation theory, in line with the existence of fully formed bonds. Furthermore, while entropically disfavoured, the aforementioned existence of **A4b** upon coordination of a fourth ligand (an alkyne) is consistent with gold(III) and not with gold(I), concluding from these calculations that it is correct to talk about a gold(III) intermediate.

51 Although the electron count of such complexes in the LXZ formulation would still result formally in gold(III), complexes with Z-type ligands can be fundamentally different from either of the two oxidation states, see Moret, M.-E.; Peters, J. C. N_2 Functionalization at Iron Metallaboratranes. *J. Am. Chem. Soc.* **2011**, *133*, 18118–18121.

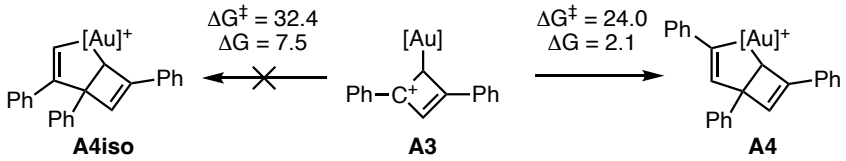

Scheme 24. Regioselective *syn*-addition of phenylacetylene to **A3**. The *anti*-addition is more disfavoured as stepwise formation of a carbocationic hidden intermediate is unavoidable.

Full regioselectivity in third alkyne addition explains the complete selectivity towards the 1,3,5-trimer.

Most other metal-catalysed cyclotrimerisations proceed through a concerted metallation in which a metallacyclopentadiene is formed, followed by insertion into a third alkyne. Alternative concerted cyclometallations with a second molecule of phenylacetylene were modelled but all transition states were found to be significantly higher in energy and, thus, non-competitive. This is interesting because in the *syn*-attack pathway eventual cyclometallation is unavoidable, thus suggesting that the η^1-cyclobutadiene complex **A3** is electron-rich enough to undergo oxidative cycloaddition, whereas the gold(I) alkyne complex, **A1**, cannot.

Experimentally, however, the reaction formed a significant amount of oligomer in almost all cases. We then focused on exploring the origin of this side-reactivity. Intermediate **A2** can be intercepted prior to its cyclisation: facile direct nucleophilic *trans*-attack of a third alkyne leads to an acyclic trimer, **B1**. This trimer can oligomerise very readily, *via* transition state **TSB2b**, leading to the main competing pathway in the gold(I)-catalysed reaction (Scheme 25). Interestingly, **B1** can also lead to the product via sequential cyclisations leading to an analogous Dewar benzene complex. Even though this process may be responsible for a fraction of the formed product, due to the greater energy differences, this is kinetically outcompeted by oligomerisation. For these reasons, we conclude that the *trans*-attack of the third alkyne primarily leads to oligomerisation, as the addition of a fourth phenylacetylene is even more favourable than before.

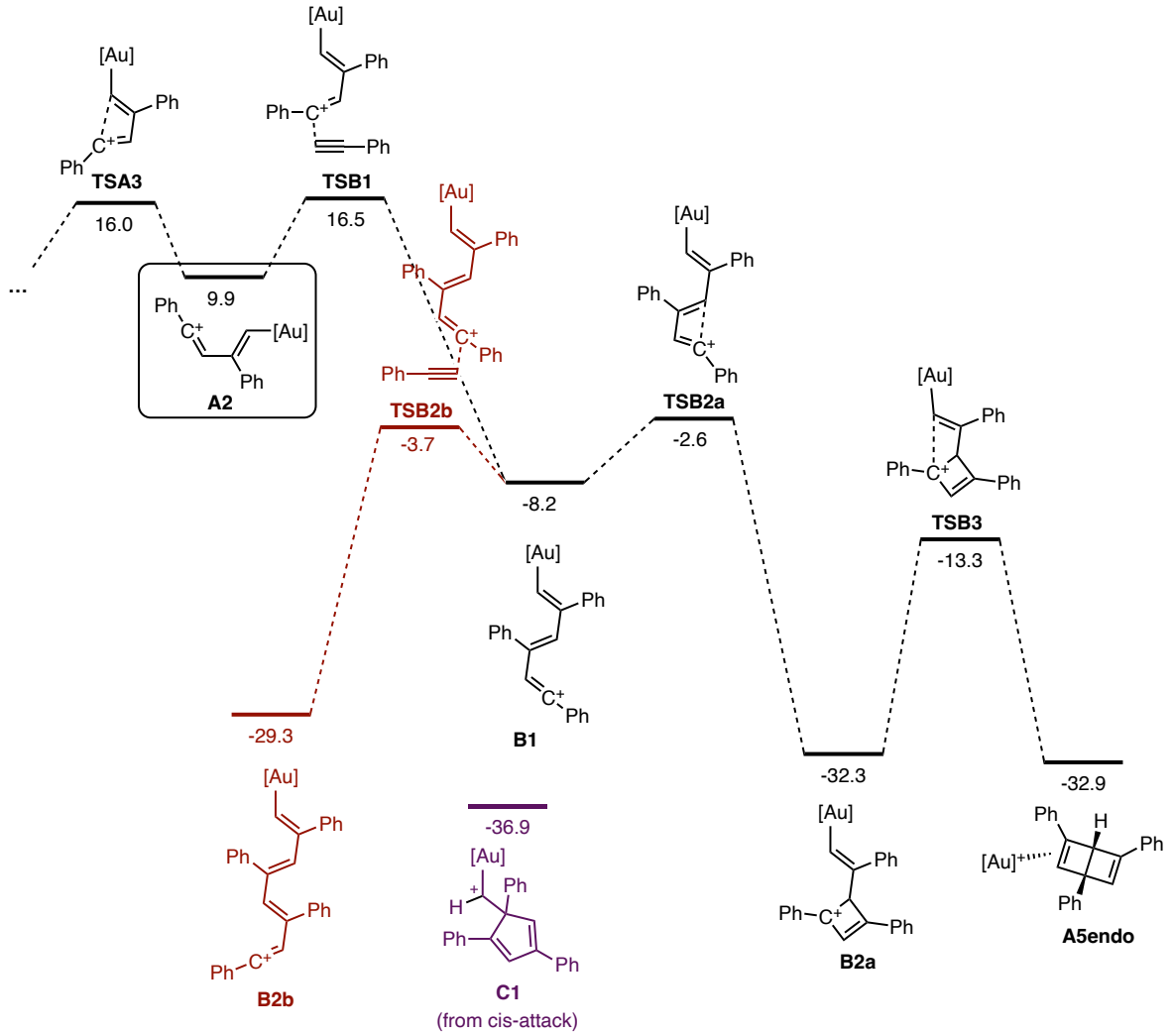

Scheme 25. Interception of **A2** with a third alkyne leads to a productive pathway (black) outcompeted by oligomerisation (red).

Cis-attack of a third alkyne (**TSC1**), while slightly disfavoured for the trimethylphosphine system, is likely more relevant when the ligand is more sterically encumbered. The transition state of *cis*-attack (**TSC1**) relaxes barrierlessly unto a carbocationic cyclopropylgold(I) species, **C1** (Scheme 26). We explored the existence of these structures previously, as detailed in **Chapter I**. This structure is an example of a gold carbenoid, being in resonance showing partial carbocationic cyclopropylgold(I) and partial gold(I) carbene character. (Figure 4).

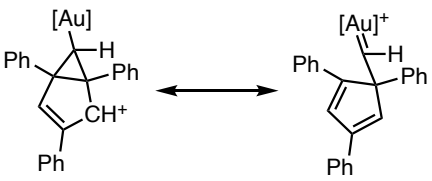

Figure 4. Resonance structures of intermediate **C1**.

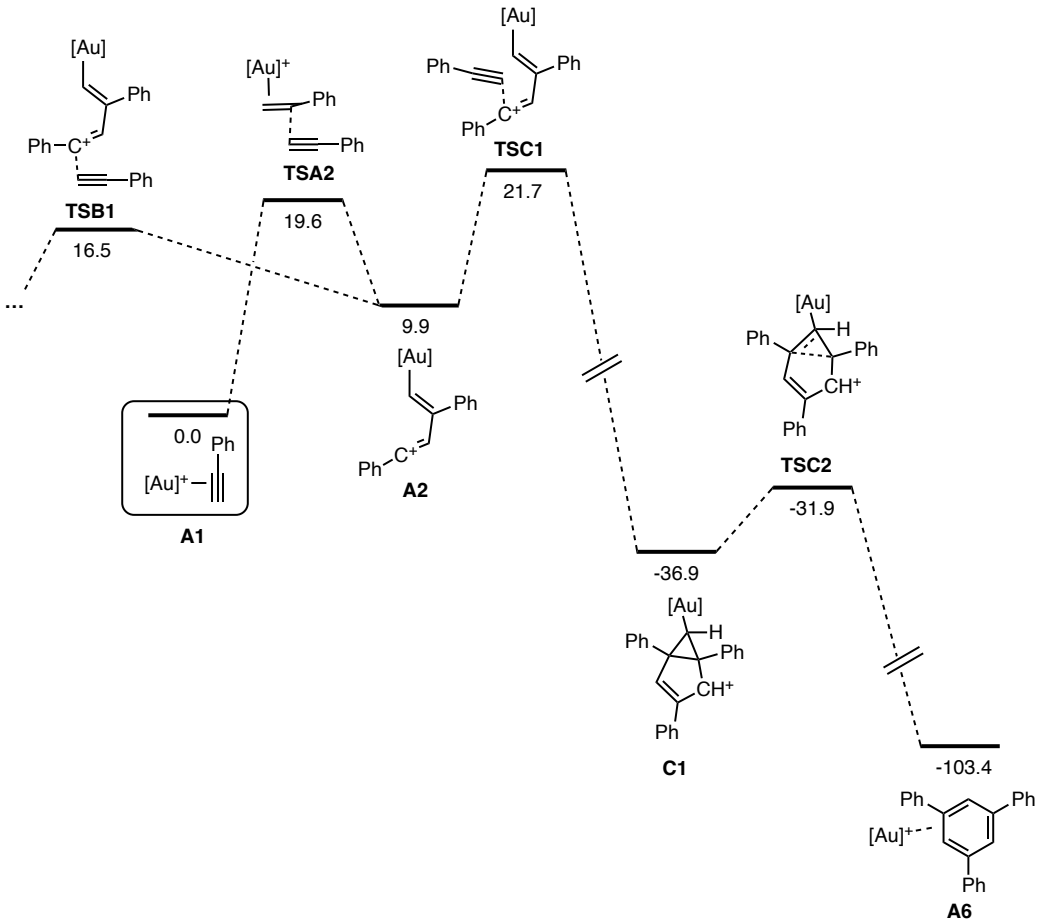

Scheme 26. Mechanism of the *cis*-attack trimerisation *via* key carbocationic cyclopropylgold(I) intermediate **C1**.

Subsequent ring-opening **TSC2** has a small energy barrier of 5 kcal mol^{-1} and leads to the product gold(I) triphenylbenzene complex. Intermediate **C1** is therefore reminiscent of the cyclopropylgold(I) intermediates or hidden intermediates explored in the work summarised in **Chapter I**, both in the description of its bonding and in its evolution.

An apparently logical alternative to reach triphenylbenzene products is a sequential deprotonation/protodemetallation mechanism. As has been discussed in the **General Introduction** and in **Chapter I**, the deprotonation of carbocationic intermediates followed by protodeauration is a well-established sequence of gold(I) catalytic cycles. If such an approach were to be present in the alkyne cyclotrimerisation, the head-to-tail selectivity would be analogous, gold(I) cyclobutadiene complexes would not be invoked as intermediates and the generation of enynes after protodemetallation would bring more nucleophilic species into the reaction. The iteroselectivity leading to cyclotrimerisation would be obtained through an irreversible 6-*endo*-dig cyclisation of a final dienyne.

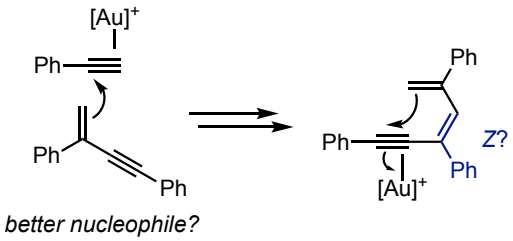

Scheme 27. Conceptual mechanism for sequential polyenyne assembly and ulterior cyclisation.

With the intention of determining the likelihood of this mechanism, we calculated the relevant structures of additions and proton shuttles. Phenylacetylene was used as the proton shuttle for two reasons: the reaction was known to work under anhydrous conditions and the alkyne was basic enough to deprotonate the acidic hydrogens of the intermediates.

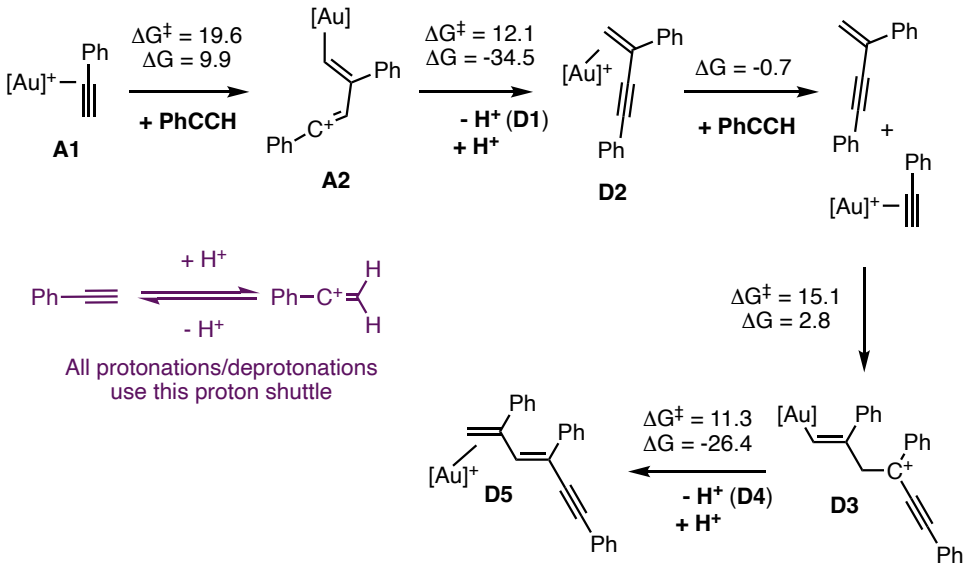

Scheme 28. Non-competitive mechanism with proton shuttle. Free energies, in kcal mol^{-1}, are higher than those in alternative mechanisms.

However, two main observations were made: firstly, the barriers were significantly higher than those for cyclisation; and secondly, the reaction was intermolecular and addition of the alkyne would always be preferred. **TSD1** was already unlikely to be accessible in the reaction mixture. Additionally, even if the product was formed, the addition of the third alkyne would preferentially afford *E*-dienyne **D5**, which cannot undergo 6-*endo*-dig cyclisation.

It can be argued that the proton shuttle model was not representative of the real system, or that other pathways with protodemetallation that were not explored could be responsible for the formation of triphenylbenzene. For this reason, we decided to run a series of control experiments that, in combination with these computational results, would bring more robust evidence to discard these pathways.

1,3-Diphenylbutenyne (**2.43**) was synthesised independently in a Sonogashira coupling of phenylacetylene and α-bromostyrene. Three control experiments were run (Scheme 29). Enyne **2.43**

was stirred under the reaction conditions with or without the addition of phenylacetylene. The reaction with added phenylacetylene gave only 3% yield of triphenylbenzene, which was significantly lower than if 1,3-diphenylbutenyne had not been added. In the absence of phenylacetylene, only unassignable oligomers formed.

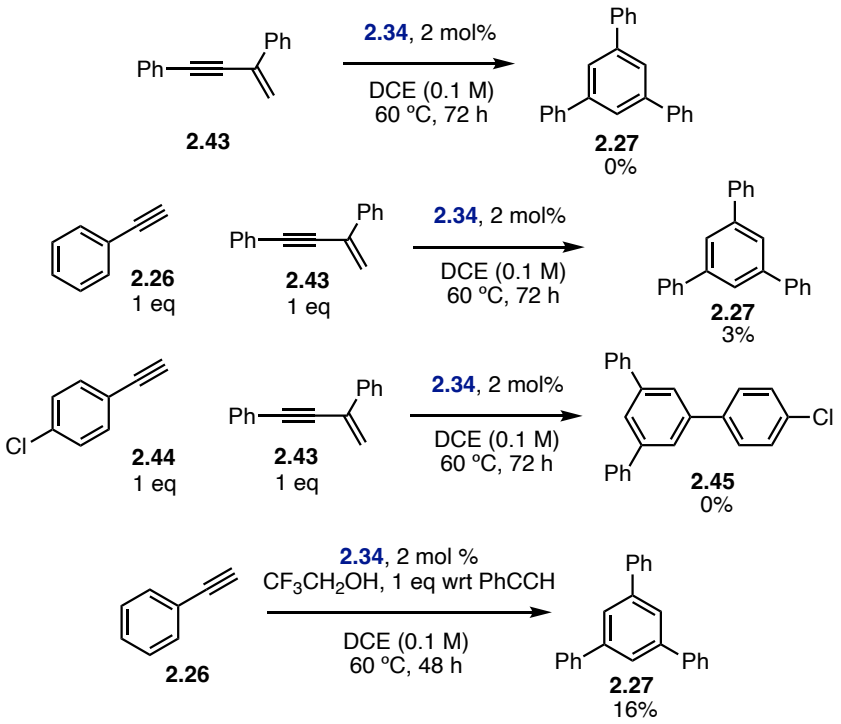

Scheme 29. Control experiments confirming that proton-shuttle mechanisms do not operate in the alkyne cyclotrimerisation.

A third reaction was run with *para*-chlorophenylacetylene, as this alkyne homotrimerised only sluggishly and because, if the heterotrimer was detected, it would only be able to come from the reaction with **2.43.**

Finally, the model reaction with [JohnPhosAu] was carried out using one equivalent of trifluoroethanol to aid in any protodemetallation/deprotonation processes. However, the yield obtained was comparable to the reaction in the absence of additive. Therefore, all the above evidence was consistent and pointed to the same interpretation: the gold(I)-catalysed cyclotrimerisation of alkynes is not mediated by proton shuttles.

With all these proposed mechanisms, the ones that can feasibly coexist in the reaction mixture are presented in Scheme 30. The discarded photochemical pathways and protodemetallation sequences are excluded.

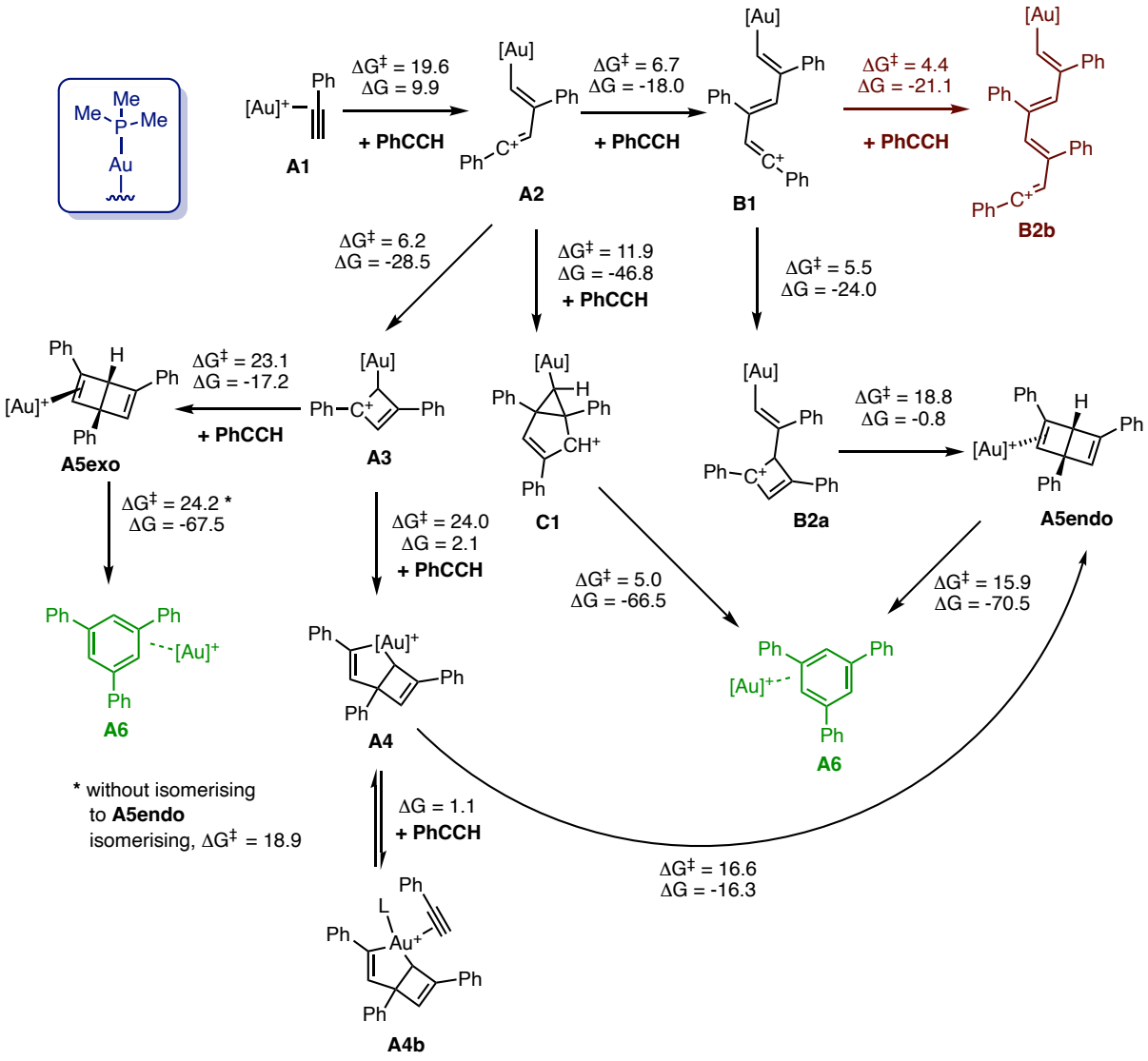

Scheme 30. Mechanisms responsible for the gold(I)-catalysed 1,3,5-selective cyclotrimerisation of phenylacetylene and main route for side-product formation (red, oligomerisation). **C1** is not competitive with trimethylphosphine but is shown for completeness. Free energy in kcal mol^{-1} at B3LYP-D3/6-311+G(d,p) + SDD, PCM (dichloromethane).

While the energy difference between **TSA3** and **TSB1** does not fully match the observed experimental preference for oligomerisation, this barrier should be expected to be quite small to coincide with the experimental ratio. The results are within DFT error and are consistent with the observed yield dependence on concentration.

We then proceeded to calculate parts of the same productive and competing mechanisms with two different ligands: trimethyl phosphite, as a less electron-rich variant, and JohnPhos, to see whether sterics changed any energy barriers considerably.

The model with trimethyl phosphite as a ligand (Scheme 31, note: geometries prefixed with **L1**) shows a very similar difference in energy between the cyclobutadiene cyclisation and trimer formation, with

L1TSA3 being 0.8 kcal mol^{-1} lower in energy than the *trans* incorporation of a third alkyne (**L1TSB1**). The barriers for the *anti*- (**L1TSA5exo**) and *syn*- (**L1TSA4**) attack onto the cyclobutadiene complex now favour the *syn*-attack and, therefore, the cyclometallation pathway. As was discussed in the case of trimethylphosphine, these small energy differences are comparatively unimportant to discriminate between the possible mechanisms and suggest a degree of coexistence between both routes to the product.

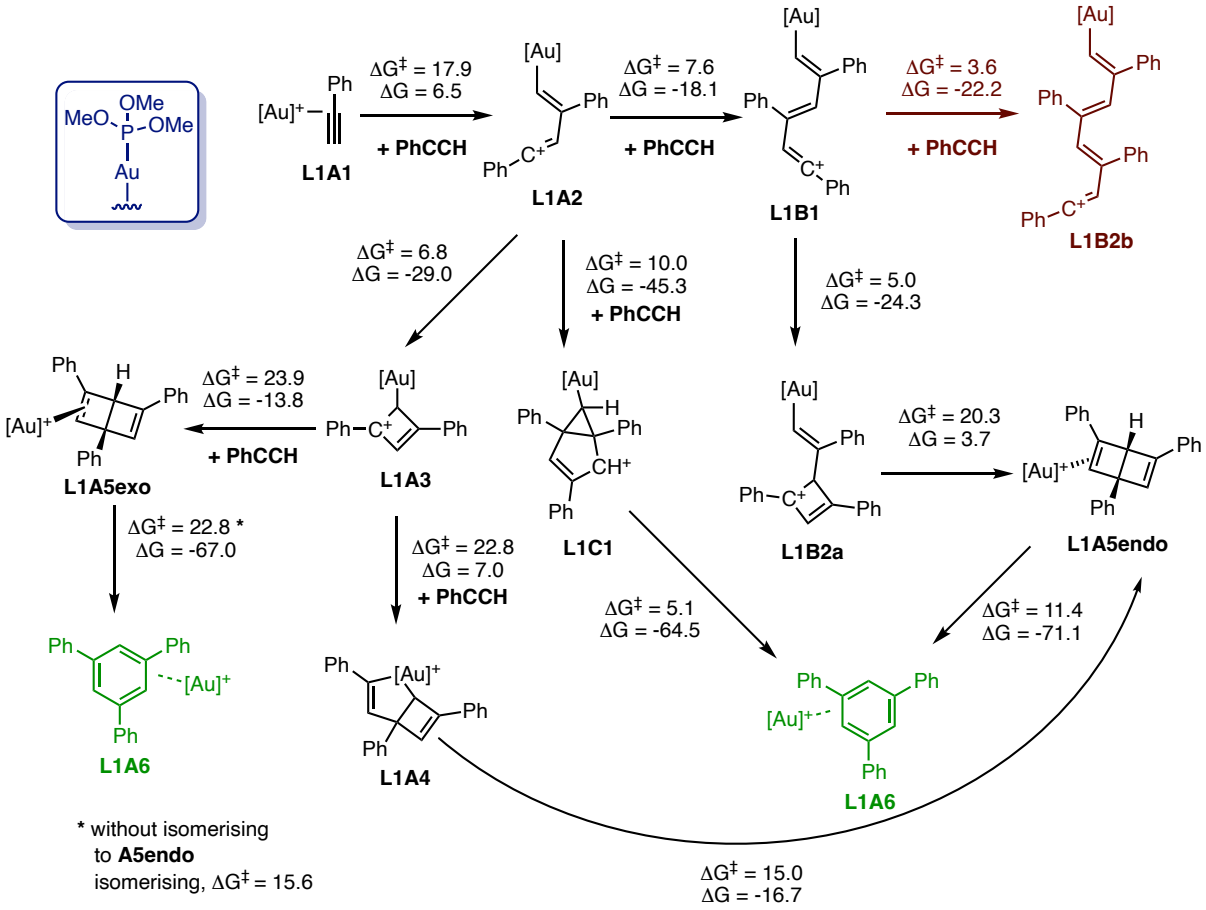

Scheme 31. Mechanism of 1,3,5-selective cyclotrimerisation using trimethyl phosphite as a ligand. Main route for side-product formation shown in red (oligomerisation). Free energy in kcal mol^{-1} at B3LYP-D3/6-311+G(d,p) + SDD, PCM (dichloromethane).

Conversely, using JohnPhos as a ligand showed several more important differences (Scheme 32). The gold(I) η^1-cyclobutadiene complex formation through **L2TSA3** is now preferred by 2.7 kcal mol^{-1}, which supports the experimental evidence that sterics play a role in the selectivity of the reaction. The imperfect match with the exact experimental ratios observed is a combination of kinetics resulting from concentrations and the limiting inherent DFT error even at acceptable levels of theory.

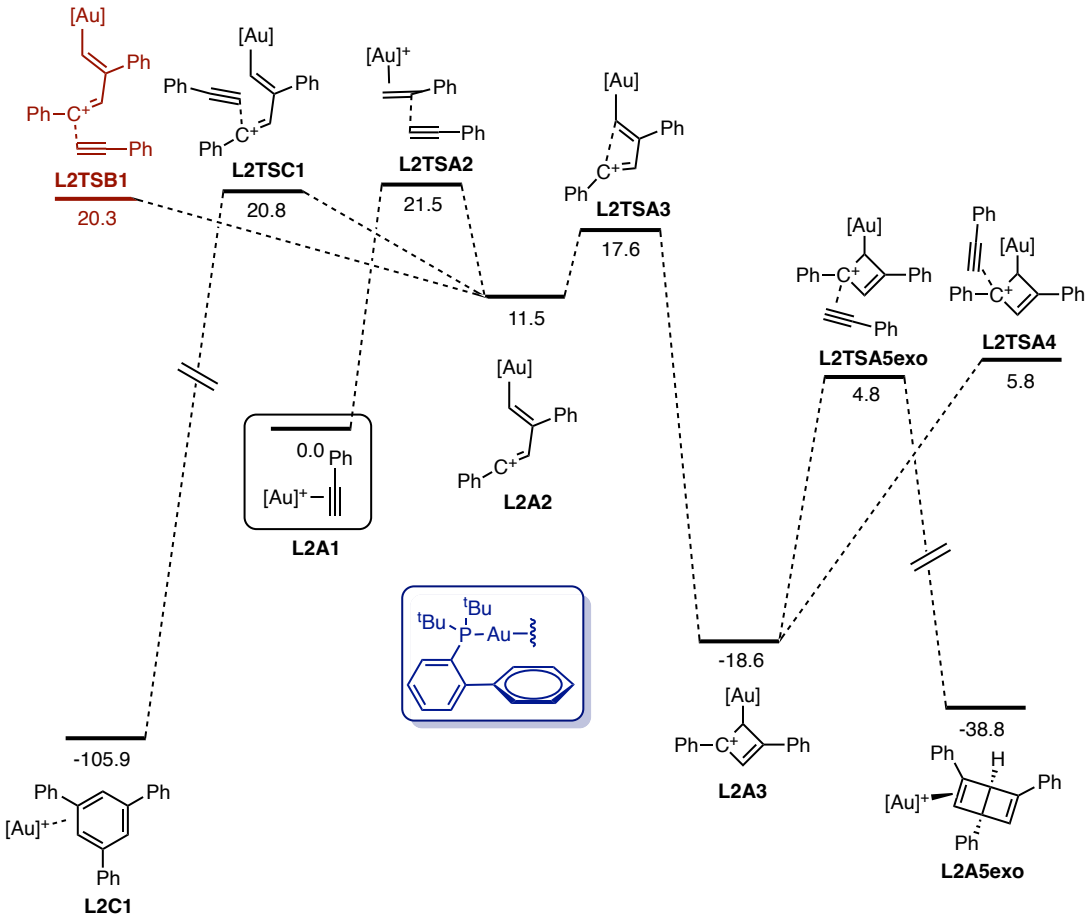

Scheme 32. Mechanism of 1,3,5-selective cyclotrimerisation using JohnPhos as a ligand. Main route for side-product formation shown in red (oligomerisation). Free energy in kcal mol^{-1} at B3LYP-D3/6-311+G(d,p) + SDD, PCM (dichloromethane).

In addition, the formation of the Dewar benzene switches from the *endo*-attack selectivity observed for (through **L2TSA4**) to an *exo*-attack mechanism (through **L2TSA5exo**), although due to the small energy difference of 1.0 kcal mol^{-1}, both mechanisms are expected to coexist within error. While the *syn*-attack **TSC1** to form cyclopropylgold **L2C1** is still not more favourable than the *anti*-attack **TSB1**, they are almost identical in energy with a 0.5 kcal mol^{-1} calculated energy difference, which lies in the error range, in line with our initial hypothesis that the undesired *anti*-attack could be sensitive to sterics. The free energies calculated with the JohnPhos model would predict a preference for trimerisation with respect to oligomerisation, which is not experimentally observed. Further refinement of the results by studying the possible conformations was not undertaken.

Intramolecular [2+2+2]-Cycloadditions and Formal 1,2,3-Trimerisation

The intramolecular reaction led to a very peculiar observation: the formation of the expected 1,3,5-cyclotrimerised product was accompanied by a formal 1,2,3-trisubstituted product (Scheme 33). A note should be made that the substitution pattern of this pathway when applied to intermolecular reactions is still 1,3,5-trisubstituted, because even if there is a complete cleavage of one of the alkynes, the aryl groups would not be *ortho* to each other for the reasons that were explained in the mechanistic analysis. However, and in order to differentiate the pathway from the usual 1,3,5-pathway with retained carbon-carbon connectivity, we will refer to these products as 1,2,3-cyclotrimers notwithstanding the ambiguity in the nomenclature.

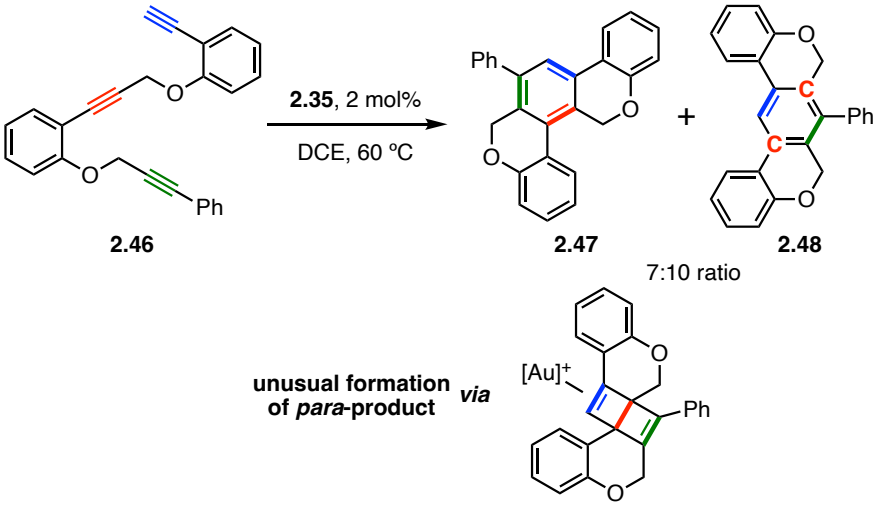

Scheme 33. Cyclotrimerisation of **2.46** gave mixtures of **2.47** and **2.48**; the latter requires cleavage of a triple bond.

These observations are explained by our proposed mechanism: the formed Dewar benzene intermediates cleave their internal bond upon aromative isomerisation to benzene. The internal bond in the Dewar benzene comes from one of the bonds in the key gold(I) cyclobutadiene intermediate, of which two bonds were newly formed but the other two were present in the alkyne. Hence, the full cleavage of one of the original alkynes is not only possible but, for some intramolecular substrates, favoured. This is shown in Scheme 34.

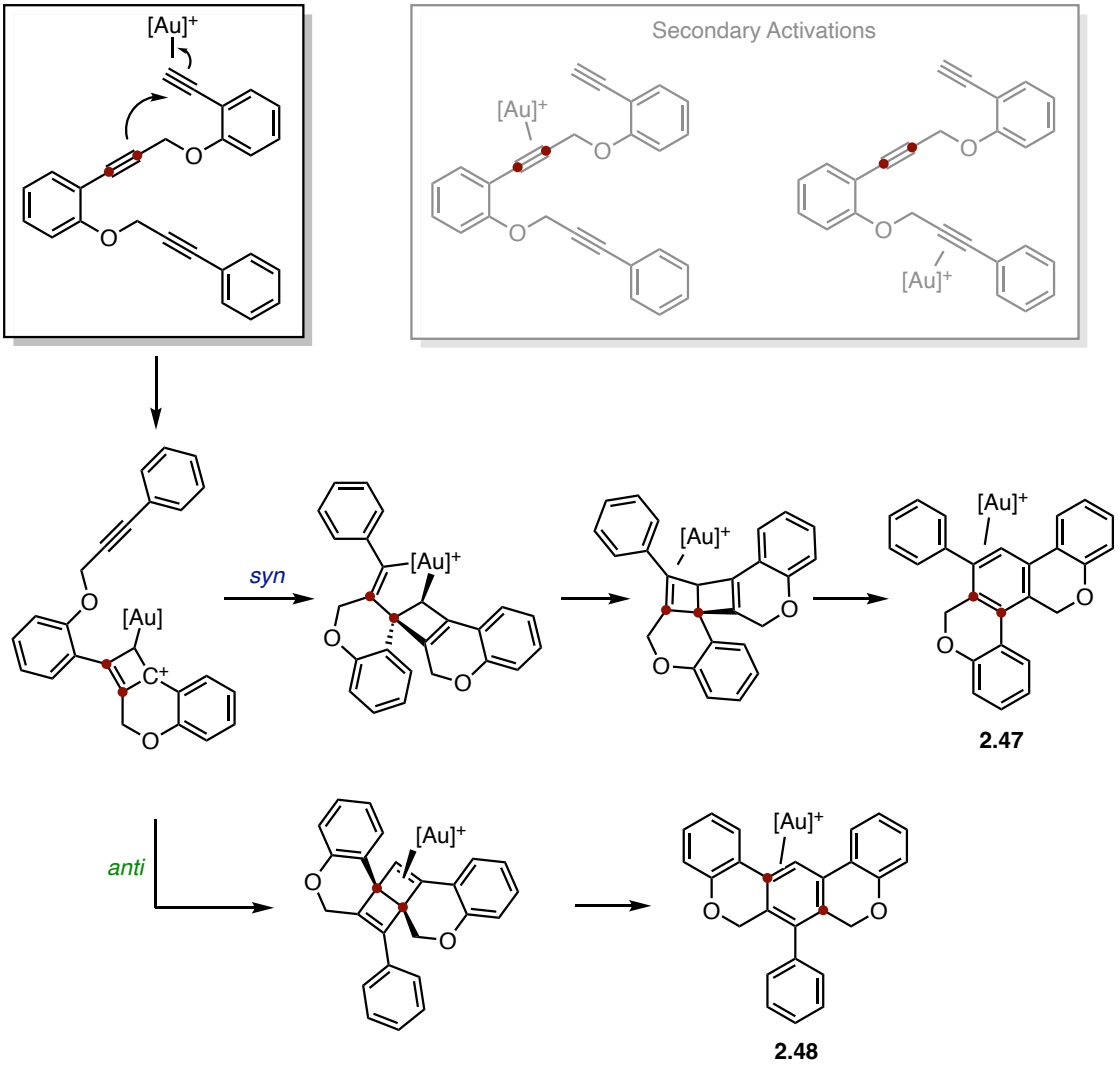

Scheme 34. Main proposed pathways to the formal 1,2,3-cyclotrimerised product through *syn*- or *anti*-attack, assuming activation of the terminal alkyne is favoured.

The proposed preference for activating the terminal alkyne instead of an internal alkyne is twofold: in addition to intermolecular trimerisations only accessible for terminal alkynes (in line with the known higher reactivity of terminal alkynes in gold(I) catalysis), the pathways stemming from activation of either of the internal alkynes require an initial 8-*endo*-dig cyclisation or form intermediates with much higher strain (Scheme 35).

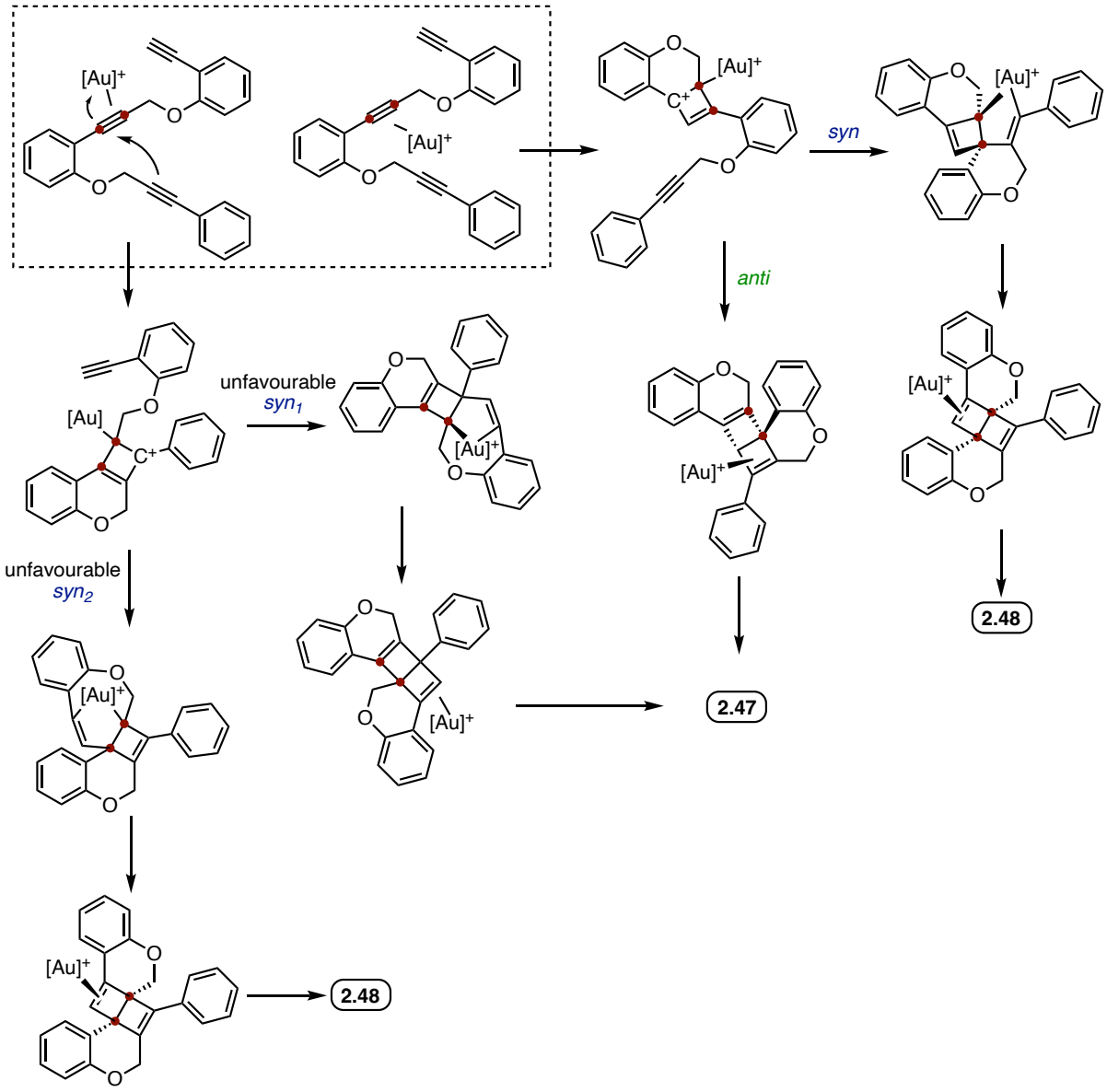

Scheme 35. Pathways derived from initial activation of the middle alkyne of triyne **2.46**.

An attempt to perform a 1,2,3-cyclotrimerisation forcing aryl groups to remain *ortho* to each other was carried out on a glycerol triether substrate, **2.49** (Scheme 36). We had anticipated the formation of an admittedly strained tricyclic species, although preliminary DFT calculations suggested that the product was thermodynamically accessible. Hydrogenation would result in the benzylic cleavage to give 1,2,3-trimethyl-4,5,6-triphenylbenzene, an unequivocal 1,2,3-trisubstitution pattern.

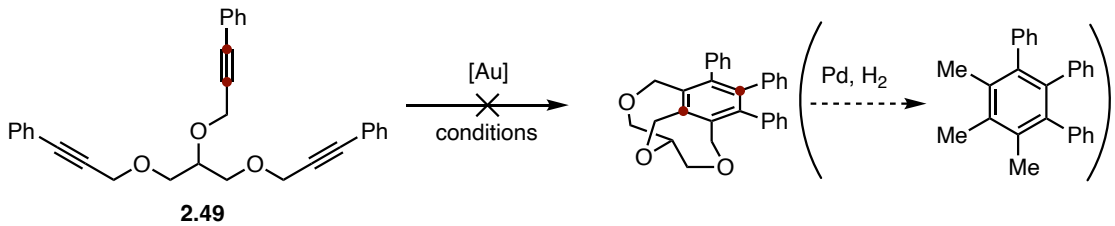

Scheme 36. Failed cyclotrimerisation of a triether.

However, subjecting the substrate to typical conditions (cationic [^{t}BuXPhosAu(NCMe)]SbF_6, 3 mol%, 60 ºC) led to no conversion after 20 h. Increasing the temperature to 80 ºC similarly showed no conversion even after 68 h. Finally, adding more gold(I) catalyst up to 11 mol% and stirring at 80 ºC led to starting material decomposition. This failed experiment suggested that internal alkynes are particularly difficult to activate, thereby confirming that the formation of the first studied intramolecular products, **2.47** and **2.48**, likely proceeded through terminal alkyne activation and *anti*-attack.

Conclusions

We have developed the gold(I)-catalysed 1,3,5-selective cyclotrimerisation of alkynes, both intermolecularly and intramolecularly. By tailoring the reaction conditions and choice of ligand, as well as taking advantage of the large concentration dependence, we reached low to moderate yields for a variety of terminal arylalkynes. While Buchwald phosphines and some NHC ligands were found to perform best, oligomers still formed as the major product, whereas tris(biphenyl)phosphine afforded cleaner mixtures but in a 1:1 dimer:1,3,5-trimer selectivity.

Investigating its mechanism, we found that, as opposed to the most frequent mechanisms, gold mediates this reaction through the initial formation of a gold(I) η^1-cyclobutadiene complex, strictly regioselective formation of a Dewar benzene and final gold-catalysed isomerisation thereof. Alternative pathways involving chain growing were expected to lead mainly to oligomerisation; on the other hand, protodemetallation-mediated mechanisms were discarded.

We also extended this reactivity to intramolecular substrates and reached products with full cleavage of one of the parent alkynes. These formal 1,2,3-cyclotrimerised products are consistent with, and unique to, the proposed mechanism. These results serve to assess the usefulness of computationally-guided reaction discovery.

Experimental Section

Computational Methods

All calculations were carried out on Gaussian09.[52] The geometry optimisations of the intermediates and transition states were performed with B3LYP[53]. In all cases, these calculations were carried out using Grimme's D3 dispersion correction[54] with the 6-31G(d) basis set[55] for non-metal atoms and the SDD[56] basis set and ECP for gold. Single-point energy calculations were performed with the 6-311+G(d,p) basis set for non-metal atoms and SDD basis set and ECP for gold. The implicit polarisable continuum model (PCM)[57] for dichloromethane was used in all calculations and the cationic complexes were modelled with the exclusion of the counter-anions. All stationary points were verified by the absence of imaginary vibrations and transition states confirmed by IRC[58] calculations with the LQA or DVV algorithms. For problematic cases in which Hratchian and Schlegel's damped velocity Verlet algorithm (DVV)[59] failed, steep optimisations with force constant calculations were performed to relax the transition state most of the way to the minima, followed by small-step optimisation calculating force constants to reach the minima. The reported free energies were calculated at 298 K and 1 atm. NBO analysis was performed with the NBO3.0 program[60] with B3LYP-D3, the 6-311+G(d,p) basis set for non-metal atoms and SDD basis set and ECP for gold.

52 Gaussian 09, Revision B.1, Frisch, M. J., Trucks, G. W., Schlegel, H. B., Scuseria, G. E., Robb, M. A., Cheeseman, J. R., Scalmani, G., Barone, V., Mennucci, B., Petersson, G. A., Nakatsuji, H., Caricato, M., Li, X., Hratchian, H. P., Izmaylov, A. F., Bloino, J., Zheng, G., Sonnenberg, J. L., Hada, M., Ehara, M., Toyota, K., Fukuda, R., Hasegawa, J., Ishida, M., Nakajima, T., Honda, Y., Kitao, O., Nakai, H., Vreven, T., Montgomery, J. A., Peralta, Jr. J. E., Ogliaro, F., Bearpark, M., Heyd, J. J., Brothers, E., Kudin, K. N., Staroverov, V. N., Kobayashi, R., Normand, J., Raghavachari, K., Rendell, A., Burant, J. C., Iyengar, S. S., Tomasi, J., Cossi, M., Rega, N., Millam, J. M., Klene, M., Knox, J. E., Cross, J. B., Bakken, V., Adamo, C., Jaramillo, J., Gomperts, R., Stratmann, R. E., Yazyev, O., Austin, A. J., Cammi, R., Pomelli, C., Ochterski, J. W., Martin, R. L., Morokuma, K., Zakrzewski, V. G., Voth, G. A., Salvador, P., Dannenberg, J. J., Dapprich, S., Daniels, A. D., Farkas, Ö., Foresman, J. B., Ortiz, J. V., Cioslowski, J., Fox, D. J. Gaussian, Inc., Wallingford CT 2009.

53 (a) Becke, A. D. *J. Chem. Phys.* **1993**, *98*, 5648; (b) Becke, A. D. *J. Chem. Phys.* **1993**, *98*, 1372; c) Lee, C.; Yang, W.; Parr, R. G. *Phys. Rev. B* **1988**, *37*, 785.

54 Grimme, S. Density Functional Theory with London Dispersion Corrections. *WIREs Comput Mol Sci* **2011**, *1*, 211–228.

55 Hehre, W. J.; Ditchfield, R.; Pople, J. A. Self–Consistent Molecular Orbital Methods. XII. Further Extensions of Gaussian–Type Basis Sets for Use in Molecular Orbital Studies of Organic Molecules. *J. Chem. Phys.* **1972**, *56*, 2257–2261.

56 Andrae, D.; Häußermann, U.; Dolg, M.; Stoll, H.; Preuß, H. Energy-adjusted ab initio pseudopotentials for the second and third row transition elements. *Theor. Chim. Acta* **1990**, *77*, 123–141.

57 Cancès, E.; Mennucci, B.; Tomasi, J. A new integral equation formalism for the polarizable continuum model: Theoretical background and applications to isotropic and anisotropic dielectrics. *J. Chem. Phys.* **1997**, *107*, 3032−3041.

58 Gonzalez, C.; Schlegel, H. B. Reaction path following in mass-weighted internal coordinates. *J. Phys. Chem.* **1990**, *94*, 5523−5527.

59 Hratchian, H. P.; Schlegel, H. B. Following Reaction Pathways Using a Damped Classical Trajectory Algorithm. *J. Phys. Chem. A* **2002**, *106*, 165–169.

60 Glendening, E. D.; Badenhoop, J. K.; Reed, A. E.; Carpenter, J. E.; Bohmann, J. A.; Morales, C. M.; Weinhold, F. NBO, 5.0 Theoretical Institute, University of Wisconsin: Madison, WI, 2011.

General Experimental Methods

Anhydrous reactions were performed under nitrogen or argon in solvents dried by passing through an activated alumina column on a PureSolv^{TM} solvent purification system (Innovative Technologies, Inc., MA). Otherwise, HPLC-grade solvents were used. Reactions were followed by GC-MS, UHPLC-MS, TLC (thin layer chromatography) or ^{1}H NMR analysis on aliquots. Analytical thin layer chromatography was carried out using TLC aluminium sheets with 0.2 mm of silica gel (Merck 60 F_{254}) using UV light as the visualizing agent, and an acidic solution of vanillin in ethanol or a basic aqueous solution of $KMnO_4$ as stains. UHPLC-MS analyses were carried out on an Agilent Technologies 1290 Infinity II instrument with single-quad detector using APCI for the ionisation. Purifications by chromatography were carried out using flash grade silica gel (SDS Chromatogel 60 ACC, 40-63 mm) or preparative thin-layer chromatography plates (Analtech, 1000 μm or 2000 μm). The reported yields refer to isolated pure compounds or, in the case of isolation as pure mixtures as ratios, weighed and the ratio determined by NMR and subsequently validating with an internal standard. NMR spectra were recorded at 298 K on a Bruker Avance 300, Bruker Avance 400 Ultrashield or a Bruker Avance 500 Ultrashield apparatus. The signals are given as δ / ppm (multiplicity, coupling constant (Hertz), number of protons) downfield from tetramethylsilane, with calibration on the residual solvent used (δ_H = 7.26 ppm and δ_C = 77.16 ppm for $CDCl_3$). Mass spectra were recorded on a Waters UPLC-QqTOF (Maxis Impact, Bruker Daltonics) with ESI and APCI, or a Waters Alliance HPLC-TOF (MicroTOF Focus, Bruker Daltonics) with ESI and APCI. Melting points were determined using a Büchi melting point apparatus or MP70 Melting Point System (Mettler Toledo). X-ray diffraction was carried out on a Bruker APEX Duo instrument with Mo Kα Microfocus source E025 IuS anode and an APEX DUO detector, or a Rigaku MicroMax-007HF, with Mo Kα radiation rotating anode and a Pilatus 200K detector.

Synthetic Procedures and Characterisation Data

General procedure for the cyclotrimerisation of alkynes

To a solution of alkyne (0.3 mmol, 3 eq) in dichloroethane (0.1 M) was added [*t*BuXPhosAu(NCMe)]SbF_6 (0.006 mmol, 2 mol %). The vial was sealed and the mixture stirred at 60 ºC for 16-48 h. The reaction was quenched by adding a drop of Et_3N, concentrated *in vacuo* and purified by preparative TLC.

1,3,5-Triphenylbenzene (2.26)

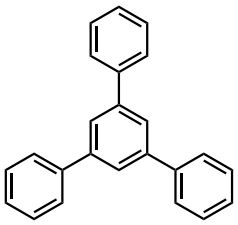

The title compound was prepared by following the general procedure using phenylacetylene (44.7 mg, 0.438 mmol). The crude product was purified by preparative TLC (7:1 CyH:PhMe). Isolated as a white solid (14.6 mg, 33%). **^{1}H NMR** (400 MHz, $CDCl_3$) δ 7.80 (s, 3H), 7.74 – 7.67 (m, 6H), 7.52 – 7.47 (m, 6H), 7.43 – 7.38 (m, 3H) ppm.

Spectral data consistent with the values reported in the literature.[61]

1,3,5-Tris(4-*tert*-butylphenyl)benzene (2.37)

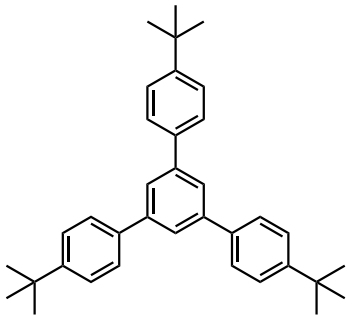

The title compound was prepared by following the general procedure using 4-tert-butylphenylacetylene (54.1 mg, 0.342 mmol). The crude product was purified by preparative TLC (1:1 CyH:PhMe). Isolated as a white solid (20.0 mg, 37%). **^{1}H NMR** (400 MHz, $CDCl_3$) δ 7.80 (s, 3H), 7.70 – 7.64 (m, 6H), 7.56 – 7.52 (m, 6H), 1.42 (s, 27H) ppm.

Spectral data consistent with the values reported in the literature. [doi/10.1021/om8002703]

1,3,5-Tris(4-[1,1'-biphenyl])benzene (2.38)

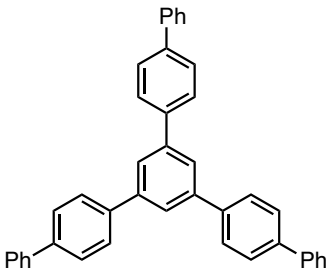

The title compound was prepared by following the general procedure using 4-ethynyl-1,1'-biphenyl (52.2 mg, 0.293 mmol). The crude product was purified by preparative TLC (1:1 CyH:PhMe). Isolated as a white solid (17.2 mg, 33%). **^{1}H NMR** (400 MHz, $CDCl_3$) δ 7.93 (s, 3H), 7.87 – 7.82 (m, 6H), 7.78 – 7.75 (m, 6H), 7.72 – 7.37 (m, 15H) ppm.

Spectral data consistent with the values reported in the literature.[61]

61 Joosten, A.; Soueidan, M.; Denhez, C.; Harakat, D.; Hélion, F.; Namy, J.-L.; Vasse, J.-L.; Szymoniak, J. Multimetallic Zirconocene-Based Catalysis: Alkyne Dimerization and Cyclotrimerization Reactions. *Organometallics* **2008**, *27*, 4152–4157.

1,3,5-Tris(4-tolyl)benzene (2.39)

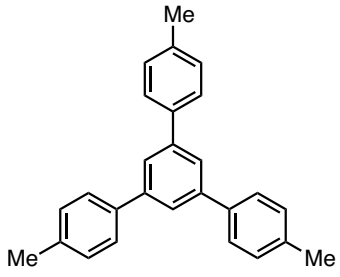

The title compound was prepared by following the general procedure using 4-methylphenylacetylene (39.0 mg, 0.336 mmol). The crude product was purified by preparative TLC (3:1 hexanes:PhMe). Isolated as a white solid (10.6 mg, 27%). **^{1}H NMR** (400 MHz, $CDCl_3$) δ 7.81 (s, 3H), 7.69 – 7.64 (m, 6H), 7.37 – 7.34 (m, 6H), 2.48 (s, 9H) ppm.

Spectral data consistent with the values reported in the literature.[61]

1,3,5-Tris(4-fluoro-3-methylphenyl)benzene (2.40)

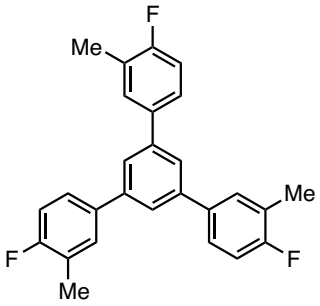

The title compound was prepared by following the general procedure using 4-fluoro-3-methylphenylacetylene (44.1 mg, 0.329 mmol). The crude product was purified by preparative TLC (3:1 hexanes:PhMe). Isolated as a white solid (13.5 mg, 31%). **^{1}H NMR** (500 MHz, $CDCl_3$) δ 7.64 (s, 3H), 7.48 (dd, J = 7.3, 2.4 Hz, 3H), 7.45 (ddd, J = 7.6, 4.9, 2.4 Hz, 3H), 7.11 (dd, J = 9.4, 8.4 Hz, 3H), 2.37 (d, J = 2.0 Hz, 9H) ppm. **^{13}C{^{1}H} NMR** δ 161.38 (d, J = 245.8), 141.76, 137.00 (d, J = 3.6 Hz), 130.55 (d, J = 5.1 Hz), 126.31 (d, J = 7.9 Hz), 125.36 (d, J = 17.6 Hz), 124.86, 115.51 (d, J = 22.5 Hz), 14.86 (d, J = 3.4 Hz) ppm. **^{19}F{^{1}H} NMR** δ -119.43 ppm.

2-(trimethylsilylethynyl)phenol (2.50)

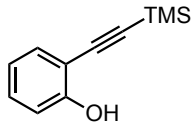

A solution of 2-iodophenol (440.0 mg, 2.00 mmol), TMS-acetylene (235.7 mg, 2.40 mmol, 1.2 eq), $(Ph_3P)PdCl_2$ (17.7 mg, 0.04 mmol, 2 mol %), copper(I) iodide (15.2 mg, 0.08 mmol, 4 mol %) in THF (5 mL, 0.4 M) was degassed by bubbling with argon and triethylamine (0.56 mL, 4.0 mmol, 2 eq) was added over a flow of argon. The mixture was stirred at 35 ºC for 22 h. After completion, the mixture was concentrated, filtered through a silica pad (4:1 CyH:EtOAc) and concentrated. The crude was used without further purification.

3-Phenylpropargyl 2-iodophenyl ether (2.51)

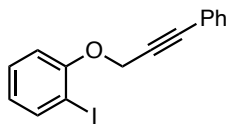

A solution of 2-iodophenol (350.0 mg, 1.59 mmol), 3-phenylpropyn-1-ol (231.3 mg, 1.75 mmol, 1.1 eq) and triphenylphosphine (418.1 mg, 1.59 mmol, 1 eq) in dry and degassed THF (4 mL, 0.4 M) was cooled to 0 ºC. To the stirred solution, DIAD (0.32 mL, 1 eq) was added dropwise and the reaction mixture was then allowed to stir at 23 ºC for 2 hours. The reaction was quenched with aqueous NaOH (0.5 M, 5 mL) and the mixture extracted with diethyl ether (2x). The combined organic fractions were washed with saturated brine (1x), dried with $MgSO_4$ and concentrated. The crude product was purified by column chromatography on silica (cyclohexane) to afford the title product as a colourless oil (528.0 mg, 99%). **HRMS** (APCI) *m/z*:

$[M+H]^+$ calculated for $C_{15}H_{12}IO$ = 334.9927; found 334.9925. The spectral data matched literature values.[62]

2-Propargyloxy(trimethylsilylethynyl)benzene (2.52)

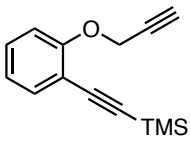

Crude **2.50** (324.2 mg) and potassium carbonate (588.5 mg, 4.26 mmol, 2.5 eq) were dissolved/suspended in dimethylformamide (8.5 mL, 0.2 M). Propargyl bromide (150 µL, 1.1 eq) was added and the mixture was stirred at 23 ºC overnight. Saturated aqueous NH_4Cl (30 mL) was added and the mixture extracted with Et_2O (2x). The combined organic fractions were washed with saturated brine, dried with $MgSO_4$ and concentrated. The crude was purified by column chromatography (10:1 to 6:1 CyH:EtOAc) yielding the title product as a yellowish oil (330.7 mg, 73% over two steps). **^{1}H NMR** (500 MHz, $CDCl_3$) δ 7.44 (dd, *J* = 7.6, 1.7 Hz, 1H), 7.28 (ddd, *J* = 8.8, 7.6, 2.0 Hz, 1H), 7.02 (dd, *J* = 8.4, 1.0 Hz, 1H), 6.94 (td, *J* = 7.5, 1.0 Hz, 1H), 4.78 (d, *J* = 2.4 Hz, 2H), 2.51 (t, *J* = 2.4 Hz, 1H), 0.26 (s, 9H) ppm. **^{13}C{^{1}H} NMR** (126 MHz, $CDCl_3$) δ 158.6, 134.3, 129.8, 121.7, 113.6, 101.0, 99.1, 81.6, 78.6, 75.9, 56.9, 0.2 ppm. **HRMS** (APCI) *m/z*: $[M+H]^+$ calculated for $C_{14}H_{17}OSi$ = 229.1043; found 229.1038.

2-[(3-phenylpropargyloxy)phenyl]propargyloxy(trimethylsilylethynyl)benzene (2.53)

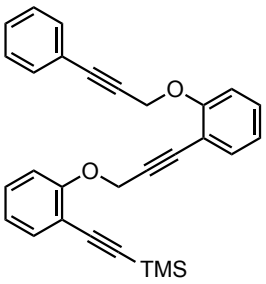

2.51 (90.0 mg, 270 µmol), **2.52** (67.7 mg, 300 µmol, 1.1 eq), $(Ph_3P)PdCl_2$ (2.4 mg, 5.4 µmol, 2 mol %) and copper(I) iodide (2.1 mg, 11 µmol, 4 mol %) were dissolved in degassed triethylamine (0.7 mL, 0.4 M). The mixture was stirred at 40 ºC for 14 h. The reaction mixture was diluted with EtOAc (10 mL), to which saturated aqueous $NaHCO_3$ (25 mL) was added, and extracted with EtOAc (2x). The combined organic fractions were washed with saturated brine (10 mL), dried with $MgSO_4$ and concentrated. Purification by column chromatography (2:1 CyH:PhMe) afforded the title product as an orange oil (34.6 mg, 30%). **^{1}H NMR** (500 MHz, $CDCl_3$) δ 7.45 (1H, dd, J = 1.7, 7.7 Hz), 7.44-7.39 (3H, m), 7.33-7.28 (5H, m), 7.20 (1H, d, J=8.4, 1.0 Hz), 7.10 (1H, d, J=8.5, 1.0 Hz), 6.95 (1H, td, J= 6.4, 1Hz), 6.92 (1H, td, J= 6.4, 1Hz), 5.06 (2H, s), 4.97 (2H, s), 0.28 (9H, s) ppm. **^{13}C{^{1}H} NMR** (126 MHz, $CDCl_3$) δ 158.9, 158.6, 134.2, 134.0, 131.9, 130.0, 129.9, 128.8, 128.4, 122.4, 121.4, 121.4, 113.9, 113.5, 113.3, 112.6, 101.3, 98.9, 88.3, 87.7, 83.9, 83.8, 57.9, 57.5, 0.2 ppm.

62 Paul, K.; Jalal, S.; Kundal, S.; Jana, U. Synthesis of Fused Dibenzofuran Derivatives via Palladium-Catalyzed Domino C–C Bond Formation and Iron-Catalyzed Cycloisomerization/Aromatization. *J. Org. Chem.* **2016**, *81*, 1164–1174.

2-[(3-phenylpropargyloxy)phenyl]propargyloxyphenylacetylene (2.46)

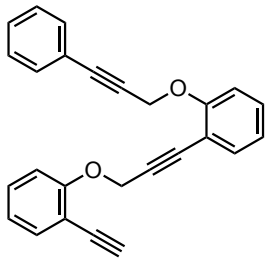

2.53 (34.1 mg, 78.5 μmol) was dissolved in tetrahydrofuran (0.4 mL, 0.2 M) and tetrabutylammonium fluoride (1M in THF, 86 μL, 1.1 eq) was added to the solution. The reaction was stirred at 23 ºC for 16 h. Filtration through silica with dichloromethane followed by purification by preparative TLC (toluene) afforded the product as a yellow oil (20.7 mg, 73%). **^{1}H NMR** (400 MHz, $CDCl_3$) δ 7.47 (dd, *J* = 7.6, 1.8 Hz, 1H), 7.44 – 7.38 (m, 3H), 7.36 – 7.28 (m, 5H), 7.24 (dd, *J* = 8.5, 1.1 Hz, 1H), 7.10 (dd, *J* = 8.5, 1.0 Hz, 1H), 6.93 (tt, *J* = 7.5, 1.2 Hz, 2H), 5.07 (s, 2H), 4.95 (s, 2H), 3.31 (s, 1H) ppm. **^{13}C{^{1}H} NMR** (101 MHz, $CDCl_3$) δ 159.1, 158.7, 134.3, 134.1, 131.9, 130.2, 130.1, 128.8, 128.4, 122.4, 121.5, 121.3, 113.4, 113.3, 112.5, 112.1, 88.1, 87.7, 84.1, 83.8, 81.5 (alkyne ***C***H), 80.1 (alkyne ***C***CH), 57.7, 57.6 ppm.

3-Phenylpropargyl alcohol (2.54)

Iodobenzene (2.10 g, 10.3 mmol), propargyl alcohol (693 mg, 12.4 mmol, 1.2 eq), bis(triphenylphosphine)palladium dichloride (90.5 mg, 0.21 mmol, 2 mol %) and copper iodide (78.6 mg, 0.41 mmol, 4 mol %) were stirred in degassed THF and triethylamine (2.9 mL, 20.6 mmol, 2 eq) was added via syringe over a flow of argon. The mixture was stirred at 23 ºC for 9 h, after which the mixture was concentrated *in vacuo*, dry-loaded on silica and purified by column chromatography (4:1 CyH:EtOAc). The product was obtained as a yellow oil (1.35 g, 99%). The spectral data matched literature values.[63]

14-phenyl-1*H*,7*H*-benzo[1,2-*c*:3,4-*c′*]dichromene (2.47) and 7-phenyl-6*H*,8*H*-benzo[1,2-*c*:5,4-*c′*]dichromene (2.48)

Triyne **2.46** (20.7 mg, 57 μmol) was dissolved in dichloroethane (0.6 mL, 0.1 M) and [*t*BuXPhosAu(NCMe)]SbF_6 (1.0 mg, 1.1 μmol, 2 mol%) was added as a solid, with the solution rapidly turning green. The mixture was stirred at 60 ºC for 36 h, with the reaction gradually turning blackish. After this time, the reaction was quenched with one drop of triethylamine and concentrated. Purification of the crude by preparatory TLC (1:1 CyH:PhMe) afforded a 7:10 mixture of **2.47**:**2.48** (total 2.6 mg, 13%).

63 Tao, R.; Yin, Y.; Duan, Y.; Sun, Y.; Sun, Y.; Cheng, F.; Pan, J.; Lu, C.; Wang, Y. Fe(OTf)$_3$-Catalyzed Tandem Meyer-Schuster Rearrangement/Intermolecular Hydroamination of 3-Aryl Propargyl Alcohols for the Synthesis of Acyclic β-Aminoketones. *Tetrahedron* **2017**, *73*, 1762–1768.

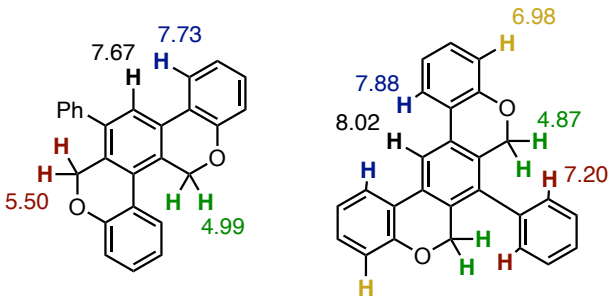

2.47 **2.48**

Characteristic peaks of **2.47**: **^{1}H NMR** (400 MHz, $CDCl_3$) δ 7.73 (dd, *J* = 7.7, 1.6 Hz, 1H), 7.67 (s, 1H), 7.05 (dd, *J* = 8.1, 1.1 Hz, 1H), 5.50 (s, 2H), 4.99 (s, 2H) ppm. *Assignment:* NOEs show no contact between 7.73 dd and OCH_2. Contact between 5.50 ppm and Ph by analogy to **2.48**. Shielded aromatic is one of the two protons *ortho* to oxygen, dd multiplicity matches, but the ring was not assigned.

Characteristic peaks of **2.48**: **^{1}H NMR** (400 MHz, $CDCl_3$) δ 8.06 (s, 1H), 7.88 (dd, *J* = 7.8, 1.6 Hz, 2H), 7.22 – 7.19 (m, 2H), 6.98 (dd, *J* = 8.1, 1.2 Hz, 2H), 4.86 (s, 4H) ppm. *Assignment:* NOE contact between OCH_2 and multiplet centred at 7.20 ppm, none between methylene and 7.88 ppm (analogy to **2.47**). Shielded aromatic is *ortho* to oxygen and dd multiplicity matches.

1,2,3-Tris(3-phenylpropargyloxy)propane (2.49)

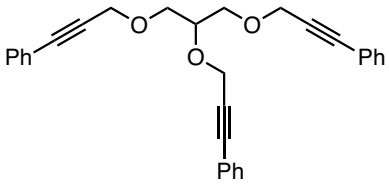

Sodium hydride (60% wt. dispersion, 189 mg, 4.73 mmol, 3.6 eq) was dissolved in degassed dimethylformamide (3.2 mL). To the stirred solution was added, over a flow of nitrogen, glycerol (121.0 mg, 1.31 mmol) in dimethylformamide (1.2 mL). After visible hydrogen evolution ceased, propargyl bromide (516 mg, 4.34 mmol, 3.3 eq) was added dropwise to the mixture. The reaction was heated at 60 ºC for 90 min and then stirred at 23 ºC for 16 h. After this time, saturated aqueous NH_4Cl (30 mL) was added and the mixture was extracted with ethyl acetate (3x). The combined organic fractions were washed with saturated brine, dried with Na_2SO_4 and concentrated. The crude did not warrant further purification and was used directly in the next step.

Iodobenzene (885 mg, 4.34 mmol, 3.3 eq), crude 1,2,3-tris(propargyloxy)propane (271.0 mg, 1.31 mmol), $(Ph_3P)_2PdCl_2$ (34.7 mg, 79 µmol, 6 mol%) and copper(I) iodide (30.1 mg, 158 µmol, 12 mol%) were dissolved in tetrahydrofuran (9 mL) and degassed by bubbling with argon. Triethylamine (1.1 mL, 800 mg, ca 8 mmol, 6 eq) was added by syringe over a flow of argon. The reaction was stirred at 23 ºC for 17 h. After this time, the mixture was concentrated and dry-loaded on silica gel for chromatographic separation. Column chromatography (10:1 CyH:EtOAc) afforded the title compound as an orange oil (510.0 mg, 89%). **^{1}H NMR** (400 MHz, $CDCl_3$) δ 7.45 (dt, *J* = 6.2, 1.8 Hz, 6H), 7.34 – 7.25 (m, 9H), 4.62 (s, 2H), 4.46 (s, 4H), 4.10 (p, *J* = 5.0 Hz, 1H), 3.84 (qd, *J* = 10.3, 5.0 Hz, 4H) ppm. **^{13}C{^{1}H} NMR**

(101 MHz, $CDCl_3$) δ 131.9, 131.9, 128.5, 128.5, 128.4, 128.3, 122.8, 122.7, 86.6, 86.3, 85.5, 85.1, 76.5, 69.8, 59.5, 58.5 ppm.

Di-*tert*-butyl(3',5'-di-*tert*-butyl-[1,1'-biphenyl]-2-yl)phosphine (2.55)

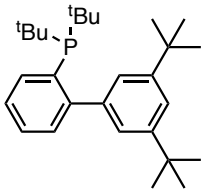

A flame-dried Schlenk tube under argon was charged with magnesium turnings (62.3 mg, 2.56 mmol, 2.3 eq), 1-bromo-3,5-di-*tert*-butylbenzene (300.2 mg, 1.12 mmol) and dry THF (1.35 mL, 0.8 M). The mixture was stirred at 65 ºC and 1,2-dibromoethane (4 µL, 50 µmol, 0.04 eq) added to activate the magnesium. After stirring at 65 ºC for 30 minutes, 1,2-dibromobenzene (264.2 mg, 1.12 mmol, 1.0 eq) was added over a flow of argon. The mixture was stirred for 2 hours at the same temperature and then allowed to cool to room temperature. Copper(I) cyanide (99.7 mg, 1.12 mmol, 1.0 eq) and di-*tert*-butylchlorophosphine (241.7 mg, 1.34 mmol, 1.2 eq) were added sequentially to the reaction mixture and the sealed Schlenk tube was stirred at 75 ºC for 37 hours. Th reaction was cooled to room temperature before quenching with aqueous NH_4Cl (20 mL) and extracted with ethyl acetate (3x). The combined organic fractions were washed with saturated brine (15 mL), dried over Na_2SO_4 and concentrated. The crude product was purified by column chromatography (30:1 to 10:1 CyH:EtOAc) followed by preparative TLC (20:1 pentane:Et_2O) affording the title product as a colourless oil/resin (244.4 mg, 53%). **^{1}H NMR** (500 MHz, CD_2Cl_2) δ 7.92 (dt, J = 7.4, 1.6 Hz, 1H), 7.39 (ddd, J = 7.3, 1.6, 0.8 Hz, 1H), 7.37 (t, J = 1.8 Hz, 1H), 7.35 (td, J = 7.4, 1.8 Hz, 1H), 7.27 (ddd, J = 7.3, 4.1, 1.8 Hz, 1H), 7.08 (dd, J = 1.8, 0.6 Hz, 2H), 1.36 (s, 18H), 1.15 (d, J = 11.6 Hz, 18H) ppm. **^{13}C{^{1}H} NMR** (126 MHz, CD_2Cl_2) δ 152.97 (d, *J* = 33.4 Hz), 149.79, 143.93 (d, *J* = 7.2 Hz), 136.42 (d, *J* = 27.5 Hz), 135.97 (d, *J* = 3.2 Hz), 130.97 (d, *J* = 6.0 Hz), 128.78, 125.74 (d, *J* = 3.7 Hz), 120.10, 35.31, 33.08 (d, *J* = 25.7 Hz), 31.90, 31.13 (d, *J* = 15.7 Hz) ppm**.** **^{31}P{^{1}H} NMR** (202 MHz, CD_2Cl_2) δ 21.7 ppm. **HRMS** (APCI) *m/z*: $[M+H]^+$ calculated for $C_{28}H_{44}P$ = 411.3175; found 411.3171.

Di-*tert*-butyl(3',5'-di-*tert*-butyl-[1,1'-biphenyl]-2-yl)phosphinegold(I) chloride (2.34b)

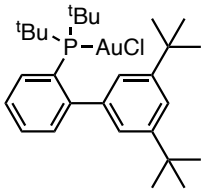

2.55 (94.9 mg, 231 µmol) was dissolved in dichloromethane (7.7 mL, 0.03 M) and chloro(dimethylsulfide)gold (69.4 mg, 236 µmol, 1.02 eq) was added as a solid. The solution was stirred at 23 ºC for 80 minutes, filtered through Teflon and concentrated to afford the complex as a white solid (148.6 mg, quant.). **^{1}H NMR** (500 MHz, CD_2Cl_2) δ 7.89 (td, J = 7.5, 1.4 Hz, 1H), 7.54 – 7.46 (m, 3H), 7.31 (ddd, J = 7.3, 4.3, 1.7 Hz, 1H), 6.92 (d, J = 1.8 Hz, 2H), 1.40 (d, J = 15.4 Hz, 18H), 1.35 (s, 18H) ppm. **^{13}C{^{1}H} NMR** (126 MHz, CD_2Cl_2) δ 151.81 (d, *J* = 14.0 Hz), 150.81, 141.81 (d, *J* = 6.7 Hz), 134.22 (d, *J* = 2.8 Hz), 133.48 (d, *J* = 7.3 Hz), 130.84 (d, *J* = 2.3 Hz), 127.00 (d, *J* = 6.7 Hz), 126.58 (d, *J* = 45.6 Hz), 124.27, 122.61, 38.17 (d, *J* = 25.5 Hz), 35.32, 31.76, 31.20 (d, *J* = 6.9 Hz) ppm. **^{31}P{^{1}H} NMR** (202 MHz, CD_2Cl_2) δ 63.09 ppm. **HRMS** (ESI) *m/z*: $[M+Na]^+$ calculated for $C_{28}H_{43}AuClNaP$ = 665.2349; found 665.2372.

2.5.4 Crystal Structures

Crystal data and structure refinement for EGP-04-C12LT.

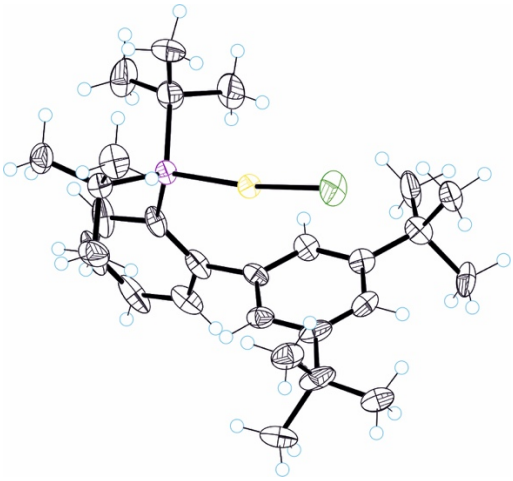

Identification code	EGP-04-C12LT		
Empirical formula	$C_{56}H_{86}Au_2Cl_2P_2$		
Formula weight	1286.02		
Temperature/K	100.00		
Crystal system	triclinic		
Space group	P-1		
a/Å	9.86042(9)	α/°	76.5366(17)
b/Å	12.7819(3)	β/°	88.2835(12)
c/Å	22.9958(4)	γ/°	88.8307(12)
Volume/Å^3	2817.09(9)		
Z	2		
ρ_{calc}g/cm^3	1.516		
μ/mm^{-1}	5.387		
F(000)	1288.0		
Crystal size/mm^3	0.6 × 0.1 × 0.1		
Radiation	MoKα (λ = 0.71073)		
2Θ range for data collection/°	3.276 to 65.444		
Index ranges	-14 ≤ h ≤ 14, -19 ≤ k ≤ 19, -34 ≤ l ≤ 34		
Reflections collected	33314		
Independent reflections	33314 [R_{int} = ?, R_{sigma} = 0.0369]		
Data/restraints/parameters	33314/261/706		
Goodness-of-fit on F^2	1.044		
Final R indexes [I>=2σ (I)]	R_1 = 0.0582, wR_2 = 0.1603		
Final R indexes [all data]	R_1 = 0.0793, wR_2 = 0.1784		
Largest diff. peak/hole / e Å^{-3}	2.92/-2.11		

Computed Structures and Energies

Table 5. Trimethylphosphinegold(I)-catalysed cyclotrimerisation main intermediates and transition states. B3LYP-D3/6-31G(d)+SDD(Au); PCM (dichloromethane); HLT: B3LYP-D3/6-311+G(d,p)+SDD(Au)

Code	E / Hartree	G / Hartree	E_{HLT} / Hartree
A1	-905.20983	-905.03014	-905.35674
A2	-1213.62892	-1213.34558	-1213.85353
A3	-1213.68366	-1213.39541	-1213.90394
A4	-1522.11381	-1521.71788	-1522.41721
A5exo	-1522.14606	-1521.75000	-1522.44801
A6	-1522.25362	-1521.85658	-1522.55662
A5endo	-1522.14033	-1521.74540	-1522.44217
C1	-1522.14763	-1521.75224	-1522.44899
B1	-1522.09112	-1521.70314	-1522.39576
B2a	-1522.14045	-1521.74602	-1522.44038
B2b	-1830.56165	-1830.06519	-1830.94674
TSA2	-1213.60358	-1213.32499	-1213.83323
TSA3	-1213.62255	-1213.33712	-1213.84578
TSA4	-1522.07341	-1521.68282	-1522.37686
TSA5exo	-1522.06996	-1521.68268	-1522.37504
TSA6exo	-1522.10506	-1521.71167	-1522.40680
TSA5endo	-1522.08750	-1521.69265	-1522.38974
TSA6endo	-1522.11574	-1521.72100	-1522.41662
TSC1	-1522.03881	-1521.65134	-1522.34763
TSB1	-1522.03940	-1521.65797	-1522.34986
TSC2	-1522.13881	-1521.74382	-1522.44054
TSB2a	-1522.08662	-1521.69559	-1522.39000
TSB3	-1522.10800	-1521.71501	-1522.40894
TSB2b	-1830.50792	-1830.01877	-1830.89875

Table 6. Trimethylphosphinegold(I)-catalysed cyclotrimerisation intermediates and transition states in the triplet state, protodemetallation mechanisms, minor resting states or non-competitive alternatives. B3LYP-D3/6-31G(d)+SDD(Au); PCM (dichloromethane); HLT: B3LYP-D3/6-311+G(d,p)+SDD(Au)

Code	E / Hartree	G / Hartree	E_{HLT} / Hartree

A3-T	-1213.63719	-1213.35328	-1213.86006
TSA4-T	-1522.02958	-1521.64206	-1522.33318
A4-T	-1522.06663	-1521.67739	-1522.36954
TSA5b-T	-1522.04051	-1521.65081	-1522.34374
A5b-T	-1522.07095	-1521.67957	-1522.37429
A5b-S	-1522.05711	-1521.66370	-1522.35934
A4b	-1830.54122	-1830.04237	-1830.92719
TSE1	-1213.59838	-1213.31897	-1213.82953
E1	-1213.64513	-1213.35976	-1213.86867
TSE2	-1213.64141	-1213.35426	-1213.86396
E2	-1213.68431	-1213.39416	-1213.90594
D1	-1213.22059	-1212.94843	-1213.45400
D2	-1213.68311	-1213.39768	-1213.91061
D3	-1522.11918	-1521.72706	-1522.42287
D4	-1521.69095	-1521.31232	-1522.00392
D4iso	-1521.68711	-1521.30951	-1522.00118
D5	-1522.15651	-1521.76477	-1522.46453
D5iso	-1522.15210	-1521.76072	-1522.46095
TSD1	-1522.02901	-1521.64956	-1522.33911
TSD4	-1522.08828	-1521.70203	-1522.39729
TSA4iso	-1522.05647	-1521.66737	-1522.36207
A4iso	-1522.10290	-1521.70758	-1522.40787

Table 7. Metal-free starting materials and products: intermediates and transition states. B3LYP-D3/6-31G(d); PCM (dichloromethane); HLT: B3LYP-D3/6-311+G(d,p)

Code	E / Hartree	G / Hartree	E_{HLT} / Hartree
PhCCH	-308.39751	-308.31837	-308.48800
$PhCCH_2^+$	-308.80883	-308.71856	-308.88827
dimer	-616.86973	-616.68712	-617.03974
dienyne	-925.33667	-925.04941	-925.58742
trienyne	-1233.80406	-1233.40827	-1234.13526
A8	-925.32381	-925.03309	-925.56807
TSA7	-925.28000	-924.99001	-925.52559
A7	-925.44402	-925.14699	-925.68856

Table 8. Trimethyl phosphite gold(I)-catalysed cyclotrimerisation main intermediates and transition states. B3LYP-D3/6-31G(d)+SDD(Au); PCM (dichloromethane); HLT: B3LYP-D3/6-311+G(d,p)+SDD(Au)

Code	E / Hartree	G / Hartree	E_{HLT} / Hartree
L1A1	-1130.88726	-1130.69718	-1131.10298
L1A2	-1439.31107	-1439.01750	-1439.60497
L1A3	-1439.36508	-1439.06830	-1439.65448
L1A4	-1747.78988	-1747.38325	-1748.16204
L1A5exo	-1747.82372	-1747.41806	-1748.19419
L1A6	-1747.93245	-1747.52413	-1748.30362
L1A5endo	-1747.81722	-1747.41136	-1748.18783
L1C1	-1747.82728	-1747.42203	-1748.19774
L1B1	-1747.77391	-1747.37526	-1748.14779
L1B2a	-1747.82339	-1747.41865	-1748.19262
L1B2b	-2056.24440	-2055.73906	-2056.69868
L1TSA2	-1439.28350	-1438.99425	-1439.58242
L1TSA3	-1439.30281	-1439.00810	-1439.59533
L1TSA4	-1747.75821	-1747.35755	-1748.13083
L1TSA5exo	-1747.75209	-1747.35416	-1748.12633
L1TSA6exo	-1747.78588	-1747.38176	-1748.15626
L1TSA5endo	-1747.76710	-1747.36078	-1748.13777
L1TSA6endo	-1747.79851	-1747.39348	-1748.16875
L1TSC1	-1747.72210	-1747.32615	-1748.10026
L1TSB1	-1747.72190	-1747.32850	-1748.10158
L1TSC2	-1747.81885	-1747.41371	-1748.18956
L1TSB2a	-1747.76888	-1747.36858	-1748.14140
L1TSB3	-1747.79013	-1747.38598	-1748.15967
L1TSB2b	-2056.19103	-2055.69204	-2056.65122

Table 9. JohnPhos gold(I)-catalysed cyclotrimerisation intermediates and transition states. B3LYP-D3/6-31G(d)+SDD(Au); PCM (dichloromethane); HLT: B3LYP-D3/6-311+G(d,p)+SDD(Au)

Code	E / Hartree	G / Hartree	E_{HLT} / Hartree
L2A1	-1563.90952	-1563.44144	-1564.22672
L2A2	-1872.32934	-1871.75403	-1872.72451
L2A3	-1872.38374	-1871.80620	-1872.77474
L2A5exo	-2180.85315	-2180.16709	-2181.32428

L2C1	-2180.96386	-2180.27335	-2181.43559
L2TSA2	-1872.30160	-1871.73322	-1872.70169
L2TSA3	-1872.32296	-1871.74560	-1872.71684
L2TSA4	-2180.77438	-2180.09342	-2181.24806
L2TSA5exo	-2180.77154	-2180.09305	-2181.24714
L2TSC1	-2180.73885	-2180.06295	-2181.21907
L2TSB1	-2180.73862	-2180.06319	-2181.21938

Chapter III

Bimetallic Complexes: Design, Reactivity and Cooperativity

Introduction

Metal catalysis, which permeates the development of modern synthetic chemistry, had mainly focused on the development of well-defined monometallic species. However, in many cases, the intermediacy of higher-order clusters was later discovered or explored further as active species in well-known catalytic reactions, including palladium-catalysed cross couplings and click reactions.[1,2,3,4] Even in gold(I) catalysis, generally understood as simpler models with outer-sphere mechanisms, there is growing evidence that many reactions might require more than one catalyst unit.[5] Because of the many examples of *in situ* formation of active bimetallic catalysts and the dearth of rational approaches therein, the idea of harnessing metal reactivity through the design of polymetallic systems gained traction.[6]

With the rapid development of reactions that required metal co-catalysts, there was a surge in interest in the study of more complex bimetallic systems.[7] The applications of bimetallic complexes in the cooperative activation of small molecules and hydroformylation already proved the potential impact of bimetallic catalysis from an early stage.[8] Heterobimetallic complexes, incorporating two different metals, have sparked interest due to the potential of using the orthogonal electronic properties of two different elements and access novel reactivity.[6] The strategies devised for their syntheses are often tailored to specific systems,[9] generally seeking to limit the undesired homobimetallic complex formation.[10]

As one of the examples mentioned in **Chapter II** of this manuscript and, thus, showing the effects of non-trivial cooperativity between metal-centres, the 1,3,5-cyclotrimerisation of phenylacetylene can be carried out catalytically, but not substoichiometrically, with a bimetallic ruthenium-molybdenum

1 Appleby, K. M.; Dzotsi, E.; Scott, N. W. J.; Dexin, G.; Jeddi, N.; Whitwood, A. C.; Pridmore, N. E.; Hart, S.; Duckett, S. B.; Fairlamb, I. J. S. Bridging the Gap from Mononuclear Pd^{II} Precatalysts to Pd Nanoparticles: Identification of Intermediate Linear $[Pd_3(XPh_3)_4]^{2+}$ Clusters as Catalytic Species for Suzuki–Miyaura Couplings (X = P, As). *Organometallics* **2021**, *40*, 3560–3570.

2 Ye, J.; Gagliardi, L.; Cramer, C. J.; Truhlar, D. G. Single Ni Atoms and Ni_4 Clusters Have Similar Catalytic Activity for Ethylene Dimerization. *Journal of Catalysis* **2017**, *354*, 278–286.

3 Jeddi, N.; Scott, N. W. J.; Fairlamb, I. J. S. Well-Defined Pd_n Clusters for Cross-Coupling and Hydrogenation Catalysis: New Opportunities for Catalyst Design. *ACS Catal.* **2022**, *12*, 11615–11638.

4 Jin, L.; Tolentino, D. R.; Melaimi, M.; Bertrand, G. Isolation of Bis(Copper) Key Intermediates in Cu-Catalyzed Azide-Alkyne "Click Reaction." *Sci. Adv.* **2015**, *1*, e1500304.

5 Ramos, M.; Poater, J.; Villegas-Escobar, N.; Gimferrer, M.; Toro-Labbé, A.; Cavallo, L.; Poater, A. Phenoxylation of Alkynes through Mono- and Dual Activation Using Group 11 (Cu, Ag, Au) Catalysts. *Eur. J. Inorg. Chem.* **2020**, 1123–1134.

6 Campos, J. Bimetallic Cooperation across the Periodic Table. *Nat. Rev. Chem.* **2020**, *4*, 696–702.

7 Pye, D. R.; Mankad, N. P. Bimetallic Catalysis for C–C and C–X Coupling Reactions. *Chem. Sci.* **2017**, *8*, 1705–1718.

8 Van Den Beuken, E. K.; Feringa, B. L. Bimetallic Catalysis by Late Transition Metal Complexes. *Tetrahedron* **1998**, *54*, 12985–13011.

9 Ostapowicz, T. G.; Fryzuk, M. D. Anionic Tantalum Dihydride Complexes: Heterobimetallic Coupling Reactions and Reactivity toward Small-Molecule Activation. *Inorg. Chem.* **2015**, *54*, 2357–2366.

10 Lewis, D. J.; Glover, P. B.; Solomons, M. C.; Pikramenou, Z. Purely Heterometallic Lanthanide(III) Macrocycles through Controlled Assembly of Disulfide Bonds for Dual Color Emission. *J. Am. Chem. Soc.* **2011**, *133*, 1033–1043.

catalyst.[11] Beyond its synthetic applicability, the formation of the rarer regioisomer stems from the combined activity of both metals.

In spite of this, heterobimetallic catalysts often show only trivial differences (those from minor steric and electronic effects), such as in the analogous alkyne cyclotrimerisation catalysed by a gold-nickel complex.[12] In this example, the cyclotrimerisation is mediated by nickel and results in identical selectivity patterns to those observed with monometallic complexes, as well as neither increasing nor decreasing its activity.

Although aurophilic interactions have been used to facilitate the formation of homo- and heterometallic complexes, or small clusters, these have mainly been explored photophysically.[13],[14] However, there are examples of catalysis with small gold clusters that display reactivity in the same line as gold(I) complexes.[15,16] The changes in reactivity were found to be relatively minor with respect to the parent monometallic complexes and cooperativity as such for these systems was, at best, residual. Moreover, although aurophilicity showed potential in the construction of small catalytically active clusters, the rational design and modification of such systems is somewhat limited.

Perhaps one of the key developments in gold(I) bimetallic cooperativity is that reported by Blum and coworkers.[17] In their work, a gold(I) triflate catalyses the cyclisation of an allenyl or alkynylcarboxylate allyl ester **3.1**. Deallylation of the cationic intermediate with a palladium catalyst, and subsequent Tsuji-Trost-like reactivity, with the vinylgold species **3.3** as a nucleophile, affords product **3.4** (Scheme 1). The generation of a stronger allyl electrophile upon cyclisation, which enables the vinylgold to function as a nucleophile, allows the reaction to proceed. In the absence of gold(I) catalyst, no product formation was observed.

11 Adams, R. D.; Babin, J. E.; Tasi, M. The nature of alkyne oligomerization on the face of a mixed-metal trinuclear cluster. *Organometallics* **1987**, *6*, 2247–2248.

12 Cluff, K. J.; Bhuvanesh, N.; Blümel, J. Monometallic Ni^0 and Heterobimetallic Ni^0/Au^I Complexes of Tripodal Phosphine Ligands: Characterization in Solution and in the Solid State and Catalysis. *Chem. Eur. J.* **2015**, *21*, 10138–10148.

13 Catalano, V. J.; Moore, A. L. Mono-, Di-, and Trinuclear Luminescent Silver(I) and Gold(I) N-Heterocyclic Carbene Complexes Derived from the Picolyl-Substituted Methylimidazolium Salt: 1-Methyl-3-(2-Pyridinylmethyl)-1H-Imidazolium Tetrafluoroborate. *Inorg. Chem.* **2005**, *44*, 6558–6566.

14 Kaub, C.; Lebedkin, S.; Bestgen, S.; Köppe, R.; Kappes, M. M.; Roesky, P. W. Defined Tetranuclear Coinage Metal Chains. *Chem. Commun.* **2017**, *53*, 9578–9581.

15 Smirnova, E. S.; Echavarren, A. M. A Hexanuclear Gold Cluster Supported by Three-Center-Two-Electron Bonds and Aurophilic Interactions. *Angew. Chem. Int. Ed.* **2013**, *52*, 9023–9026.

16 Pei, X.; Pereira, A.; Smirnova, E. S.; Echavarren, A. M. Small Gold(I) and Gold(I)–Silver(I) Clusters by C−Si Auration. *Chem. Eur. J.* **2020**, *26*, 7309–7313.

17 Shi, Y.; Roth, K. E.; Ramgren, S. D.; Blum, S. A. Catalyzed Catalysis Using Carbophilic Lewis Acidic Gold and Lewis Basic Palladium: Synthesis of Substituted Butenolides and Isocoumarins. *J. Am. Chem. Soc.* **2009**, *131*, 18022–18023.

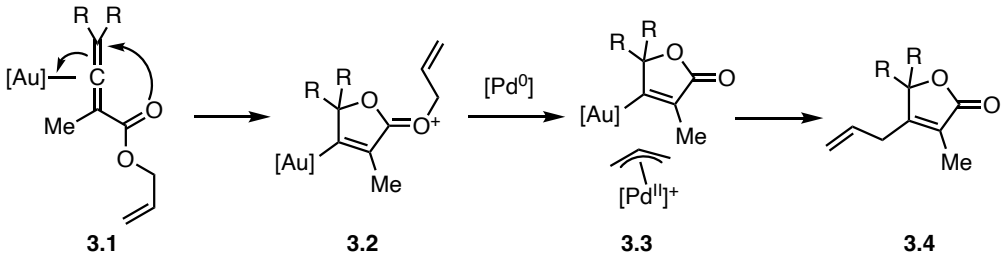

Scheme 1. Butenolide synthesis through cooperative gold–palladium catalysis.

Well-defined homogeneous heterobimetallic catalysts containing gold have been reported, including metalloligand-type metal-metal bonded species and purported cooperative redox chemistry.[18][19],[20] Their reactivity, while comparatively underdeveloped when viewed alongside the richer heterometallic chemistry of other metals (such as ruthenium, palladium or rhodium), has been explored and unique catalytic transformations attainable with such bimetallic systems has been attributed to the metal-metal cooperativity. For example, heterobimetallic complexes with gold have been found to be bridged by a dinitrogen molecule, showcasing the possibilities in frustrated Lewis pair-like activation.[21] Other small-molecule activations are also known, such as the activation of dihydrogen with a gold-platinum complex, with theoretical studies supporting the cooperativity between both metals.[22] These examples reveal how gold(I) centres can take part in reactivity not usually associated with this metal.

The performance of bridged bimetallic gold(I) complexes has been assessed in a range of classic catalytic organometallic transformations. In the field of alkene isomerisations, cationic $[(Ph_3P)_3Ru(CO)H_2AuPPh_3](PF_6)$ **3.7** –allegedly containing two bridging hydride ligands– outperformed monometallic ruthenium precursor **3.8** in the isomerisation of 1-pentene to 2-pentene. However, most remarkably, the selectivity switched to the *E*-alkene when the bimetallic complex was used.[23] It is worth noting that true full three-centre two-electron bonds in hydride-bridged heterobimetallic complexes with two hydride bonds to gold(I) have been described since, but both bonds tend to be fully equivalent.[24]

18 Hanusch, F.; Munz, D.; Sutter, J.; Meyer, K.; Inoue, S. A Zwitterionic Heterobimetallic Gold–Iron Complex Supported by Bis(*N*-Heterocyclic Imine)Silyliumylidene. *Angew Chem Int Ed* **2021**, *60*, 23274–23280.

19 Buchwalter, P.; Rosé, J.; Braunstein, P. Multimetallic Catalysis Based on Heterometallic Complexes and Clusters. *Chem. Rev.* **2015**, *115*, 28–126.

20 McNair, R. J.; Nilsson, P. V.; Pignolet, L. H. Synthesis and x-ray structural characterization of a bimetallic rhodium-gold complex with bridging 2-[bis(diphenylphosphino)methyl]pyridine (PNP) ligands. *Inorg. Chem.* **1985**, *24*, 1935–1939.

21 Specklin, D.; Coffinet, A.; Vendier, L.; Del Rosal, I.; Dinoi, C.; Simonneau, A. Synthesis, Characterization, and Comparative Theoretical Investigation of Dinitrogen-Bridged Group 6-Gold Heterobimetallic Complexes. *Inorg. Chem.* **2021**, *60*, 5545–5562.

22 Zhang, L.; Hu, S.; Yang, L.; Li, W.; Li, S.; Wang, W.; Zeng, G. H_2 Activation by Heterobimetallic Gold(I)/Platinum(0) Complex: Theoretical Understanding of Electronic Processes and Prediction on More Active Species. *J. Phys. Chem. C* **2020**, *124*, 4525–4533.

23 Gomez-Sal, M. P.; Gannon, P. R.; Blaine, C. A.; Boyle, P. D.; Mueting, A. M.; Pignolet, L. H. Heterobimetallic Au-Os and Au-Ru Hydrido Complexes. X-Ray Crystal and Molecular Structures of $[Au_2Os(H)_3(PPh_3)_5]PF_6$ and $[AuRu(H)_2(CO)(PPh_3)_4]PF_6$. *Inorg. Chem.* **1988**, *27*, 3301–3308.

24 Rocchigiani, L.; Klooster, W. T.; Coles, S. J.; Hughes, D. L.; Hrobárik, P.; Bochmann, M. Hydride Transfer to Gold: Yes or No? Exploring the Unexpected Versatility of Au···H−M Bonding in Heterobimetallic Dihydrides. *Chem. Eur. J.* **2020**, *26*, 8267–8280.

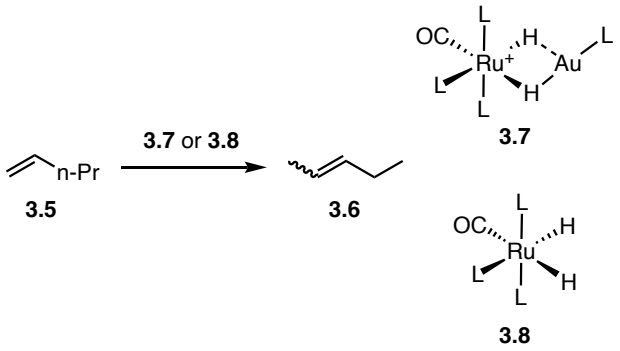

Scheme 2. Alkene isomerisation with a heterobimetallic catalyst. **3.7** favoured ***E*-3.6** but relative ratios were not reported.

Heterobimetallic gold-copper complexes with a bridging hydride were also characterised and found to be remarkably selective catalysts in the reaction of carbon dioxide with pinacolborane (Scheme 3).[25] Even though this catalyst is reported to be inferior to most other known transition metal catalysts for this transformation, the monometallic copper(I) nor gold(I) complexes are less active catalysts in this reaction and are much less selective, confirming their cooperativity.

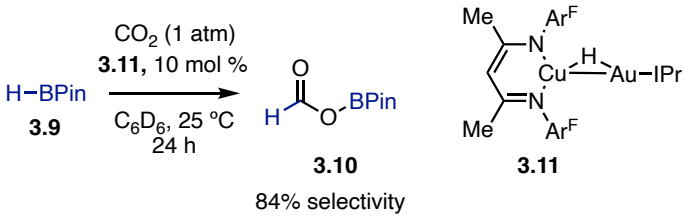

Scheme 3. Hydroboration of carbon dioxide catalysed by a gold(I)-copper(I) bimetallic complex.

Homotrimetallic gold complexes have been found to be photoactive by themselves, catalysing the aminoalkylation or carboarylation of alkenes.[26] Mechanistically, this reaction is very different to most gold(I) catalysis involving halogen atom transfer to the photoexcited gold cluster. Hence, the subsequent cluster chemistry bridging classical homogeneous catalysis and nanoparticles, thus exhibiting other kinds of reactivity.

Most metal cooperativity is observed in metal-metal bonded systems, or clusters, as well as metals joined by non-innocent bridging ligands. However, this is by no means the exclusive manner in which a bimetallic system can exhibit such synergistic effects. The design of ditopic ligand platforms to harness the reactivity of the daughter systems has been a main focus of research, especially due to the

25 Hicken, A.; White, A. J. P.; Crimmin, M. R. Selective Reduction of CO_2 to a Formate Equivalent with Heterobimetallic Gold- - -Copper Hydride Complexes. *Angew. Chem. Int. Ed.* **2017**, *56*, 15127–15130.

26 Fang, Q.; Han, J.; Qin, M.; Li, W.; Zhu, C.; Xie, J. Trinuclear Gold-Catalyzed 1,2-Difunctionalization of Alkenes. *Angew. Chem. Int. Ed.* **2023**, *62*, e202305121.

easier access to a much wider range of well-defined bimetallic complexes through simpler coordination chemistry in a more predictable manner.[27]

Photoredox chemistry has been one of the areas in which spatially separated cooperating bimetallic complexes have been sought. Duhme-Klair and coworkers tethered a bis(pyridine)phenanthroline ruthenium(II) photoactivator to a thiosemicarbazone complex of molybdenum(VI). Photoactivation of this complex allowed the two-electron transfer in the oxygen atom transfer to triphenylphosphine (Scheme 4).[28] The rapid electron transfer is proposed to prevent comproportionating catalyst deactivation that is present in intermolecular systems.

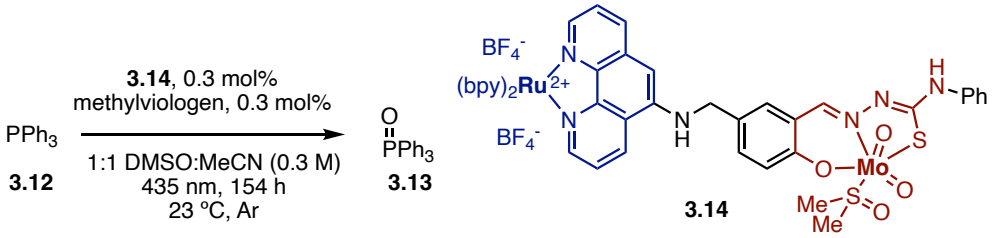

Scheme 4. Photocatalysed oxygen atom transfer to triphenylphosphine.

The same conceptual approach was used in photoredox gold(I) catalysis using a photoactive ruthenium(II) centre and a tethered gold(I) complex with a paracyclophane backbone.[29] The bimetallic complex was found to catalyse the arylative Meyer-Schuster rearrangement of arylpropargyl alcohols (Scheme 5), which had been reported previously for intermolecular co-catalysis.[30] Unfortunately, the yields were somewhat lower than those obtained with the intermolecular combination of two monometallic catalysts, indicating that photoredox chemistry with gold might not be aided by tethered bimetallic arrangements.

27 Gatus, M. R. D.; Bhadbhade, M.; Messerle, B. A. Highly Versatile Heteroditopic Ligand Scaffolds for Accommodating Group 8, 9 & 11 Heterobimetallic Complexes. *Dalton Trans.* **2017**, *46*, 14406–14419.

28 Ducrot, A. B.; Coulson, B. A.; Perutz, R. N.; Duhme-Klair, A.-K. Light-Induced Activation of a Molybdenum Oxotransferase Model within a Ru(II)–Mo(VI) Dyad. *Inorg. Chem.* **2016**, *55*, 12583–12594.

29 Knoll, D. M.; Zippel, C.; Hassan, Z.; Nieger, M.; Weis, P.; Kappes, M. M.; Bräse, S. A Highly Stable, Au/Ru Heterobimetallic Photoredox Catalyst with a [2.2]Paracyclophane Backbone. *Dalton Trans.* **2019**, *48*, 17704–17708.

30 Tlahuext-Aca, A.; Hopkinson, M. N.; Garza-Sanchez, R. A.; Glorius, F. Alkyne Difunctionalization by Dual Gold/Photoredox Catalysis. *Chem. Eur. J.* **2016**, *22*, 5909–5913.

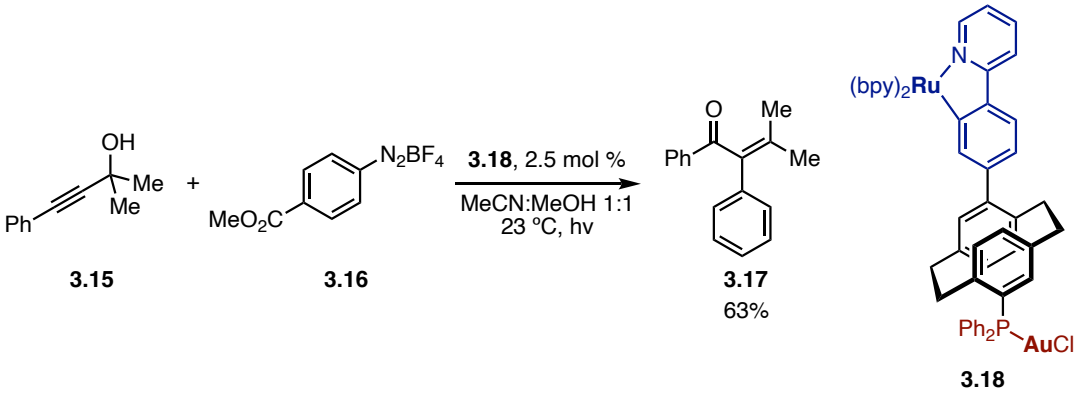

Scheme 5. Arylative Meyer-Schuster rearrangement of propargyl alcohols catalysed by a heterobimetallic AuRu complex.

One similar tethered ligand design in gold catalysis for use in photoredox was described in 2022.[31] The prototypical photoactivation of diazonium salts, trapped by the gold(I) centre, was set to react further with diethyl phosphite to form arylphosphonates (Scheme 6). The authors claim that these gold-ruthenium complexes outperformed the intermolecular analogues; however, the catalyst loading (at 10 mol %) was significantly higher than all literature reports with intermolecular gold(I) ruthenium photoredox chemistry. Interestingly, in any case, the best catalyst was not the one with the shorter Au-Ru distance.

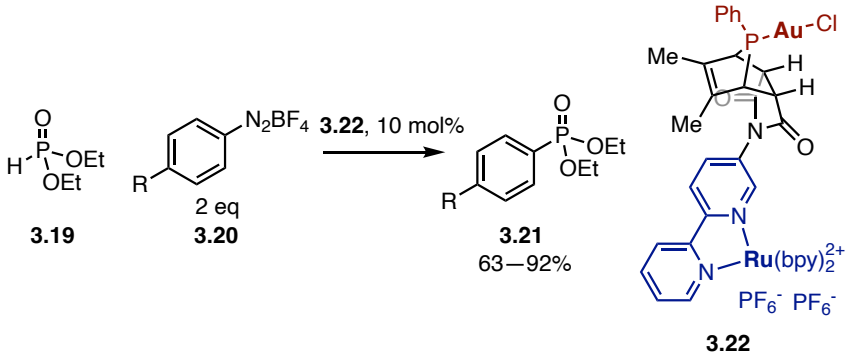

Scheme 6. Photoredox-mediated preparation of arylphosphonates with a heterobimetallic [AuRu] complex.

Other tethered gold(I)-containing heterobimetallic catalysts have been studied. Among them, [AuIr] **3.25** was found to lead to the selective formation of benzylanilines from nitrobenzene and benzyl alcohol (Scheme 7).[32] Using combinations of monometallic rhodium or iridium and gold complexes in the same reaction led to lower yield and selectivity towards the diphenylimine product. Such a shift in

31 Bayer, L.; Birenheide, B. S.; Krämer, F.; Lebedkin, S.; Breher, F. Heterobimetallic Gold/Ruthenium Complexes Synthesized via Post-functionalization and Applied in Dual Photoredox Gold Catalysis. *Chem. Eur. J.* **2022**, *28*, e202201856.

32 Böhmer, M.; Kampert, F.; Tan, T. T. Y.; Guisado-Barrios, G.; Peris, E.; Hahn, F. E. Ir^{III}/Au^{I} and Rh^{III}/Au^{I} Heterobimetallic Complexes as Catalysts for the Coupling of Nitrobenzene and Benzylic Alcohol. *Organometallics* **2018**, *37*, 4092–4099.

selectivity towards what probably resulted from ulterior transfer hydrogenation was suggested to originate from the different electronic environment in the bimetallic complex. The catalyst loading could also be lowered further, down to 0.1 mol %, when the heterobimetallic complex was used.

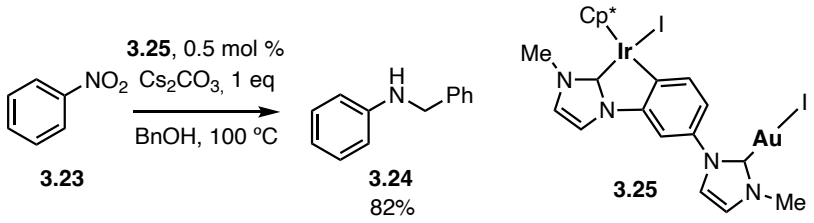

Scheme 7. Reductive benzylation of nitrobenzene to benzylaniline catalysed by a gold-iridium heterobimetallic complex.

What can be seen in most of these designs is that proximity between the two metal centres usually results in less widely-applicable protocols to synthesise these complexes. Conversely, when modular syntheses of bimetallic complexes are proposed, these often place the metals too far apart to leverage their chemistry in cooperative catalysis (with the exception of photocatalysis, as discussed earlier). Hashmi and co-workers' recent report on the preparation of gold-palladium bimetallic complexes[33] result in long distances between the two metal atoms (**3.26**) and, moreover, the ligand tethers are flexible enough to freely rotate the metals away from each other. This severely limits the practicality of such systems in cooperative catalysis when compared to the usage of two independent monometallic complexes. A similar situation arises with the gold palladium complexes prepared by the group of Huynh (**3.27**).[34]

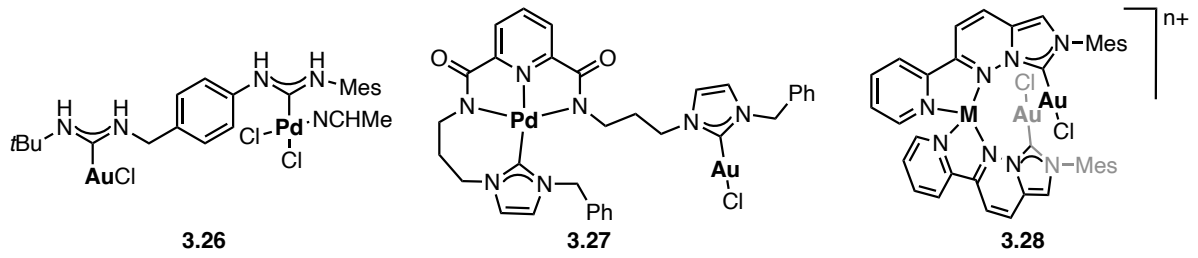

Figure 1. Example of [AuPd] complexes reported by Hashmi or Huynh and coworkers, and bimetallic complexes with a tighter arrangement reported by Sawamura and coworkers.

There has been recent progress in tailoring ditopic ligands to address the issue of proximity between the metal centres in gold chemistry. In spite of this, the systems have only rarely been applied in catalysis. The problems are related to the dicoordinated nature of gold(I) and, most importantly, the need for one of the two coordination sites to bind a substrate. For this reason, while multidentate ligands

33 Dietl, M. C.; Vethacke, V.; Keshavarzi, A.; Mulks, F. F.; Rominger, F.; Rudolph, M.; Mkhalid, I. A. I.; Hashmi, A. S. K. Synthesis of Heterobimetallic Gold(I) Palladium(II) Bis(Acyclic Diaminocarbene) Complexes via the Isonitrile Route. *Organometallics* **2022**, *41*, 802–810.

34 Teng, Q.; Huynh, H. V. (Hetero)Bimetallic and Tetranuclear Complexes of Pincer-Bridged N-Heterocyclic Carbene Ligands. *Organometallics* **2018**, *37*, 4119–4127.

have been used successfully with other metals, they have limited applications with gold(I) unless a ligand is hemilabile. Scaffold that are otherwise highly effective in placing the metal atoms in close proximity, such as Iwamoto and Ishii's tetrapyridyl ligand,[35] coordinatively saturate gold(I) and limit their catalytic applications.

One such example is the NHC-bipyridine ligand designed as a scaffold for gold(I)-zinc(II) cooperative catalysis.[36] While the bimetallic complexes were generated *in situ* and, thus, were not characterised,[37] Sawamura and coworkers showed that both metals were required to form the product. Attempting to run the reaction with two monometallic catalysts, by using a JohnPhosAuCl with addition of 2 mol% of 2,2'-bipyridine as a ligand for the zinc acetylacetonate only resulted in traces of the products. The unoptimised conditions with the heterobimetallic system yielded **3.31** in 75% yield, increasing to 98% after optimisation. This would constitute one of the first cases in which ligand platform preorganisation is required to achieve bimetallic catalysis with gold(I). This is very peculiar, as the almost identical addition of phenols to diphenylacetylene performed well with two separate monometallic catalysts (gold and copper, in this case).[38]

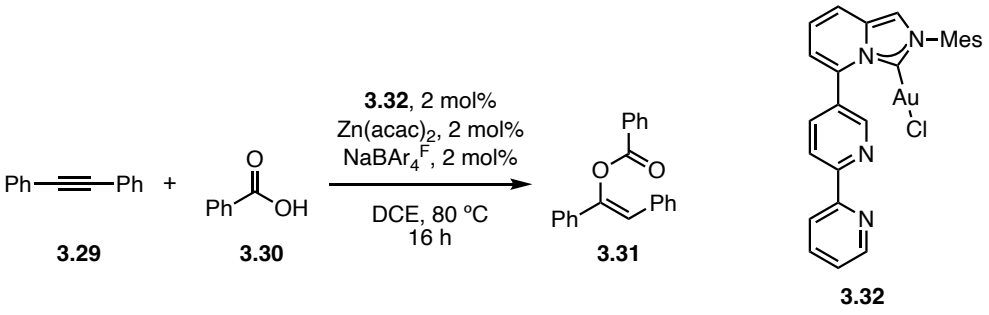

Scheme 8. Example of the [AuZn] complex catalysed addition of carboxylic acids to alkynes.

Another NHC-NN ditopic ligand framework was very recently studied as a platform to prepare a variety of gold(I)-3d metal complexes.[39] Unlike a previous report of luminescent NHC-bipyridine complexes,[40] these new designs would not be as flexible and the two metal centres are placed closer together. The Au_2M derived from the ditopic ligand (**3.28**, Figure 1) was suggested to have Au-M interactions due to the short contacts in the crystal structure, the QTAIM analysis indicating the presence of a bond critical point and IGMH methods. However, while the short distances obtained to the gold(I) nucleus are

35 Iwamoto, T.; Sotome, Y.; Ishii, Y. Binuclear Complexes Supported by a Tetrapyridyl Ligand with a Bending Anthraquinodimethane Linker. *ACS Org. Inorg. Au* **2023**, *3*, 305–311.

36 Rawat, V. K.; Higashida, K.; Sawamura, M. Construction of Heterobimetallic Catalytic Scaffold with a Carbene-Bipyridine Ligand: Gold–Zinc Two-Metal Catalysis for Intermolecular Addition of *O* -Nucleophiles to Nonactivated Alkynes. *ACS Catal.* **2022**, *12*, 8325–8330.

37 A model with zinc dichloride was crystallised instead.

38 Lazreg, F.; Guidone, S.; Gómez-Herrera, A.; Nahra, F.; Cazin, C. S. J. Hydrophenoxylation of Internal Alkynes Catalysed with a Heterobimetallic Cu-NHC/Au-NHC System. *Dalton Trans.* **2017**, *46*, 2439–2444.

39 Kitabayashi, A.; Ono, Y.; Taketsugu, T.; Sawamura, M.; Higashida, K. Dimetal-Binding Scaffold 2-(Pyridin-2-yl)Imidazo [1,5- *b*]Pyridazine-7-ylidene: Synthesis of Trinuclear Heterobimetallic Complexes Involving Gold-Metal Interactions. *Chem. Eur. J.* **2023**, e202301673.

40 Kaub, C.; Lebedkin, S.; Li, A.; Kruppa, S. V.; Strebert, P. H.; Kappes, M. M.; Riehn, C.; Roesky, P. W. Bimetallic d^{10}-Metal Complexes of a Bipyridine Substituted N-Heterocyclic Carbene. *Chem. Eur. J.* **2018**, *24*, 6094–6104.

interesting in their own right, steric influences can be responsible for the observed distortions. Similarly, using QTAIM as the sole method to determine bonding interactions can be problematic.[41,42] Notwithstanding the specific nature of the close contact between the metals, the proximity of such an interaction is likely to affect the coordination chemistry and catalytic performance of the gold(I) centres.

Toste and co-workers reported a bimetallic effect in the reductive elimination of homobimetallic digold complexes, not necessarily involving mixed gold(I)–gold(III) systems.[43] These bimetallic complexes, tethered by the bis(diphenylphosphino)methane ligand or a close analogue, were able to undergo reductive elimination several orders of magnitude faster than other gold(III) complexes. The cooperative reaction proceeded through the intermediacy of gold-gold bonded dimers that underwent more facile reductive elimination to the parent gold(I)–gold(I) complex (Scheme 9).

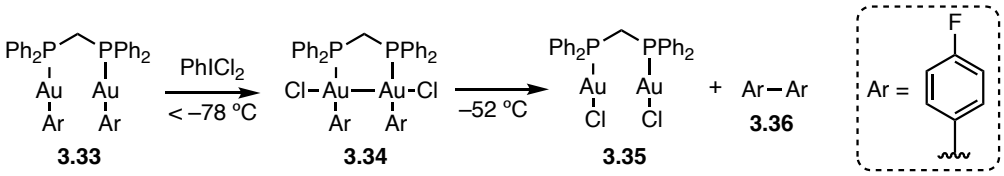

Scheme 9. Bimetallic reductive elimination from a digold complex was much faster than from monometallic gold complexes.

Finally, the application of bimetallic catalysis to induce enantioselectivity is a developing field in gold chemistry.[44] One of the main ways in which these lines have shown better results than monometallic gold(I) systems is the formation of chiral nucleophiles by coordination to the second metal, overcoming the widespread problem with outer-sphere attack in gold(I) catalysis.[45,46]

Despite the various advances in this respect, there are to the best of our knowledge no examples in which chiral gold heterobimetallic complexes act with both metals cooperatively to induce enantioselectivity. Preorganisation in such complexes strictly limits the number of possible conformations, a commonly sought-after feature in enantioselective catalyst design. Given the increasing number of reactions known for heterobimetallic complexes with gold, it is expected that these new approaches to enantioselectivity will be studied in the near future.

41 Foroutan-Nejad, C.; Shahbazian, S.; Marek, R. Toward a Consistent Interpretation of the QTAIM: Tortuous Link between Chemical Bonds, Interactions, and Bond/Line Paths. *Chem. Eur. J.* **2014**, *20*, 10140–10152.
42 Wick, C. R.; Clark, T. On Bond-Critical Points in QTAIM and Weak Interactions. *J. Mol. Model.* **2018**, *24*, 142.
43 Wolf, W. J.; Winston, M. S.; Toste, F. D. Exceptionally Fast Carbon–Carbon Bond Reductive Elimination from Gold(III). *Nat. Chem.* **2014**, *6*, 159–164.
44 Ambegave, S. B.; Shubham; More, T. R.; Patil, N. T. Gold-Based Enantioselective Bimetallic Catalysis. *Chem. Commun.* **2023**, *59*, 8007–8016.
45 Ge, S.; Zhang, Y.; Tan, Z.; Li, D.; Dong, S.; Liu, X.; Feng, X. Bimetallic Catalytic Tandem Reaction of Acyclic Enynones: Enantioselective Access to Tetrahydrobenzofuran Derivatives. *Org. Lett.* **2020**, *22*, 3551–3556.
46 Hu, X.; Tang, X.; Zhang, X.; Lin, L.; Feng, X. Catalytic asymmetric Nakamura reaction by gold(I)/chiral N,N′-dioxide-indium(III) or nickel(II) synergistic catalysis. *Nat. Commun.* **2021**, *12*, 3012.

Objectives

The design of a scaffold to support a range of bimetallic complexes, ideally placing a second metal in the vicinity of a gold(I) centre, is a question worth addressing. As explained in the introduction, most designs tend to require a trade-off between atomic proximity and applicability of the synthetic protocol to different metals. Having such an easily accessible ligand platform would allow the determination of intramolecular cooperativity effects and explore the non-trivial effects on their reactivity or coordination chemistry.

For these reasons, the objective of the project presented in this chapter was to access a well-defined system, to prove its value as a versatile tool to access a variety of bimetallic complexes and explore their reactivity. By achieving these results, we would seek to investigate the influence of bimetallic effects in gold complexes.

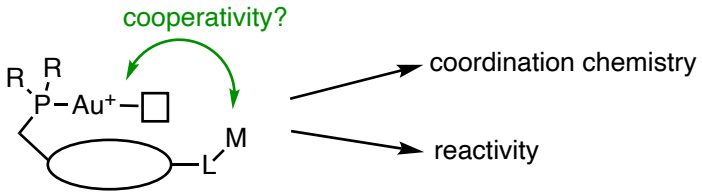

Figure 2. Proposed model for the design of bimetallic complexes.

We also intended to prepare the first gold(I)-gold(III) homobimetallic complexes with potential applications in catalysis, as well as to study the effects of its reactivity both experimentally and *in silico*. In particular, we wanted to explore whether non-trivial cooperativity can be observed (in which both metals are required to be in the same complex) and how this would compare to other d^8 metal complexes.

Results and Discussion

Synthesis of Bimetallic Complexes

We oriented the design of the ligand to a ditopic scaffold with the following properties: initial selective coordination of gold(I) to one site, known catalytic activity of analogous monometallic gold complexes, and a chelating second site that is able to coordinate a wide range of metals.

In order to fulfil the two first requirements, a phosphine ligand was chosen for ligation to gold(I). Together with NHC complexes, phosphine complexes of gold have been explored in catalysis for various transformations, including those presented in other chapters of this manuscript. Furthermore, the affinity of gold(I) towards soft coordination sites such as that offered by a phosphine were considered a promising option to avoid poor selectivity in the coordination of this metal. A NN bidentate moiety was chosen for the intermediate softness of nitrogen, the likely reversible coordination to gold(I) and the abundance of examples with similar scaffolds. Among these, the iminopyridine and bipyridine fragments were chosen for our ligand design.

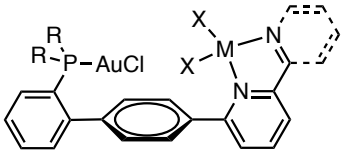

Figure 3. Ditopic PNN ligand design with a divalent metal on the second coordination site.

The design also drew ideas from previous ligand designs in gold(I) enantioselective catalysis in which the interaction of the substrate with the ligand generally happened *trans* to the phosphine ligand. Intending a similar geometric arrangement for cooperativity and proximity to the coordinated substrate, a *para*-substituted JohnPhos scaffold was chosen as the basis for the ligand framework. The bulky groups and biphenyl platform stabilise the gold(I) centre, as is generally seen in known gold(I) complexes; additionally, the bipyridine fragment ensures ligation of a second metal enhanced by the chelate effect.

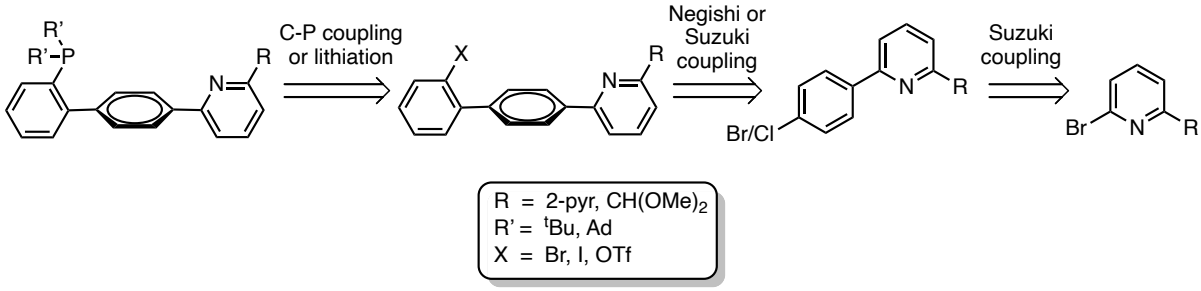

Scheme 10. General retrosynthetic analysis for phosphine–bipyridine and phosphine–iminopyridine scaffolds.

The ligand design was also considered in terms of the ease of synthesis, as an easily scalable synthesis would ensure that the quantity of precursor complexes would not become a bottleneck in any subsequent experiments. The synthesis would involve sequential palladium-catalysed cross-couplings; selectivity would be achieved by making use of different halogen substituents or a phenol that could later be triflated.

The initial target ligand was the iminopyridine variant. We first considered this design due to its redox non-innocence and more modular preparation. Usage of a chloro substituent completely stopped further couplings, whereas mixtures favouring the double-Suzuki product were obtained when 4-bromophenylboronic acid was used as a coupling partner in spite of the limiting stoichiometry. Even though the couplings gave an excellent yield, in the case of **3.38** with chlorophenyl, or worked reasonably well, for **3.39** with bromophenyl, the ulterior lithiation was not achieved under various conditions.

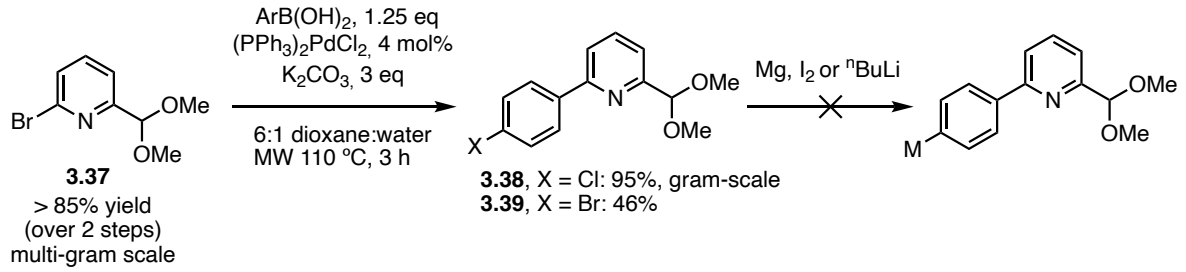

Scheme 11. Synthetic approach and attempted metal-halogen exchanges.

For this reason, we decided to pursue an alternative method by coupling the aryl chloride to a 2-hydroxyphenylboronic acid. As the aryl chloride made the second Suzuki coupling more challenging, using SPhos as a Buchwald phosphine suitable for the activation of C-Cl bonds showed better results (Scheme 12).

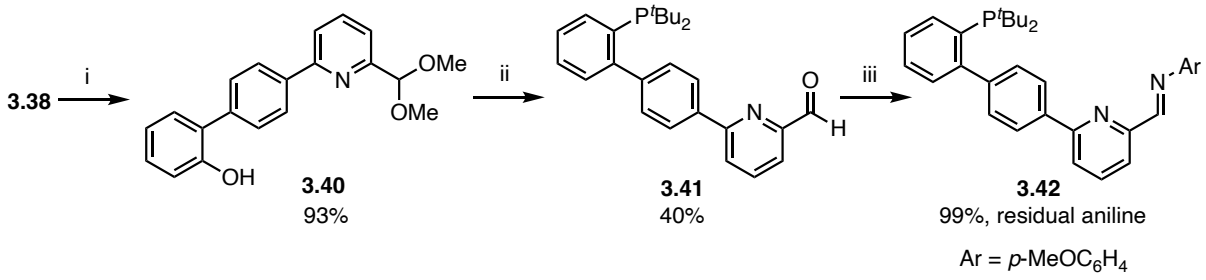

Scheme 12. Formation of phosphine–iminopyridine ligand. i. 2-hydroxyphenylboronic acid (1.4 eq), $PdCl_2$ (4 mol%), SPhos (8 mol%), K_2CO_3 (3 eq), 6:1 dioxane:H_2O (0.1 M), MW 90 ºC, 3 h; ii. $PhNTf_2$ (1.1 eq), K_2CO_3 (3 eq), dioxane (0.2 M), MW 120 ºC, 75 min; then NaO^tBu (1.2 eq), $Pd(OAc)_2$ (5 mol%), dppf (6 mol%), $^tBu_2PH$ (1.3 eq), MW 150 ºC, 4 h; then HCl (aq), 55 ºC, 3.5 h; iii. *p*-methoxyaniline (1.05 eq), 23 ºC, 24 h.

After formation of phenol **3.40**, a three-step one-pot sequence was devised to form the phosphine–aldehyde precursor to the iminopyridine. Triflation, phosphine coupling and hydrolysis afforded **3.41** and worked reasonably well with no intermediate purification (Scheme 12). The iminopyridine was formed by condensation of 4-methoxyaniline; however, the product was too unstable on silica or neutral alumina so the reaction could not be monitored easily by TLC nor purified by chromatography. Sublimation of residual aniline yielded relatively pure ligand **3.42** with some detectable aniline. Unfortunately, coordination of gold(I) formed some metallic gold –perhaps due to residual aniline– and the monometallic complex could not be obtained in pure form. No further purification could be carried out due to crystallisation problems or stability towards hydrolysis.

Because of these issues, we changed our design to a phosphine–bipyridine ligand as this should be significantly more robust and allow purification at all stages, with the only drawback being a less modular retrosynthetic approach.

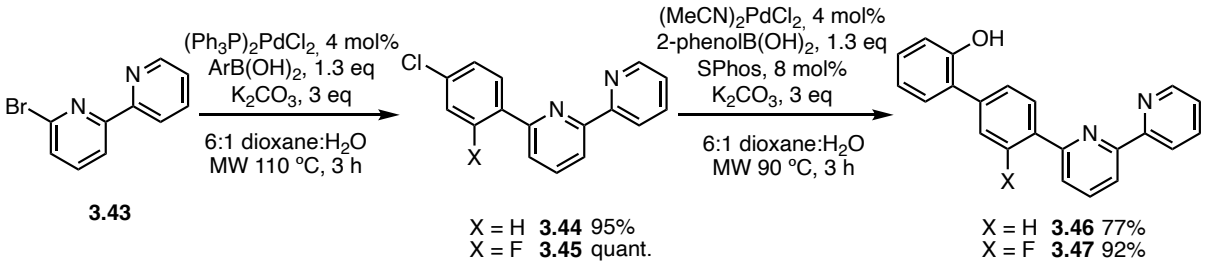

Scheme 13. Optimised synthesis of the phenol precursors to phosphine–bipyridine ligands.

Initially, starting with a bipyridine fragment, we installed a *para*-chlorophenyl group in excellent yield (Scheme 13). In an attempt to use SPhos in the same manner as in the iminopyridine synthesis, the first trials gave promising results but scaling up and subsequent repeats only gave low to moderate yields. Erratic yields were ascribed to the formation of inactive bipyridine palladium complexes. Attempts to use zinc salt additives to saturate the bipyridine coordination sites were unsuccessful, with an HTE optimisation suggesting that SPhos and RuPhos were optimal (Table 1). However, preforming the palladium complex before addition of the starting material afforded **3.46** and **3.47** in good to excellent yields.

Fluorinated analogues were also prepared with the intention of following speciation in later coordination studies by ^{19}F NMR. Under the same conditions, the Suzuki couplings gave excellent yields even higher than those with the non-fluorinated substrates.

Table 1. High-throughput experimentation results for Suzuki coupling to **3.44**. UV yields of **3.46** referenced to internal standard (biphenyl), uncorrected. Dioxane (0.2 M), 90 ºC, 4.5 h. [Pd], 4 mol%; **L**, 8 mol%; base, 2 eq; zinc salt, 1 eq.

		$(MeCN)_2PdCl_2$				$Pd(OAc)_2$			
		K_2CO_3	K_3PO_4	NaOAc	Et_3N	K_2CO_3	K_3PO_4	NaOAc	Et_3N
-[a]	**L1**[b]	80.3	70.1	39.5	15.0	73.7	63.6	41.4	21.5
	L2[b]	27.5	9.8	1.0	6.9	8.7	6.2	2.1	4.8
	L3[b]	80.8	66.8	31.2	4.5	75.7	66.4	39.2	13.7
	L4[b]	45.0	23.8	2.7	2.4	16.9	19.3	2.8	4.6
$ZnBr_2$	**L1**	4.3	3.2	0.1	0.1	3.4	2.2	0.2	0.2
	L2	1.7	0.0	0.0	0.3	0.0	0.0	0.0	0.2
	L3	0.5	0.2	0.1	0.1	0.4	0.3	0.5	0.0
	L4	3.6	2.0	0.0	1.6	3.0	0.8	0.1	1.2
$Zn(OTf)_2$	**L1**	0.0	0.2	0.5	1.2	0.0	0.3	1.7	0.8
	L2	0.0	0.0	0.0	0.2	0.0	0.0	0.0	0.1
	L3	0.0	0.0	0.6	0.5	0.0	0.2	1.4	0.5
	L4	1.0	1.1	0.4	0.2	0.0	0.1	0.0	0.0

[a] No additive added. [b] $\mathbf{L_1}$: SPhos, $\mathbf{L_2}$: ^{t}BuXPhos, $\mathbf{L_3}$: RuPhos, $\mathbf{L_4}$: ^{t}BuDavePhos.

Finally, triflation of the phenol generated a suitable partner for phosphine coupling to either di-*tert*-butyl or diadamantylphosphine, yielding **3.49** and **3.50** (Scheme 14). This transformation was run in dioxane with the intention of running the phosphine coupling in a one-pot procedure. In fact, when the intermediate triflate product was purified before phosphine coupling, similar yields were obtained. Both di-*tert*-butyl and diadamantyl phosphines were used in the coupling, with similar results, and metallation with dimethylsulfidegold(I) chloride yielded the monometallic gold complexes **3.51** and **3.52** quantitatively.

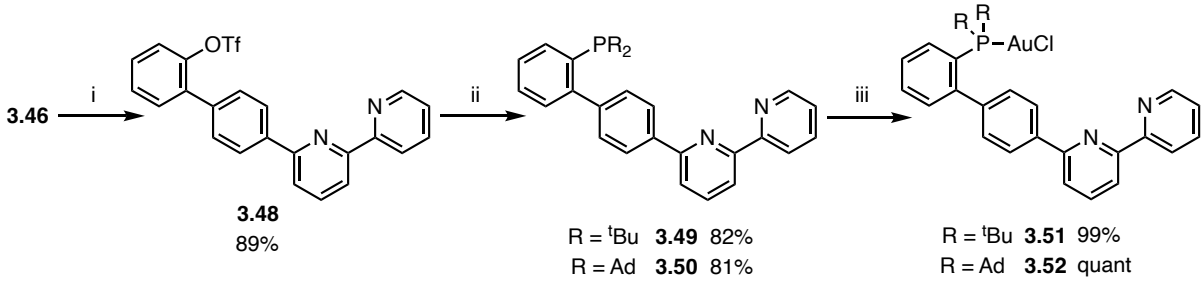

Scheme 14. Preparation of monogold(I) phosphine–bipyridine complexes from phenol **3.44**. i. $PhNTf_2$ (1.1 eq), K_2CO_3 (1.2 eq), dioxane (0.2 M), MW 120 ºC, 105 min; ii. R_2PH (1.1-1.3 eq), $Pd(OAc)_2$ (5 mol%), dppf (6 mol%), dioxane (ca. 0.1 M), MW 150 ºC, 4 h; iii. Me_2SAuCl (1.05 eq), CH_2Cl_2 (0.05 M), 23 ºC, 45 min.

A protocol was devised for the complexation of a range of metal halides to the bipyridine fragment: dissolution of the corresponding gold(I) complex and metal halide in a dichloromethane:acetone, dichloromethane:propanol or a similar mixture capable of solubilising both starting materials would allow complexation to take place. Removal of the solvent *in vacuo* followed by redissolution in dichloromethane and filtering through a Teflon syringe filter (rinsing with dichloromethane) would recover the soluble heterobimetallic complex while removing the insoluble metal salts. In this manner, heterobimetallic [AuRu^{III}], [AuCu^{II}], [AuCo^{II}] and [AuPd^{II}] complexes were synthesised.

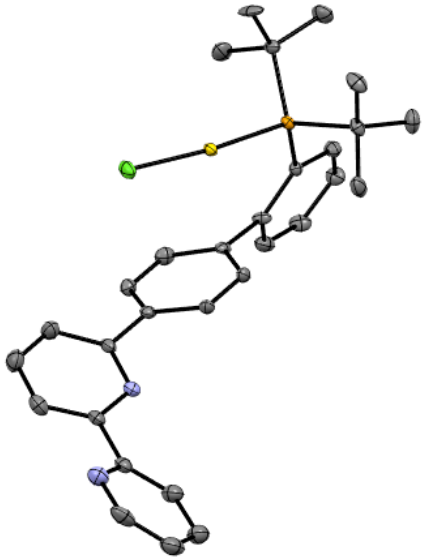

Figure 4. Crystal structure of gold(I) complex **3.51**. Hydrogen atoms removed for clarity.

Monogold(I) complex **3.51** displays similar interatomic distances to JohnPhosAuCl, as expected from a sterically and electronically very similar complex. The closest contact between gold and the lower ring of the biphenyl scaffold is to the *ipso* carbon, at 3.040(4) Å (cf. JohnPhosAuCl at 3.114(4) Å)[47] (Figure 4).

47 Grirrane, A.; Álvarez, E.; García, H.; Corma, A. Deactivation of Cationic Cu ^{I} and Au ^{I} Catalysts for A ^{3} Coupling by CH $_{2}$ Cl $_{2}$: Mechanistic Implications of the Formation of Neutral Cu ^{I} and Au ^{I} Chlorides. *Angew. Chem. Int. Ed.* **2014**, *53*, 7253–7258.

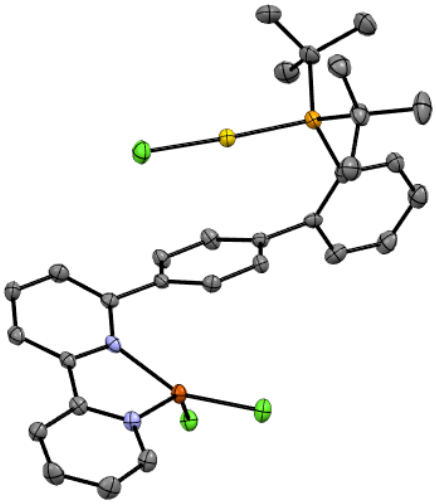

Figure 5. Crystal structure of [AuCu]·$C_2H_4Cl_2$ chloride complex **3.53**. Hydrogen atoms and solvent of crystallisation removed for clarity.

The [AuCu] complex, **3.53**, was crystallised as a dichloroethane solvate and shows a coordination sphere around Cu^{II} that is exactly halfway between tetrahedral and square planar (Figure 5). Its τ_4 parameter, as defined by Houser and coworkers,[48] is of 0.535. As a τ_4 of 0 would be fully square planar, whereas 1 would be a fully tetrahedral geometry, the copper atom in this complex can be described as being in the entatic state, as referred to in bioinorganic chemistry.[49] The gold–C_{ipso} contact is nonetheless comparable to JohnPhosAuCl, at 3.096(5) Å.

In contrast, [AuCo] complex **3.54**, which was crystallised as the bromide, was tetrahedral and had a τ_4 parameter of 0.828 (Figure 6). The preparation of this complex was analogous to the previous ones but using two equivalents of the metal halide. The formation of the gold(I) bromide complex suggests facile halogen exchange with the metal salts. The gold atom is closest not to the *ipso* carbon but to the *ortho* carbon of the biphenyl, but this is likely due to crystal packing effects – the distance is comparable at 3.078(5) Å.

48 Yang, L.; Powell, D. R.; Houser, R. P. Structural Variation in Copper(i) Complexes with Pyridylmethylamide Ligands: Structural Analysis with a New Four-Coordinate Geometry Index, τ_4. *Dalton Trans.* **2007**, *9*, 955–964.
49 Comba, P. Coordination Compounds in the Entatic State. *Coord. Chem. Rev.* **2000**, *200–202*, 217–245.

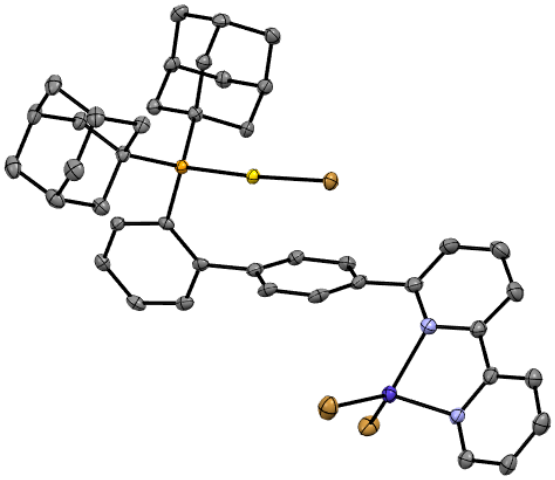

Figure 6. Crystal structure of [AuCo] bromide complex **3.54**. Hydrogen atoms removed for clarity.

Unfortunately, the standard [AuRu^{III}] complex resisted crystallisation. All attempts to form potentially photoactive {LAu}Ru(bipy)$_2$ **3.55** or similar complexes such as **3.56**, following adapted procedures, failed probably due to the steric crowding.

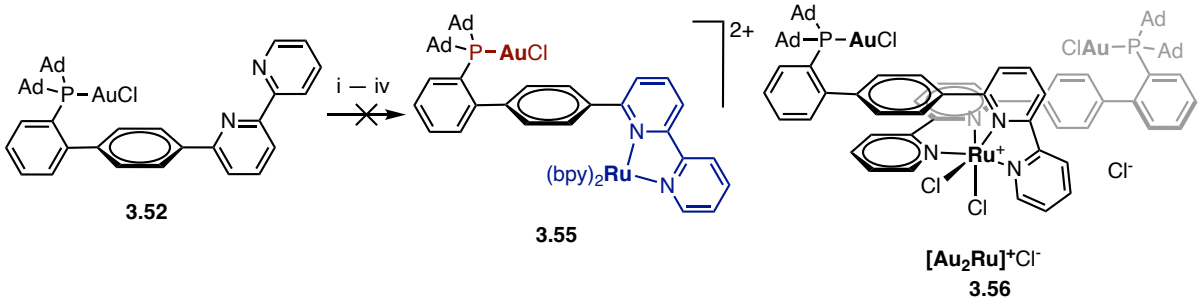

Scheme 15. Failed preparation of tris or bis(bipyridine) ruthenium complexes. i. $RuCl_3 \cdot nH_2O$ (1 eq), 2,2'-bipyridine (2 eq), DMF (0.2 M), MW 140 ºC; ii. $[Ru(bpy)_2Cl_2]SbF_6$ (1 eq), $AgNO_3$ (0 or 2 eq), MeCN (0.2 M), 80 ºC, 16 h; iii. $Ru(bpy)_2Cl_2$ (1 eq), $AgNO_3$ (0 or 2 eq), MeCN (0.2 M), 80 ºC, 16 h, then NH_4BF_4; iv. $RuCl_3 \cdot nH_2O$ (1 eq), DMF (0.2 M), MW 150 ºC, 6 h.

However, one of the attempts to form **3.56** in dimethylformamide at high temperatures with microwave irradiation afforded our only crystal structure of a [AuRu] complex, **3.57**, in which the ruthenium centre is trivalent or divalent, thus coordinating one (43%, Ru^{III}) or two (57%, Ru^{II}) additional carbonyl ligands from the thermal decomposition of dimethylformamide and had spontaneously chlorinated 35% of the *ortho*-position of the ligand (Figure 7). The chlorines on the aryl ring were found on both sides of the ring as different conformations (potentially atropoisomers) in a 57:43 ratio. The chlorination of the middle ring would have to result from reaction with the coordinated ruthenium chloride species, as no other chloride sources were used (the gold(I) chloride is not a reasonable source).

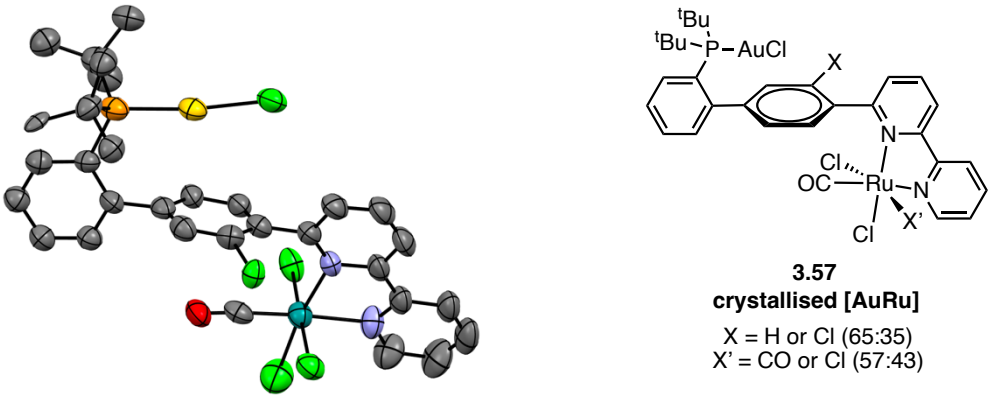

Figure 7. Crystal structure of [AuRu]·2 $C_4H_8O_2$ chloride complex **3.57** and schematic molecular structure of all species in the crystal. Hydrogen atoms, disorder, rotamer of chloroarene, non-chlorinated species, solvent of crystallisation and $Ru^{II}Cl_2(CO)_2$-containing species removed for clarity.

For our intended bimetallic cooperativity, or at least to justify the ligand design as a scaffold for future investigations, the coordinated substrates should lie close to the second metal centre. In order to probe this, we synthesised two different alkynylgold(I) complexes which would serve as a dummy substitution representative of a typical organic substrate (Scheme 16). In addition, these complexes could be used for stoichiometric experiments after a second metallation.

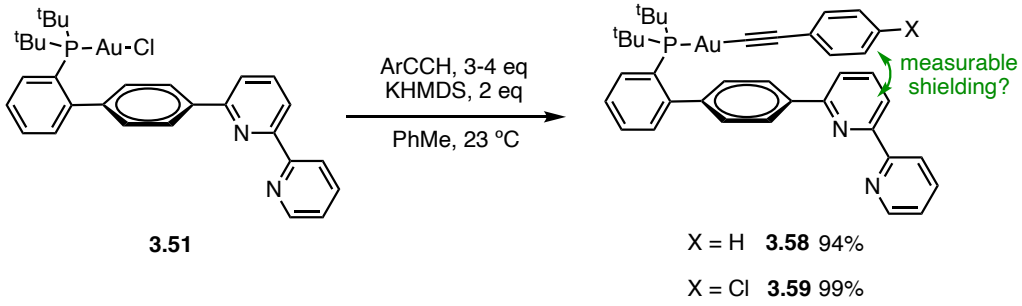

Scheme 16. Synthesis of arylacetylide monometallic gold(I) complexes.

For a substrate to be relatively close to the bipyridine coordination site, the aryl should lie approximately on top of one of the bipyridine rings. Our hypothesis was that, for such geometries, the ring current would shield the protons on the aryl and this could be observable. Analogous JohnPhosAu phenylacetylide showed all phenyl multiplets above 7.2 ppm.[50] Only very modest effects were observed, as a ^{1}H NMR spectrum of **3.58** in CD_2Cl_2 showed the phenylacetylide multiplets from 6.95–6.70 ppm. In the case of **3.59**, the two 2H multiplets of the AA'MM' system appeared centred around 6.78 and 6.63 ppm. These shifts were marginally further upfield than usually found, with the variations being, at

50 Manbeck, G. F.; Kohler, M. C.; Porter, M. R.; Stockland Jr., R. A. P–H Activation Using Alkynylgold Substrates: Steric and Electronic Effects. *Dalton Trans.* **2011**, *40*, 12595.

best, very modest at << 1 ppm, which is likely a result of torsional freedom and unhindered bond rotation.

Reactivity, Coordination Chemistry and Computational Studies[51]

We then endeavoured to study the reactivity of several of these complexes. Unfortunately, most reactions attempted were unsuccessful or did not show any significant cooperativity.

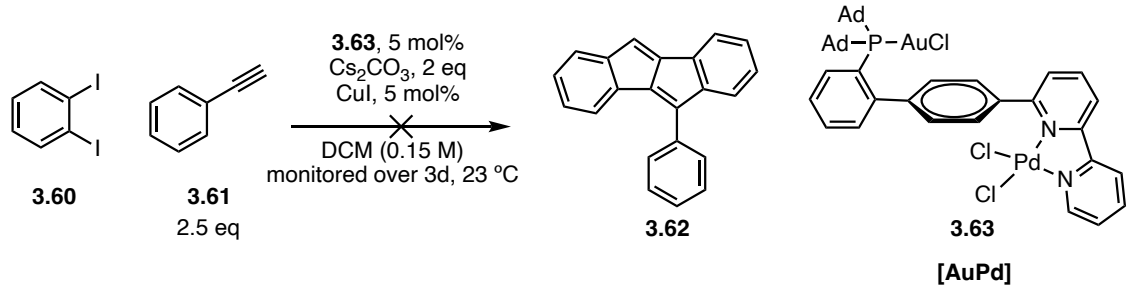

Scheme 17. Unsuccessful Sonogashira/diyne cyclisation with [AuPd] **3.63**.

The cyclisation of alkynylchalcone **3.64** was explored in the presence of phenylsilane and found to form deoxygenated dihydrobenzo[*a*]fluorene **3.65** (Scheme 18). While some gold(I)-catalysed enyne rearrangements have been known to form dihydrobenzo[*a*]fluorenes, the connectivity in the product is different with respect to the starting material.[52] In the reaction with [AuRu] **3.66**, it is the aryl on the enone that undergoes a Friedel-Crafts-type vinylation. The connectivity is therefore analogous to that found in a Brønsted acid-catalysed transformation,[53] suggesting a Lewis catalysed pathway operates in our system. In our case the reaction is over within 75 minutes and the product is fully deoxygenated, presumably through a ruthenium-catalysed hydrosilylation. Interestingly, the use of either a gold(I) catalyst or an *in situ* generated ruthenium bipyridine complex led to only unreacted starting material under the same conditions. Ruthenium complexes of triphenylarsine could perform the same transformation in lower yields.

51 Part of the experiments described in this section were done in collaboration with Dr. Víctor García.
52 García-García, P.; Rashid, M. A.; Sanjuán, A. M.; Fernández-Rodríguez, M. A.; Sanz, R. Straightforward Synthesis of Dihydrobenzo[*a*]Fluorenes through Au(I)-Catalyzed Formal [3 + 3] Cycloadditions. *Org. Lett.* **2012**, *14*, 4778–4781.
53 Mandal, M.; Balamurugan, R. Triflic Acid-Mediated Expedient Synthesis of Benzo[*a*]Fluorenes and Fluorescent Benzo[*a*]Fluorenones. *Adv. Synth. Catal.* **2018**, *360*, 1453–1465.

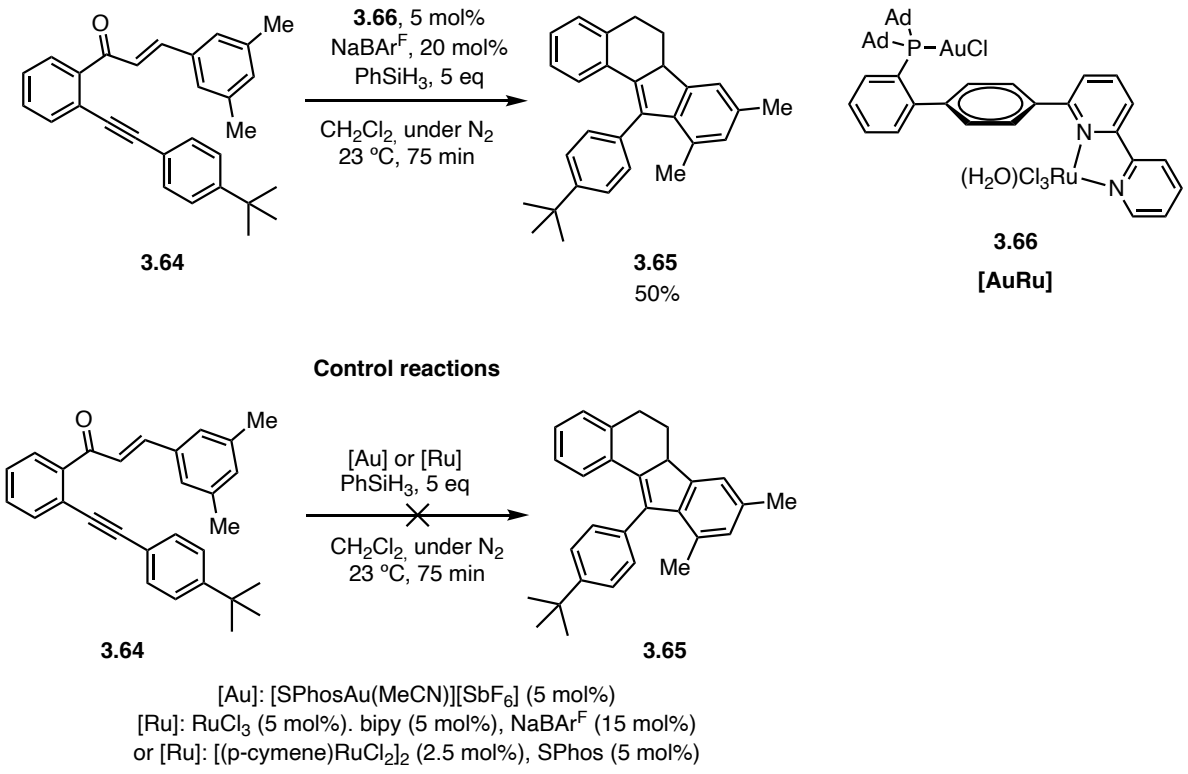

Scheme 18. Deoxygenative cyclisation of alkynylchalcones catalysed by a [AuRu] complex.

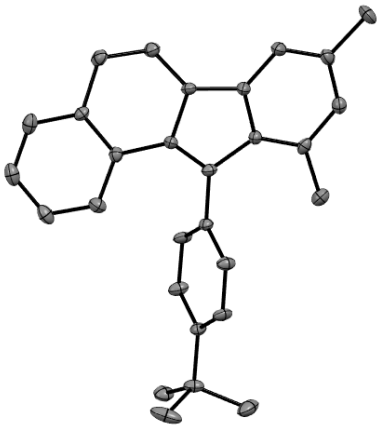

Figure 8. Crystal structure (ORTEP diagram, 50% ellipsoids) of one of the equivalent **3.65** present in the unit cell. Hydrogen atoms omitted for clarity.

Attempts to carry out a previously reported[54] photochemical alkoxycyclization-arylation sequence with the same [AuRu] catalyst were not successful.

54 Mayans, J. G.; Suppo, J.-S.; Echavarren, A. M. Photoredox-Assisted Gold-Catalyzed Arylative Alkoxycyclization of 1,6-Enynes. *Org. Lett.* **2020**, *22*, 3045–3049.

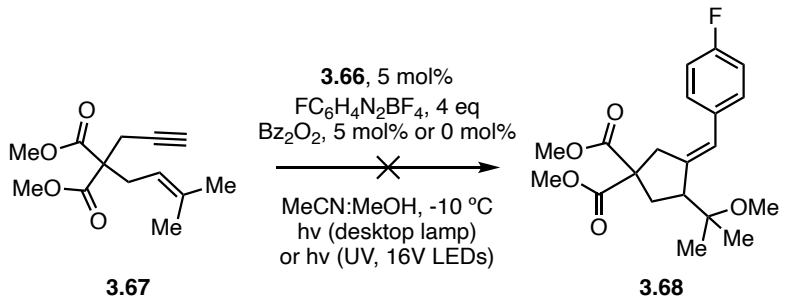

Scheme 19. Failed photoredox chemistry attempted with [AuRu] complex.

Subsequent tests with [AuCu] **3.53** or [AuCo] **3.54** in photoredox reactions were unsuccessful, and applying these complexes in common gold(I) cyclisations resulted in lower yields and no significant changes in selectivity.

In addition to these simpler coordinated complexes, we endeavoured to synthesise cyclometallated complexes. The bipyridine ligand could be a directing group for the *ortho*-C-H activation of the middle phenyl ring. These complexes would place a second metal in close proximity to the gold(I) centre. We focused on obtaining the monocationic [$Au^{I}Au^{III}$] complex and the neutral [AuPt] and [AuPd] complexes. These three complexes would all have a square planar d^8 metal centre.

Initial tests with gold(III) acetate in acetic acid, followed by the required ligand and weakly-coordinated anion exchanges, afforded the product **3.69** in good yields.[55] With a gold(I)-carbon distance of only 2.937(3) Å (0.42 Å shorter than the sum of van der Waals radii), this is to the best of our knowledge the shortest gold-carbon contact in gold(I) Buchwald phosphine complexes (Figure 9). NBO calculations on the crystal structure found almost no bonding interaction between these atoms (less than 5.5 kcal mol^{-1}), in line with the known absence of interaction in analogous gold-phenyl contacts.[56] The dihedral angle of the biphenyl scaffold is more flattened than usual for gold complexes, with a torsional angle of 63.5(5) º, but crystal packing effects could be at least partly responsible for this.

55 See Experimental Section for details.
56 Pérez-Galán, P.; Delpont, N.; Herrero-Gómez, E.; Maseras, F.; Echavarren, A. M. Metal-Arene Interactions in Dialkylbiarylphosphane Complexes of Copper, Silver, and Gold. *Chem. Eur. J.* **2010**, *16*, 5324–5332.

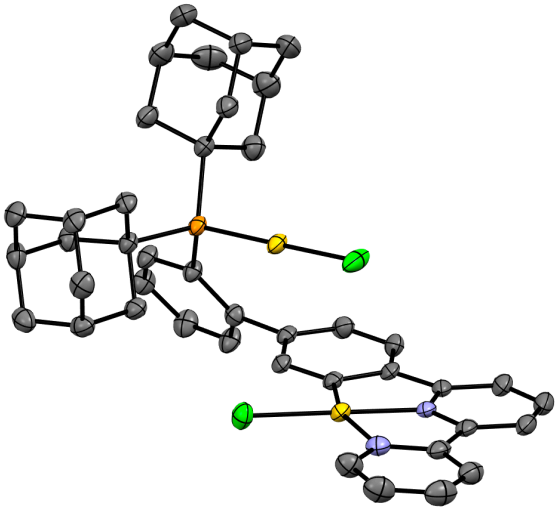

Figure 9. Crystal structure of [AuAu]PF_6·PhMe complex **3.69**. Hydrogen atoms, counteranion and toluene (solvate) removed for clarity.

Perhaps as a consequence of the torsion, the gold(I) chloride Cl atom displays a moderately short interatomic distance to the cyclometallated gold(III) atom, at 3.418(1) Å; NBO calculations did not find any significant bonding, but some degree of interaction would not be surprising as it lies only 20º off the axial coordination site of the metal. The preference of gold(III) to form square planar complexes might explain the relatively weak interaction between these two atoms, which might have been stronger for non-d^8 metals.

The synthesis of these cyclometallated complexes proved not to be as trivial as the simpler coordination complexes that we previously prepared: we were ultimately unable to carry out the synthesis at larger scales and repeating the reaction with the original amounts gave varying yields. We were unable to ascertain whether the reproducibility issues arose from the cyclometallation itself or from the complex workup and purification.

Alternatives known to work for similar ligands, using trifluoroacetic acid,[57] were also problematic and failed to afford even modest quantities of the complex. Cyclometallation methods explored also included microwave irradiation of aqueous mixtures, *in situ* addition of sodium hexafluoroantimonate with sodium tetrachloroaurate to aid in the halide abstraction, and also attempts to directly isolate the presumed gold(I) chloride–gold(III) acetate tetraacetoxyaurate(III) intermediate to avoid solubility problems in the purification. None of these methods were successful.

57 Langseth, E. Synthesis and Reactivity of Gold(III) Complexes, Doctoral Thesis, University of Oslo, **2014,** .

Finally, following a modified procedure with sodium tetrachloroaurate, performing the metallation in the presence of silver triflate, was found to be a reproducible way of accessing the homobimetallic [$Au^{I}Au^{III}$] complex in excellent yields.

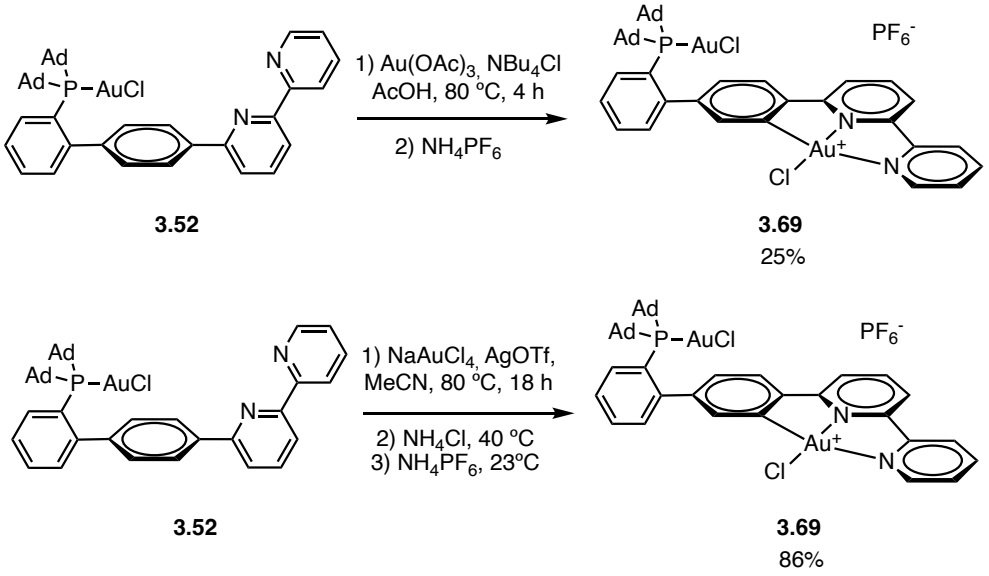

Scheme 20. Cyclometallation procedures for gold(I) gold(III) bimetallic complexes.

With the aim of preforming dicationic and tricationic [AuAu] complexes, the abstraction of the halides of **3.69** was performed with a chloride scavenger (Scheme 20). Even with higher amounts of silver hexafluorophosphate at 80 ºC, only dicationic complex **3.70** was isolated. Further tests with more electron-rich nitriles were not carried out.

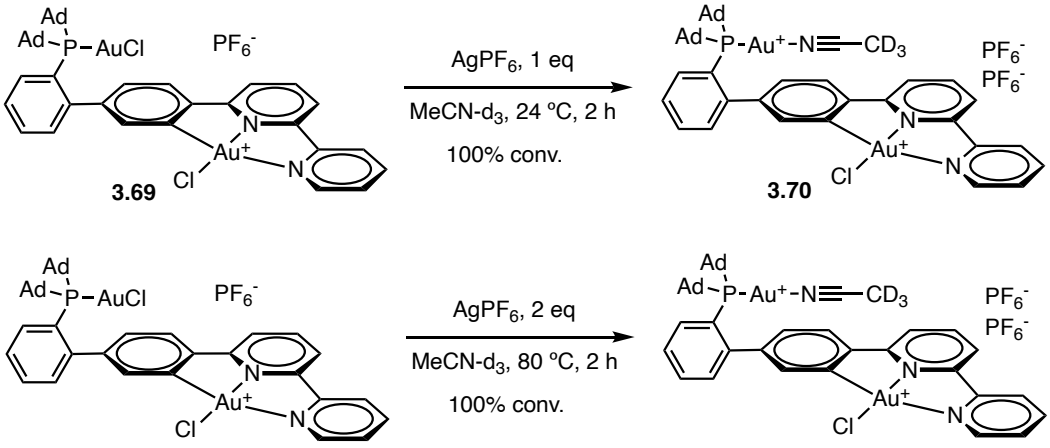

Scheme 21. Synthesis of dicationic [AuAu] complex **3.70**. The tricationic complex was not formed.

With the aim of expanding the reactivity of the cyclometallated complexes and understanding the impact of the second metal centre, we explored their fundamental coordination chemistry with a combined computational and experimental approach.

In a first approach, we ran a series of calculations for cyclometallated [AuAu], [AuPd] and [AuPt] to find their thermodynamic preferences in transmetallation or coordination and isolate the effect of charge build-up by using isoelectronic Pt(II) as a neutral comparison model for Au(III). These calculations were carried out with B3LYP-D3 as in previously described computational work, using the SDD basis set and corresponding ECP for the metal atoms. Weakly coordinating anions were excluded and solvation was modelled in dichloromethane as a model organic solvent using PCM. The reason for using solvation for these calculations, which in principle were aimed to describe the basic properties of the metal complexes, was to prevent strong Coulombic interactions from dominating (as is the case in vacuum) and changing the results. The specific choice of solvent is therefore less important and dichloromethane was used as a model due to known solubility and catalytic applicability.

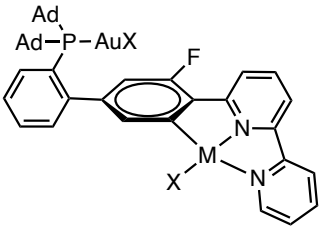

M = Au(III), Pd(II), Pt(II)
X = Cl, ethynyl, Ph; or HCCH, C_2H_4, MeCN

(charges vary)

Table 2. Relative energies (kcal mol^{-1}) of L{AuCl}{M'X} with respect to L{AuX}{M'Cl}. Positive energies favour coordination of X to Au(I).

	Ethynyl	**Phenyl**	**HCCH**	**C_2H_4**	**MeCN**
Au(III)	-9.9	-19.0	14.4	12.1	9.2
Pd(II)	1.3	2.7	-1.7	-0.7	-2.0
Pt(II)	-6.6	-5.5	-2.4	-3.1	-3.0

Assuming that the energy changes are roughly independent of metal–chloride bonding and, thus, the relative energies relatively comparable to the substrate affinities, the monocationic palladium and platinum refer coordinating the neutral ligand at the d^8 metal. However, in the dicationic [$Au^{I}Au^{III}$] complex, the preference is reversed as a result of the build-up of charge on the centre.

To model the relative ease of formation from the dichloride precursors of the three complexes, we performed model calculations on simple isodesmic exchange systems. The thermodynamics of the transmetallation from $RSnMe_3$ were calculated, with concomitant formation of trimethyltin chloride.

Table 3. Reaction free energies (kcal mol^{-1}) of $[AuM]Cl_2$ + $RSnMe_3$ --> [AuM]ClR + Me_3SnCl. The [AuM]ClR considered is the most stable isomer, which are the ones with transmetallation to M for M = Au^{III}, Pt^{II}, but to Au^{I} for M = Pd^{II}.

	Ethynyl	**Transmetallation selectivity**	**Phenyl**	**Transmetallation selectivity**	**Remaining chloride**
Au(III)	-11.0	9.9	-20.3	19.0	Au(I)-Cl
Pd(II)	-2.1	1.3	-1.0	2.7	Pd(II)-Cl
Pt(II)	-8.2	6.6	-6.5	5.5	Au(I)-Cl

Interestingly, both third-row metal complexes favour the transmetallation to the d^8 metal, whereas the palladium complex preferentially formed the gold(I)-aryl or gold(I)-alkynyl complex.

We then modelled the halide abstraction step, again, with a simplified thermodynamic treatment and no modelling of the kinetic process. In this case, a reference using the ligand exchange with cationic $[Ag(MeCN)_4]^+$ to $(MeCN)_3AgCl$ was used. This does not take into account lattice energy of AgCl. Because of the exclusion of lattice energy, this reaction driven by salt precipitation may show endergonic values even for experimentally known halide abstraction. However, it allows the direct comparison between the different M-Cl abstraction energies.

As a corollary, the stability of the [AuM](NCMe)(Cl) vs $[AuM](NCMe)_2$ + $[AuM]Cl_2$ was assessed, which, if there is a possible comproportionation or disproportionation mechanism, could result in differently coordinated species in solution. (Note: such a pathway is likely to exist, because it is analogous to halide abstraction by Ag).

Table 4. Model chloride abstraction energies and comproportionation energy. Free energy in kcal mol^{-1} at B3LYP-D3/6-311+G(d,p) + SDD.

	Au(I)-Cl	**M-Cl**	**Both Cl atoms**	**Comproportionation**
Au(III)	13.1	22.3	42.0	15.9
Pd(II)	1.3	-0.8	7.6	9.1
Pt(II)	0.6	-3.0	5.8	10.4

The data suggest that abstraction of any halide in the [AuPd] or [AuPt] complexes is easier than in the digold analogue, an expected behaviour as a consequence of forming the dicationic complex. However, it is particularly noteworthy that even abstracting two chlorides from the neutral complexes is still more favoured than abstracting the first one from the digold complex.

Regardless of the absolute energies for halide abstraction, the following are clear from the model:

(1) Charge build-up is disfavoured, with tricationic [AuAu] particularly higher in energy.

(2) Both [AuPd] and [AuPt] would abstract the M(II) chloride first.

(3) A mixture of species would comproportionate to the singly abstracted species in all cases.

The expected experimental consequences are that abstraction of a single chloride is unlikely to lead to reactivity of the doubly abstracted complex, dicationic complexes likely being easily accessible for [AuPd] and [AuPt], whereas the fully tricationic [AuAu] complex might not be possible to form with a simple salt metathesis.

The cyclometallated gold(III) atom is, due to torsional constraints, unlikely to undergo reductive elimination due to the required TS geometry. To confirm the extent to which the arylgold(III) species would be inert, we calculated the two transition states linking **A1** to the product of reductive elimination (as isomers **A2**, **A3** and **A4**). Both **TSA2** and **TSA3** were completely inaccessible, even though **TSA2** was modestly more stabilised through serendipitous intramolecular chloride-bridge interactions.

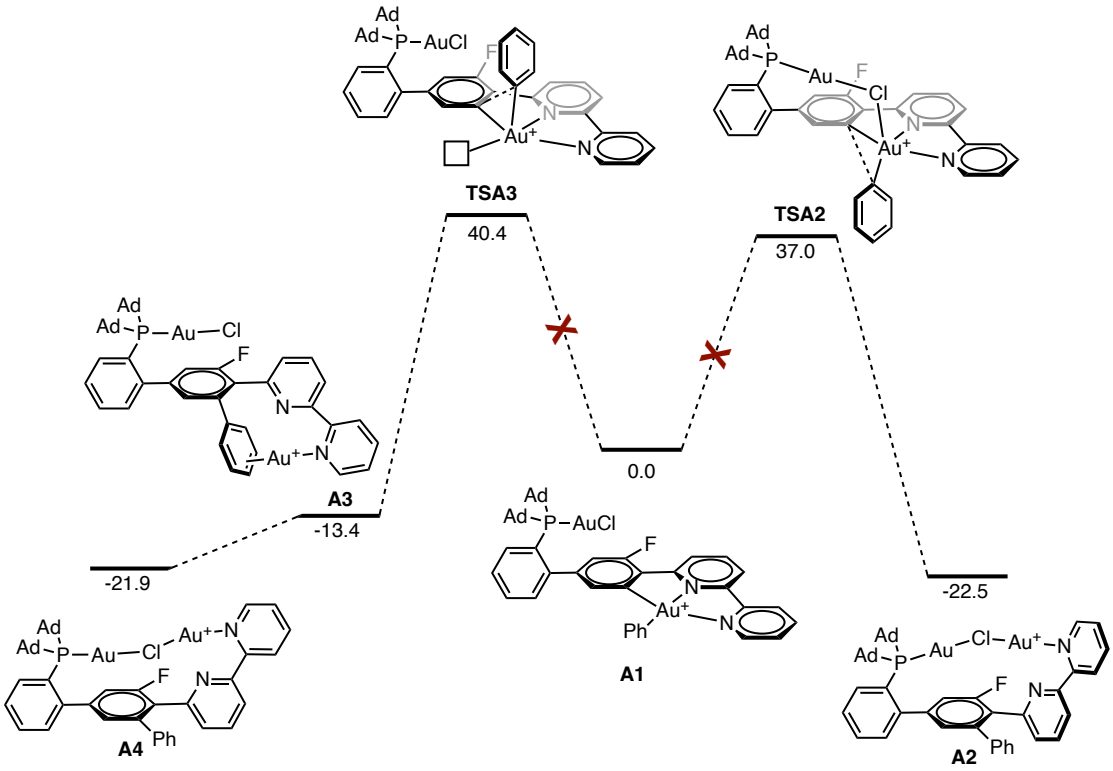

Scheme 22. Calculated (unfeasible) reductive elimination from [{$Au^{I}Cl$}{$Au^{III}Ph$}]. Free energy in kcal mol^{-1}.

As the modelled ligand exchanges with neutral complexes (tables 2 and 4) were calculated on mixed complexes with halides, the charge build-up on the metal centres could determine a significant proportion of the energy differences. This is because especially in the case of the dicationic [AuAu] complexes, the localisation of charge on the Au^{III} would be much higher when a neutral ligand is attached to it, instead of the anionic chloride. That observation can also be made from the differeces in

energy when abstracting either of the chlorides as collected in Table 5. For this reason, we modelled analogous ligand exchanges but starting from the doubly chloride-abstracted bis(acetonitrile) complexes, isolating the affinity to each substrate from the effect of the charge.

Table 5. Relative energies of gold(I)-d^8 metal bimetallic complexes with different ligands, referenced to the bis(acetonitrile) complexes.

Au-L M-L	**MeCN** **MeCN**	**HCCH** **MeCN**	**MeCN** **HCCH**	**C_2H_4** **MeCN**	**MeCN** **C_2H_4**	**Acetone** **MeCN**	**MeCN** **Acetone**
Au(III)	0.0	4.7	11.8	3.3	8.2	2.0	3.1
Pd(II)	0.0	3.7	5.8	2.8	3.3	4.0	4.2
Pt(II)	0.0	2.8	5.2	2.5	2.8	4.0	5.8

The gold(I) centre in tricationic [AuAu] is less alkynophilic than the same atom when the d^8 metal centre is Pd or Pt, probably due to the electron-withdrawing effect of the dicationic gold(III) atom and, perhaps, due to its through-space effects. The increase in affinity for acetone with respect to the other complexes is a consequence of the same phenomenon.

A very attractive gold(I)-gold(III) cooperative process would be bimetallic reductive elimination.[43] However, and as discussed earlier, these were described to require the generation of formal Au(II)-Au(II) metal-metal bonded compounds, facilitating the reductive elimination. In our case, the cyclometallated gold(III) centre blocks the required pathway.

Even though Au-Au reductive elimination is unlikely to be possible, it has been found computationally that insertion reactions –from Au(I)-R onto a suitable acceptor on Au(III)– are feasible both energetically and geometrically (Scheme 23). *Ipso*-attack of a model arylgold(I) **TSB2** was favoured over *ortho*-attack **TSB3** forming the corresponding gold(III) enolate intermediates **B2** and **B3**. Any quantitative interpretation of the results is not possible at this stage, as experimental evidence would be required to assess any side-reactivity. Moreover, catalytically, this transformation would be very challenging because of the high cost associated to forming the dicationic gold(III) centre. Any further experimental investigations would be limited to stoichiometric tests.

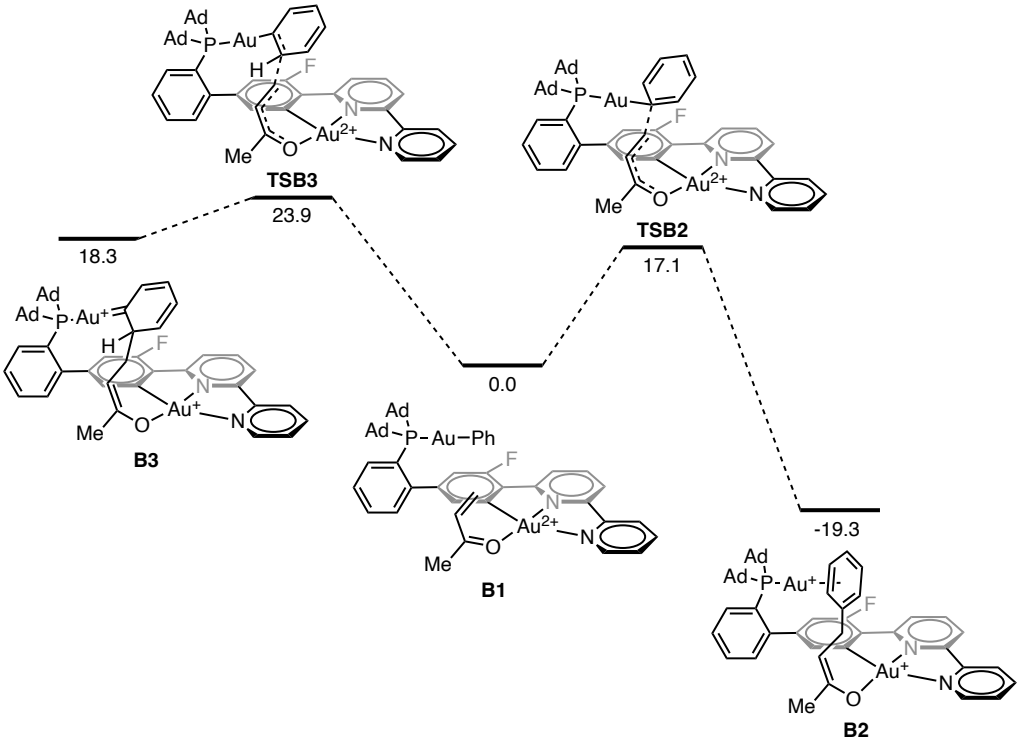

Scheme 23. Conjugate *ipso*-addition (favoured, right) and *ortho*-addition (disfavoured, left) of gold(I)-phenyl to a coordinated enone. Free energies in kcal mol^{-1} at B3LYP-D3/6-311+G(d,p) + SDD, PCM (dichloromethane).

The potential for self-activation chloride abstraction in [AuAu] **3.69** was then assessed, where aided by the Au(III). This was done by modelling the associative interchange transition state, **TSC2**, with acetylene. The activation energy was found to be only 18.1 kcal mol^{-1} and the next minimum **C2** at 15.5 kcal mol^{-1}, making this self-activation a real possibility (Scheme 24).

The same process was modelled with AdJohnPhosAuCl, known not to react or, at best, to perform very sluggishly in the absence of a chloride scavenger (Scheme 25). The highest barrier for the chloride displacement with AdJohnPhos, **TSD3**, reached 20.1 kcal mol^{-1}, with the next minimum **D3** at 19.0 kcal mol^{-1}. All transition states were relaxed by using the DVV algorithm for the IRC calculation, as well as steep optimisations. While all of these barriers are perfectly accessible at room temperature, which is also the case of AdJohnPhos, any further reactivity would have to proceed with a 15.5 kcal mol^{-1} or 19.0 kcal mol^{-1} handicap, respectively.

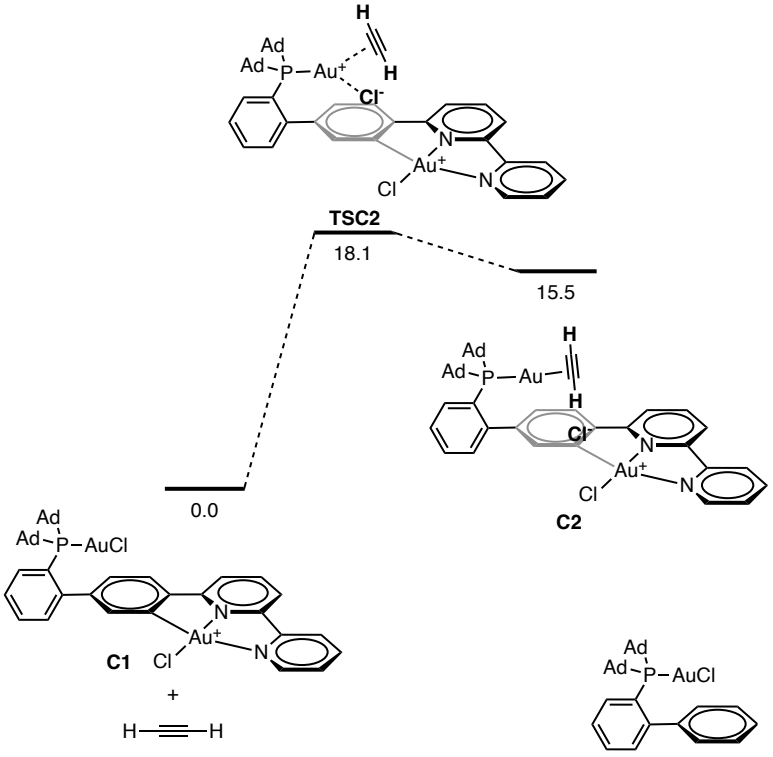

Scheme 24. Self-abstraction modelled for [AuAu] complex **3.69** by displacement with an alkyne. Free energies in kcal mol^{-1} at B3LYP-D3/6-311+G(d,p) + SDD, PCM (dichloromethane).

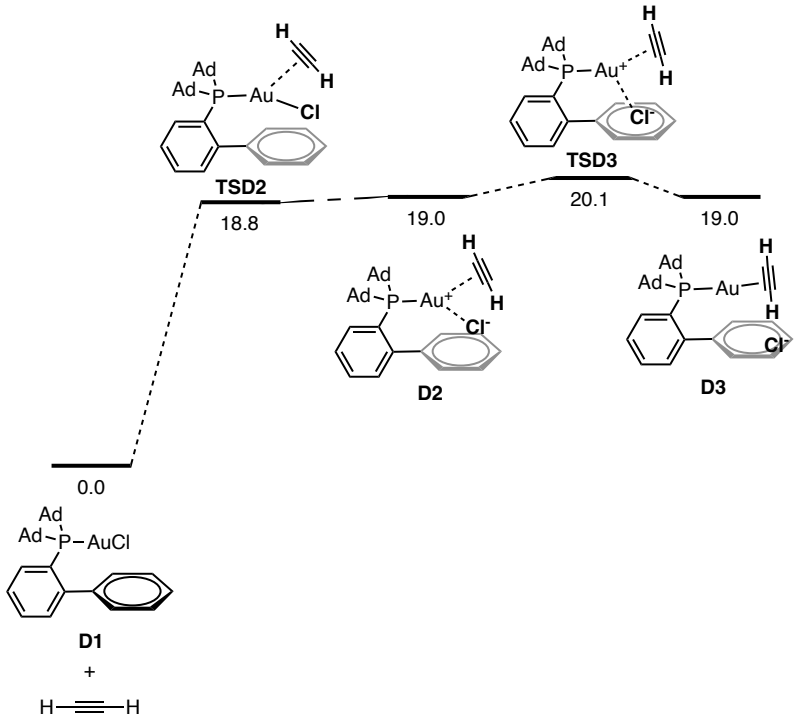

Scheme 25. Self-abstraction modelled for AdJohnPhos gold(I) chloride by displacement with an alkyne. **TSD2** has a higher electronic energy than **D2**. Free energies in kcal mol^{-1} at B3LYP-D3/6-311+G(d,p) + SDD, PCM (dichloromethane).

Unexpectedly, a high-energy intermediate was located for the chloride displacement from AdJohnPhosAuCl, constituting a two-step process and showing a real tricoordinate gold(I) minimum **D2** (confirmed by both IRC relaxations and vibrational analysis). While the free energy profile seems to show a lower energy transition state **TSD2** than high-energy intermediate **D2**, this is only due to the entropic contribution as its electronic energy is lower.

Uniquely for self-activating systems, the origin of the stabilisation of the abstracted complex **C2** and the TS leading to it does not seem to be a strong supramolecular interaction of a covalent nature, but rather an ionic interaction with the gold(III) cation.

Inspired by these computational results suggesting facile chloride displacement and given the interest in self-activating gold(I) complexes, we decided to try the digold complex in silver-free catalysis. We selected a number of model reactions to understand this reactivity.

Propargylamides are known to undergo divergent reactivity under gold(I) or gold(III) catalysis, with the former yielding an exocyclic methyleneoxazoline whereas the latter affords a methyloxazole through later isomerisation.

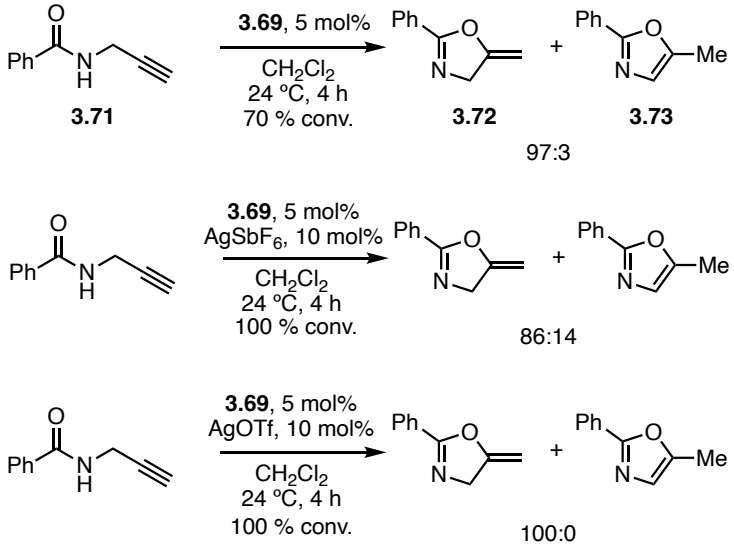

Scheme 26. Cyclisation of N-propargylbenzamide with digold catalyst **3.69** changing the chloride scavenger silver(I) salt.

In the absence of chloride scavengers, the reaction reached 70% conversion after only 4 hours and the products **3.72** and **3.73** were formed in a 97:3 ratio, which is attributed to the gold(I) reactivity. This is the first example of a gold catalyst that undergoes self-activation by Coulombic stabilisation of the charge-separated species.

Addition of excess silver hexafluoroantimonate led to full conversion of the starting material, but in this case a larger proportion of oxazole **3.73** was present, indicating at least some mediation of gold(III).

However, as gold(III) is able to isomerise the products formed by gold(I) catalysis, it is possible that the isomerisation took place at a later stage.

Nevertheless, usage of silver triflate as a halide abstractor led to full conversion and exclusive formation of methyleneisoxazole **3.72**. This result suggests that the coordinating strength of the counteranion has a direct effect on the outcome of the reaction. If the triflate does replace the chloride on gold(III), it remains tightly bound and prevents it from getting involved in catalysis.

Other chloride scavenger-free reactions tested included the alkoxycyclisation of 2-prenylphenylacetylene, the migration-cyclopropanation of styrene with a propargylic ester and the pronucleophile-trapped cyclisation of an alkynylenone. All these reactions showed full conversion in the absence of silver or sodium salts (Scheme 27).

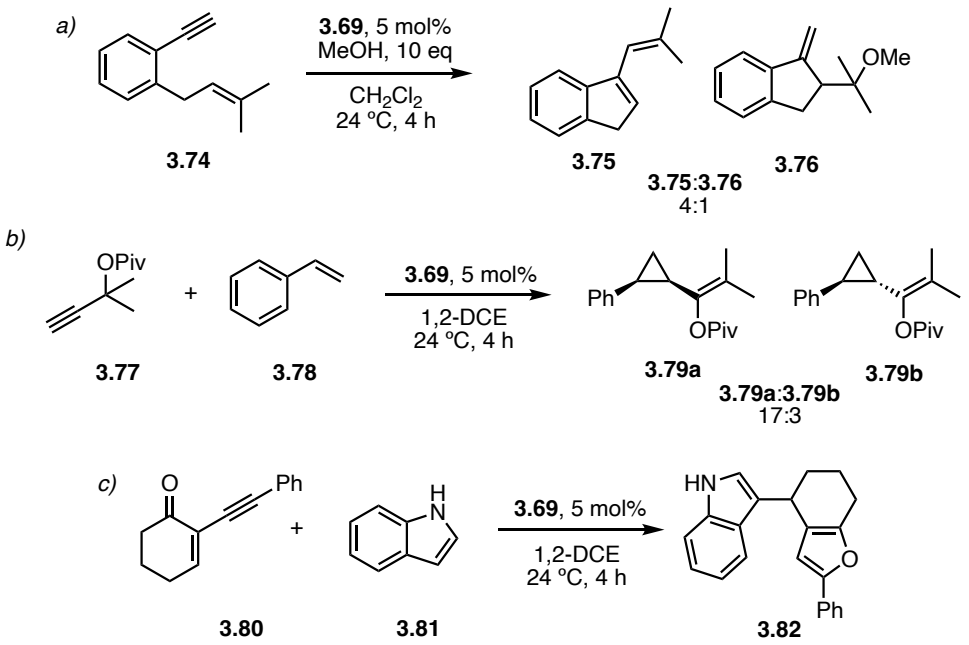

Scheme 27. Self-activating test reactions with [AuAu] complex **3.69** in the absence of halide abstractors. Full conversion reached in all cases.

We then approached the intramolecular cyclisation of indoles with alkynes, specifically, the selectivity in the 7-*exo*-dig against the 8-*endo*-dig cyclisation. These substrates had been investigated in early publications in gold catalysis.[58,59] More concretely, these reactions had prompted interest because of the contrasting reactivity of different gold species: gold(I) complexes were found to catalyse the 7-*exo*-dig cyclisation whereas gold(III) chloride or unligated gold(I) chloride formed the 8-*endo*-dig product selectively.

58 Ferrer, C.; Echavarren, A. M. Gold-Catalyzed Intramolecular Reaction of Indoles with Alkynes: Facile Formation of Eight-Membered Rings and an Unexpected Allenylation. *Angew. Chem. Int. Ed.* **2006**, *45*, 1105–1109.

59 Ferrer, C.; Amijs, C. H. M.; Echavarren, A. M. Intra- and Intermolecular Reactions of Indoles with Alkynes Catalyzed by Gold. *Chem. Eur. J.* **2007**, *13*, 1358–1373.

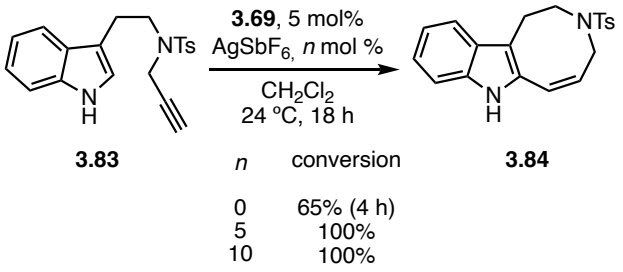

Scheme 28. Cyclisation of an indolylalkyne displaying full 8-*endo*-dig selectivity. No other products were formed.

The selectivity that we report when using the digold complex was atypical, being the opposite to that observed with JohnPhos (Scheme 28). The 8-*endo*-dig product was the only product irrespective of the equivalents of silver salt used, or whether any scavenger was used at all (although the self-activation version resulted in slower reactions). It is proposed that the greater electrophilicity provided by the proximity to an intrinsically cationic gold(III) to be the origin of this shift, as the gold(III) atom is unlikely to be catalytically active unless full abstraction is achieved.

Nevertheless, a limitation of the self-activating chemistry is seen in the failed attempts to perform [4+2] cycloadditions with model 1,6-enynes, in which no reactivity was observed under standard conditions. These reactions as well as other related cycloisomerisations have generally been challenging with self-activated gold catalysts.[60]

After studying the reactivity of complex **3.69** we focused our efforts on understanding the role of Au(III) in the complex. We first used different transmetallating agents in stoichiometric experiments with **3.69** (Scheme 29). While allyltributylstannane did not show reactivity, NMR analysis of the reaction with organomagnesium compounds showed complex mixtures.

60 Franchino, A.; Martí, À.; Nejrotti, S.; Echavarren, A. M. Silver-Free Au(I) Catalysis Enabled by Bifunctional Urea- and Squaramide-Phosphine Ligands via H-Bonding. *Chem. Eur. J.* **2021**, *27*, 11989–11996.

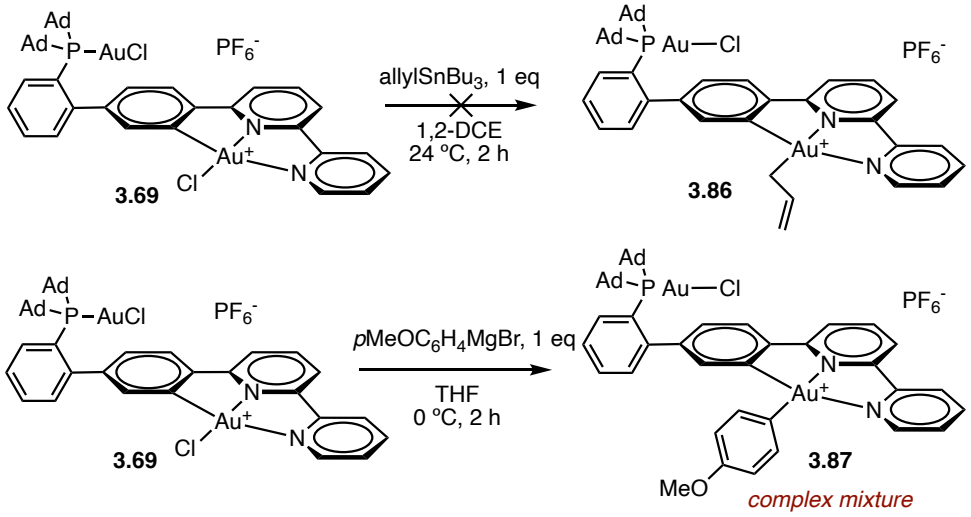

Scheme 29. Transmetallation reactions with complex **3.69**.

Conclusions

A ditopic phosphine–bipyridine ligand was successfully designed as a scaffold for the synthesis of bimetallic complexes, enabling us to delve into their reactivity and studying their coordination chemistry through structural characterisation. The chosen approach involved a ditopic ligand, carefully designed to accommodate gold(I) and a second metal in proximity, providing the framework for investigating intramolecular cooperativity effects and their impact on reactivity.

We report the structural characterisation of several coordination complexes accessible through a standardised sequential metallation procedure making use of hard and soft ligand preferences. The successful preparation of various heterobimetallic complexes, including [AuRu], [AuCu], [AuCo] and [AuPd], exemplifies the applicability of the site-selective complexation concept in the synthetic protocol. This work also allowed the determination of the shortest known non-covalent Au-phenyl contact in a Buchwald phosphine complex, as well as an example of a copper(II) bipyridine complex with a strongly distorted geometry.

The computational chemistry investigations provided a deeper understanding of the reactivity landscape. Notably, our calculations shed light on the factors governing transmetallation and coordination chemistry in cyclometallated [AuAu], [AuPd], and [AuPt] complexes. The impact of charge build-up emerged as a crucial factor, influencing the stability and selectivity of the complexes. Additionally, our exploration of ligand exchange reactions showed the combined effect of charge distribution and substrate affinity, showing how highly charged complexes could show orthogonal reactivity to neutral ones.

The DFT prediction of an accessible self-activation of the gold(I) atom in the digold complex was confirmed experimentally. The outcomes of the reactions that were explored suggested gold(I) was mediating the silver-free reactions; however, when enough chloride scavenger was used, there was indirect evidence of residual gold(III) activity. These results highlight the importance and functionality of computational chemistry in *a priori* exploratory coordination chemistry and catalysis.

Experimental Section

Computational Methods

All calculations were carried out on Gaussian09.[61] The geometry optimisations of the complexes were performed with B3LYP[62] using Grimme's D3 dispersion correction[63] with the 6-31G(d) basis set[64] for non-metal atoms and the SDD[65] basis set and ECP for all metals. Single-point energy calculations were performed with the 6-311+G(d,p) basis set for non-metal atoms and SDD basis set and ECP for all metals. The implicit polarisable continuum model (PCM)[66] for dichloromethane was used in all calculations and the cationic complexes were modelled with the exclusion of the counteranions. All stationary points were verified by the absence of imaginary vibrations and transition states confirmed by IRC[67] calculations. The reported free energies were calculated at 298 K and 1 atm.

General Experimental Methods

Anhydrous reactions were performed under nitrogen or argon in solvents dried by passing through an activated alumina column on a PureSolv^{TM} solvent purification system (Innovative Technologies, Inc., MA) or bought as dry solvents stored over 4Å MS. Dry deuterated NMR solvents, where required, were stored over 4Å MS. Otherwise, HPLC-grade solvents were used. Reactions were followed by GC-MS, UHPLC-MS, TLC (thin layer chromatography) or ^{1}H NMR analysis on aliquots. Analytical thin layer chromatography was carried out using TLC aluminium sheets with 0.2 mm of silica gel (Merck 60 F_{254}) using UV light as the visualizing agent, and an acidic solution of vanillin in ethanol or a basic aqueous solution of $KMnO_4$ as stains. UHPLC-MS analyses were carried out on an Agilent Technologies 1290 Infinity II instrument with single-quad detector using APCI for the ionisation. Purifications by

61 Gaussian 09, Revision B.1, Frisch, M. J., Trucks, G. W., Schlegel, H. B., Scuseria, G. E., Robb, M. A., Cheeseman, J. R., Scalmani, G., Barone, V., Mennucci, B., Petersson, G. A., Nakatsuji, H., Caricato, M., Li, X., Hratchian, H. P., Izmaylov, A. F., Bloino, J., Zheng, G., Sonnenberg, J. L., Hada, M., Ehara, M., Toyota, K., Fukuda, R., Hasegawa, J., Ishida, M., Nakajima, T., Honda, Y., Kitao, O., Nakai, H., Vreven, T., Montgomery, J. A., Peralta, Jr. J. E., Ogliaro, F., Bearpark, M., Heyd, J. J., Brothers, E., Kudin, K. N., Staroverov, V. N., Kobayashi, R., Normand, J., Raghavachari, K., Rendell, A., Burant, J. C., Iyengar, S. S., Tomasi, J., Cossi, M., Rega, N., Millam, J. M., Klene, M., Knox, J. E., Cross, J. B., Bakken, V., Adamo, C., Jaramillo, J., Gomperts, R., Stratmann, R. E., Yazyev, O., Austin, A. J., Cammi, R., Pomelli, C., Ochterski, J. W., Martin, R. L., Morokuma, K., Zakrzewski, V. G., Voth, G. A., Salvador, P., Dannenberg, J. J., Dapprich, S., Daniels, A. D., Farkas, Ö., Foresman, J. B., Ortiz, J. V., Cioslowski, J., Fox, D. J. Gaussian, Inc., Wallingford CT 2009.

62 (a) Becke, A. D. *J. Chem. Phys.* **1993**, *98*, 5648; (b) Becke, A. D. *J. Chem. Phys.* **1993**, *98*, 1372; c) Lee, C.; Yang, W.; Parr, R. G. *Phys. Rev. B* **1988**, *37*, 785.

63 Grimme, S. Density Functional Theory with London Dispersion Corrections. *WIREs Comput Mol Sci* **2011**, *1*, 211–228.

64 Hehre, W. J.; Ditchfield, R.; Pople, J. A. Self–Consistent Molecular Orbital Methods. XII. Further Extensions of Gaussian–Type Basis Sets for Use in Molecular Orbital Studies of Organic Molecules. *J. Chem. Phys.* **1972**, *56*, 2257–2261.

65 Andrae, D.; Häußermann, U.; Dolg, M.; Stoll, H.; Preuß, H. Energy-adjusted ab initio pseudopotentials for the second and third row transition elements. *Theor. Chim. Acta* **1990**, *77*, 123–141.

66 Cancès, E.; Mennucci, B.; Tomasi, J. A new integral equation formalism for the polarizable continuum model: Theoretical background and applications to isotropic and anisotropic dielectrics. *J. Chem. Phys.* **1997**, *107*, 3032−3041.

67 Gonzalez, C.; Schlegel, H. B. Reaction path following in mass-weighted internal coordinates. *J. Phys. Chem.* **1990**, *94*, 5523−5527.

chromatography were carried out using flash grade silica gel (SDS Chromatogel 60 ACC, 40-63 mm) or preparative thin-layer chromatography plates (Analtech, 1000 μm or 2000 μm). The reported yields refer to isolated pure compounds or, in the case of isolation as pure mixtures as ratios, weighed and the ratio determined by NMR and subsequently validating with an internal standard. NMR spectra were recorded at 298 K on a Bruker Avance 300, Bruker Avance 400 Ultrashield or a Bruker Avance 500 Ultrashield apparatus. The signals are given as δ / ppm (multiplicity, coupling constant (Hertz), number of protons) downfield from tetramethylsilane, with calibration on the residual solvent used (δ_H = 7.26 ppm and δ_C = 77.16 ppm for $CDCl_3$). Mass spectra were recorded on a Waters UPLC-QqTOF (Maxis Impact, Bruker Daltonics) with ESI and APCI, a Waters Alliance HPLC-TOF (MicroTOF Focus, Bruker Daltonics) with ESI and APCI or, for MALDI, a Bruker Daltonics Autoflex spectrometer. Melting points were determined using a Büchi melting point apparatus or MP70 Melting Point System (Mettler Toledo). X-ray diffraction was carried out on a Bruker APEX Duo instrument with Mo Kα Microfocus source E025 IuS anode and an APEX DUO detector, or a Rigaku MicroMax-007HF, with Mo Kα radiation rotating anode and a Pilatus 200K detector.

Synthetic Procedures and Characterisation Data

N-propargylbenzamide,[60] 2-prenylphenylacetylene,[60] 2-phenylethynyl-2-cyclohexen-1-one,[60] and N-tosyl-N-propargyl-2-(3-indolyl)-ethylamine[68] were prepared according to literature procedures.

6-bromopicolinaldehyde dimethyl acetal (3.37)

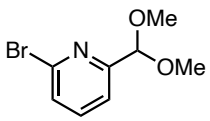

6-bromopicolinaldehyde (2.50 g, 13.4 mmol) and *p*-toluenesulfonic acid hydrate (510 mg, 2.7 mmol, 0.2 eq) were dissolved in methanol (45 mL) and trimethyl orthoformate (7.4 mL, 67 mmol, 5 eq) added. The solution was stirred at 23 ºC for 6 h. After this time, it was quenched with saturated aqueous $NaHCO_3$ and extracted with ethyl acetate (3x). The combined organic fractions were washed with saturated brine, dried over $MgSO_4$ and concentrated. Pale yellow oil (2.95 g, 95%). **^{1}H NMR** (400 MHz, $CDCl_3$) δ 7.59 (t, *J* = 7.7 Hz, 1H), 7.52 (dd, *J* = 7.6, 1.1 Hz, 1H), 7.45 (dd, *J* = 7.7, 1.1 Hz, 1H), 5.30 (s, 1H), 3.41 (s, 6H) ppm. **^{13}C{^{1}H} NMR** (101 MHz, $CDCl_3$) δ 158.9, 141.6, 139.1, 128.2, 120.1, 103.7, 54.2 ppm.

6-(4-chlorophenyl)picolinaldehyde dimethyl acetal (3.38)

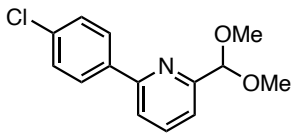

3.37 (1.000 g, 4.3 mmol), bis(triphenylphosphine)palladium(II) chloride (75.8 mg, 172 μmol, 4 mol%), potassium carbonate (1.79 g, 12.9 mmol, 3 eq) and 4-chlorophenylboronic acid (842 mg, 5.39 mmol, 1.25 eq) were dissolved in 6:1 dioxane:water (15 mL : 2.5 mL, 0.25 M) and degassed by bubbling with argon. The

68 Zhu, P.-L.; Zhang, Z.; Tang, X.-Y.; Marek, I.; Shi, M. Gold- and Silver-Catalyzed Intramolecular Cyclizations of Indolylcyclopropenes for the Divergent Synthesis of Azepinoindoles and Spiroindoline Piperidines. *ChemCatChem* **2015**, *7*, 595–600.

mixture was stirred with microwave irradiation at 110 ºC for 3 h. The reaction was worked up with saturated aqueous NH_4Cl and extracted with diethyl ether (2x). The combined organic fractions were washed with saturated brine, dried over Na_2SO_4 and concentrated. The crude product was purified by column chromatography (6:1 CyH:EtOAc), yielding the title compound as a colourless oil/semisolid (1.068 g, 94%). **^{1}H NMR** (400 MHz, $CDCl_3$) δ 7.99 – 7.93 (m, 2H), 7.79 (t, *J* = 7.8 Hz, 1H), 7.65 (dd, *J* = 7.9, 1.0 Hz, 1H), 7.51 (dd, *J* = 7.7, 1.0 Hz, 1H), 7.46 – 7.40 (m, 2H), 5.41 (s, 1H), 3.46 (s, 6H) ppm.

4'-(6-(dimethoxymethyl)pyridin-2-yl)-[1,1'-biphenyl]-2-ol (3.40)

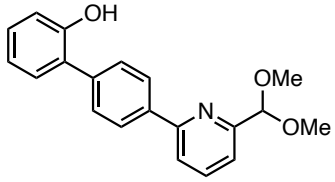

To a microwave vial were added **3.38** (315.1 mg, 1.20 mmol), SPhos (39 mg, 96 µmol, 8 mol%), palladium(II) chloride (8.5 mg, 48 µmol, 4 mol%), potassium carbonate (495 mg, 3.6 mmol, 3 eq) and 2-hydroxyphenylboronic acid (230.7 mg, 1.67 mmol, 1.4 eq). The products were dissolved in dioxane (4 mL) and water (0.7 mL), roughly in a 6:1 ratio, then degassed by bubbling with argon. The mixture was heated with microwave irradiation at 90 ºC for 3 h. Upon completion, the reaction was worked up with the addition of saturated aqueous NH_4Cl and extracted with diethyl ether (3x). The combined organic fractions were washed with saturated brine, dried over Na_2SO_4 and concentrated. Purification by column chromatography (CyH:EtOAc gradient up to 10%), then a second column chromatography (4:1 DCM:CyH to DCM) afforded the title product as a pale yellow oil or foam (357.0 mg, 93%).

^{1}H NMR (400 MHz, $CDCl_3$) δ 8.15 – 8.11 (m, 2H), 7.83 (t, *J* = 7.7 Hz, 1H), 7.74 (dd, *J* = 7.9, 1.1 Hz, 1H), 7.61 – 7.57 (m, 2H), 7.54 (dd, *J* = 7.6, 0.9 Hz, 1H), 7.31 – 7.24 (m, 2H), 7.03 – 6.98 (m, 2H), 5.47 (br s, 1H), 5.46 (s, 1H), 3.48 (s, 6H) ppm. **^{13}C{^{1}H} NMR** (101 MHz, $CDCl_3$) δ 157.6, 156.3, 152.8, 138.6, 138.1, 137.7, 130.3, 129.6, 129.4, 128.0, 127.9, 121.0, 120.5, 119.8, 116.1, 104.9, 54.3 ppm.

6-(2'-(di-*tert*-butylphosphaneyl)-[1,1'-biphenyl]-4-yl)picolinaldehyde (3.41)

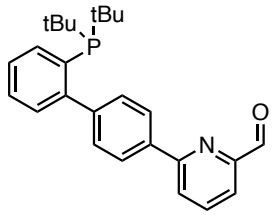

3.40 (93.1 mg, 0.29 mmol), phenyl bistriflimide (114 mg, 0.32 mmol, 1.1 eq) and potassium carbonate (120 mg, 0.87 mmol, 3 eq) were dissolved or suspended in dioxane (3.3 mL, ca 0.1 M). The mixture was heated at 120 ºC for 75 minutes with microwave irradiation. When full conversion was observed by UHPLC-MS, the reaction mixture was allowed to cool to room temperature.

To the aryl triflate reaction mixture were added sodium *tert*-butoxide (33.4 mg, 0.35 mmol, 1.2 eq), dppf (9.6 mg, 17 µmol, 6 mol%) and $Pd(OAc)_2$ (3.3 mg, 14 µmol, 5 mol%). The mixture was then degassed by bubbling with argon. Di-*tert*-butylphosphine (55.0 mg, 0.38 mmol, 1.3 eq) was added by syringe. The mixture was heated to 150 ºC with microwave irradiation for 4 h, then poured into 37% HCl (0.5 mL) in dioxane (3 mL) and stirred at 55 ºC for 3.5 h. After this time, saturated aqueous $NaHCO_3$ (50 mL) was added and the mixture extracted with ethyl acetate (3x). The combined organic

fractions were washed with saturated brine, dried over Na_2SO_4 and concentrated. Purification by column chromatography (9:1 CyH:EtOAc) yielded the product as an oil (47.3 mg, 40%).

^{1}H NMR (500 MHz, CD_2Cl_2) δ 10.16 (d, *J* = 0.8 Hz, 1H), 8.12 – 8.10 (m, 2H), 8.06 (dd, *J* = 7.9, 1.1 Hz, 1H), 7.99 – 7.94 (m, 2H), 7.90 (dd, *J* = 7.6, 1.1 Hz, 1H), 7.42 – 7.38 (m, 3H), 7.32 – 7.28 (m, 2H), 1.17 (d, *J* = 11.7 Hz, 17H) ppm. **^{31}P{^{1}H} NMR** (202 MHz, CD_2Cl_2) δ 21.4 ppm.

(*E*)-1-(6-(2'-(di-*tert*-butylphosphaneyl)-[1,1'-biphenyl]-4-yl)pyridin-2-yl)-*N*-(4-methoxyphenyl)methanimine (3.42) = L^1

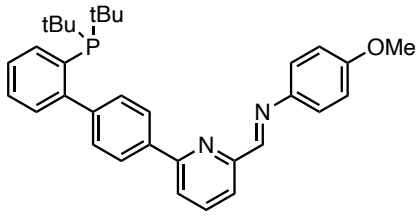

To a solution of **3.41** (27.5 mg, 68 µmol) in toluene (0.2 mL) was added *p*-methoxyaniline (8.8 mg, 72 µmol, 1.05 eq). After stirring for 24 h at 23 ºC, the solvent was removed by rotary evaporation at 50 ºC and the excess aniline removed under high vacuum at 60 ºC. Yellow resin (34.3 mg, 99%). The compound was unstable on silica and on alumina and was not purified.

^{1}H NMR (500 MHz, CD_2Cl_2) δ 8.74 (s, 1H), 8.15 (dd, *J* = 7.2, 1.5 Hz, 1H), 8.09 – 8.06 (m, 2H), 7.97 – 7.94 (m, 1H), 7.91 (td, *J* = 7.5, 0.6 Hz, 1H), 7.88 (dd, *J* = 7.8, 1.5 Hz, 1H), 7.43 (tdd, *J* = 7.4, 1.6, 0.8 Hz, 1H), 7.39 – 7.37 (m, 3H), 7.33 – 7.29 (m, 1H), 7.16 – 7.12 (m, 1H), 7.07 – 7.04 (m, 1H), 7.00 – 6.96 (m, 2H), 3.85 (s, 3H), 1.17 (d, *J* = 11.7 Hz, 18H) ppm. **^{31}P{^{1}H} NMR** (202 MHz, CD_2Cl_2) δ 21.2 ppm.

L^{1}AuCl (3.85)

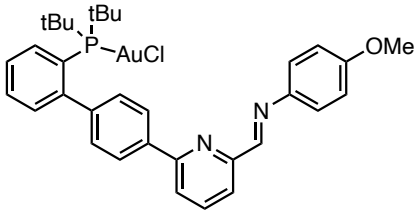

To a solution of **3.42** (L^1) (34.7 mg, 68 µmol) in dichloromethane (1.2 mL) was added (dimethylsulfide)gold(I) chloride (22.1 mg, 75.0 µmol, 1.1 eq). The reaction turned hazy dark reddish with some brown precipitate (Au). After 1 h, filtration through Teflon syringe filters and concentration by rotary evaporation yielded the title compound as dark brown crystals (43.4 mg, 86%).

^{1}H NMR (400 MHz, CD_2Cl_2) δ 8.74 (s, 1H), 8.19 – 8.14 (m, 1H), 8.11 (t, *J* = 7.9 Hz, 2H), 7.99 (dd, *J* = 7.9, 3.6 Hz, 1H), 7.91 (q, *J* = 8.3 Hz, 2H), 7.61 – 7.51 (m, 3H), 7.36 (dd, *J* = 10.2, 7.7 Hz, 3H), 7.30 (d, *J* = 7.8 Hz, 2H), 6.97 (d, *J* = 8.9 Hz, 1H), 3.84 (s, 3H), 1.42 (dd, *J* = 15.6, 1.0 Hz, 18H) ppm. **^{31}P{^{1}H} NMR** (162 MHz, CD_2Cl_2) δ 63.3 ppm.

6-(4-chlorophenyl)-2,2'-bipyridine (3.44)

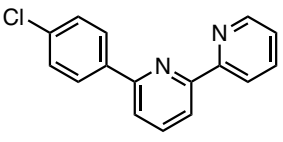

In a microwave vial, 6-bromo-2,2'-bipyridine (974.7 mg, 4.15 mmol), 4-chlorophenylboronic acid (810.4 mg, 5.18 mmol, 1.25 eq), $(Ph_3P)_2PdCl_2$ (72.9 mg, 0.166 mmol, 4 mol %) and potassium carbonate (1.719 g, 12.44 mmol, 3 eq) were dissolved in 6:1 dioxane:water (16.5 mL, 0.25 M), sealed with a MW cap and

degassed by bubbling with argon. The mixture was heated with microwave irradiation at 110 ºC for 3 hours. Full conversion was confirmed by UHPLC-MS. The reaction was quenched with saturated aqueous $NaHCO_3$ and the aqueous phase extracted with diethyl ether (3x). The combined organic fractions washed with brine, dried with Na_2SO_4, concentrated, and purified by column chromatography (PhMe or DCM, then 1:3 DCM:EtOAc) affording the title compound as a pale-yellow oil or solid (1051.0 mg, 95%, purum). **^{1}H NMR** (500 MHz, $CDCl_3$) δ 8.76 (ddd, *J* = 5.0, 1.8, 0.8 Hz, 1H), 8.67 (dt, *J* = 8.0, 1.1 Hz, 1H), 8.51 (d, *J* = 7.8 Hz, 1H), 8.13 – 8.07 (m, 2H), 8.00 – 7.95 (m, 1H), 7.93 (t, *J* = 7.8 Hz, 1H), 7.78 (dd, *J* = 7.9, 0.9 Hz, 1H), 7.50 – 7.46 (m, 2H), 7.46 – 7.43 (m, 1H) ppm. **^{13}C{^{1}H} NMR** (126 MHz, $CDCl_3$) δ 155.7, 155.2, 147.9, 138.7, 138.3, 137.6, 135.5, 129.1, 128.4, 124.4, 122.2, 120.8, 120.3 ppm. **HRMS** (ESI) *m/z*: $[M+H]^+$ calculated for $C_{16}H_{12}ClN_2$ = 267.0684; found 267.0682.

Alternatively, the compound could be purified by filtering through a silica plug (1:1 CyH:EtOAc), leading to a ca 94% purity product.

6-(4-chloro-2-fluorophenyl)-2,2'-bipyridine (3.45)

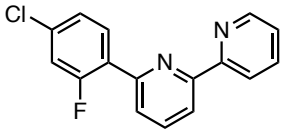

In a microwave vial, 6-bromo-2,2'-bipyridine (270.0 mg, 1.15 mmol), 4-chloro-2-fluorophenylboronic acid (230.3 mg, 1.32 mmol, 1.15 eq), $(Ph_3P)_2PdCl_2$ (20.2 mg, 45.4 µmol, 4 mol %) and potassium carbonate (476 mg, 3.45 mmol, 3 eq) were dissolved in 6:1 dioxane:water (4.5 mL, 0.25 M), sealed with a MW cap and degassed by bubbling with argon. The mixture was heated with microwave irradiation at 110 ºC for 3 hours. Full conversion was confirmed by UHPLC-MS. The reaction was quenched with saturated aqueous $NaHCO_3$ and the aqueous phase extracted with diethyl ether (3x). The combined organic fractions washed with brine, dried with Na_2SO_4, concentrated, and purified by column chromatography (6:1 to 3:1 CyH:EtOAc) affording the title compound as a colourless oil (327.0 mg, quant.). **^{1}H NMR** (400 MHz, $CDCl_3$) δ 8.72 (d, *J* = 4.9 Hz, 1H), 8.59 – 8.52 (m, 1H), 8.44 (d, *J* = 7.8 Hz, 1H), 8.19 (t, *J* = 8.5 Hz, 1H), 7.91 (t, *J* = 7.8 Hz, 1H), 7.88 – 7.82 (m, 2H), 7.39 – 7.33 (m, 1H), 7.31 (ddd, *J* = 8.5, 2.0, 0.7 Hz, 1H), 7.23 (dd, *J* = 11.0, 2.1 Hz, 1H) ppm. **^{19}F{^{1}H} NMR** (376 MHz, $CDCl_3$) δ -114.11 ppm.

6-(2'-hydroxy-4-biphenyl)-2,2'-bipyridine (3.46)

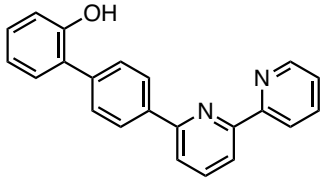

$(MeCN)_2PdCl_2$ (11.9 mg, 0.06 mmol, 4 mol %) and SPhos (62.5 mg, 0.15 mmol, 8 mol %) were dissolved in minimal dioxane and stirred for 5 minutes. Potassium carbonate (525.6 mg, 3.80 mmol, 2 eq), a solution of chloroarene **3.44** (507.2 mg, 1.9 mmol) in dioxane (9.5 mL, 0.2 M) and 2-hydroxyphenylboronic acid (367.2 mg, 2.66 mmol, 1.4 eq) were sequentially added. The reaction mixture was degassed by bubbling with Ar and the reaction was stirred for 4.5 hours at 90 ºC. Full conversion was observed by UHPLC-MS. Workup and extraction with saturated aqueous NH_4Cl and EtOAc, followed by column chromatography on silica (4:1 CyH:EtOAc, then up to 1:1 CyH:EtOAc) yielded the product as a crystalline white solid (476.8 mg, 77%). **^{1}H NMR** (500 MHz, CD_2Cl_2) δ 8.69

(ddd, *J* = 4.8, 1.8, 0.9 Hz, 1H), 8.65 (dt, *J* = 8.0, 1.1 Hz, 1H), 8.40 (dd, *J* = 7.7, 1.0 Hz, 1H), 8.30 – 8.24 (m, 2H), 7.93 (t, *J* = 7.8 Hz, 1H), 7.88 (ddd, *J* = 8.0, 7.5, 1.8 Hz, 1H), 7.85 (dd, *J* = 7.8, 1.0 Hz, 1H), 7.67 – 7.62 (m, 2H), 7.38 – 7.33 (m, 2H), 7.28 (ddd, *J* = 8.1, 7.4, 1.7 Hz, 1H), 7.03 (td, *J* = 7.5, 1.2 Hz, 1H), 6.99 (dd, *J* = 8.1, 1.1 Hz, 1H), 5.67 (s, 1H) ppm. **^{13}C{^{1}H} NMR** (126 MHz, CD_2Cl_2) δ 156.7, 156.3, 156.3, 153.4, 149.6, 139.1, 138.7, 138.4, 137.5, 130.9, 130.0, 129.8, 128.4, 128.0, 124.4, 121.6, 121.4, 120.8, 120.0, 116.5 ppm. **HRMS** (ESI) *m/z*: $[M+H]^+$ calculated for $C_{22}H_{17}N_2O$ = 325.1335; found 325.1333; $[M+Na]^+$ calculated for $C_{22}H_{16}N_2NaO$ = 347.1155; found 347.1155. **Melting point** (cyclohexane/EtOAc) 165–167 ºC. **FTIR** (neat): 3065 (br w), 2939 (w), 2879 (w), 2746 (w), 2706 (w), 2596 (w), 1577 (m), 1556 (m), 1449 (m), 1431 (m), 1388 (w), 1268 (m), 1107 (w), 1005 (w), 763 (m), 750 (m) cm^{-1}.

6-(2'-hydroxy-3-fluoro-4-biphenyl)-2,2'-bipyridine (3.47)

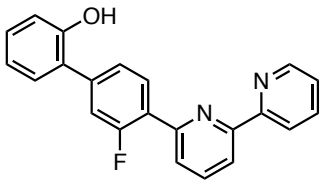

$(MeCN)_2PdCl_2$ (19.7 mg, 45.9 µmol, 4 mol %) and SPhos (37.7 mg, 91.9 µmol, 8 mol %) were dissolved in minimal dioxane and stirred for 5 minutes. Potassium carbonate (317.4 mg, 2.30 mmol, 2 eq), a solution of chloroarene **3.45** (327.0 mg, 1.15 mmol) in dioxane (9.5 mL, 0.2 M) and 2-hydroxyphenylboronic acid (221.8 mg, 1.61 mmol, 1.4 eq) were sequentially added. The reaction mixture was degassed by bubbling with Ar and the reaction was stirred for 5 hours at 90 ºC. Full conversion was observed by UHPLC-MS. Workup and extraction with saturated aqueous NH_4Cl and EtOAc, followed by column chromatography on silica (4:1 CyH:EtOAc, then up to 3:1 CyH:EtOAc) yielded the product as a white solid (360.4 mg, 92%). **^{1}H NMR** (400 MHz, $CDCl_3$) δ 8.70 (ddd, *J* = 4.8, 1.8, 0.9 Hz, 1H), 8.58 (dt, *J* = 8.0, 1.1 Hz, 1H), 8.39 (dd, *J* = 7.0, 1.8 Hz, 1H), 8.28 (apparent t, *J* = 8.2 Hz, 1H), 7.94 – 7.88 (m, 2H), 7.86 (ddd, *J* = 8.0, 7.6, 1.9 Hz, 1H), 7.45 (dd, *J* = 8.0, 1.7 Hz, 1H), 7.36 – 7.27 (m, 4H), 7.06 – 6.98 (m, 2H), 5.65 (br s, 1H, OH) ppm. **^{13}C{^{1}H} NMR** (101 MHz, $CDCl_3$) δ 161.1 (d, *J* = 251.6 Hz), 156.1 (d, *J* = 25.1 Hz), 152.8, 152.2 (d, *J* = 2.8 Hz), 149.2, 140.1 (d, *J* = 8.6 Hz), 137.7, 137.1, 131.9 (d, *J* = 3.7 Hz), 130.3, 129.8, 126.9, 126.7 (d, *J* = 11.4 Hz), 125.2 (d, *J* = 3.2 Hz), 124.6 (d, *J* = 10.2 Hz), 124.0, 121.5, 121.2, 120.0, 117.2 (d, *J* = 23.9 Hz), 116.4 ppm. **^{19}F{^{1}H} NMR** (376 MHz, $CDCl_3$) δ -115.61 ppm.

6-(2'-OTf-4-biphenyl)-2,2'-bipyridine (3.48) ***with purification***

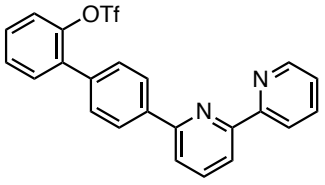

To a solution of **3.46** (476.8 mg, 1.47 mmol) and $PhNTf_2$ (577.6 mg, 1.62 mmol, 1.1 eq) in dioxane (17 mL, 0.087 M) in a microwave vial was added potassium carbonate (243.8 mg, 1.764 mmol, 1.2 eq). The mixture was heated with microwave irradiation at 120 ºC for 105 minutes. Full conversion was observed by UHPLC-MS. Water was added and the mixture extracted with EtOAc (3x), washed with brine (1x), dried with Na_2SO_4 and purified by column chromatography

(8:1 CyH:EtOAc). The product was obtained as a white solid (EtOAc/heptane) (598.6 mg, 89%). **^{1}H NMR** (500 MHz, $CDCl_3$) δ 8.71 (ddd, *J* = 4.8, 1.8, 0.9 Hz, 1H), 8.66 (dt, *J* = 8.0, 1.1 Hz, 1H), 8.39 (dd, *J* = 7.7, 1.0 Hz, 1H), 8.30 – 8.25 (m, 2H), 7.92 – 7.85 (m, 2H), 7.84 (dd, *J* = 7.8, 1.0 Hz, 1H), 7.64 – 7.60 (m, 2H), 7.56 – 7.53 (m, 1H), 7.50 – 7.41 (m, 3H), 7.35 (ddd, *J* = 7.5, 4.8, 1.2 Hz, 1H) ppm. **^{19}F{^{1}H} NMR** (471 MHz, $CDCl_3$) δ -73.83 ppm. **^{13}C{^{1}H} NMR** (126 MHz, $CDCl_3$) δ 156.4, 155.8, 155.8, 149.1, 147.0, 139.2, 137.9, 137.2, 136.4, 135.3, 132.1, 129.9, 129.6, 129.3, 128.8, 127.1, 124.0, 122.3, 121.6, 120.5, 119.8, 118.4 (q, *J* = 320.7 Hz) ppm. **HRMS** (ESI) *m/z*: $[M+H]^+$ calculated for $C_{23}H_{16}F_3N_2O_3S$ = 457.0828; found 457.0819.

6-(2'-OTf-4-biphenyl)-2,2'-bipyridine (3.48) ***for one-pot phosphine coupling***

To a solution of **3.46** (245.5 mg, 0.76 mmol) and $PhNTf_2$ (297.4 mg, 0.83 mmol, 1.1 eq) in dioxane (8.7 mL, 0.087 M) in a microwave vial was added potassium carbonate (376.5 mg, 2.73 mmol, 3.6 eq). The mixture was heated with microwave irradiation at 120 ºC for 75 minutes. Full conversion was observed by UHPLC-MS. Used to prepare **3.49** or **3.50**.

(4'-(6-[2,2'-bipyridyl])-2-biphenyl)-2,2'-tBu_2P (3.49) ***one pot*** **= L^{3}**

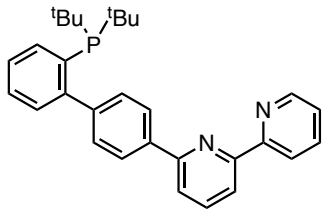

To the reaction mixture of **3.48** were added palladium acetate (5 mol %) and dppf (6 mol %). The solution was degassed by bubbling thoroughly with Ar. Di-*tert*-butylphosphine (1.3 eq) was added by syringe. The mixture was then heated at 150 ºC for 4 hours. Full conversion was observed by UHPLC-MS. After workup with saturated aqueous $NaHCO_3$ and extraction with diethyl ether (3x), the crude product was purified by column chromatography (conditions to be improved; 5:1:1 PhMe:DCM:THF or 50:1 DCM:MeOH best so far). The product was obtained as a white foam (82%). **^{1}H NMR** (400 MHz, $CDCl_3$) δ 8.70 (ddd, *J* = 4.8, 1.9, 0.9 Hz, 1H), 8.67 (dt, *J* = 8.0, 1.1 Hz, 1H), 8.35 (dd, *J* = 7.6, 1.2 Hz, 1H), 8.19 – 8.14 (m, 2H), 7.95 – 7.91 (m, 1H), 7.91 – 7.82 (m, 3H), 7.42 – 7.30 (m, 6H), 1.16 (d, *J* = 11.6 Hz, 18H) ppm. **^{13}C{^{1}H} NMR** (101 MHz, $CDCl_3$) δ 156.7, 156.5, 155.8, 149.2, 145.0 (d, *J* = 7.0 Hz), 137.8, 137.3, 137.0, 135.8 (d, *J* = 27.5 Hz), 135.6 (d, *J* = 3.3 Hz), 131.2 (d, *J* = 4.0 Hz), 130.7 (d, *J* = 6.1 Hz), 129.8, 128.6, 127.7, 126.1, 125.9, 123.8, 121.6, 120.4, 119.3, 33.0 (d, *J* = 25.0 Hz), 30.9 (d, *J* = 15.3 Hz) ppm. **^{31}P{^{1}H} NMR** (162 MHz, $CDCl_3$) δ 21.3 ppm.

(4'-(6-[2,2'-bipyridyl])-2-biphenyl)-Ad_2P (3.50) ***from purified precursor*** **= L^{4}**

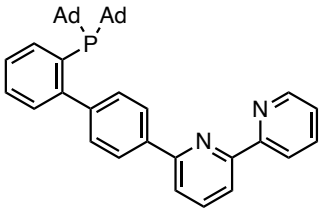

A microwave vial was charged with (a magnetic stirrer bar,) potassium carbonate (261.4 mg, 1.89 mmol, 2.5 eq), palladium acetate (8.5 mg, 37.8 µmol, 5 mol %) and dppf (25.2 mg, 45.4 µmol 6 mol %), and brought into the glovebox. Diadamantylphosphine (251.8 mg, 0.832 mmol 1.1 eq) was added and the vial sealed and brought outside. A degassed solution of **3.48** (345.4 mg, 0.757 mmol) in dioxane (8.7 mL, 0.087 M) was added via syringe to the other reagents. The mixture was heated at 150 ºC with microwave irradiation for 4 hours and the conversion was checked by UHPLC-MS. After workup with saturated aqueous $NaHCO_3$ and extraction with diethyl ether (3x), the crude was purified by column chromatography (DCM to remove impurity, then 1:1 DCM:EtOAc). The tertiary phosphine was obtained as an off-white foam (371.2 mg, 81%).**^{1}H NMR** (500 MHz, CD_2Cl_2) δ 8.73 – 8.70 (m, 2H), 8.42 (dd, *J* = 7.6, 1.1 Hz, 1H), 8.20 – 8.17 (m, 2H), 7.98 (dt, *J* = 7.1, 1.8 Hz, 1H), 7.93 (t, *J* = 7.7 Hz, 1H), 7.88 (tt, *J* = 7.8, 1.4 Hz, 2H), 7.48 – 7.43 (m, 2H), 7.43 – 7.40 (m, 2H), 7.35 (dddd, *J* = 7.4, 4.2, 3.1, 1.5 Hz, 2H), 2.02 – 1.98 (m, 6H), 1.92 (dq, *J* = 6.1, 3.2 Hz, 12H), 1.71 (d, *J* = 3.1 Hz, 12H) ppm. **^{13}C{^{1}H} NMR** (126 MHz, CD_2Cl_2) δ 156.9, 156.8, 156.3, 152.0, 151.8, 149.7, 145.8 (d, *J* = 7.3 Hz), 138.3, 137.5 (d, *J* = 31.9 Hz), 137.4, 133.8, 133.6, 131.6 (d, *J* = 3.7 Hz), 131.0 (d, *J* = 6.2 Hz), 128.8, 126.2, 124.3, 121.6, 120.7, 119.6, 42.5 (d, *J* = 12.9 Hz), 38.0 (d, *J* = 25.1 Hz), 37.5, 29.6 (d, *J* = 8.5 Hz) ppm. **^{31}P{^{1}H} NMR** (162 MHz, C_6D_6) δ 23.2 ppm. **HRMS** (ESI) *m/z*: $[M+H]^+$ calculated for $C_{42}H_{46}N_2P$ = 609.3393; found 609.3402.

L^{3}AuCl (3.51)

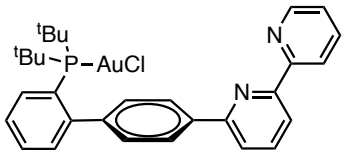

To a solution of L^3 **3.49** (356.9 mg, 0.67 mmol) in dichloromethane (13.5 mL, 0.05 M) was added (dimethylsulfide)gold(I) chloride (208.0 mg, 0.70 mmol, 1.05 eq). After stirring at room temperature for 45 minutes, the solution was filtered through a Teflon syringe filter (washed with some dichloromethane), some heptane added and concentrated to afford an off-white solid (537.0 mg, 99%). Crystals suitable for X-ray diffraction were grown by layering (CH_2Cl_2/heptane). **^{1}H NMR** (500 MHz, C_6D_6) δ 8.82 (dt, *J* = 8.0, 1.1 Hz, 1H), 8.66 (dd, *J* = 7.8, 1.0 Hz, 1H), 8.59 (ddd, *J* = 4.8, 1.8, 0.9 Hz, 1H), 8.36 – 8.33 (m, 2H), 8.00 (dd, *J* = 7.8, 1.0 Hz, 1H), 7.47 – 7.42 (m, 1H), 7.39 (t, *J* = 7.8 Hz, 1H), 7.29 – 7.26 (m, 2H), 7.14 (ddd, *J* = 7.7, 4.4, 1.6 Hz, 1H), 7.04 (tt, *J* = 7.5, 1.5 Hz, 1H), 6.88 – 6.83 (m, 2H), 6.81 – 6.77 (m, 1H), 6.73 (ddd, *J* = 7.4, 4.8, 1.2 Hz, 1H), 1.02 (d, *J* = 15.4 Hz, 18H) ppm. **^{13}C{^{1}H} NMR** (126 MHz, C_6D_6) δ 157.3 (d, *J* = 13.8 Hz), 156.0, 150.6 (d, *J* = 13.7 Hz), 149.2, 142.5 (d, *J* = 6.4 Hz), 141.1, 137.8, 136.6, 134.6, 133.6 (d, *J* = 2.4 Hz), 133.5 (d, *J* = 7.3 Hz), 130.6 (d, *J* = 2.3 Hz), 129.7, 129.4, 128.6, 123.8, 123.5, 122.3, 121.6, 119.9, 37.4 (d, *J* = 25.3 Hz), 30.6 (d, *J* = 6.8 Hz) ppm. **^{31}P{^{1}H} NMR** (202 MHz, C_6D_6) δ 59.3 ppm. **HRMS** (ESI) *m/z*: $[M+H]^+$ calculated for $C_{30}H_{34}AuClN_2P$ = 685.1808; found 685.1817; $[M+Na]^+$ calculated for $C_{30}H_{33}AuClN_2NaP$ = 707.1628; found 707.1629.

L^4AuCl (3.52)

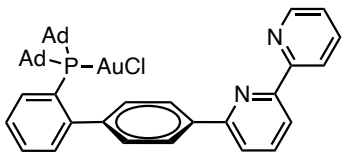

To a solution of L^4 **3.50** (351.2 mg, 0.58 mmol) in dichloromethane (11.5 mL, 0.05 M) was added (dimethylsulfide)gold(I) chloride (178.4 mg, 0.60 mmol, 1.05 eq). After stirring at room temperature for 16 hours (NOTE: purely practical, metallation is over within 2 hours), the solution was filtered through a Teflon syringe filter (washed with some dichloromethane), some heptane added and concentrated to afford an off-white solid (484.0 mg, quant.). **^{1}H NMR** (500 MHz, CD_2Cl_2) δ 8.69 (ddd, *J* = 4.8, 1.8, 0.9 Hz, 1H), 8.66 (dt, *J* = 8.0, 1.1 Hz, 1H), 8.39 (dd, *J* = 7.7, 1.1 Hz, 1H), 8.19 – 8.17 (m, 2H), 7.98 (dd, *J* = 7.8, 1.1 Hz, 1H), 7.95 – 7.91 (m, 2H), 7.86 (td, *J* = 7.7, 1.8 Hz, 1H), 7.59 – 7.52 (m, 2H), 7.34 (dddd, *J* = 10.0, 7.5, 4.5, 1.7 Hz, 2H), 7.32 – 7.29 (m, 2H), 2.24 (ddt, *J* = 11.6, 5.4, 3.0 Hz, 6H), 2.15 (ddt, *J* = 11.9, 5.9, 2.8 Hz, 6H), 2.01 (dt, *J* = 5.8, 3.0 Hz, 6H), 1.70 (q, *J* = 2.6 Hz, 12H) ppm. **^{13}C{^{1}H} NMR** (126 MHz, CD_2Cl_2) δ 157.1 (d, *J* = 19.0 Hz), 156.0, 150.8 (d, *J* = 12.9 Hz), 149.6, 143.7 (d, *J* = 6.6 Hz), 140.0, 138.2, 137.3, 135.3 (d, *J* = 2.3 Hz), 133.7 (d, *J* = 7.2 Hz), 130.9 (d, *J* = 2.2 Hz), 130.3, 127.8, 127.1 (d, *J* = 6.6 Hz), 124.3, 124.2, 124.0, 121.7, 121.6, 119.7, 43.1 (d, *J* = 23.6 Hz), 42.7 (d, *J* = 2.6 Hz), 36.9 (d, *J* = 1.5 Hz), 29.4 (d, *J* = 9.8 Hz) ppm. **^{31}P{^{1}H} NMR** (202 MHz, CD_2Cl_2) δ 64.7 ppm. **HRMS** (ESI) *m/z*: $[M+H]^+$ calculated for $C_{42}H_{46}AuClN_2P$ = 841.2747; found 841.2741; $[M+Na]^+$ calculated for $C_{42}H_{45}AuClN_2NaP$ = 863.2567; found 863.2559.

L^3Au(phenylacetylide) (3.58)

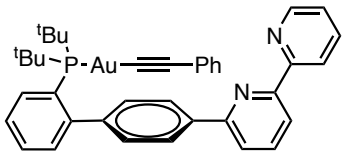

To a solution of L^3AuCl **3.51** (96.7 mg, 140 µmol) and phenylacetylene (57.6 mg, 570 µmol, 4 eq) in toluene (0.7 mL) was added potassium hexamethyldisilazide (56 mg, 280 µmol, 2 eq) and the mixture stirred for 2 hours at 23 ºC. The reaction was quenched with water and diluted with ethyl acetate. Saturated brine was added, the layers separated and the aqueous phase extracted with ethyl acetate (2x). The combined organic fractions were dried with anhydrous sodium sulfate, concentrated by rotary evaporation. Purification by column chromatography (7:1 toluene:acetonitrile) yielded the gold phenylacetylide as an off-white solid (99.9 mg, 94%). **^{1}H NMR** (400 MHz, C_6D_6) δ 8.82 (dt, *J* = 8.0, 1.1 Hz, 1H), 8.66 (dd, *J* = 7.8, 0.9 Hz, 1H), 8.59 (ddd, *J* = 4.8, 1.9, 0.9 Hz, 1H), 8.52 – 8.49 (m, 2H), 7.81 (dd, *J* = 7.8, 1.0 Hz, 1H), 7.51 (ddd, *J* = 8.0, 6.6, 1.4 Hz, 1H), 7.38 – 7.34 (m, 2H), 7.28 – 7.20 (m, 4H), 7.07 – 6.95 (m, 4H), 6.82 (dd, *J* = 5.1, 2.0 Hz, 2H), 6.73 (ddd, *J* = 7.4, 4.7, 1.2 Hz, 1H), 1.09 (d, *J* = 14.8 Hz, 18H) ppm. **DEPT-135 ^{13}C{^{1}H} NMR** (101 MHz, C_6D_6) δ 149.0, 137.4, 136.2, 134.3, 133.0 (d, *J* = 7.1 Hz), 132.0, 130.0, 129.5, 128.3, 128.1, 127.6, 126.3, 125.1, 123.2, 121.3 (d, *J* = 2.9 Hz), 119.5, 30.5 (d, *J* = 7.0 Hz) ppm. **^{31}P{^{1}H} NMR** (162 MHz, C_6D_6) δ 67.8 ppm.

L^3Au(*p*-chlorophenylacetylide) (3.59)

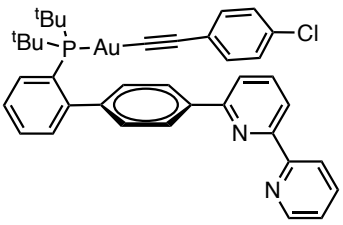

To a solution of L^3AuCl **3.51** (35.1 mg, 51 μmol) and *p*-chlorophenylacetylene (21.0 mg, 154 μmol, 3 eq) in toluene (0.3 mL) was added potassium hexamethyldisilazide (20 mg, 102 μmol, 2 eq) and the mixture stirred for 15 hours at 23 ºC. The reaction was quenched with water, diluted with dichloromethane and extracted with dichloromethane (2x). The combined organic fractions were dried with anhydrous sodium sulfate, concentrated by rotary evaporation, washed with minimal heptane and dried under high vacuum to remove residual *p*-chlorophenylacetylene. White powder (39.9 mg, 99%). **^{1}H NMR** (500 MHz, CD_2Cl_2) δ 8.69 (ddd, *J* = 4.8, 1.8, 0.9 Hz, 1H), 8.62 (dt, *J* = 8.0, 1.1 Hz, 1H), 8.36 – 8.32 (m, 2H), 8.28 (dd, *J* = 7.8, 0.9 Hz, 1H), 7.93 (ddd, *J* = 8.4, 6.9, 1.5 Hz, 1H), 7.87 – 7.81 (m, 2H), 7.63 (t, *J* = 7.8 Hz, 1H), 7.59 – 7.50 (m, 2H), 7.38 – 7.32 (m, 4H), 6.80 – 6.77 (m, 2H), 6.65 – 6.60 (m, 2H), 1.44 (d, *J* = 15.0 Hz, 18H) ppm. **^{13}C{^{1}H} NMR** (126 MHz, CD_2Cl_2) δ 156.9, 156.4, 156.1, 150.4 (d, *J* = 15.1 Hz), 149.6, 143.9 (d, *J* = 6.2 Hz), 139.3, 138.0, 137.2, 136.0, 135.2, 133.4 (d, *J* = 7.3 Hz), 133.2, 131.4, 131.0, 130.9, 130.3, 128.1, 127.9, 127.5 (d, *J* = 6.0 Hz), 125.2 (d, *J* = 2.6 Hz), 124.2, 121.6, 121.0, 119.7, 101.0 (d, *J* = 23.5 Hz), 38.0 (d, *J* = 22.5 Hz), 31.4 (d, *J* = 6.9 Hz) ppm. **^{31}P{^{1}H} NMR** (202 MHz, CD_2Cl_2) δ 67.6 ppm.

L^3{AuCl}{$CuCl_2$} (3.53)

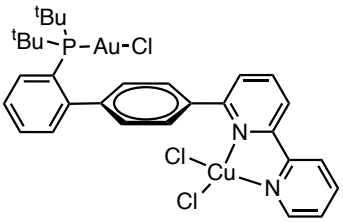

To a solution of L^3AuCl **3.51** (82.4 mg, 0.12 mmol) in a 1:1 mixture of 1-propanol:acetone (12.0 mL) was added copper(II) choride (18.0 mg, 0.13 mmol, 1.1 eq) and stirred at 23 ºC, with the mixture gradually turning orange. After 19 h, the solvent was removed *in vacuo*. The orange residue was redissolved in dichloromethane and filtered through a Teflon syringe filter (washing with dichloromethane 2x), concentrated to ca. 1 mL and precipitated with heptane (3 mL). The supernatant was removed with a pipette to remove any organic impurities. The remaining solid and residual solvent were dried in vacuo to afford the title bimetallic complex as an orangeish brown powder (87.2 mg, 89%). Crystals suitable for X-ray diffraction were grown by vapour diffusion of pentane into a dichloroethane solution. **HRMS** (MALDI) *m/z*: $[M\text{-}Cl]^+$ calculated for $C_{30}H_{33}AuCl_2CuN_2P$ = 782.0715; found = 782.0715. **Melting point** (CH_2Cl_2/heptane): >190 ºC (dec.). **FTIR** (neat): 3077 (w), 2958 (w), 1597 (m), 1569 (w), 1450 (s), 1375 (m), 1204 (s), 1140 (m), 942 (w), 819 (w), 786 (s, bpy C-H bend), 763 (m, "top" Ar C-H bend), 601 (w) cm^{-1}.

L^4{AuBr}{$CoBr_2$} (3.54)

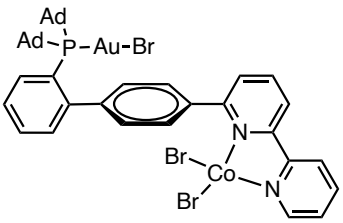

To a solution of L^4AuCl **3.52** (41.7 mg, 50 μmol) in a 1:1 mixture of ethyl acetate:dichloroethane (1.2 mL) with a drop of water was added cobalt(II) bromide (18.0 mg, 0.13 mmol, 2 eq) and stirred at 23 ºC for 24 h. The mixture was concentrated *in vacuo* to yield the product mixed

with hydrated cobalt(II) halides. The solid was dissolved in dichloromethane and filtered through a Teflon syringe filter (washing with dichloromethane 2x). After the addition of heptane, the product was concentrated to yield [AuCo] as a deep turquoise solid (51.8 mg, 95%). Crystals suitable for X-ray diffraction were grown from an acetonitrile:dichloromethane solution at 45 ºC. **^{1}H pNMR** (400 MHz, CD_2Cl_2) δ 29.45, 7.23, 6.90, 4.52, 4.21, 4.00, 3.77, 2.83, 2.06, 1.92, 1.44, 1.18, 0.95, 0.78, 0.54, -0.03, -0.33, -0.77, -1.51, -2.44, -4.78, -9.55, -10.16, -10.46, -13.06, -18.03, -18.73, -19.63, -28.18, -32.59, -33.09 ppm. **^{31}P{^{1}H} pNMR** (162 MHz, CD_2Cl_2) δ 61.8 ppm. **HRMS** (MALDI) *m/z*: $[M\text{-}Br]^+$ calculated for $C_{30}H_{33}AuBr_2CoN_2P$ = 1022.0679; found = 1022.0635. **Melting point** (CH_2Cl_2/heptane): >240 ºC (dec.). **FTIR** (neat): 2903 (s, Ad), 2849 (s, Ad), 1598 (m), 1570 (w), 1450 (s), 1206 (m), 1142 (m), 819 (w), 778 (m), 530 (w) cm^{-1}.

L^4{AuCl}{PdCl$_2$} (3.63)

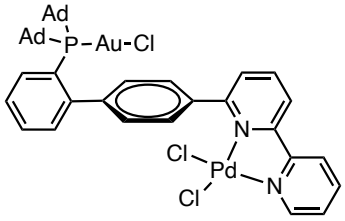

To a solution of L^{4}AuCl (74.8 mg, 89 μmol) in dichloromethane (1.8 mL) was added bis(benzonirile)palladium(II) chloride (34.1 mg, 89 μmol, 1 eq) and stirred at 23 ºC for 3 h, during which the solution became cloudy. The mixture was concentrated *in vacuo* to give a mixture of orange and yellow solids. The solid was dissolved in dichloromethane and filtered through a Teflon syringe filter (washing with dichloromethane 2x). After the addition of heptane, the product was concentrated to yield [AuPd] as a yellow solid (68.1 mg, 75%). **Melting point** (CH_2Cl_2/heptane): >215 ºC (dec.). **FTIR** (neat): 3054 (w), 2902 (s, Ad), 2848 (m, Ad), 1596 (m), 1424 (m), 1203 (m), 1141 (m), 942 (w), 774 (m), 601 (w) cm^{-1}.

L^4{AuCl}{AuCl} (3.69) Procedure A

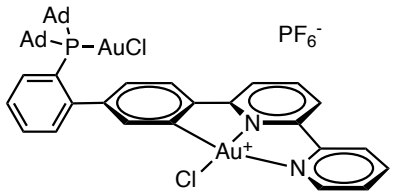

Gold(III) acetate (22.5 mg, 0.06 mmol, 1.0225 eq) and L^{4}AuCl **3.52** (49.5 mg, 0.059 mmol) were dissolved in acetic acid (2 mL, 0.03 M) and stirred at 80 ºC for 3 hours. Ammonium chloride (31.5 mg, 0.59 mmol, 10 eq) was added and the mixture stirred for 1 hour. After cooling, the mixture was filtered through a Teflon syringe filter, rinsed with acetic acid (2x) and ethyl acetate (1x) to give a yellow solution that was concentrated *in vacuo* to give a viscous red gel. The semisolid residue was redissolved in a 1:1 MeOH:EtOAc solution of ammonium hexafluorophosphate (95.9 mg, 0.59 mmol, 10 eq), concentrated and redissolved in MeOH with minimum EtOAc. The product was fully precipitated with deionised water, filtered through paper, the solid washed with water and recovered by redissolving the residue on the filter with dichloromethane. The solution was then concentrated and dried under high vacuum. The redissolved solid in dichloromethane was re-filtered through a Teflon syringe filter to remove residual ammonium salts and concentrated to give the product as a yellow powder (66.6 mg, 93%). Crystals suitable for X-ray

diffraction were grown from a toluene solution with minimal *o*-difluorobenzene at 50 ºC. **^{1}H NMR** (400 MHz, CD_2Cl_2) δ 8.99 – 8.96 (m, 1H), 8.55 (dt, *J* = 8.0, 1.1 Hz, 1H), 8.45 (td, *J* = 7.9, 1.7 Hz, 2H), 8.33 – 8.29 (m, 1H), 8.11 (ddd, *J* = 8.2, 6.9, 0.9 Hz, 1H), 7.96 (dddd, *J* = 9.6, 7.2, 5.5, 1.8 Hz, 2H), 7.72 (d, *J* = 7.9 Hz, 1H), 7.68 – 7.59 (m, 3H), 7.44 – 7.41 (m, 1H), 7.31 (dd, *J* = 7.9, 1.6 Hz, 1H), 2.24 – 1.98 (m, 18H), 1.75 – 1.65 (m, 12H) ppm. **^{31}P{^{1}H} NMR** (202 MHz, CD_2Cl_2) δ 65.36 (s, 1P), -141.48 (hex, $^1J_{PF}$ = 712.6 Hz, 1P) ppm. **HRMS** (ESI) *m/z*: $[M+H]^+$ calculated for $C_{42}H_{44}Au_2Cl_2N_2P$ = 1071.1945; found = 1071.1928. **Melting point** (CH_2Cl_2/heptane): >190 ºC (dec.). **FTIR** (neat): 2904 (s, Ad), 2850 (m, Ad), 1601 (w), 1566 (w), 1503 (w), 1445 (m), 1201 (s), 1136 (m), 838 (s), 776 (m), 607 (w), 557 (m) cm^{-1}.

L^4{AuCl}{AuCl} (EGP-05-P16) Procedure B

A solution of L^{4}AuCl **3.52** (100 mg, 119 µmol), sodium tetrachloroaurate (43 mg, 119 µmol, 1 eq) and silver triflate (92 mg, 357 µmol, 3 eq) were dissolved in acetonitrile (8 mL) and stirred at 80 ºC for 18 hours. The reaction mixture was cooled to 40 ºC, ammonium chloride (60 mg, 8 eq) was added and the mixture stirred for 3 hours. The solution was filtered through Teflon, the solid residue washed with dichloromethane (1x) and the filtrate concentrated *in vacuo*. The crude digold complex was then redissolved in dichloromethane (2 mL) and ammonium hexafluorophosphate (80 mg, 4 eq, solution in 1 mL MeOH) and stirred for 30 minutes. The mixture was concentrated, redissolved in dichloromethane and filtered through Teflon syringe filters, washing with dichloromethane (2x). Concentration of the filtrate afforded the title bimetallic complex as a yellow powder (122 mg, 84%). Analytical data of this product matched that of the complex prepared with Procedure A, but subsequent repeats with procedure B were more reproducible in the scale-up.

Substrates and Reactions

2'-(4-(*tert*-butyl)phenylethynyl)acetophenone (3.86)

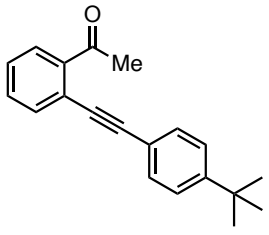

A solution of 2'-iodoacetophenone (1550 mg, 6.30 mmol), 4-*tert*-butylphenylacetylene (1200 mg, 7.56 mmol, 1.2 eq), bis(triphenylphosphine)palladium(II) chloride (44 mg, 63 µmol, 1 mol%) and copper(I) iodide (24 mg, 126 µmol, 2 mol%) in anhydrous tetrahydrofuran (12.6 mL, 0.5 M) was degassed by bubbling with argon. To the stirring solution was added triethylamine (1.8 mL, 12.6 mmol, 2 eq) and the solution turned black. The reaction was stirred at 23 ºC for 18 hours. After completion, the mixture was filtered through diatomaceous earth and washed with ethyl acetate. Saturated aqueous ammonium chloride was then added and the mixture extracted with ethyl acetate (3x). The combined organic fractions were dried over Na_2SO_4 and

concentrated by rotary evaporation. Purification by column chromatography (10:1 CyH:EtOAc) afforded the title compound as an orange oil (1690 mg, 97%). **^{1}H NMR** (400 MHz, $CDCl_3$) δ 7.75 (ddd, *J* = 7.8, 1.5, 0.6 Hz, 1H), 7.62 (ddd, *J* = 7.7, 1.4, 0.6 Hz, 1H), 7.50 – 7.45 (m, 3H), 7.43 – 7.37 (m, 3H), 2.80 (s, 3H), 1.33 (s, 9H) ppm.

(*E*)-1-(2-((4-(*tert*-butyl)phenyl)ethynyl)phenyl)-3-(3,5-dimethylphenyl)prop-2-en-1-one (3.64)

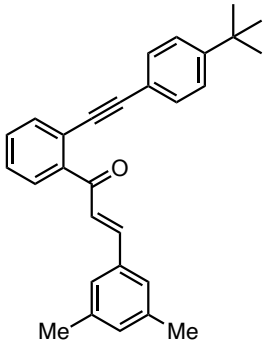

To a cooled solution of **3.86** (1511 mg, 5.47 mmol)and 3,5-dimethylbenzaldehyde (880 mg, 6.56 mmol, 1.2 eq) in ethanol (14 mL, 0.4 M) at 0 ºC was added dropwise aqueous sodium hydroxide (660 mg, 3 eq, 2 M in water). The temperature was allowed to rise to 23 ºC, the mixture sonicated for 30 minutes and stirred for 12 hours at the same temperature. The mixture was added to saturated aqueous NH_4Cl and extracted with diethyl ether (2x). The organic fractions were dried over Na_2SO_4 and concentrated by rotary evaporation. Column chromatography (1:2 CyH:PhMe) yielded the title chalcone as a yellow oil (1998 mg, 89%). **^{1}H NMR** (500 MHz, C_6D_6) δ 7.87 (d, *J* = 15.9 Hz, 1H), 7.78 – 7.73 (m, 2H), 7.55 – 7.51 (m, 1H), 7.44 – 7.41 (m, 2H), 7.03 – 6.99 (m, 4H), 6.98 – 6.96 (m, 2H), 6.70 (td, *J* = 1.7, 0.9 Hz, 1H), 1.97 (q, *J* = 0.7 Hz, 6H), 1.07 (s, 9H) ppm. **^{13}C{^{1}H} NMR** (126 MHz, C_6D_6) δ 192.5, 151.9, 144.4, 142.9, 138.3, 135.5, 133.3, 132.3, 131.9, 130.8, 129.4, 128.5, 126.9, 126.0, 125.6, 122.3, 120.4, 96.4, 88.5, 34.7, 31.1, 21.0 ppm.

11-(4-(*tert*-butyl)phenyl)-8,10-dimethyl-6,6a-dihydro-5*H*-benzo[*a*]fluorene (3.65)*, by [AuRu]-catalysed deoxygenative alkynylchalcone cyclisation*

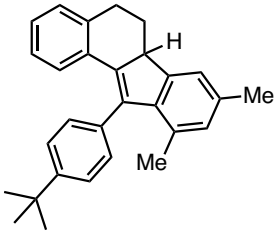

Chalcone **3.64** (75.2 mg, 192 µmol), phenylsilane (118 µL, 960 µmol, 5 eq) and sodium tetrakis[3,5-bis(trifluoromethyl)phenyl]borate (34.0 mg, 38.3 µmol, 20 mol%) were dissolved in dichloromethane (1.5 mL) and degassed by bubbling with argon. To the stirred reaction mixture was added a degassed solution of [AuRu] complex **3.66** (8.6 mg, 9.6 µmol, 5 mol%) in dichloromethane (0.5 mL) by syringe. After 75 minutes, two drops of triethylamine were added to quench the reaction, with the mixture dry loaded on silica gel. Purification by column chromatography (cyclohexane or 17:2 pentane:toluene) afforded the product as a white solid (66.8 mg, 92%). Crystallisation from ethyl acetate at -20 ºC afforded crystals suitable for XRD. **^{1}H NMR** (500 MHz, C_6D_6) δ 7.49 (dd, *J* = 8.0, 1.9 Hz, 1H), 7.40 (dd, *J* = 8.0, 2.1 Hz, 1H), 7.31 (ddd, *J* = 7.8, 5.5, 1.6 Hz, 1H), 7.26 (dd, *J* = 8.0, 2.1 Hz, 1H), 7.18 (dd, *J* = 7.9, 1.9 Hz, 1H), 7.10 (d, *J* = 1.4 Hz, 1H), 7.00 (d, *J* = 7.5 Hz, 1H), 6.90 (td, *J* = 7.5, 1.4 Hz, 1H), 6.79 (s, 1H), 6.76 (d, *J* = 7.6 Hz, 1H), 3.49 (dd, *J* = 13.4, 4.4 Hz, 1H), 2.88 (dd, *J* = 12.6, 5.2 Hz, 1H), 2.80 (ddd, *J* = 16.8, 5.2, 1.5 Hz, 1H), 2.42 (dtd, *J* = 12.1, 5.1, 2.0 Hz, 1H), 2.30 (s, 3H), 1.95 (s, 3H), 1.58 (qd, *J* = 12.8, 5.2 Hz, 1H), 1.26 (s, 9H) ppm. **^{13}C{^{1}H} NMR** (126 MHz, C_6D_6) δ 150.4, 147.3, 142.0, 141.9, 138.5, 137.7, 137.4, 134.6, 133.3, 131.8, 131.4,

130.5, 129.4, 128.9, 127.1, 127.0, 126.3, 126.0, 125.8, 121.7, 49.2, 34.6, 31.5, 31.1, 29.3, 21.4, 20.0 ppm. **HRMS** (APCI) *m/z*: $[M+H]^+$ calculated for $C_{29}H_{31}$ = 379.2420; found = 379.2422. **Melting point** (EtOAc): 192.5–194.0 ºC.

Control reaction with [SPhosAu(NCMe)]SbF_6

Chalcone **3.64** (37.6 mg, 96 μmol) and phenylsilane (59 μL, 480 μmol, 5 eq) were dissolved in dichloromethane (0.8 mL) and degassed by bubbling with argon. To the stirred reaction mixture was added a degassed solution of [SPhosAu(NCMe)]SbF_6 (3.1 mg, 4.8 μmol, 5 mol%) in dichloromethane (0.3 mL) by syringe. Aliquots were taken for UHPLC-MS analysis. After 18 hours, no conversion was observed. Quenching with triethylamine and running a crude NMR showed only starting material.

Control reaction with ruthenium chloride and bipyridine ligand

6-(4-chlorophenyl)-2,2'-bipyridine (2.0 mg, 7.4 μmol, 5 mol%) and ruthenium(III) chloride hydrate (2.0 mg, 7.4 μmol, 5 mol%) were dissolved/suspended in degassed dichloromethane (1.8 mL) and stirred for 10 minutes at 23 ºC. Chalcone **3.64** (58.0 mg, 148 μmol), sodium tetrakis[3,5-bis(trifluoromethyl)phenyl]borate (26.2 mg, 30 μmol, 20 mol%) and phenylsilane (90 μL, 740 μmol, 5 eq) were sequentially added over a flow of argon. Aliquots were taken for UHPLC-MS analysis. After 18 hours, no conversion was observed. Filtering through silica gel and running a crude NMR showed only starting material.

[AuAu] cyclisation of N-propargylbenzamide under silver-free conditions

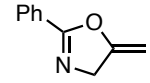

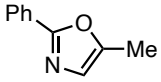

To a solution of N-propargylbenzamide (16 mg, 0.10 mmol) in dichloromethane (1 mL, 0.1 M) was added **3.69** (6.1 mg, 5.0 μmol, 5 mol%). The mixture was stirred at 24 ºC for 4 h, after which the reaction was quenched with a drop of triethylamine and concentrated *in vacuo*. Conversion determined by NMR: 70%. Product ratio **3.72**:**3.73** of 97:3. NMR data consistent with literature values.[69]

[AuAu] cyclisation of N-propargylbenzamide with silver hexafluoroantimonate

To a solution of N-propargylbenzamide (8 mg, 50 μmol) in dichloromethane (1 mL, 0.05 M) was added **3.69** (3.0 mg, 2.5 μmol, 5 mol%) and silver hexafluoroantimonate (1.8 mg, 5.2 μmol, 10 mol%). The mixture was stirred at 24 ºC for 4 h, after which the reaction was quenched with a drop of triethylamine and concentrated *in vacuo*. Conversion determined by NMR: 100%. Product ratio **3.72**:**3.73** of 86:14.

69 Tzouras, N. V.; Gobbo, A.; Pozsoni, N. B.; Chalkidis, S. G.; Bhandary, S.; Van Hecke, K.; Vougioukalakis, G. C.; Nolan, S. P. Hydrogen Bonding-Enabled Gold Catalysis: Ligand Effects in Gold-Catalyzed Cycloisomerizations in Hexafluoroisopropanol (HFIP). *Chem. Commun.* **2022**, *58*, 8516–8519.

[AuAu] cyclisation of N-propargylbenzamide with silver trifluoromethanesulfonate

To a solution of N-propargylbenzamide (8 mg, 50 µmol) in dichloromethane (1 mL, 0.05 M) was added **3.69** (3.0 mg, 2.5 µmol, 5 mol%) and silver trifluoromethanesulfonate (1.8 mg, 7.0 µmol, 10 mol%). The mixture was stirred at 24 ºC for 4 h, after which the reaction was quenched with a drop of triethylamine and concentrated *in vacuo*. Conversion determined by NMR: 100%. Product ratio **3.72**:**3.73** of 100:0.

Hydroamination of phenylacetylene and one-pot hydrolysis

To a solution of phenylacetylene (10 mg, 100 µmol) in dichloromethane (0.5 mL, 0.2 M) was added **3.69** (3 mg, 5 µmol, 5 mol%) and aniline (46 mg, 0.5 mmol, 5 eq). The mixture was stirred at 24 ºC for 24 h. After this time, aqueous HCl (1 M, 1 mL) was added and stirred for 30 minutes. The biphasic mixture was then extracted with EtOAc (3x), dried over $MgSO_4$ and concentrated in vacuo. Full conversion to acetophenone with NMR data consistent with literature values.[70]

3-prenylindene (3.75) and 2-(2-methoxyisopropyl)-1-methyleneindane (3.76)

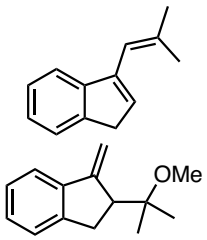

To a solution of 2-prenylphenylacetylene (9 mg, 50 µmol) and methanol (21 µL, 0.5 mmol, 10 eq) in dichloromethane (1 mL, 0.05 M) was added **3.69** (3 mg, 2.5 µmol, 5 mol%). The mixture was stirred at 24 ºC for 4 h, then quenched with a drop of triethylamine and concentrated, showing full conversion. Skeletal rearrangement product **3.75** and alkoxycyclisation product **3.76** were found in a 4:1 ratio. NMR data consistent with literature values.[71,60]

***cis*- (3.79a) and *trans*-1-(2-phenylcyclopropyl)isobutenyl pivalate (3.79b)**

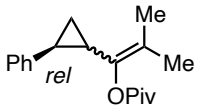

To a solution of 2-methylbut-3-yn-2-yl pivalate (16.8 mg, 100 µmol) and styrene (20.8 mg, 200 µmol, 2 eq) in 1,2-dichloroethane (1 mL, 0.1 M) was added **3.69** (6.1 mg, 5.0 µmol, 5 mol%). The reaction was stirred at 24 ºC for 4 h, quenched with a drop of triethylamine and concentrated *in vacuo*. Products formed as a *cis*:*trans* (**3.79a**:**3.79b**) mixture in a 17:3 ratio. NMR data consistent with literature values.[72]

4-(2-indolyl)-2-phenyl-4,5,6,7-tetrahydrobenzofuran (3.82)

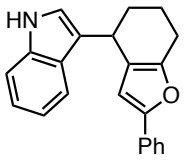

To a solution of 2-(phenylethynyl)-2-cyclohexen-1-one (19.7 mg, 100 µmol) and indole (23.5 mg, 200 µmol, 2 eq) in 1,2-dichloroethane (1 mL, 0.1 M) was added **3.69** (6.1 mg, 5.0 µmol, 5 mol%). The reaction was stirred at 24 ºC for 4 h, quenched with

70 Roydhouse, M. D.; Motherwell, W. B.; Constantinou, A.; Gavriilidis, A.; Wheeler, R.; Down, K.; Campbell, I. Ozonolysis of Some Complex Organic Substrates in Flow. *RSC Adv.* **2013**, *3*, 5076.

71 Álvarez-Pérez, M.; Frutos, M.; Viso, A.; Fernández De La Pradilla, R.; De La Torre, M. C.; Sierra, M. A.; Gornitzka, H.; Hemmert, C. Gold(I)-Catalyzed Cycloisomerization–Dimerization Cascade of Benzene-Tethered 1,6-Enynes. *J. Org. Chem.* **2017**, *82*, 7546–7554.

72 Johansson, M. J.; Gorin, D. J.; Staben, S. T.; Toste, F. D. Gold(I)-Catalyzed Stereoselective Olefin Cyclopropanation. *J. Am. Chem. Soc.* **2005**, *127*, 18002–18003.

a drop of triethylamine and concentrated *in vacuo*. Full conversion. **3.82** (yield n. d.), NMR data consistent with literature values.[60]

(*Z*)-3-tosyl-2,3,4,7-tetrahydro-1*H*-azocino[5,4-*b*]indole (3.84)

Silver-free 8-*endo*-dig cyclisation

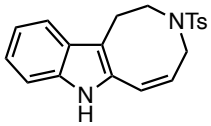

To a solution of N-tosyl-N-propargyl-2-(3-indolyl)-ethylamine (35.2 mg, 100 μmol) in dichloromethane (1 mL, 0.1 M) was added **3.69** (6.1 mg, 5 μmol, 5 mol%). The reaction was stirred at 24 ºC for 4 h, after which a drop of triethylamine was added to quench it, the mixture filtered through Celite and concentrated *in vacuo*. Conversion determined by NMR: 65%, with only product **3.84** observed. **^{1}H NMR** (500 MHz, $CDCl_3$) δ 7.55 – 7.51 (m, 2H), 7.42 (dq, *J* = 8.0, 0.9 Hz, 1H), 7.32 (dt, *J* = 8.0, 0.7 Hz, 1H), 7.26 – 7.24 (m, 2H), 7.18 – 7.15 (m, 2H), 6.50 (dt, *J* = 11.3, 1.2 Hz, 1H), 5.85 (dt, *J* = 11.2, 6.6 Hz, 1H), 3.98 (dd, *J* = 6.7, 1.2 Hz, 2H), 3.56 – 3.54 (m, 2H), 2.99 – 2.96 (m, 2H), 2.35 (s, 3H) ppm.

8-*endo*-dig cyclisation with 1:1 [AuAu]:[Ag]

To a solution of N-tosyl-N-propargyl-2-(3-indolyl)-ethylamine (35.2 mg, 100 μmol) in dichloromethane (1 mL, 0.1 M) was added **3.69** (6.1 mg, 5 μmol, 5 mol%) and silver hexafluoroantimonate (1.7 mg, 5 μmol, 5 mol%). The reaction was stirred at 24 ºC for 18 h, after which a drop of triethylamine was added to quench it, the mixture filtered through Celite and concentrated *in vacuo*. Conversion determined by NMR: 100%, with only product **3.84** observed.

8-*endo*-dig cyclisation with 1:2 [AuAu]:[Ag]

To a solution of N-tosyl-N-propargyl-2-(3-indolyl)-ethylamine (35.2 mg, 100 μmol) in dichloromethane (1 mL, 0.1 M) was added **3.69** (6.1 mg, 5 μmol, 5 mol%) and silver hexafluoroantimonate (3.4 mg, 10 μmol, 10 mol%). The reaction was stirred at 24 ºC for 18 h, after which a drop of triethylamine was added to quench it, the mixture filtered through Celite and concentrated *in vacuo*. Conversion determined by NMR: 100%, with only product **3.84** observed.

Crystal Structures

Crystal data and structure refinement for mo_VP05_0m.

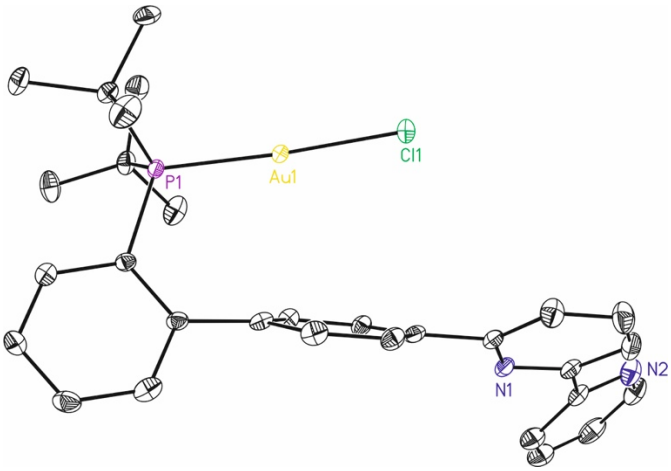

Identification code	mo_VP05_0m		
Empirical formula	$C_{30}H_{33}AuClN_2P$		
Formula weight	684.97		
Temperature/K	100(2)		
Crystal system	orthorhombic		
Space group	P 2_1 2_1 2_1		
a/Å	9.5918(7)	α/°	90
b/Å	14.8873(11)	β/°	90
c/Å	18.5922(14)	γ/°	90
Volume/Å^3	2654.9(3)		
Z	4		
ρ_{calc}g/cm^3	1.714		
μ/mm^{-1}	5.724		
F(000)	1352		
Crystal size/mm^3	0.2 × 0.1 × 0.1		
Radiation	MoKα (λ = 0.71073)		
Θ range for data collection/°	1.752 to 30.194°		
Index ranges	-13 ≤ h ≤ 13,-21 ≤ k ≤ 20,-26 ≤ l ≤ 26		
Reflections collected	34965		
Independent reflections	7318 [R(int) = 0.0290]		
Data/restraints/parameters	7318/0/322		
Goodness-of-fit on F^2	0.995		
Final R indexes [I>=2σ (I)]	R_1 = 0.0168, wR_2 = 0.0407		
Final R indexes [all data]	R_1 = 0.0174, wR_2 = 0.0409		
Largest diff. peak/hole / e Å^{-3}	1.709/-0.926		

Crystal data and structure refinement for mo_VP07b_0m_a.

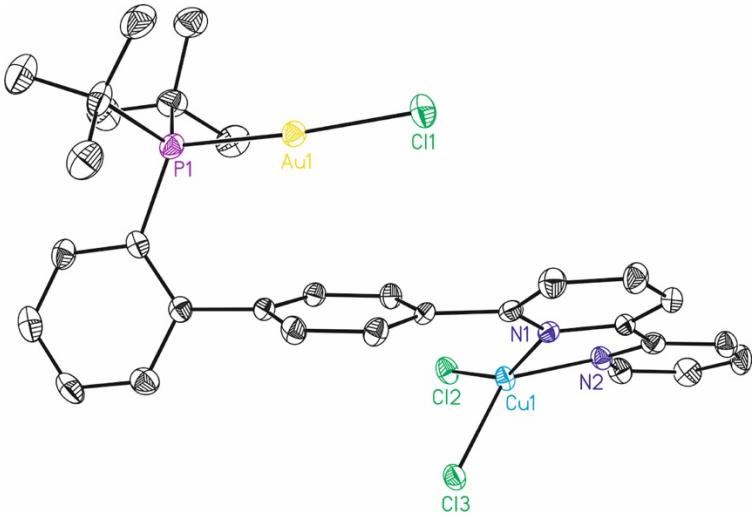

Identification code	mo_VP07b_0m_a		
Empirical formula	$C_{32}H_{37}N_2PCuAuCl_3$		
Formula weight	918.36		
Temperature/K	100(2)		
Crystal system	monoclinic		
Space group	$P2_1/c$		
a/Å	13.0860(8)	α/°	90
b/Å	15.8795(10)	β/°	97.454(2)
c/Å	16.4518(10)	γ/°	90
Volume/Å^3	3389.8(4)		
Z	4		
ρ_{calc}g/cm^3	1.799		
μ/mm^{-1}	5.417		
F(000)	1804		
Crystal size/mm^3	0.10 × 0.05 × 0.05		
Radiation	MoKα (λ = 0.71073)		
Θ range for data collection/°	1.569 to 25.680		
Index ranges	$-15 \le h \le 15$, $-19 \le k \le 19$, $-20 \le l \le 20$		
Reflections collected	80270		
Independent reflections	6431 [R_{int} = 0.0506]		
Data/restraints/parameters	6431/32/412		
Goodness-of-fit on F^2	1.047		
Final R indexes [I>=2σ (I)]	R_1 = 0.0319, wR_2 = 0.0837		
Final R indexes [all data]	R_1 = 0.0384, wR_2 = 0.0878		
Largest diff. peak/hole / e Å^{-3}	2.519/-1.498		

Crystal data and structure refinement for egp-vp18.

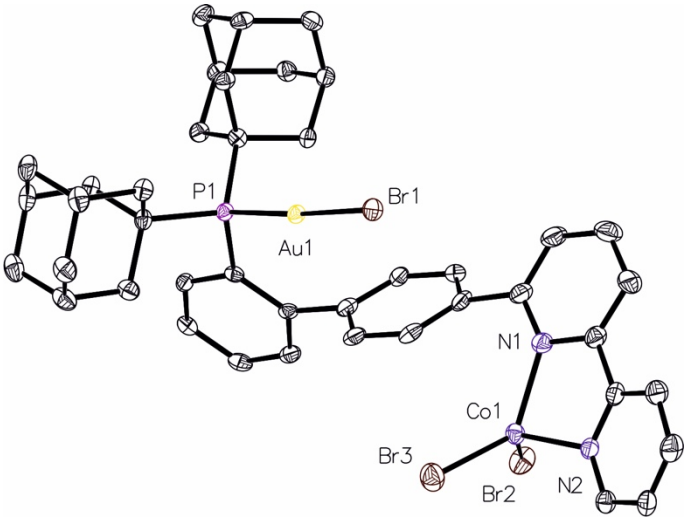

Identification code	egp-vp18		
Empirical formula	$C_{42}H_{45}N_2PCoAuBr_3$		
Formula weight	1104.39		
Temperature/K	100.15		
Crystal system	monoclinic		
Space group	$P2_1/c$		
a/Å	15.7759(2)	α/°	90
b/Å	14.9319(2)	β/°	94.3670(10)
c/Å	16.1594(2)	γ/°	90
Volume/Å^3	3795.52(8)		
Z	4		
ρ_{calc}g/cm^3	1.933		
μ/mm^{-1}	7.532		
F(000)	2148.0		
Crystal size/mm^3	0.15 × 0.03 × 0.02		
Radiation	MoKα (λ = 0.71073)		
2Θ range for data collection/°	5.056 to 57.3		
Index ranges	$-21 \leq h \leq 21$, $-19 \leq k \leq 19$, $-21 \leq l \leq 19$		
Reflections collected	79366		
Independent reflections	9160 [R_{int} = 0.0478, R_{sigma} = 0.0362]		
Data/restraints/parameters	9160/0/451		
Goodness-of-fit on F^2	1.027		
Final R indexes [I>=2σ (I)]	R_1 = 0.0328, wR_2 = 0.0816		
Final R indexes [all data]	R_1 = 0.0505, wR_2 = 0.0887		
Largest diff. peak/hole / e Å^{-3}	1.91/-2.46		

Crystal data and structure refinement for VP10LT.

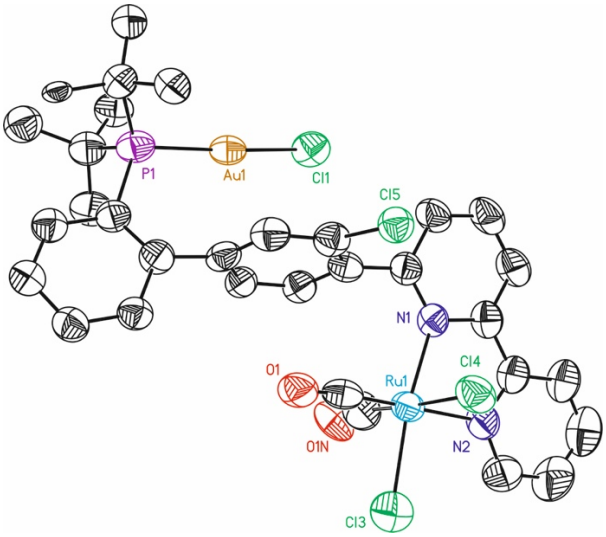

Identification code	VP10LT		
Empirical formula	$C_{39.37}H_{47.85}AuCl_{3.77}N_2O_{5.47}PRu$		
Formula weight	1099.40		
Temperature/K	100(2)		
Crystal system	monoclinic		
Space group	$P2_1/n$		
a/Å	21.5873(5)	α/°	90
b/Å	10.85138(19)	β/°	110.560(2)
c/Å	21.7634(4)	γ/°	90
Volume/Å^3	4773.41(19)		
Z	4		
ρ_{calc}g/cm^3	1.530		
μ/mm^{-1}	3.671		
F(000)	2176		
Crystal size/mm^3	0.30 × 0.04 × 0.03		
Radiation	MoKα (λ = 0.71073)		
Θ range for data collection/°	2.286 to 29.367		
Index ranges	$-29 \le h \le 25$, $-14 \le k \le 14$, $-26 \le l \le 29$		
Reflections collected	90943		
Independent reflections	12302 [R_{int} = 0.0723]		
Data/restraints/parameters	12302/1656/945		
Goodness-of-fit on F^2	1.063		
Final R indexes [I>=2σ (I)]	R_1 = 0.0710, wR_2 = 0.1890		
Final R indexes [all data]	R_1 = 0.1319, wR_2 = 0.2268		
Largest diff. peak/hole / e Å^{-3}	3.280/-1.069		

Crystal data and structure refinement for epgphvp16lt.

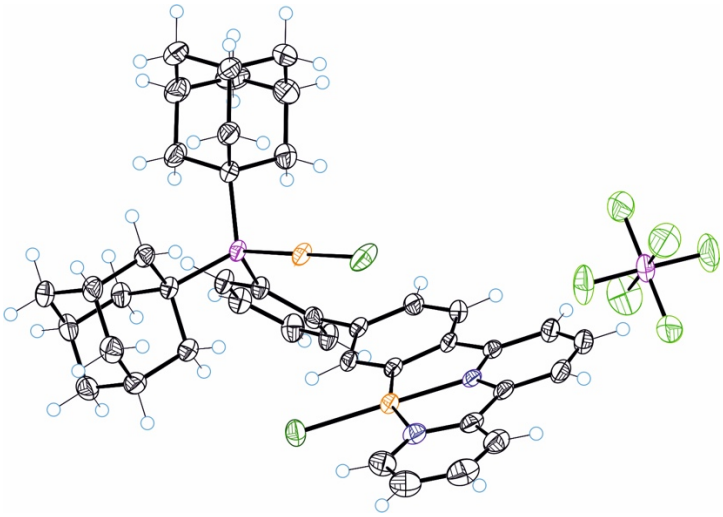

Identification code	iciq 291a-21 epgphvp16lt 20211209		
Empirical formula	$C_{49}H_{53}N_2Au_2P_2Cl_2F_6$		
Formula weight	1310.70		
Temperature/K	100(2)		
Crystal system	monoclinic		
Space group	$P2_1/c$		
a/Å	16.7185(2)	α/°	90
b/Å	26.7811(4)	β/°	105.3184(15)
c/Å	10.41119(15)	γ/°	90
Volume/Å^3	4495.91(12)		
Z	4		
ρ_{calc}g/cm^3	1.936		
μ/mm^{-1}	6.772		
F(000)	2548.0		
Crystal size/mm^3	0.05 × 0.04 × 0.01		
Radiation	MoKα (λ = 0.71073)		
2Θ range for data collection/°	4.332 to 64.342		
Index ranges	$-22 \leq h \leq 24$, $-38 \leq k \leq 39$, $-15 \leq l \leq 15$		
Reflections collected	138189		
Independent reflections	15039 [R_{int} = 0.0478, R_{sigma} = 0.0313]		
Data/restraints/parameters	15039/0/569		
Goodness-of-fit on F^2	1.029		
Final R indexes [I>=2σ (I)]	R_1 = 0.0314, wR_2 = 0.0758		
Final R indexes [all data]	R_1 = 0.0498, wR_2 = 0.0834		
Largest diff. peak/hole / e Å^{-3}	2.20/-2.06		

Crystal data and structure refinement for EGPVRD.

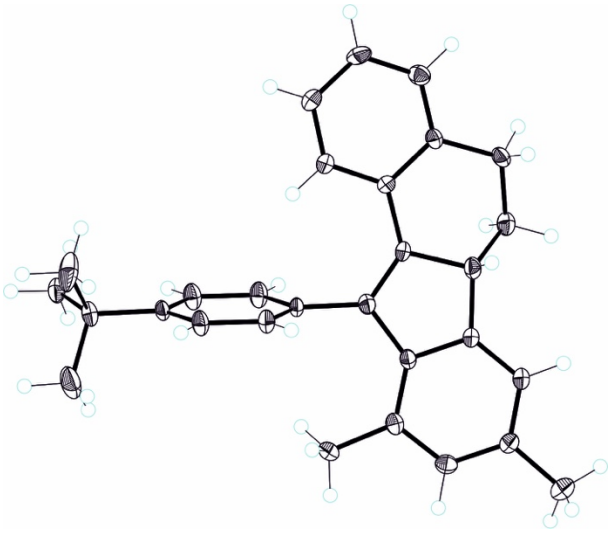

Identification code	EGPVRD		
Empirical formula	$C_{58}H_{60}$		
Formula weight	757.06		
Temperature/K	100.02		
Crystal system	orthorhombic		
Space group	$Pna2_1$		
a/Å	15.0883(14)	α/°	90
b/Å	11.5657(13)	β/°	90
c/Å	24.876(3)	γ/°	90
Volume/Å^3	4341.0(8)		
Z	4		
ρ_{calc}g/cm^3	1.158		
μ/mm^{-1}	0.065		
F(000)	1632.0		
Crystal size/mm^3	0.05 × 0.04 × 0.04		
Radiation	MoKα (λ = 0.71073)		
2Θ range for data collection/°	3.884 to 61.802		
Index ranges	$-13 \leq h \leq 21$, $-16 \leq k \leq 11$, $-35 \leq l \leq 17$		
Reflections collected	34762		
Independent reflections	9690 [R_{int} = 0.0756, R_{sigma} = 0.0745]		
Data/restraints/parameters	9690/1005/1061		
Goodness-of-fit on F^2	1.061		
Final R indexes [I>=2σ (I)]	R_1 = 0.0672, wR_2 = 0.1692		
Final R indexes [all data]	R_1 = 0.0902, wR_2 = 0.1859		
Largest diff. peak/hole / e Å^{-3}	0.43/-0.34		

Computed Structures and Energies

E and G correspond to calculations performed with 6-31G(d) for non-metals, whereas E_{HLT} are the single-point energies using 6-311+G(d,p). Unless otherwise specified, B3LYP-D3 was used with implicit solvation with PCM (dichloromethane).

Table 6. Energies of substrates used in **Chapter III**. B3LYP-D3/6-31G(d)+SDD(Au); PCM (dichloromethane); HLT: B3LYP-D3/6-311+G(d,p)+SDD(Au)

Substrate	E / Hartree	G / Hartree	E_{HLT} /Hartree
C_2H_4	-78.58768	-78.55804	-78.61748
HCCH	-77.32702	-77.31927	-77.35992
Me_2CO	-193.16137	-193.10553	-193.22869
$HCCSnMe_3$	-199.86683	-199.77849	-199.94028
$PhSnMe_3$	-354.77101	-354.61557	-354.88163
Me_3SnCl	-583.37428	-583.30169	-583.45272
MeCN	-132.75920	-132.73761	-132.80457
$Ag(MeCN)_4$	-677.97439	-677.85172	-678.13315
$Ag(MeCN)_3Cl$	-1005.58979	-1005.51388	-1005.74625

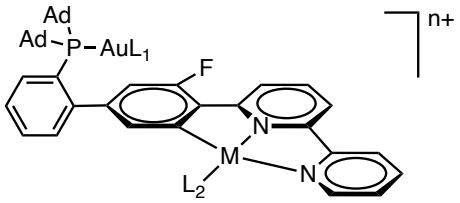

Figure 10. Model complex for coordination chemistry.

Table 7. Energies of gold(I)-d^8 metal complexes in different coordination environment. Charges vary for Au(III) and Pd(II)/Pt(II). B3LYP-D3/6-31G(d)+SDD(Au); PCM (dichloromethane); HLT: B3LYP-D3/6-311+G(d,p)+SDD(Au)

M	L_1	L_2	Charge	E / Hartree	G / Hartree	E_{HLT} /Hartree
Au	MeCN	MeCN	3	-2713.88877	-2713.10147	-2714.45618
Au	MeCN	Cl	2	-3041.55158	-3040.81025	-3042.11619
Au	Cl	MeCN	2	-3041.53445	-3040.79518	-3042.09946
Au	Cl	Cl	1	-3369.18668	-3368.49325	-3369.74897
Pd	MeCN	MeCN	2	-2706.30118	-2705.51775	-2706.87141
Pd	MeCN	Cl	1	-3033.92807	-3033.18928	-3034.49672

Pd	Cl	MeCN	1	-3033.93112	-3033.19315	-3034.49912
Pd	Cl	Cl	0	-3361.54739	-3360.85312	-3362.11406
Pt	MeCN	MeCN	2	-2697.78845	-2697.00443	-2698.35877
Pt	MeCN	Cl	1	-3025.41271	-3024.67404	-3025.98148
Pt	Cl	MeCN	1	-3025.41784	-3024.67947	-3025.98593
Pt	Cl	Cl	0	-3353.03068	-3352.33711	-3353.59728
Au	Ph	Cl	1	-3140.59371	-3139.81473	-3141.18272
Au	Cl	Ph	1	-3140.62339	-3139.84452	-3141.21280
Pd	Ph	Cl	0	-3132.95049	-3132.17309	-3133.54479
Pd	Cl	Ph	0	-3132.94539	-3132.16808	-3133.54036
Pt	Ph	Cl	0	-3124.43485	-3123.65701	-3125.02917
Pt	Cl	Ph	0	-3124.44232	-3123.66498	-3125.03741
Au	CCH	Cl	1	-2985.68772	-2984.97695	-2986.23977
Au	Cl	CCH	1	-2985.70209	-2984.99226	-2986.25468
Pd	CCH	Cl	0	-2978.04763	-2977.33810	-2978.60447
Pd	Cl	CCH	0	-2978.04521	-2977.33569	-2978.60245
Pt	CCH	Cl	0	-2969.53129	-2968.82167	-2970.08777
Pt	Cl	CCH	0	-2969.54238	-2968.83140	-2970.09958
Au	C_2H_4	Cl	2	-2987.37625	-2986.62621	-2987.92496
Au	Cl	C_2H_4	2	-2987.35605	-2986.60693	-2987.90475
Pd	C_2H_4	Cl	1	-2979.75354	-2979.00846	-2980.30626
Pd	Cl	C_2H_4	1	-2979.75589	-2979.00987	-2980.30832
Pt	C_2H_4	Cl	1	-2971.23832	-2970.49263	-2971.79122
Pt	Cl	C_2H_4	1	-2971.24499	-2970.49807	-2971.79739
Au	HCCH	Cl	2	-2986.11046	-2985.38718	-2986.66058
Au	Cl	HCCH	2	-2986.08834	-2985.36454	-2986.63814
Pd	HCCH	Cl	1	-2978.48768	-2977.76746	-2979.04209
Pd	Cl	HCCH	1	-2978.49100	-2977.77067	-2979.04495
Pt	HCCH	Cl	1	-2969.97275	-2969.25313	-2970.52692
Pt	Cl	HCCH	1	-2969.97851	-2969.25739	-2970.53231
Au	C_2H_4	MeCN	3	-2659.71330	-2658.91670	-2660.26503
Au	MeCN	C_2H_4	3	-2659.70719	-2658.90918	-2660.25874
Pd	C_2H_4	MeCN	2	-2652.12727	-2651.33468	-2652.68100
Pd	MeCN	C_2H_4	2	-2652.12483	-2651.33321	-2652.67920
Pt	C_2H_4	MeCN	2	-2643.61483	-2642.82162	-2644.16883

Pt	MeCN	C_2H_4	2	-2643.61451	-2642.82031	-2644.16930
Au	HCCH	MeCN	3	-2658.44713	-2657.67749	-2659.00022
Au	MeCN	HCCH	3	-2658.43829	-2657.66654	-2658.99105
Pd	HCCH	MeCN	2	-2650.86038	-2650.09557	-2651.41604
Pd	MeCN	HCCH	2	-2650.85959	-2650.09216	-2651.41540
Pt	HCCH	MeCN	2	-2642.34842	-2641.58329	-2642.90462
Pt	MeCN	HCCH	2	-2642.34763	-2641.57987	-2642.90349
Au	Me_2CO	MeCN	3	-2774.29177	-2773.46985	-2774.87742
Au	MeCN	Me_2CO	3	-2774.29255	-2773.46842	-2774.87792
Pd	Me_2CO	MeCN	2	-2766.70536	-2765.88390	-2767.29289
Pd	MeCN	Me_2CO	2	-2766.70146	-2765.88278	-2767.28989
Pt	Me_2CO	MeCN	2	-2758.19271	-2757.37062	-2758.78028
Pt	MeCN	Me_2CO	2	-2758.18615	-2757.36665	-2758.77483

Table 8. Energies for the conjugate additions and reductive elimination on **A1** and **B1**. B3LYP-D3/6-31G(d)+SDD(Au); PCM (dichloromethane); HLT: B3LYP-D3/6-311+G(d,p)+SDD(Au)

Code	E / Hartree	G / Hartree	E_{HLT} /Hartree
A1	-3140.62339	-3139.84452	-3141.21280
TSA2	-3140.55916	-3139.78272	-3141.15134
A2	-3140.65706	-3139.87794	-3141.24884
TSA3	-3140.55686	-3139.77986	-3141.14660
A3	-3140.64322	-3139.86601	-3141.23254
A4	-3140.65381	-3139.87664	-3141.24604
B1	-2911.42365	-2910.55686	-2912.04268
TSB2	-2911.39984	-2910.53081	-2912.01770
B2	-2911.46356	-2910.59128	-2912.07892
TSB3	-2911.39274	-2910.52234	-2912.00826
B3	-2911.40429	-2910.53136	-2912.01963

Table 9. Energies for the self-activation of **C1** and **D1**. B3LYP-D3/6-31G(d)+SDD(Au); PCM (dichloromethane); HLT: B3LYP-D3/6-311+G(d,p)+SDD(Au)

Code	E / Hartree	G / Hartree	E_{HLT} /Hartree
C1	-3269.95523	-3269.25054	-3270.48347
TSC2	-3347.27565	-3346.54721	-3347.83059

C2	-3347.27728	-3346.55046	-3347.83311
D1	-2180.46684	-2179.88139	-2180.84934
TSD2	-2257.78781	-2257.17667	-2258.19719
D2	-2257.78897	-2257.17738	-2258.19747
TSD3	-2257.78403	-2257.17287	-2258.19528
D3	-2257.78475	-2257.17324	-2258.19728

General Conclusions

This Doctoral Thesis analyses gold(I)-catalysed cycloisomerisations both from a mechanistic and a synthetic perspective, together with the preparation of novel bimetallic complexes. The research collected in this manuscript has led to the following conclusions:

Firstly, our computational explorations into the nature of the intermediates formed in the cyclisations of 1,5-enynes and 1,5-allenenes suggested that a variety of gold(I) cyclopropylcarbene and open form carbocationic vinylgold species are tautomers both in *exo*-dig and *endo*-dig cyclisations. The existence of specific tautomers is strictly substrate-dependent and most 1,5-enynes and allenenes favour the cyclopropylcarbene forms more strongly than comparable 1,6-enynes.

We have discovered the factors leading to exocyclic and endocyclic cleavage in the single-cleavage rearrangement of 1,6-enynes, as well as the origin of the experimentally observed stereoconvergence. These factors have been ascribed to a balance of steric and electronic factors that explain the substrate dependence previously observed experimentally and we correctly predict the outcomes of several borderline cases that were confirmed experimentally.

In addition, computational models for cyclisation and alkoxycyclisation of 1,6-enynes were devised, accounting for the role of alcohol as a nucleophile or as a base and shedding light on the nuclearity of the relevant reactive clusters. We also explore the mechanism for the erosion of enantioselectivity of such products when fewer equivalents of alcohol were used, pointing to a reversible 1,2-hydride shift pathway which becomes kinetically accessible with lower concentrations of alcohol. Moreover, we discard proton-catalysed pathways due to the facile protodemetallation, although proton shuttles prove important.

We have developed a 1,3,5-selective cyclotrimerisation of terminal alkynes and explored its mechanism comprehensively with DFT and key control experiments. Thereby, we determined that gold(I) η^1-cyclobutadiene and Dewar benzene intermediates are involved and result in the 1,3,5-selectivity. Guided by these insights, we achieved to carry out the counterintuitive intramolecular formal 1,2,3-cyclotrimerisation.

Finally, the design of a new scaffold based on a phosphine-bipyridine ditopic ligand framework allowed the easily scalable preparation of heterobimetallic complexes, as well as the first mixed-valence digold complexes to be used in catalysis. As well as carrying out the structural characterisation of most complexes, we tested the catalytic performance of a number of bimetallic complexes. Our computational investigations suggested that Coulombic stabilisation would be enough to perform self-activating gold(I) catalysis, which was confirmed for a series of reactions.